Synthesis and Characterization of Multifunctional Macromonomers and Photoacid Generators for the Modification of Hydrogels

von der Fakultät Energie-, Verfahrens- und Biotechnik der

Universität Stuttgart zur Erlangung der Würde eines

Doktors der Naturwissenschaften (Dr. rer. nat.)

genehmigte Abhandlung

vorgelegt von

Karishma Katharina Reinold, geb. Adatia

geboren am 17.06.1989 in Memmingen

Hauptberichter: Prof. Dr. Günter E. M. Tovar

Mitberichterin: Prof. Dr. Sabine Laschat

Tag der mündlichen Prüfung: 09.07.2020

_____

Dedicated to my dad

.

Table of contents

_____

Declaration of Authorship

I hereby certify that the dissertation entitled „Synthesis and Characterization of Multifunctional Macromonomers and Photoacid Generators for the Modification of Hydrogels" is entirely my own work except where otherwise indicated. Passages and ideas from other sources have been clearly indicated.

Karishma Reinold

Erklärung über die Eigenständigkeit der Dissertation

Ich versichere, dass ich die vorliegende Dissertationsschrift mit dem Titel „Synthesis and Characterization of Multifunctional Macromonomers and Photoacid Generators for the Modification of Hydrogels" selbständig verfasst und dass ich keine anderen als die angegebenen Quellen und Hilfsmittel benutzt habe. Aus fremden Quellen entnommene Passagen und Gedanken sind als solche kenntlich gemacht.

Karishma Reinold

I.   Acknowledgements

First of all I want to thank my supervisor Prof. Dr. Günter E. M. Tovar for supporting me as a PhD student at the Institute of Interfacial Process Engineering and Plasma Technology of the University of Stuttgart. I am grateful for the opportunity to do my PhD research in such a free and multidisciplinary environment. I especially appreciated the freedom to develop my own ideas and to get excellent scientific guidance during fruitful discussions.

I also want to thank the second assessor of this thesis Prof. Dr. Sabine Laschat for evaluating my thesis with a second opinion and for supervising my students. Her deep knowledge about organic chemistry was highly valuable for our collaboration.

My special thank goes to my scientific advisor Dr. Alexander Southan. Without him and my supervisor Prof. Dr. Günter E. M. Tovar I would not be the scientist I am today. His critical questions and his scientific precision helped me to grow beyond myself. I appreciate his unrelenting support throughout the whole research.

I am deeply thankful for my time at Stanford University. Thank you so much, Prof. Curt Frank, for inviting me and making this dream come true! It was probably the best time of my life! I had great experiences on a personal and scientific level. For me Stanford is truly a place to flourish!

It was also a pleasure for me to supervise our students. Thank you Vanessa Fronk, Oliver Gorke, Andre Michele, Michael Tran and Manuel Häußler for your contributions.

My sincere thank goes to Dr. Michael Schweickert, who helped me with the TEM measurements. I enjoyed learning and working with him so much.

I also want to thank all lab members and cooperation partners for their support and the productive atmosphere. Especially the discussions with Tobias Götz and Dr. Christiane Claaßen were very valuable for me.

Furthermore, I want to thank Prof. Dr. Thomas Hirth and Dr. Markus Wolperdinger for extending the facilities of the Fraunhofer IGB laboratories and research infrastructure for this study.

_____

I am thankful to the Evonik Foundation for financially supporting me through their generous PhD scholarship.

Melanie Dettling, Regina Buck, Sarah Schmidt, Nadine Dannehl and Larissa Kutscha, I will never forget your incredible support. I thank you from the bottom of my heart and I am sure our friendship will last far beyond this PhD.

Last but not least I want to thank my family. My mum, Peter and Martina. There are no words which could express my gratefulness to you. Thank you for always being on my side. Without each and everyone of you, I would never have come so far.

II.   Structure of the thesis

This dissertation thesis begins with a summary in english language (section 1) and a "Zusammenfassung" in german language (section 2). In section 3 the introduction guides the reader towards the scientific background of this research and leads towards the aim of work and hypotheses (section 4).

The results are shown and discussed in section 5 – 8, whereby section 5 "Hydrogels with multiple clickable anchor points: synthesis and characterization of poly(furfuryl glycidyl ether)-*block*-poly(ethylene glycol) macromonomers" and section 6 "Structure-property relations of amphiphilic poly(furfuryl glycidyl ether)-*block*-poly(ethylene glycol) macromonomers at the air-water interface" are both published in *Polymer Chemistry* (RSC). Section 7 comprises preliminary experiments for the functionalization of the air-hydrogel interface. The following section (section 8) "Coumarin-4-ylmethyl and *p*-hydroxyphenacyl-based photoacid generators with high solubility in aqueous media: synthesis, stability and photolysis" is published in *ChemPhotoChem* (Wiley-VCH).

Section 9 "Discussion of hypotheses" evaluates the results in reference to the hypotheses from section 4. The dissertation thesis ends with the main conclusions of this research and an outlook to future applications in section 10.

III. Abbreviations and Symbols

^{13}C NMR	carbon nuclear magnetic resonance spectroscopy
^1H NMR	proton nuclear magnetic resonance spectroscopy
2D	two dimensional
3D	three dimensional
3PP	3-phenyl-1-propanol
4-DMAP	*N,N*-dimethylpyridin-4-amine
4-VBC	4-vinylbenzyl chloride
A	area per molecule
Aam	acrylamide
ABC	amphiphilic block copolymers
A_c	constant trough area
ACN	acetonitrile
AcOH	acetic acid
AFM	atomic force microscopy
AGE	allyl glycidyl ether
Ala-Ala	di-alanine
ANOVA	analysis of variance
A_o	area per molecule at the onset
a_o	trough area at the isotherm onset
AROP	anionic ring opening polymerization

ATP	adenosine triphosphate
ATR-IR	attenuated total reflection infrared spectra
A_λ	absorbance at specific wavelength
B	block length ratio
Boc	*tert*-butyloxycarbonyl
c	concentration
c4m	coumarin-4-ylmethyl
c4m-OH	7-[bis(carboxymethyl) amino]-4-(hydroxymethyl)-coumarin
C_{DA}	conversion of Diels-Alder reaction
c_g	abundance of gray scale value
c_{max}	maximum solubility
$c_{max,a}$	maximum solubility in alkaline solution
c_d	maximum solubility of diluted solution
$c_{max,w}$	maximum solubility in water
cmc	critical micelle concentration
$Đ$	molar mass dispersities
d	path length
DAGA	*N,N*-diallyl glycidyl amine
DBAG	*N,N*-dibenzyl glycidyl amine
DCM	dichlormethane
DCTB	*trans*-2-[3-(4-*tert*-Butylphenyl)-2-methyl-2-propenylidene]-malononitrile
d_f	dilution factor

DMF	*N,N*-dimethylformamide
$Đ_{MS}$	molar mass dispersity determined by mass spectrometry
DMSO	dimethylsulfoxide
DPM	diphenylmethane
DPMK	diphenylmethyl potassium
DSC	differential scanning calorimetry
$Đ_{SEC}$	molar mass dispersity determined by size exclusion chromatography
EDC	1-ethyl-3-(3-dimethylaminopropyl)carbodiimide
EDS	equilibrium degree of swelling
EEGE	ethoxy ethyl glycidyl ether
EO	ethylene oxide
Et	ethyl
EtOAC	ethyl acetate
EtOH	ethanol
f	functionalization degree
FGE	furfuryl glycidyl ether
f_m	mass fraction
FT-IR	fourier-transform infrared
g	average gray scale value
h	hour
HEPES	hydroxyethyl piperazineethanesulfonic acid
HLB	hydrophilic-lipophilic balance

HPLC	high performance liquid chromatography
I	fluorescence intensity
IGG	isopropylidene glyceryl glycidyl ether
Int_{BB}	integral of backbone signals in ^1H NMR
Int_{end}	end group signals in ^1H NMR spectrum
Int_{furan}	integral of furfuryl signals in ^1H NMR
Int_{ini}	initiator signals in ^1H NMR spectrum
iPrOH	isopropanol
ISC	intersystem crossing
IUPAC	International Union of Pure and Applied Chemistry
J	coupling constant
LD	lethal dose
LG	leaving group
LSM	laser scanning microscopy
m_{4VBC}	mass of 4-vinylbenyzl end group
MALDI	matrix assisted laser desorption ionization
MBA	N,N'-methylenebisacrylamide
m_{dry}	dry mass
m_e	experimentally determined mass
Me	methyl
m_{EO}	mass of ethylene oxide
MeOH	methanol
m_{FGE}	mass of furfuryl glycidyl ether

M_h	molar mass of the hydrophilic moiety
m_{ini}	mass of the initiator
MIP	maximum intensity projection
MIR	monomer-to-initiator ratio
M_l	molar mass of the lipophilic moiety
MMD	molar mass distribution
M_n	number average molar mass
$M_{n,MS}$	number average molar mass determined by mass spectrometry
$M_{n,NMR}$	number average molar mass determined by nuclear magnetic resonance spectroscopy
$M_{n,SEC}$	number average molar mass determined by size exclusion chromatography
m_{pol}	mass after polymerization
MS	mass spectrometry
M_w	weight average molar mass
$M_{w,MS}$	weight average molar mass determined by mass spectrometry
$M_{w,SEC}$	weight average molar mass determined by size exclusion chromatography
NEM	*N*-ethylmaleimide
n_{end}	number of end group protons
n_{EO}	number of ethylene oxide protons
n_{furan}	number of furfuryl protons
n_{ini}	number of initiator protons

n_p	photon flux
p	furfuryl glycidyl ether repeating units
P	peak area
p(Aam)	polyacrylamide
PAG	photoacid generator
PE	petroleum ether
PEG	poly(ethylene glycol
PEG-*b*-PFGE	poly(ethylene glycol)-*block*-poly(furfuryl glycidyl ether)
PEGDA	poly(ethylene diacrylate)
PEO	poly(ethylene oxide)
PFGE	poly(furfuryl gylcidyl ether)
PFGE$_p$-*b*-PEG$_q$	*α*-diphenylmethyl-*ω*-4-vinylbenzyl-poly(furfuryl glycidyl ether)-*block*-poly(ethylene glycol)
PFGE$_p$-*b*-PEG$_q$H	*α*-diphenylmethyl-*ω*-hydroxy-poly(furfuryl glycidyl ether)-*block*-poly(ethylene glycol)
pHBA	*p*-hydroxybenzyl alcohol
pHEMA	poly(2-hydroxyethyl methacrylate)
*p*HP	*p*-hydroxyphenacyl
pHPA	*p*-hydroxyphenylacetic acid
*p*HP-ac	*p*-hydroxyphenacylacetate
*p*HP-t	*p*-hydroxyphenacyl-2,5,8,11-tetraoxatridecan-13-oate
pK_a	logarithmic acid dissociation constant

pK_b	locarighmic base dissociation constant
PP	polypropylene
PS	polystyrene
PTFE	polytetrafluoroethylene
q	ethylene oxide repeating units
R^2	coefficient of determination
RGD	arginine-glycine-aspartic acid
RI	refractive index
RSC	royal society of chemistry
RT	room temperature
s	stability
S	surface functionality factor
s_{1h}	stability for 1 hour
s_{24h}	stability for 24 hours
s_{3h}	stability for 3 hours
SD	spirodione
SEC	size exclusion chromatography
SFR	surface functionality ranking
s_{HM}	slope of hysteresis maxima fit
SIMS	secondary-ion mass spectrometry
t	time
T_d	decomposition temperature
$T_{d,5}$	decomposition temperatures at 5% mass loss

TFA	trifluoroacetic acid
T_g	glass transition temperature
TGA	thermogravimetric analysis
THF	Tetrahydrofuran
t_{irr}	irradiation time
T_m	melting temperature
TOF	time of flight
t_s	storage time
UV	ultraviolet
V	volume
y	concentration change
y'	initial change of concentration rate
Y_g	gel yield
Y_s	synthesis yield
γ	surface tension of water with surfactant
γ_0	surface tension of water
δ	chemical shift
ΔH_m	melting enthalpy
$\Delta \pi$	surface pressure difference
$\Delta \pi_d$	surface pressure drop
ε_{max}	maximum molar absorption coefficient
Θ_m	mass surface coverage factor
Θ_n	molar surface coverage factor

λ_{max}	wavelength of the absorption maxiumum
λ_Φ	wavelength at the quantum yield
π	surface pressure
π_0	starting surface pressure
π_{HM}	surface pressure at hysteresis maximum
$\pi_{HM,1}$	surface pressure at the hysteresis maximum of the first hysteresis cycle
$\pi_{HM,5}$	surface pressure at the hysteresis maximum of the fifth hysteresis cycle
$\pi_{HM,r}$	surface pressure at the hysteresis maximum of the recovery cycle
Φ	quantum yield

1. Summary

There is a growing demand for tailor-made hydrogels with specific properties since hydrogels are used in various fields such as tissue engineering, drug delivery and cosmetics. Therefore, hydrogels need to be modified according to the desired application. For the modification of hydrogels two basic stratgies are applicable. The first strategy focusses on the modification of the polymer network and the second strategy is based on the modification of the hydrogel swelling agent. The aim of this work is to synthesize and characterize novel hydrogel modification reagents for both strategies (Figure 1). Regarding the first hydrogel modification strategy, multifunctional *α*-diphenylmethyl-*ω*-4-vinylbenzyl-poly(furfuryl glycidyl ether)-*block*-poly(ethylene glycol) (PFGE$_p$-*b*-PEG$_q$) macromonomers were synthesized and characterized. Regarding the second strategy for the potential modification of the hydrogel swelling agent, the synthesis and characterization of two photoacid generators (PAG) *p*-hydroxyphenacyl-2,5,8,11-tetraoxatridecan-13-oate (*p*HP-t) and 7-[bis(carboxy-methyl)amino]-4-(acetoxymethyl)-coumarin (c4m-ac) was investigated.
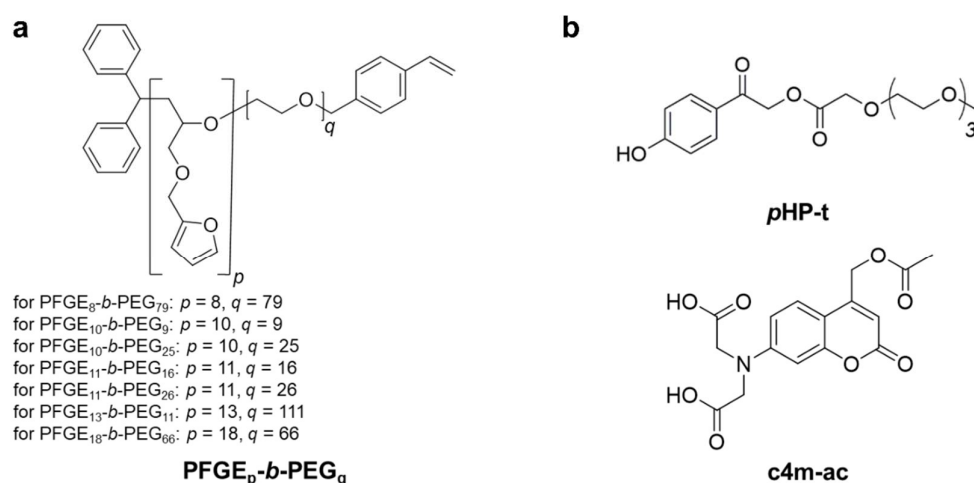
a

for PFGE$_8$-*b*-PEG$_{79}$: $p = 8$, $q = 79$
for PFGE$_{10}$-*b*-PEG$_9$: $p = 10$, $q = 9$
for PFGE$_{10}$-*b*-PEG$_{25}$: $p = 10$, $q = 25$
for PFGE$_{11}$-*b*-PEG$_{16}$: $p = 11$, $q = 16$
for PFGE$_{11}$-*b*-PEG$_{26}$: $p = 11$, $q = 26$
for PFGE$_{13}$-*b*-PEG$_{11}$: $p = 13$, $q = 111$
for PFGE$_{18}$-*b*-PEG$_{66}$: $p = 18$, $q = 66$

PFGE$_p$-*b*-PEG$_q$

b

*p*HP-t

c4m-ac

Figure 1: Aim of work with focus on the synthesis and characterization of novel hydrogel modification reagents. a) For the modification of the polymer network, *α*-diphenylmethyl-*ω*-4-vinylbenzyl-poly(furfuryl glycidyl ether)-*block*-poly(ethylene glycol) (PFGE$_p$-*b*-PEG$_q$) was chosen. b) For the potential modification of the hydrogel swelling agent, *p*-hydroxyphenacyl-2,5,8,11-tetraoxatridecan-13-oate (*p*HP-t) and 7-[bis(carboxymethyl)amino]-4-(acetoxymethyl)coumarin (c4m-ac) were synthesized and characterized.

PFGE$_p$-*b*-PEG$_q$ macromonomers were prepared as building blocks for functional hydrogels containing multiple furfuryl anchor points for post-synthetic modification reactions. These macromonomers were chosen because they exhibit a polymerizable unit for the covalent incorporation into radically cross-linked hydrogels, contain a

poly(ethylene glycol) spacer to increase flexibility and water solubility, and also have multiple, pendent furan groups, which can serve as molecular anchor points. The $PFGE_p$-b-PEG_q macromonomers were synthesized in different block length ratios ($PFGE_{10}$-b-PEG_9, $PFGE_{11}$-b-PEG_{16}, $PFGE_{11}$-b-PEG_{26}, $PFGE_{10}$-b-PEG_{25}, $PFGE_8$-b-PEG_{79}, $PFGE_{18}$-b-PEG_{66} and $PFGE_{13}$-b-PEG_{111}) *via* anionic ring opening polymerization by adjusting the monomer-to-initiator (MIR) ratio. The characterization by proton nuclear magnetic resonance spectroscopy (^{1}H NMR), carbon nuclear magnetic resonance spectroscopy (^{13}C NMR) and fourier-transform infrared (FT-IR) spectroscopy, size exclusion chromatography (SEC) and matrix assisted laser desorption ionization time of flight (MALDI TOF) mass spectrometry revealed the successful preperation of well-defined macromonomers with low molar mass dispersities $Đ$ between 1.05 and 1.12, number average molar masses $M_{n,SEC}$ between 2 330 g mol^{-1} and 6 660 g mol^{-1}, high end group functionalization degrees between 72 % and 98 % and a broad range of hydrophilic-lipophilic balance (HLB) values from 3.6 to 13.9. Differential scanning calorimetry (DSC) and thermogravimetric analysis (TGA) measurements elucidated their thermal properties such as their glass transition temperatures T_g between -43 °C and -32 °C, their melting temperatures T_m between 32 °C and 45 °C and their decomposition temperatures T_d between 369 °C and 381 °C. The surface activity of the water-soluble macromonomers was determined by bubble pressure tensiometry and showed a critical micelle concentration of around 0.3 mg mL^{-1} in aqueous solution. Furthermore, fluorescence labeling experiments with a maleimide-functionalized dye demonstrated that $PFGE_p$-b-PEG_q macromonomers were reactive in Diels-Alder reactions after their integration into polyacrylamide hydrogels by radical copolymerization. Therefore, this hydrogel modification strategy based on the introduction of multiple furan anchor points paves the way to conjugate molecules possessing maleimide groups to hydrogels using Diels-Alder click reactions.

To find out whether the macromonomers are not only able to functionalize the hydrogel bulk, but are also able to exclusively functionalize the air-hydrogel interface, deeper knowledge of the film formation and structure-property relations of $PFGE_p$-b-PEG_q macromonomers was needed. Therefore, the surface activity of the macromonomers was investigated at the air-water interface, which served as a simplified model of the air-hydrogel interface. Langmuir surface pressure-area (π-A) isotherms revealed that the macromonomers were able to form monolayers at the air-water interface and that the block lengths and the molar masses influence the isotherm shape and onset.

Smaller, more hydrophobic macromonomers (HLB < 8) showed a steeper surface pressure increase in the liquid condensed phase compared to larger, more hydrophilic macromonomers with HLB > 8. Additionally, the molecular area for the isotherm onsets increased almost linearly with growing molar mass of the macromonomers. Static and dynamic film stability measurements demonstrated limited stability of all macromonomer monolayers at the air-water interface, whereby the more hydrophilic macromonomers with HLB values > 8 showed higher film stability compared to the more hydrophobic macromonomers with HLB values < 8. This observation is in line with hysteresis experiments of the macromonomers, which displayed an almost linear increase of the monolayer degradation with rising HLB values. For the mechanism of the macromonomer monolayer at the air-water interface, we propose an interplay between a reversible folding and an irreversible submersion mechanism, based on the partial film recovery of the macromonomers after 12 hours. Taken together, the molecular structure and the film forming ability of the macromonomers at the air-water interface indicate that they are promising functionalization reagents for the air-hydrogel interface. However, we could not yet prove an exclusively functionalized air-hydrogel interface in preliminary experiments.

Regarding the second hydrogel modification strategy, the PAGs c4m-ac and pHP-t were synthesized and characterized for the potential modification of hydrogel swelling agents. They showed high solubility in water with maximum solubilities of $c_{max,w}$(c4m-ac) = 2.77 mmol L^{-1} ± 0.07 mmol L^{-1}, $c_{max,w}$(pHP-t) = 124.66 mmol L^{-1} ± 2.10 mmol L^{-1} and high solubilities under basic conditions at pH 9 with a maximum solubility in alkaline solution of $c_{max,a}$(c4m-ac) = 646.46 mmol L^{-1} ± 0.63 mmol L^{-1}, $c_{max,a}$(pHP t) = 34.68 mmol L^{-1} ± 0.62 mmol L^{-1}. The photochemical properties of both PAGs were pH-dependent, as they showed a bathochromic shift of the absorption maxima and a reduction of the maximum molar absorption coefficients in alkaline solution compared to water. For c4m-ac, the photoreactions quantum yield (Φ) at 365 nm stayed at 0.02 regardless of the pH, whereas the relatively high Φ at 310 nm of pHP-t at 0.69 in water dropped to 0.07 at pH 9. Furthermore, c4m-ac and pHP-t showed high stabilities (s_{24h} ≥ 95 %) in water for 24 h, but decreasing stability with increasing pH due to hydrolysis. We envision that our studies will contribute to an increased applicability of c4m and pHP-based PAGs in aqueous media, where high PAG concentrations are needed, such as for hydrogel modification reactions.

Overall, this research about the synthesis and characterization of $PFGE_p$-*b*-PEG_q macromonomers and c4m and *p*HP-based photoacid generators contributed to a comprehensive insight into novel hydrogel modification reagents.

2. Zusammenfassung

Da Hydrogele in verschiedensten Bereichen wie beispielsweise dem *Tissue Engineering*, dem Wirkstofftransport und in der Kosmetik verwendet werden, steigt die Nachfrage nach maßgeschneiderten Hydrogelen mit spezifischen Eigenschaften. Um Hydrogele entsprechend ihrer Anwendung zu modifizieren, gibt es prinzipiell zwei Möglichkeiten: Einerseits kann das Polymernetzwerk des Hydrogels und andererseits das Quellmedium des Hydrogels modifiziert werden. Daher fokussiert sich diese Arbeit auf die Erforschung neuartiger Reagenzien für beide Modifizierungsstrategien (Abbildung 1). Bezüglich der ersten Modifizierungsstrategie wurden multifunktionale α-Diphenylmethyl-ω-4-vinylbenzyl-poly(furfuryl glycidyl ether)-*block*-poly(ethylene glycol) ($PFGE_p$-*b*-PEG_q) Makromonomere hergestellt und charakterisiert. Im Hinblick auf die zweite Modifizierungsstrategie wurden zwei *photoacid generators* (PAGs) *p*-Hydroxyphenacyl-2,5,8,11-tetraoxatridecan-13-oate (*p*HP-t) und 7-[Bis(carboxy-methyl)amino]-4-(acetoxymethyl)coumarin (c4m-ac) synthetisiert und auf ihre zukünftige Anwendung als Reagenz für die Modifikation von Hydrogel-Quellmedien untersucht.
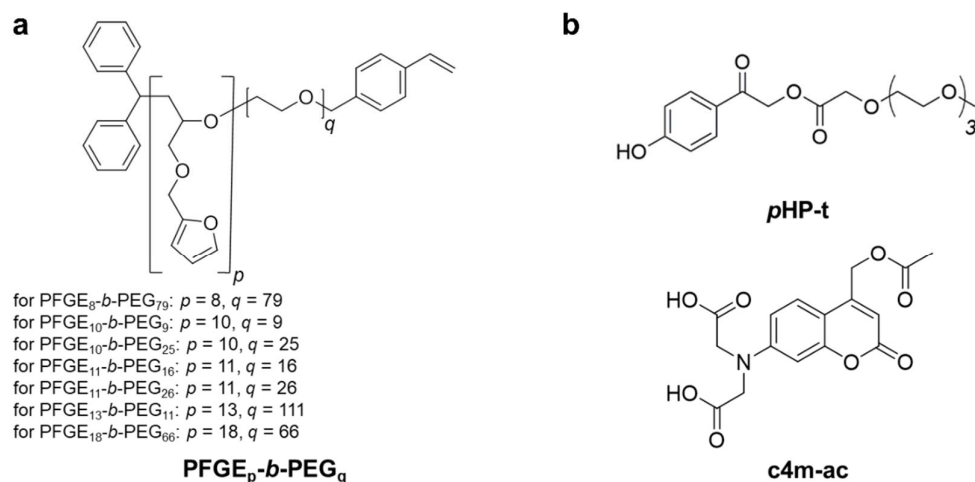

Abbildung 1: Der Schwerpunkt dieser Arbeit liegt auf der Synthese und Charakterisierung neuer Reagenzien für die Hydrogelmodifikation Für die Modifizierung der Polymernetzwerke wurden a) α-Diphenylmethyl-ω-4-vinylbenzyl-poly(furfuryl glycidyl ether)-*block*-poly(ethylene glycol) ($PFGE_p$-*b*-PEG_q) Makromonomere gewählt. Für die zuküftige Modifikation von Hydrogel-Quellmedien wurden b) *p*-Hydroxyphenacyl-2,5,8,11-tetraoxatridecan-13-oate (*p*HP-t) and 7-[Bis(carboxymethyl)amino]-4-(acetoxymethyl)coumarin (c4m-ac) synthetisiert und charkterisiert.

$PFGE_p$-*b*-PEG_q Makromonomere wurden für die Darstellung von funktionalen Hydrogelen gewählt, da sie: I) eine polymerisierbare Einheit für die kovalente Einvernetzung in radikalisch aufgebaute Hydrogelnetzwerke besitzen, II) über einen

Poly(ethylenglykol)-Spacer für erhöhte Flexibilität und Wasserlöslichkeit verfügen, sowie III) multipe Furangruppen als molekulare Ankerpunkte für post-synthetische Diels-Alder Reaktionen mit sich bringen. Mittels anionisch ringöffnender Polymerisation und der Variation des Monomer-zu-Initiator Verhältnisses wurden die PFGE$_p$-b-PEG$_q$ Makromonomere in verschiedenen Blocklängen hergestellt. Die Charakterisierung der Polymere erfolgte durch ^{1}H- und ^{13}C-Kernspinresonanz-spektroskopie, FT-IR, Gelpermeations-chromatographie und MALDI TOF Massenspektrometrie. Diese bestätigten die Synthese von wohldefinierten, eng verteilten Makromonomeren mit zahlengemittelten Molekulargewichten zwischen 2 330 g mol^{-1} und 6 660 g mol^{-1}, sowie einer sehr geringen Polydispersität von 1.05 bis 1.12. Zudem konnten hohe Endgruppen-Funktionalisierungsgrade zwischen 72 % und 98 % und eine weite Spanne an HLB-Werten von 3.6 bis 13.9 nachgewiesen werden. Zur Aufklärung der thermischen Eigenschaften wurden Wärmedurchflusskalorimetrie-Messungen und thermogravimetrische Analysen druchgeführt, die Glasübergangstemperaturen T_g zwischen -43 °C und -32 °C, Schmelztemperaturen T_m zwischen 32 °C und 45 °C, sowie Zersetzungstemperaturen T_d von 369 °C bis 381 °C zeigten. Darüber hinaus konnte durch die Messung der Oberflächenaktivität mittels Blasendrucktensiometrie eine kritische Mizellbildungskonzentration von 0.3 mg mL^{-1} der wasserlöslichen Makromonomere ermittelt werden. Zudem zeigten Fluoreszenzmarkierungs-Experimente mit einem maleimid-funktionalisierten Farbstoff, dass die Makromonomere bei Diels-Alder Reaktionen reaktiv waren, nachdem sie durch radikalische Copolymerisation in Polyacrylamid-Hydrogele integriert wurden. Daher ebnet diese Hydrogel-Modifikationsstrategie, die auf der Einführung multipler Furan-Ankerpunkte basiert, den Weg zur Kopplung von Molekülen mit Maleimidgruppen an radikalisch polymerisierte Hydrogele.

Um herauszufinden, ob die Makromonomere nicht nur in der Lage sind, die Hydrogelmasse, sondern auch die Luft-Hydrogel-Grenzfläche zu funktionalisieren, ist ein vertieftes Wissen über die Filmbildung und die Struktur-Eigenschaftsbeziehungen der Makromonomere notwendig. Daher wurde die Oberflächenaktivität der Makromonomere an der Luft-Wasser-Grenzfläche untersucht, die als vereinfachtes Modell der Luft-Hydrogel-Grenzfläche diente. Anhand von Langmuir π-A Isothermen konnte gezeigt werden, dass die Makromonomere an der Luft-Wasser-Grenzfläche Monoschichten bildeten. Zudem zeigte sich, dass die Blocklängen und die Molekulargewichte der Makromonomere die Form der Isotherme und deren Beginn

beeinflussten. Kleinere, hydrophobere Makromonomere (HLB < 8) zeigten in der flüssig-kondensierten Phase einen steileren Anstieg des Oberflächendrucks im Vergleich zu größeren, hydrophileren Makromonomeren mit HLB > 8. Zudem stieg der Platz pro Molekül an der Luft-Wasser Grenzfläche nahezu linear mit steigender Molmasse der Makromonomere. Statische und dynamische Filmstabilitätsmessungen zeigten eine eingeschränkte Stabilität aller Makromonomer-Monoschichten an der Luft-Wasser-Grenzfläche, wobei die hydrophileren Makromonomere mit HLB-Werten > 8 eine höhere Filmstabilität aufwiesen als die hydrophoberen Makromonomere mit HLB-Werten < 8. Diese Beobachtung steht im Einklang mit den Hystereseexperimenten, die einen nahezu linearen Anstieg des Degradierungs-prozesses der Makromonomer-Monolagen mit steigenden HLB-Werten zeigten. Basierend auf der Filmrückbildung der Makromonomere nach 12 Stunden, kann für den Mechanismus der Makromonomer-Monoschichten an der Luft-Wasser-Grenzfläche ein Zusammenspiel aus einem reversiblen Faltungs- und einem irreversiblen Abtauch-Mechanismus vorgeschlagen werden. Auch wenn die Grenzflächenfunktionalisierung von Hydrogelen in bisherigen Experimenten noch nicht bestätigt werden konnte, weisen die Molekülstruktur und die Filmbildungsfähigkeit an der Luft-Wasser-Grenzfläche auf das hohe Potential der Makromonomere als Grenzflächenfunktionalisierungs-Reagenzien für Hydrogele hin.

Bezüglich der zweiten Hydrogelmodifizierungs-Strategie wurden die PAGs c4m-ac und *p*HP-t synthetisiert und für die zukünftige Modifikation von Hydrogel-Quellmedien untersucht. Hierfür wurden sie hinsichtlich ihrer Löslichkeit, ihrer photochemischen Eigenschaften und ihrer Stabilität analysiert. Die PAGs zeigten eine hohe Löslichkeit in Wasser mit einer maximalen Löslichkeit von $c_{max,w}$(c4m-ac) = 2.77 mmol L^{-1} ± 0.07 mmol L^{-1}, $c_{max,w}$(*p*HP-t) = 124.66 mmol L^{-1} ± 2.10 mmol L^{-1}. Auch unter basischen Bedingungen bei pH 9 waren c4m-ac und *p*HP-t sehr gut löslich mit einer maximalen Löslichkeit von $c_{max,a}$(c4m-ac) = 646.46 mmol L^{-1} ± 0.63 mmol L^{-1} und $c_{max,a}$(*p*HP t) = 34.68 mmol L^{-1} ± 0.62 mmol L^{-1}. Die photochemischen Eigenschaften beider PAGs waren pH-abhängig, da sie eine bathochrome Verschiebung der Absorptionsmaxima und eine Reduktion der maximalen molaren Absorptionskoeffizienten in alkalischer Lösung im Vergleich zu Wasser zeigten. Für c4m-ac blieb die Quantenausbeute (Φ) unabhängig vom pH-Wert bei 0.02, während bei *p*HP-t die relativ hohe Φ von 0.69 in Wasser auf 0.07 bei pH 9 sank. Darüber hinaus zeigten c4m-ac und *p*HP-t hohe Stabilitäten (s_{24h} ≥ 95%) in Wasser für 24 h, aber abnehmende Stabilität mit

steigendem pH-Wert aufgrund von Hydrolyse. Die Erforschung der Löslichkeit, der photochemischen Eigenschaften und der Stabilität von c4m-ac und pHP-t könnte in Zukunft zu einem erhöhten Einsatz von c4m- und pHP-basierten PAGs in wässrigen Medien führen, wenn hohe PAG-Konzentrationen erforderlich sind wie beispielsweise bei der Modifikation von Hydrogel-Quellmedien.

Insgesamt trägt diese Forschungsarbeit zu einem unfassenden Wissen hinsichtlich neuartiger Reagenzien für Hydrogelmodifikationen bei, die strukturell auf $PFGE_P$-b-PEG_q Makromonomeren sowie c4m- und pHP-basierten PAGs beruhen.

3. Introduction

3.1. Hydrogels – applications, definition and preparation

Hydrogels play an important role in various fields like in biomedicine (Pellá *et al.* 2018, Tavakoli *et al.* 2017), in biotechnology (Abd El-Mohdy *et al.* 2008, Ullah *et al.* 2015), in pharmacy (Hamedi *et al.* 2018, Li *et al.* 2016), in cosmetics (Parente *et al.* 2015), in agriculture (Guilherme *et al.* 2015) and in waste water treatment (Mohammadzadeh Pakdel *et al.* 2018, Ullah *et al.* 2015). Xue *et al.* (2015) for instance used pH- and redox-sensitive hydrogels for controlled drug delivery of anticancer drugs and Atta *et al*. (Atta *et al.* 2012a) were able to remove heavy metals from waster water using polyacylamid hydrogels. Hydrogels are also very appealing as polymer scaffolds in tissue engineering because they can mimic the extracellular matrix of cells and support the growth of functional tissue (Drury *et al.* 2003, El-Sherbiny *et al.* 2013, Lee *et al.* 2001).

To understand what hydrogels are, the definition according to the International Union of Pure and Applied Chemistry (IUPAC) can be used. Gels are defined as a „non-fluid colloidal network or polymer network that is expanded throughout its whole volume by a fluid" and a hydrogel is a „gel where the swelling agent is water" (McNaught *et al.* 1997). Over the years, the term "hydrogel" evolved to gels which are swollen in aqueous solutions such as biological buffers or salt solutions (Caló *et al.* 2015, Ehrenhofer *et al.* 2018, Richter *et al.* 2007). Hereby the hydrophilic polymer network of the hydrogel is responsible for a high water binding capacity and the cross-links among the polymer chains avoid its dissolution into the aqueous phase (Akhtar *et al.* 2016, Hennink *et al.* 2002).

There are multiple ways to classify hydrogels based on their origin, their polymeric composition, their physical properties, their electrical charge or the method of preparation. However, the most frequently used classification of hydrogels is based on their cross-linking nature, which divides them into two classes of either chemically or physically cross-linked hydrogels (Ahmed 2015, Singh *et al.* 2010, Ullah *et al.* 2015). Chemically cross-linked hydrogels show covalent junctions in their polymer network, whereas the polymer network of physically cross-linked hydrogels are based on physical interactions such as chain entanglements, hydrogen bonds or ionic interactions (Figure 2) (Ahmed 2015, Garg *et al.* 2016, Hennink *et al.* 2002). In contrast

to the more permanent nature of chemically cross-linked hydrogels, physical cross-links in hydrogels can be reversible. This reversibility can for instance be triggerd by changing the pH value or the temperature of the hydrogel swelling agent (Garg *et al.* 2016, Hoffman 2012, Rosiak *et al.* 1999).
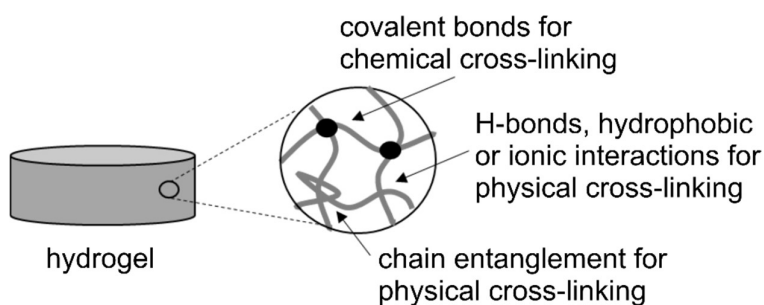

Figure 2: Hydrogel with chemical and physical cross-links. Figure changed according to Buenger *et al.* (2012).

There are numerous possibilities for the synthesis of hydrogels, whereby the two basic methods are: I) the polymerization of water-soluble monomers in the presence of multifunctional cross-linker and II) the cross-linking of hydrophilic polymers with multiple functional groups (Buwalda *et al.* 2017). The polyacrylamide ((p(Aam)) hydrogels in this work for instance, were prepared according to the first method by cross-linking acrylamide (Aam) with *N,N'*-methylenebisacrylamide (MBA) through light-initiated radical polymerization (Ayub *et al.* 2015). A schematic depiction of the cross-linking reaction between Aam and MBA is shown in Scheme 1.
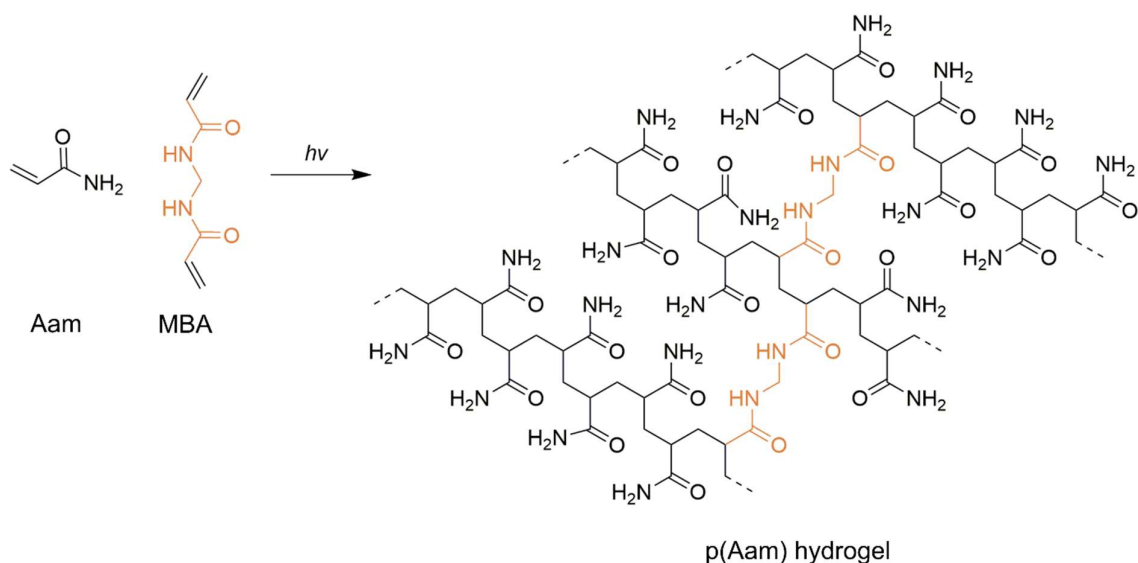
Scheme 1: Chemical cross-linking of acrylamide (Aam) and *N,N'*-methylenebisacrylamide (MBA) for the preparation of polyacrylamide ((p(Aam)) hydrogels. Figure changed according to Hermanson *et al.* (2013).

Due to the broad range of applications with specific requirements, tailor-made hydrogels with adjustable properties are in the focus of current research and the major target of this work (Buwalda *et al.* 2017, Singhal *et al.* 2016, Wu *et al.* 2018).

3.2. Hydrogel modification reactions of the polymer network

A frequently used strategy to introduce specific properties to hydrogels is the modification of hydrogels (Tallawi *et al.* 2015). This can be achieved mainly in two ways: either by tailoring the polymer network or by modifying the swelling agent of the hydrogel. In the literature the term "hydrogel modification" and "hydrogel functionalization" are not precisely defined and sometimes even used as synonyms (Kawaguchi *et al.* 1996, Yilmaz *et al.* 2011). In this work "hydrogel modification" is an umbrella term, which includes all kinds of alterations of the respective hydrogel, whereas hydrogel functionalization is a subtopic of hydrogel modifications and comprises the implementation of new functional groups, like hydroxyl (Grevesse *et al.* 2014), furan (Fan *et al.* 2015) or amine groups (Schauenburg *et al.* 2018). Furthermore the term "hydrogel functionalization" is also used for the introduction of novel functionalities into the hydrogel, such as biofunctionality (Tallawi *et al.* 2015, Tsutsumi *et al.* 2018).

As the aim of this work is to synthesize and characterize novel hydrogel modification reagents, this section is focused on the overview of hydrogel modification reactions of

the polymer networks. The introduction of hydrogel modification reactions of the swelling agents is given afterwards in section 3.5.

In the last decades the demand for hydrogels with improved properties led to an increasing number of hydrogel modifications (Buwalda *et al.* 2017, Tallawi *et al.* 2015). Common ways to alter the hydrogel bulk properties are to modify the monomer of the polymer network itself (Zhu *et al.* 2006), to copolymerize it with functional building blocks (Drumheller *et al.* 1994, Southan *et al.* 2018) or physical blending for the preparation of interpenetrating hydrogel networks (Swain *et al.* 2018). Zhu *et al*. (2006) for example tailored their hydrogel by synthesizing peptide-containing poly(ethylene diacrylate) (PEGDA) macromonomers, which enabled them to increase the bioactivity of PEGDA hydrogels. Drumheller and Hubbell (1994) in contrary copolymerized trimethylolpropane triacrylate with acrylic acid to introduce carboxyl groups to poly(ethylene glycol) (PEG) hydrogels, which were used for *N*-terminal grafting of arginine-glycine-aspartic acid (RGD) sequences to enhance cell adhesion.

Basically, most of these bulk modification methods can be broken down to either direct incorporation of hydrogel functionalization reagents, which is the substance causing the change of the hydrogel properties, or the development of a hydrogel functionalization platform for post-synthetic modification reactions. Both strategies are schematically depicted in Figure 3.
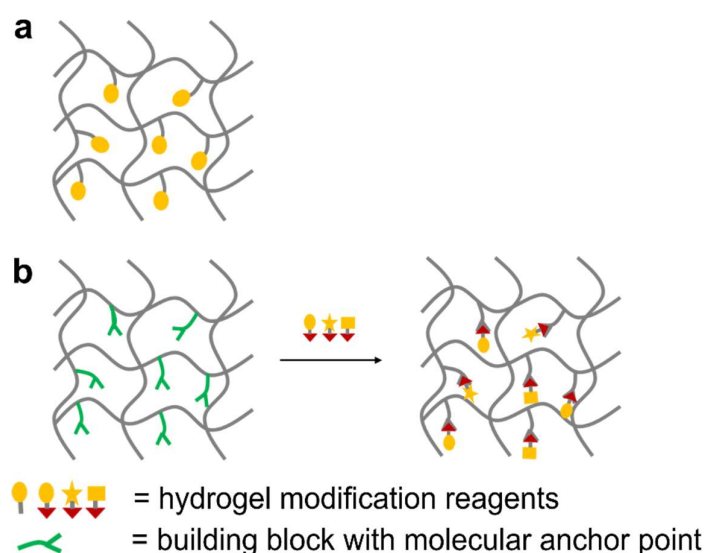

Figure 3: Hydrogel bulk modifications *via* a) directly incorporated hydrogel modification reagent and b) hydrogel functionalization platforms with building blocks, which bear molecular anchor points. These molecular anchor points can be used for post-synthetic reactions with versatile hydrogel modification reagents.

The advantage of the direct immobilization of the hydrogel functionalization reagent is that no further modification step is necessary, whereas the major drawback lies in the restricted versatility (Zhu 2010). Hydrogel functionalization platforms in contrary need a post-synthetic modification step, but are applicable to a broad variety of molecules with the respective reactive unit (Drumheller *et al.* 1994, Yigit *et al.* 2011, Zhu 2010). The functional groups in the hydrogel functionalization platform, which are used for post-synthetic modification reactions, are called (molecular) anchor points (DeForest *et al.* 2012).

Favorable anchor points are amines (Schauenburg *et al.* 2018), carboxyls (Drumheller *et al.* 1994), alkynes (Altin *et al.* 2010, Chen *et al.* 2012, Malkoch *et al.* 2006, Yilmaz *et al.* 2011), alkenes (DeForest *et al.* 2012, Gould *et al.* 2012) and furans (Baker *et al.* 2017) since they can undergo mild and efficient reactions, such as amidations or click reactions (Kolb *et al.* 2001). Backer *et al.* (2017) for example established a bifunctional hyaluronan hydrogel with independently adjustable mechanical and chemical properties by using aldehydes to control the mechanical characteristics and pendent furan groups as molecular anchor points for post-synthetic Diels-Alder reactions. This enabled them to create a well-defined matrix for the cultivation of breast cancer spheroids. An overview over this and other hydrogel functionalization platforms is given in Table 1.

Table 1: Overview over hydrogel functionalization platforms with molecular anchor points in the hydrogel, functional moieties of the modification reagent, functionalization reaction between anchor point and modification reagent as well as the field of application.

anchor point	functional moiety of modification reagent	functionalization reaction	application	reference
amine	carboxyl	amidation	functionalization platform	(Schauenburg *et al.* 2018)
carboxyl	amine	amidation	tissue engineering	(Drumheller *et al.* 1994)
carboxyl	amine	amidation	biosensors	(Kowalczyk *et al.* 2014)
alkyne	azide	CuAAc	functionalization platform	(Altin *et al.* 2010)
alkyne	azide	CuAAc	functionalization platfrom	(Yilmaz *et al.* 2011)
alkyne	azide	CuAAc	tissue engineering	(Chen *et al.* 2012)

alkene	thiol	thiol-ene	functionalization platform	(Polizzotti *et al.* 2008)
alkene	thiol	thiol-ene	functionalization platform	(DeForest *et al.* 2012)
alkene	thiol	thiol-ene	tissue engineering	(Gould *et al.* 2012)
furan	maleimide	Diels-Alder	cancer research	(Baker *et al.* 2017)
maleimide	furan	Diels-Alder	drug delivery	(Koehler *et al.* 2013)
epoxide	amine	nucleophilic ring opening reaction	tissue engineering	(Rimmer *et al.* 2007)

So far, most hydrogel functionalization platforms described in the literature only exhibit one anchor point per building block (Grevesse *et al.* 2013, Grevesse *et al.* 2014, Schauenburg *et al.* 2018, Yilmaz *et al.* 2011), so the only way to increase the amount of anchor points is to increase the building block proportion in the entire hydrogel. This makes it challenging to create high local substrate concentrations within the hydrogel, which is crucial for directed cell migration (DeLong *et al.* 2005) or specific catalyst development (Gao *et al.* 2014). Therefore, the investigation of hydrogel functionalization platforms with multiple anchor points per building block, as shown in this work, is highly relevant.

3.3. Poly(ethylene glycol)-based macromonomers – synthesis and post-synthetic click reactions

In order to explore hydrogel functionalization platforms with multiple anchor points, suitable building blocks are needed. For this, macromonomers are advantageous, because they can be polymerized like a monomer due to their polymerizable unit (McNaught *et al.* 1997). Especially, when the repeating unit of the macromonomer exhibits a functional group which can be used as anchor point, this automatically leads to a building block with multiple anchor points. Furthermore, for the homogeneous incorporation of such macromonomers in hydrogels, these macromonomers need to be water soluble so that they can get dissolved in the aqueous hydrogel precursor solution. In Figure 4, the conceptual design of suitable macromonomers for the development of hydrogel functionalization platforms with multiple anchor points is shown.

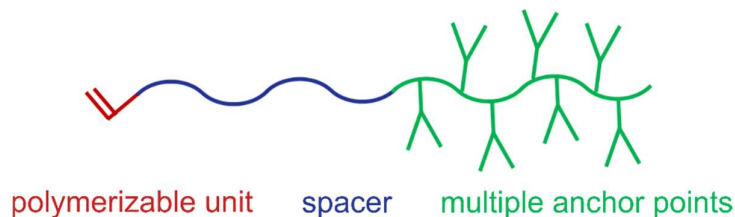polymerizable unit   spacer   multiple anchor points

Figure 4: Conceptual design of macromonomers for the development of a hydrogel functionalization platforms with multiple anchor points. The macromonomer comprises a polymerizable unit for the incorporation into the hydrogel, a spacer for sufficient flexibility and water solubility as well as multiple anchor points, which can be used for post-synthetic modification reactions.

Poly(ethylene glycol)-based polymers are attractive for the development of water-soluble macromonomers (Iijima *et al.* 1999, Masson *et al.* 1982, Pich *et al.* 2009, Spencer *et al.* 2018), as poly(ethylene glycol) (PEG) is well-known for its good water solubility (Bailey Jr. *et al.* 1959, Harris *et al.* 1982) and its low toxicity (Fruijtier-Pölloth 2005, Webster *et al.* 2009). The terms "poly(ethylene glycol)", "poly(ethylene oxide)" (PEO) and "poly(oxirane)" are hereby often used synonymously since they are all composed of the same ethylene oxide (EO) repeating unit. Strictly speaking, PEG refers to polymers with a molecular weight below 20 000 g mol^{-1} and PEO describes polymers with higher molecular weights (Southan 2013, Wenande *et al.* 2016), but the borders are blurred in the literature. Either way, PEGs and their derivatives are used in numerous applications such as cosmetics (Fiume *et al.* 2012, Jang *et al.* 2015), lubricants (Kobayashi *et al.* 2014, Kumari *et al.* 2016) and drug delivery (Chen *et al.* 2018, D'souza *et al.* 2016). They are mainly synthesized by anionic ring opening polymerization (AROP) of ethylene oxide (EO) or its derivatives, since this leads to a remarkably narrow molecular weight distribution (MWD) of PEG-based polymers with molar mass dispersities (*Đ*) below 1.1 and (almost) quantitative monomer conversion (Flory 1940, Price *et al.* 1966, Southan 2013).

Scheme 2 shows the mechanism of AROP of EO, which works analogous with other EO derivatives (Flory 1940). In the initiation step, an anionic initiator like potassium *tert*-butoxide (Price *et al.* 1966), sodium naphthalenide (Richards *et al.* 1959), or diphenylmethyl potassium (DPMK) (Masson *et al.* 1982) reacts with EO to open the epoxide ring and form an anionic alkoxide species. Hereby the relief of the strain energy of the epoxide ring is the driving force of this AROP (Brocas *et al.* 2013). The alkoxide then propagates the reaction with further EO, which results in a growing PEG-chain. To terminate the polymerization, a Brönsted acid like water is added. This polymerization exhibits a living character because under ideal conditions the growing

polymer chain does not terminate itself without a termination reagent (Flory 1940, Gee *et al.* 1959, Herzberger *et al.* 2015).

According to the mechanism a variety of functional end groups such as amines (Huang *et al.* 1996, Mahou *et al.* 2012, Schlaad *et al.* 2001), azides (Edward Semple *et al.* 2016a), thiols (Mahou *et al.* 2012), formyls (Nagasaki *et al.* 1995) and caprolactones (Rieger *et al.* 2004) can be implemented by functional initiators or respective end-capping reagents. This strategy can also be applied for the synthesis of macromonomers using unsaturated initiators (Barman *et al.* 2009, Masson *et al.* 1982, Vojkovsky *et al.* 2016) or appropriate terminations agents (Höring *et al.* 1989) to functionalize PEG-based polymers with a polymerizable moiety like vinyls and their derivatives. Masson *et al.* (1982) for example used potassium *p*-isopropenylbenzyl as initiator to synthesize PEG-macromonomers, whereas Höring and Ulbricht (1989) reported a termination with allyl bromide to obtain allyl-terminated PEGs.
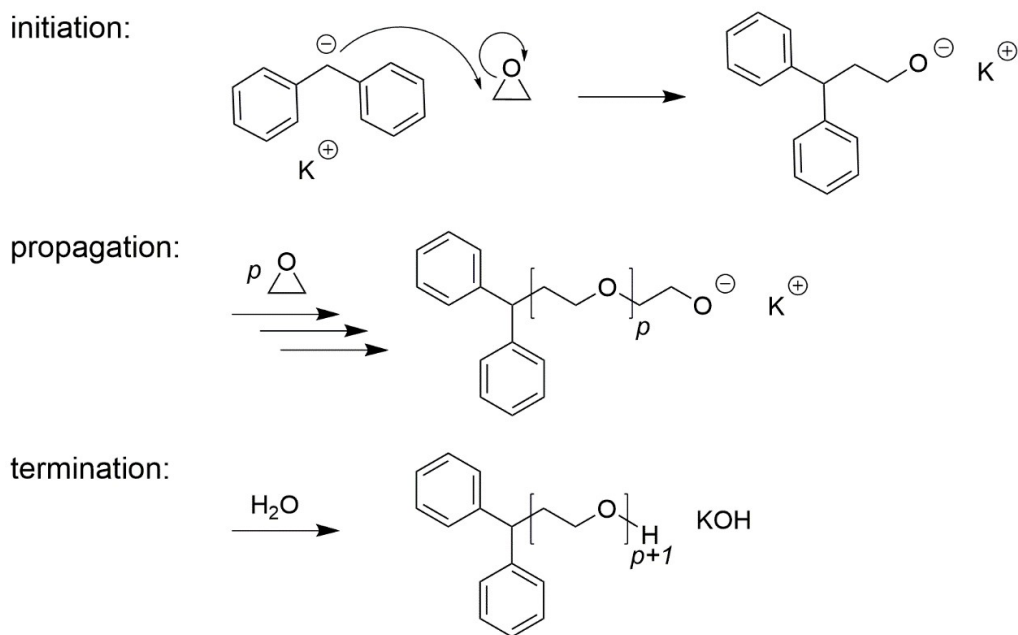

Scheme 2: Schematic representation of the anionic ring opening polymerization (AROP) of ethylene oxide (EO).

Instead of ending the living PEG-chain with a termination agent, other monomer(s) can be added to form copolymers with advanced properties (Barthel *et al.* 2013a, Gleede *et al.* 2018, Konishcheva *et al.* 2018, Yamamoto *et al.* 1999). Hereby a sequential copolymerization with EO leads to block copolymers and a concurrent addition results

in random copolymers (Obermeier *et al.* 2011b). Furthermore, the copolymerization can be diversified by using heterocycles (Gleede *et al.* 2018, Yamamoto *et al.* 1999) or functional epoxides (Klein *et al.* 2015, Mangold *et al.* 2012) as monomers. Linear PEG-based copolymers with various functional groups are summarized under the term "multifunctional PEGs" (Obermeier *et al.* 2011b). An overview of frequently used epoxides for the synthesis of multifunctional PEGs is given in Scheme 3. Multifunctional PEGs are an inspiring polymer class for the design of macromonomers with multiple anchor points.

The copolymerization of EO with furfuryl glycidyl ether (FGE) (Barthel *et al.* 2012, Barthel *et al.* 2013b, Hörenz *et al.* 2015, Wagner *et al.* 2014) and allyl glycidyl ether (AGE) (Hrubý *et al.* 2005, Koyama *et al.* 1996, Obermeier *et al.* 2011a) leads to inherent furan or allyl functional groups, which can directly be used for post-synthetic modification reactions. Ethoxy ethyl glycidyl ether (EEGE) (Dworak *et al.* 1999, Mangold *et al.* 2010b, Taton *et al.* 1994), isopropylidene glyceryl glycidyl ether (IGG) (Mangold *et al.* 2010a, Wurm *et al.* 2008), *N,N*-diallyl glycidyl amine (DAGA) (Reuss *et al.* 2012) and *N,N*-dibenzyl glycidyl amine (DBAG) (Mangold *et al.* 2011, Obermeier *et al.* 2010), in contrary, need a prior deprotection step before they can be converted into multihydroxy- or multiamino PEG copolymers, which are frequently utilized for bioconjugations (Obermeier *et al.* 2011b).

FGE   **AGE**   **EEGE**

IGG   **DAGA**   **DBAG**
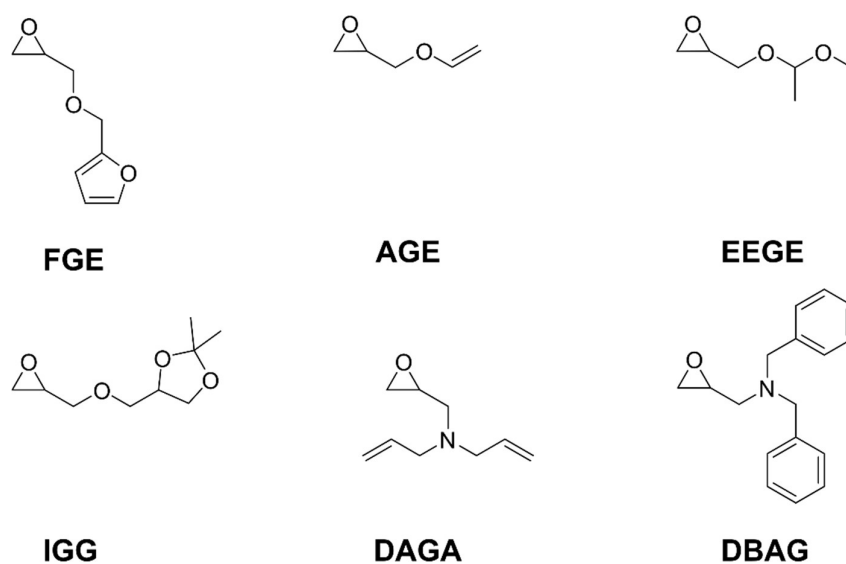
Scheme 3: Functional epoxides for the preparation of multifunctional PEGs: furfuryl glycidyl ether (FGE) (Barthel *et al.* 2012, Barthel *et al.* 2013b, Hörenz *et al.* 2015, Wagner *et al.* 2014), allyl gylcidyl ether (AGE) (Hrubý *et al.* 2005, Koyama *et al.* 1996, Obermeier *et al.* 2011a), ethoxy ethyl glycidyl ether (EEGE) (Dworak *et al.* 1999, Mangold *et al.* 2010b, Taton *et al.* 1994), isopropylidene glyceryl glycidyl

ether (IGG) (Mangold *et al*. 2010a, Wurm *et al*. 2008), *N,N*-diallyl glycidyl amine (DAGA) (Reuss *et al*. 2012), *N,N*-dibenzyl glycidyl amine (DBAG) (Mangold *et al*. 2011, Obermeier *et al*. 2010).

However, post-polymerization modification reactions based on standard organic reaction may result in low conversions and side reactions if applied on a macromolecular level (Obermeier *et al.* 2011b). Therefore, "click reactions" which are reactions exhibiting high yields, good selectivity, versatility and simplicity are a powerful tool (Kolb *et al.* 2001). The most commonly used click reactions in polymer and material science are the azide-alkyne cycloaddition (Adzima *et al.* 2011, Binder *et al.* 2007, Huisgen 1963, Liang *et al.* 2011, Rostovtsev *et al.* 2002), the thiol-ene reactions (Hoyle *et al.* 2010a, Hoyle *et al.* 2010b, Lowe 2010) and the Diels-Alder cycloadditions (Diels *et al.* 1926, Gandini 2013, Tasdelen 2011).

For the discovery of the latter, Otto Diels and Kurt Alder were jointly awarded with the noble prize in 1950 (Alder 1950). The concerted mechanism of the Diels-Alder cycloaddition relies on a 1,3-sigmatropic rearrangement between an electron-rich diene and an electron-deficient dienophile leading to the formation of two new carbon-carbon bonds within a six-membered ring. The mechanism is illustrated in Scheme 4 using the example of furan as diene and maleimide as dieneophile.
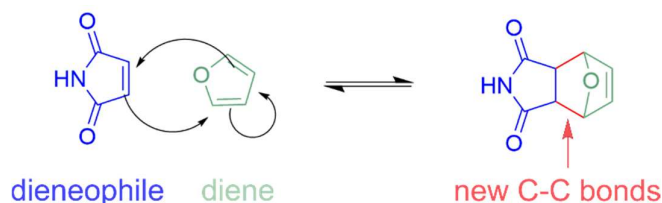

Scheme 4: Schematic mechanism of the Diels-Alder cycloaddition.

Similar Diels-Alder reactions were applied for post-synthetic modification reactions of multifunctional PEGs by Barthel *et al*. (Barthel *et al*. 2012, Barthel *et al*. 2013b). For this, they synthesized well-defined poly(ethylene glycol)-*block*-poly(furfuryl glycidyl ether) (PEG-*b*-PFGE) block copolymers with low molar mass dispersities *Đ* between 1.04 and 1.06 and used Diels-Alder click chemistry to cross-link the furan side chains of PEG-*b*-PFGE with bifunctional maleimides to prepare self-healing materials (Barthel *et al.* 2013b).

We believe that PEG-*b*-PFGE block copolymers are an excellent core structure for the synthesis of multifunctional PEG-based macromonomers in this work, because the PEG-block can provide water-solubility and flexibility (Barthel *et al*. 2012, Bolourchian

et al. 2013, Sill *et al.* 2017) and the multiple furan side chains can serve as multiple anchor points for post-synthetic Diels-Alder click reactions. Moreover, Diels-Alder reactions of furan moieties are orthogonal to radical cross-linking reactions (Laita *et al.* 1997, Pramanik *et al.* 2017). However, as described in Figure 4, a suitable macromonomer has to have a polymerizable unit for covalent incorporation. In this case the polymerizable group needs to be attached at the hydrophilic PEG-block as PEG-*b*-PFGE block copolymers form micelles in aqueous solution (Barthel *et al.* 2012), which could bury the end group from the hydrophobic block inside the micelle core. Such buried end groups are less accessible and therefore only limited applicable for the incorporation of a macromonomer into a hydrogel. Consequently the reported synthesis of Barthel *et al.* in Scheme 5 is not conducive to implement the polymerizable unit at the hydrophilic chain end.
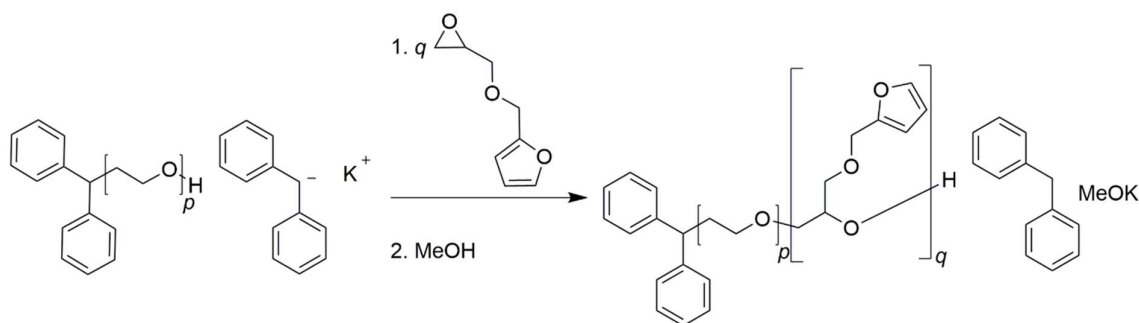
Scheme 5: Synthesis of PEO-*b*-PFGE block copolymers by Barthel *et al.* (2012).

Hence, one target of this work is to develop a sophisticated synthetic route for the synthesis of PEG-*b*-PFGE-based macromonomers with a polymerizable unit at the hydrophilic chain end.

3.4. Langmuir film balance experiments for the investigation of interfacial properties of block copolymers

As described in the last section, PEG-*b*-PFGE macromonomers are interesting for the modification of hydrogels. Based on the hydrophilic PEG-block and the hydrophobic poly(furfuryl gylcidyl ether) (PFGE)-block, PEG-*b*-PFGE block copolymers can be assigned to the class of amphiphilic block copolymers (ABC). (Barthel *et al.* 2012).

ABCs tend to form micelles in selective solvents and to self-assemble at surfaces (Otsuka *et al.* 2001), which makes them attractive for numerous applications in drug delivery (Adams *et al.* 2003b, Rösler *et al.* 2012, Yang *et al.* 2018), as emulsifiers

(Chausson *et al.* 2008, Riess *et al.* 2004) or as surface functionalization reagents (Otsuka *et al.* 2001, Tan *et al.* 1993). Many PEG-based ABCs like poly(ethylene glycol)-*b*-polylactide (Iijima *et al.* 1999), poly(ethylene glycol)-*b*-poly(-benzyl-L-aspartate) (Kataoka *et al.* 2000) and poly(ethylene glycol)-*b*-poly(caprolactone) (Allen *et al.* 2000) form core-shell micelles by segregating the insoluble hydrophobic blocks into the core and exposing the hydrophilic block (shell) to the surrounding water. Similarly, ABCs can align at aqueous interfaces in a way that the hydrophilic block is anchored in the aqueous subphase and the hydrophobic block is orientated towards the hydrophobic air (Otsuka *et al.* 2001). Both concepts are based on the minimization of the free energy (Letchford *et al.* 2007).

In order to choose appropriate ABCs for an application, it is important to gain knowledge about its characteristic values like the critical micelle concentration (cmc) and to understand its structure-property relations. The cmc is the concentration upon which the surface is saturated with amphiphilic molecules and micelles are formed in the subphase (McNaught *et al.* 1997). There are multiple ways to determine the cmc like the Nouy ring technique (Bodour *et al.* 1998, Sahebnazar *et al.* 2018), the Wilhelmy plate method (Qian *et al.* 2018) or bubble pressure tensiometry (Schramm *et al.* 1992). For these three methods the surface tension is measured in dependence of the concentration as the surface tension drops with increasing occupancy of the amphiphile at the surface and (ideally) leads into a surface tension plateau when the surface is saturated (Scholz *et al.* 2018). The cmc can be determined at the intersection of these two extrapolated lines (Figure 5).
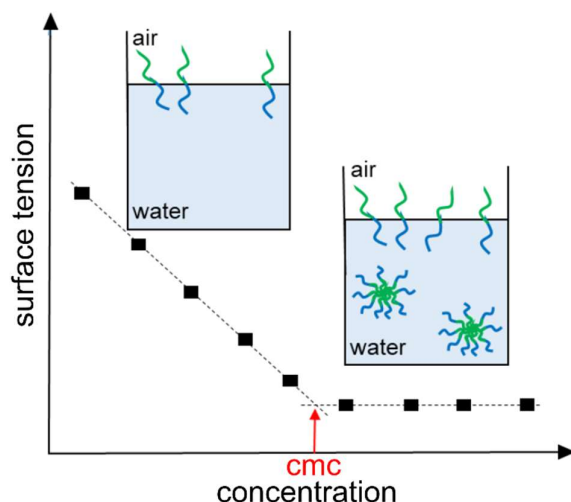
Figure 5: Schematic representation of amphiphilic block copolymers (ABCs) at the air-water interface below and above the critical micelle concentration (cmc). The cmc is determined at the intersection of concentration dependent and concentration independent region of the surface tension. The ABC consists of a hydrophilic (blue) and a hydrophobic (green) block. Figure changed according to McNaught and Wilkinson (1997).

Below the cmc, a molecular film can be formed at the air-water interface, which is interesting for studies in the field of molecular electronics (Hussain *et al.* 2009), cell biology (Yang *et al.* 2002) and nanotechnology (Ji *et al.* 2005). To study such nanoscopic films, multiple methods are reported in the literature such as conductance measurements (Sakurai *et al.* 1987, Teissié *et al.* 1985), brewster angle microscopy (Jaroque *et al.* 2019, Rodríguez Patino *et al.* 1999), X-ray diffraction (Kaganer *et al.* 1999, Kaleta *et al.* 2018), second harmonic generation (Heinz *et al.* 1983) and sum frequency generation vibrational spectroscopy (Roy *et al.* 2018, Saha *et al.* 2018).

The probably most frequently used method for the preparation and investigation of amphiphilic monolayers at the air-water interface is the Langmuir film balance technique (Langmuir 1917). It has been named after its inventor Irving Langmuir, who received the Nobel prize in 1932 for his pioneering work in surface chemistry (Langmuir 1932). Since then, Langmuir film balance experiments were applied to a broad range of surface active substances such as small molecules (Fazio *et al.* 1998, Komitov *et al.* 1994, Modlińska *et al.* 2011), polymers (Faure *et al.* 1998, Miñones *et al.* 2009), metal complexes (Liu *et al.* 1997, Yoo *et al.* 1999) and supramolecular assemblies (Culp *et al.* 2002, Ni *et al.* 2004). The Langmuir technique may provide first hand information about the formation of a monolayer, the molecular area of the amphiphile within a monolayer, phase behavior of the monolayer, its compressibility and the monolayer stability (Dynarowicz-Łątka *et al.* 2001). As a side note, in the literature the

term "Langmuir monolayer" or "Langmuir film" is utilized, even if it is not necessarily a true monomolecular film but a thin film (Dynarowicz-Łątka *et al.* 2001). Furthermore, a Langmuir monolayer which is transferred from the liquid-gas interface to a solid substrate is called Langmuir-Blodgett film (Blodgett 1935, Roberts 1985).

To prepare a Langmuir monolayer a Langmuir trough is needed, which consists of a hydrophobic trough for the water subphase, two mobile barriers that span over the water surface and a sensitive film balance (Langmuir 1917, Pockels 1891) (Figure 6).
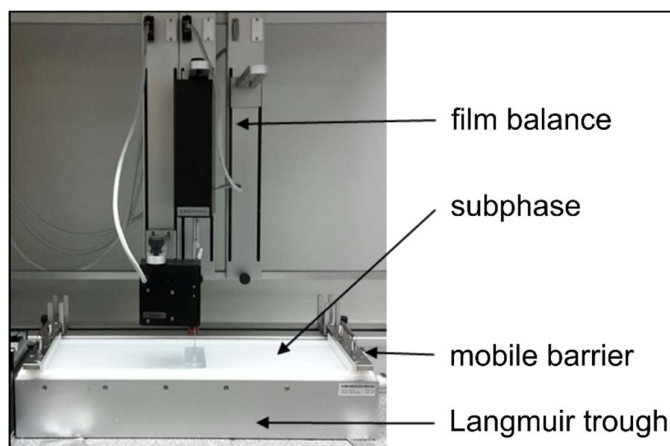

Figure 6: Representation of a Langmuir trough for the preparation of Langmuir monolayers (Langmuir 1917).

Small amounts of an amphiphile solution are deposited drop-wise on the water subphase and after the solvent is evaporated, the amphiphile spreads spontaneously as a monolayer at the air-water interface (Langmuir 1917). Since surface active molecules reduce the surface tension of water, the accumulation of amphiphiles at the air-water interface can be monitored by measuring the surface pressure (π). π is the difference between the surface tension of water (γ_0) and the surface tension of water with surfactant (γ) (McNaught *et al.* 1997). If π is measured as a function of the area per molecule (A), a surface pressure – area (π-A) isotherm can be obtained, which is characteristic for every amphiphile and provides information about the phases of the monolayer. As shown in Figure 7, the general π-A isotherm shows three characteristic phases, the "gas-like", the "liquid-like" and the "solid-like" phase (Bernardini *et al.* 2013, Roberts 1985).
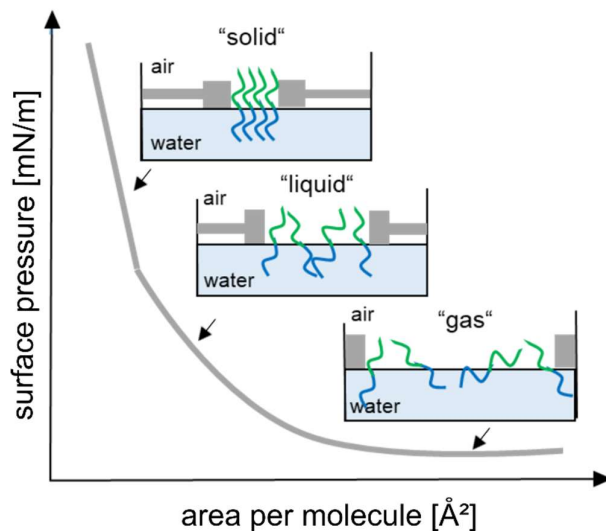
Figure 7: Idealized surface pressure – area (π-A) isotherm of a Langmuir monolayer with three distinct phases: gas, liquid and solid phase. The level of ordering within the monolayer phases is shown schematically, whereby the hydrophobic block of the amphiphile is colored in green and the hydrophilic block in blue. Figure changed according to Bernardini *et al.* (2013).

The surface-active molecules are in a "gas-like" or "expanded" phase, if they have a lot of space at the air-water interface where they rarely interact with each other. In this state almost no work is required to compress the monolayer and the free energy of the aqueous subphase remains unchanged, which leads to a nearly constant surface pressure (Dynarowicz-Łątka *et al.* 2001). By compressing the mobile barriers of the Langmuir trough, the area available for each amphiphile is reduced leading to a partial ordering of the amphiphiles in the monolayer, whereby the molecules start interacting with each other. In this "liquid-like" or "liquid expanded" state the surface tension is affected by the increased density of the surfactants at the air-water interface, which results in a surface pressure rise starting at the onset. Upon further compression a "solid-like" or "liquid condensed" region is formed, in which the surfactants are highly ordered. Herein the monolayer is relatively uncompressible so that small area changes result in a high surface pressure increase (Dynarowicz-Łątka *et al.* 2001). Thus, the isotherm slope in solid-like phase is very steep. If the monolayer is compressed beyond the collapse pressure, multilayer formation can occur (Lee 2008).

There is vast literature on the usage of π-A isotherm measurements for the exploration of amphiphilic monolayers (Brugger *et al.* 2010, Dynarowicz-Łątka *et al.* 2001, Nutting *et al.* 1939, Shimizu *et al.* 2015), like from the Frank group (Kampf *et al.* 1999). They investigated the monolayer stability and molecular conformation of PEG-based poly(benzyl ether) monodendrons, which are hyperbranched macromolecule with a

functional group at its focal point. They found out that longer hydrophilic tails improved the film stability and that each additional EO repeating unit increased the collapse pressure by 3 mN m^{-1} to 4 mN m^{-1}. Furthermore, they showed that the molecular area of their amphiphile at the air-water interface grew linearly with the molecular weight (Kampf *et al.* 1999).

As novel PEG-*b*-PFGE macromonomers will be synthesized in this work, which should be amphiphilic based on the hydrophilic PEG-block and the hydrophobic PFGE-block, it is valuable to investigate whether they are able to form Langmuir monolayers. These films could be used to explore the surface characteristics and structure-property relations of PEG-*b*-PFGE macromonomers at the air-water interface. The gained knowledge could enhance hydrogel surface functionalization experiments since the air-water interface is a simplification of the air-hydrogel precursor interface.

3.5. Hydrogel modification reactions triggered by swelling agents – solvent responsive hydrogels

For the functionalization of hydrogels, the focus until now was on the modification of the hydrogel network and its respective modification reagents. Beyond this, it is also possible to modify hydrogels by altering their swelling agent to introduce new tailor made properties (Ullah *et al.* 2015). Such hydrogels are summarized under the term solvent responsive hydrogels.

Depending on the pH, the solvent composition and the ionic strength of the hydrogel swelling agent, the swelling properties, the rheological behavior and the microstructure of solvent responsive hydrogels can be specifically tuned (Bossard *et al.* 2006, Shahi *et al.* 2017, Ullah *et al.* 2015, Wang *et al.* 2011). This hydrogel modification strategy based on the swelling agent is in particular interesting for applications in drug delivery (Gupta *et al.* 2002, Park *et al.* 2004, Sadeghi *et al.* 2008), sensor technology (Richter *et al.* 2008, Yew *et al.* 2007) and hygiene industry (Shahi *et al.* 2017). Recently, Qin *et al.* (2018) published a solvent responsive hydrogel with reversible self folding behaviour, which can switch between a 2D-sheet and 3D-tube formation depending on the solvent composition and exposure (Qin *et al.* 2018). Furthermore, Ozbas *et al.* (2004) tuned the visoelastic properties of peptide hydrogels by modulating the ionic strength of the swelling medium.

Shifting the pH of the swelling agent is also a simple and efficient aproach to modify hydrogels. Such pH sensitive hydrogels have gained a lot of attention over the years and are mostly of anionic or cationic nature (Dolatabadi-Farahani *et al.* 2006, Park *et al.* 2004, Sadeghi *et al.* 2008). They exhibit pendent ionic groups like carboxyls (Jianqi *et al.* 2002) or amines (Nebhani *et al.* 2016), which donate or accept protons according to the pH (Ullah *et al.* 2015). If the net charge of the hydrogel increases above the logarithmic acid dissociation constant (pK_a) or respectivly below the locarighmic base dissociation constant (pK_b), the elctrostatic repulsive forces grow and lead to higher osmotic swelling forces. This causes a volume change of the pH sensitive hydrogels (Ullah *et al.* 2015). Park *et al.* (2004) for example prepared pH switchable poly(vinyl alcohol-*graft* acrylic acid) hydrogels for controlled drug release, which enabled them to release insulin from the hydrogel in a simulated gastric fluid of pH 1.2 and to withold it in a simulated interstinal fluid at pH 6.8.

In 2015 Feng *et al.* introduced a hydrogel functionalization strategy, which converted pH responsive hydrogels into light responsive hydrogels by using photoacid generators (PAG) (Feng *et al.* 2015). They described a poly(acrylamide-*co*-N-vinylimidazole) shape memory hydrogel, which can bend when treated with a mixture of metal ions, because of complexation reactions between the imidazole groups of the hydrogel and the added metal ions. So from a 2D perspective, the hydrogel bends from a linear form (Figure 8a) to a "u-shaped" form (Figure 8b) due to complexations. After ultraviolot (UV) irradiation the hydrogel returns into its original linear shape (Figure 8c), based on the UV-induced photolysis of the diphenyliodonium nitrate PAG in the hydrogel swelling media. The photoreaction shifts the pH below the pK_a of the imidazole groups (pK_a ~ 5.8) and results in a rescission of the complexation effect (Feng *et al.* 2015). This PAG-triggered shape recovery mechanism of the hydrogel is schematically shown in Figure 8.
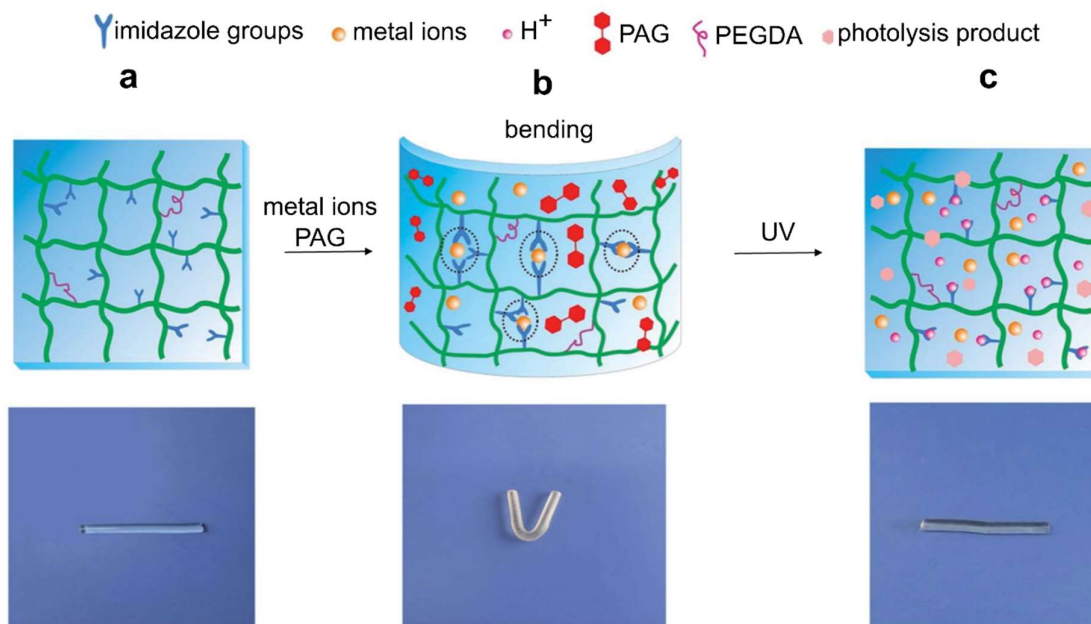
Figure 8: Schematic representation of photoacid generator (PAG) -triggered UV responsive shape memory hydrogel (Feng *et al.* 2015). The shape of this solvent responsive hydrogel can be modified reversibly by the pH of the hydrogel swelling agent. Figure changed according to Feng *et al.* (2015).

The main advantage of the above described light-induced hydrogel modification approach lies in its external, spatio-temporal control. This appealing feature was also recognized by Satoh *et al.* (2015), Dunne *et al.* (2016) and Francis *et al.* (2017), who used PAGs to functionalize their hydrogel systems. Therefore, the investigation of suitable PAGs as hydrogel modification reagents is highly relevant for current hydrogel research (Dunne *et al.* 2016, Feng *et al.* 2015, Francis *et al.* 2017, Satoh *et al.* 2015).

3.6. Photoacid generators – applications, classification and photolysis mechanism

A good overview of PAGs, which are compounds that generate acids upon irradiation with light, is given by Shirai and Tsunooka (1996) as well as recently by Martin *et al.* (2018). PAGs are applied in a wide range of areas like in photodynamic therapy (Fadhel *et al.* 2016, Yue *et al.* 2013), protecting group chemistry (Klán *et al.* 2013a, Shirai *et al.* 1996), microelectronics (Mizoguchi *et al.* 1996, Sugita *et al.* 2018), adhesives (Bomze *et al.* 2015), inks (Schlögl *et al.* 2012), polymerization initiations (Crivello *et al.* 1979, Klikovits *et al.* 2017) and polymer functionalization (Feng *et al.* 2015, Francis *et al.* 2017). Schlögl *et al.* (2012) for instance published a sophisticated implementation of PAGs in the field of 3D printed polymer foams. They matched the acid release during the PAG photolysis with the curing process of 3D printed

polyacrylamide films. As the photo released acid could directly react with carbonate particles from the polymer precursor solution, this led to the *in situ* formation of the blowing agent CO_2. By balancing the curing process and the foaming speed through the irradiation parameters and the PAG concentration, they generated 3D printed polymeric foams.

According to the application, either strong electrolyte or weak electrolyte PAGs are used, which are the two categories in which PAGs can be classified. As shown in Scheme 6, strong electrolyte PAGs often consist of an diarylhalonium (Crivello *et al.* 1977, Pappas *et al.* 1984), aryldiazonium (Smets *et al.* 1980), triarylsulfonium (Crivello *et al.* 1981, Saeva *et al.* 1985) or triarylphosphonium (Komoto *et al.* 1994, Neckers *et al.* 1984) cation and an halogen complex anion.
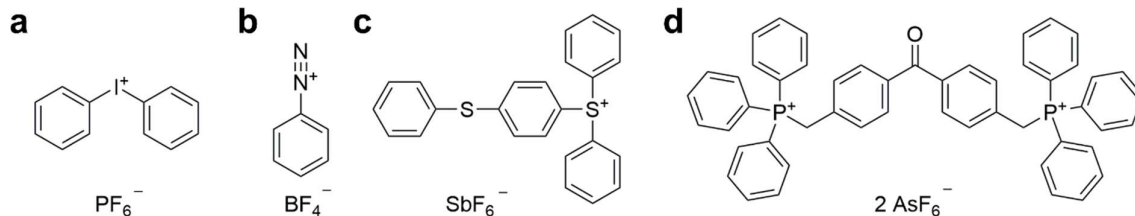
Scheme 6: Molecular structure of frequently used strong electrolyte photoacid generators (PAGs) based on a) diarylhalonium, b) aryldiazonium, c) triarylsulfonium and d) triarylphosphonium moeities.

Strong electrolyte PAGs mainly photodissociate *via* radical pathways and abstract protons from their surrounding compounds like their solvent to release Brønsted or Lewis acids (Martin *et al.* 2018). Exemplarily, the photolysis mechanism of strong electrolyte diaryliodonium PAGs under UV irradiation is illustrated in Scheme 7. The excited iodonium compound efficiently decomposes to an aryliodo radical-cation, an aryl radical and an anion (Crivello *et al.* 1977). This process occurs quickly as the bond energy of the C-I bond is very low (~ 27 kcal mol^{-1}) (Crivello *et al.* 1977). The next step involves a hydrogen abstraction form the solvent, which was confirmed by deuteration experiments using acetonitrile-d_3. In the end the protonated iodoaromatic species deprotonates to 4-iodophenyl and a free acid (Crivello *et al.* 1977).

RH = solvent, e.g. CH₃CN
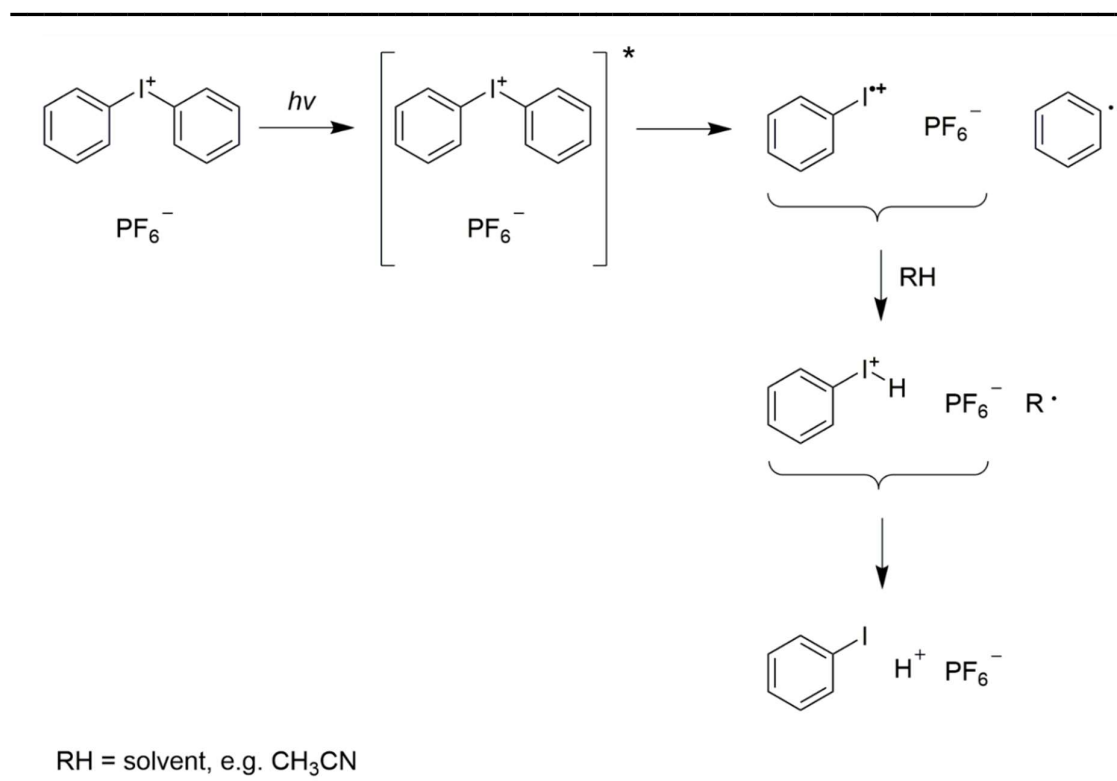
Scheme 7: Photolysis mechanism of diarylliodonium hexafluorophosphate under UV irradiation (Crivello *et al.* 1977). For clarity only the major photolysis pathway is demonstrated.

Many strong electrolyte PAGs show good thermal stability and are commercially available, but show pronounced toxicity. Diaryliodonium hexafluoroantimonate for instance is highly toxic with an oral lethal dose (LD_{50}) of 40 mg kg^{-1} for rats (Shirai *et al.* 1996). Furthermore strong electrolyte PAGs are often only applicable in a small wavelength window, which limits their application (Martin *et al.* 2018). One way to overcome this, is by using photosensitizers like anthracene (Schlögl *et al.* 2012) or setoflavin T (Crivello *et al.* 1978), which nevertheless are toxic.

Weak electrolyte PAGs in contrary can be used in a wide wavelength range depending on their molecular structure (Martin *et al.* 2018). Furthermore, they are often soluble in a variety of solvents and polymer matrices, which makes them attractive for various applications (Martin *et al.* 2018). A comprehensive overview of prominent weak electrolyte PAGs like *o*-nitrobenzyls, *p*-hydroxyphenacyls (*p*HP) and coumarin-4-ylmethyls (c4m) from Scheme 8, is given by Klan *et al.* (2013b).
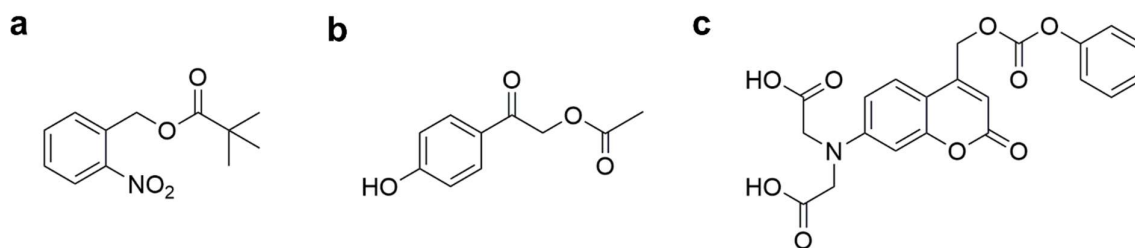
Scheme 8: Molecular structure of frequently used weak electrolyte photoacid generators (PAGs) based on a) *o*-nitrobenzyl (Reichmanis *et al.* 1985), b) *p*-hydroxyphenacyl (Zhang *et al.* 1999) and c) coumarin-4-ylmethyl (c4m) (Hagen *et al.* 2008) moieties.

The photochemistry of the *o*-nitrobenzyl group has been studied for more than 100 years (Ciamician *et al.* 1901). Since then, many mechanistic studies have been published (Gaplovsky *et al.* 2005, Il'ichev *et al.* 2004, Schmierer *et al.* 2010, Schwörer *et al.* 2001) and *o*-nitrobenzylic PAGs were widely used because of their high yielding and fast photoreaction (Shirai *et al.* 1996). However, there are major drawbacks of *o*-nitrobenzyl compounds based on the formation of toxic and water-insoluble side products such as *o*-nitroso aromatic ketones (Barth *et al.* 1997, Givens *et al.* 2012). Moreover, these side products absorb the irradiation wavelengths of the parent *o*-nitrobenzyl derivative more strongly, which automatically lowers the efficiency of the desired photoreaction (Givens *et al.* 2012).

A good alternative to *o*-nitrobenzyic PAGs are *p*-hydroxyphenacyl (*p*HP) and coumarin-4-ylmethyl (c4m) PAGs as they exhibit a very efficient photolysis reaction with inert and water soluble photoproducts (Du *et al.* 2001). Furthermore, they show good synthetic accessibility, are water soluble and can be used in physiological applications (Givens *et al.* 2012). Based on this, I focused my research on these two core structures. Therefore, *p*HP and c4m PAGs will be explained in more detail in the following two subsections.

3.6.1. *p*-Hydroxyphenacyl-based photoacid generators

In 1996 pioneering work on *p*HP PAGs was published by Givens and Park (1996), who reported the efficient photorelease of adenosine triphosphate (ATP) from ATP-caged *p*HPs. This was historically based on studies of Anderson and Reese (1962) as well as Sheehan and Umezawa (1973), who suggested phenacyl groups as photoremovable protecting groups. Since then *p*HPs have been applied in various fields such as enzyme catalysis (Geibel *et al.* 2000), protecting group chemistry (Givens *et al.* 2012), neurotransmitter release (Kandler *et al.* 1998) or signal tracking

of neuronal networks (Givens *et al.* 2012, Givens *et al.* 2000). The key benefit of *p*HPs lies in their ease of synthesis, their water solubility, their high yielding photocleavage and their biological compatibility (Givens *et al.* 2012). Furthermore, the UV absorption profile of the photo products differ significantly from the *p*HP reactants (Givens *et al.* 2012, Klán *et al.* 2013b).

Multiple *p*HP caged derivatives are accessible *via* nucleophilic substitution of commercially available *p*-hydroxyphenacyl bromide with the respective nucleophile (Kaila *et al.* 2007). In Scheme 9, this facile approach is demonstrated for 2-(4-hydroxyphenyl)-2-oxoethyl acetate (*p*HP-caged acidic acid), which in modified form works for amino acid-, peptide- or nucleotide-caged *p*HPs as well (Givens *et al.* 1996, Givens *et al.* 2000, Klán *et al.* 2013b).
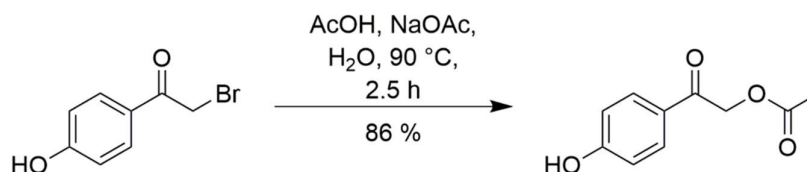
Scheme 9: Synthesis of 2-(4-hydroxyphenyl)-2-oxoethyl acetate (Kaila *et al.* 2007). In modified form this synthetic approach can also be used for the synthesis of other *p*-hydroxyphenacyl (*p*HP)-caged derivatives like amino acid-, peptide- or nucleotide-caged *p*HPs.

The caged molecule can then be release through UV irradiation between 250 nm – 350 nm (Givens *et al.* 2012). Mechanistically the photocleavage is based on the Favorskii-rearrangement, which was confirmed by laser flash photolysis studies (Givens *et al.* 2008) and quantum chemical calculations (Klíčová *et al.* 2012). As shown in Scheme 10, *p*HP derivatives (pHPX) are initially excited to their singlet state (S_1) and then undergo rapid intersystem crossing (ISC) to the triplet state (T_1) (Givens *et al.* 2008). This leads to a triplet phenoxide biradical (^{3}PB) by abstracting the leaving group (X). In the next step, a putative spirodione (SD) is formed (Givens *et al.* 2008), which despite extensive effort (Chen *et al.* 2006, Givens *et al.* 2008, Ma *et al.* 2005) could not be detected yet. It is said that the two main reasons which are causing the detection difficulties of the spirodione are that the formation rate is slower than its lifetime and that the spirodione is optically transparent in the range of 300 nm – 700 nm (Givens *et al.* 2008). Nevertheless the occurance of *p*-hydroxyphenylacetic acid (pHPA) and *p*-hydroxybenzyl alcohol (pHBA) are strong hints towards a SD intermediate, because pHPA can be formed through a ring opening reaction of the SD

with water and pHBA can be generated *via* decarbonylation of the SD and subsequent water addition (Givens *et al.* 2008).
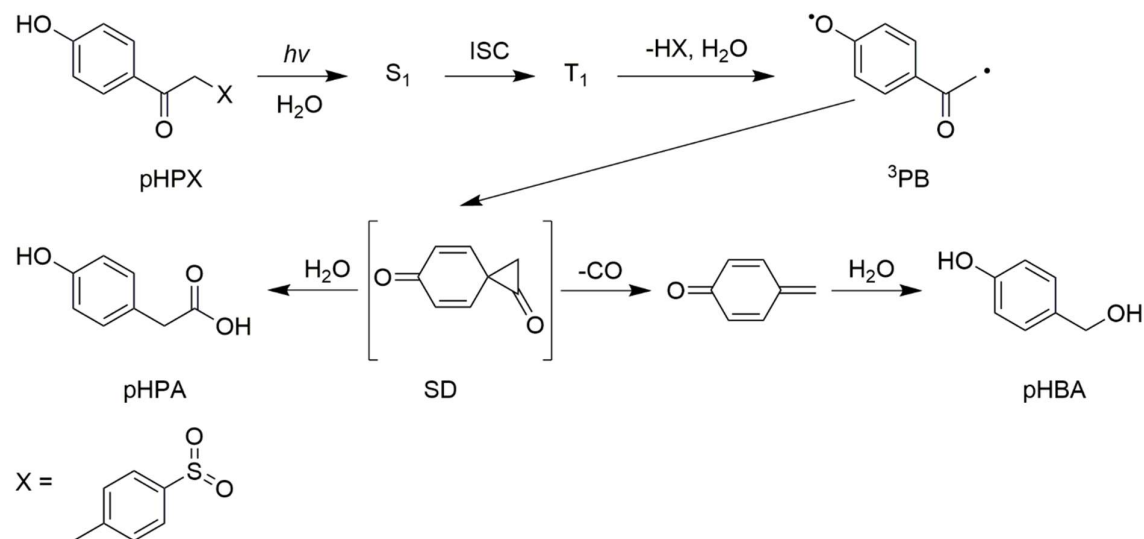
Scheme 10: Photolysis mechanism of *p*-hydroxyphenacyl (*p*HP) derivatives based on the Favorskii rearrangement. Figure according to (Givens *et al.* 2008).
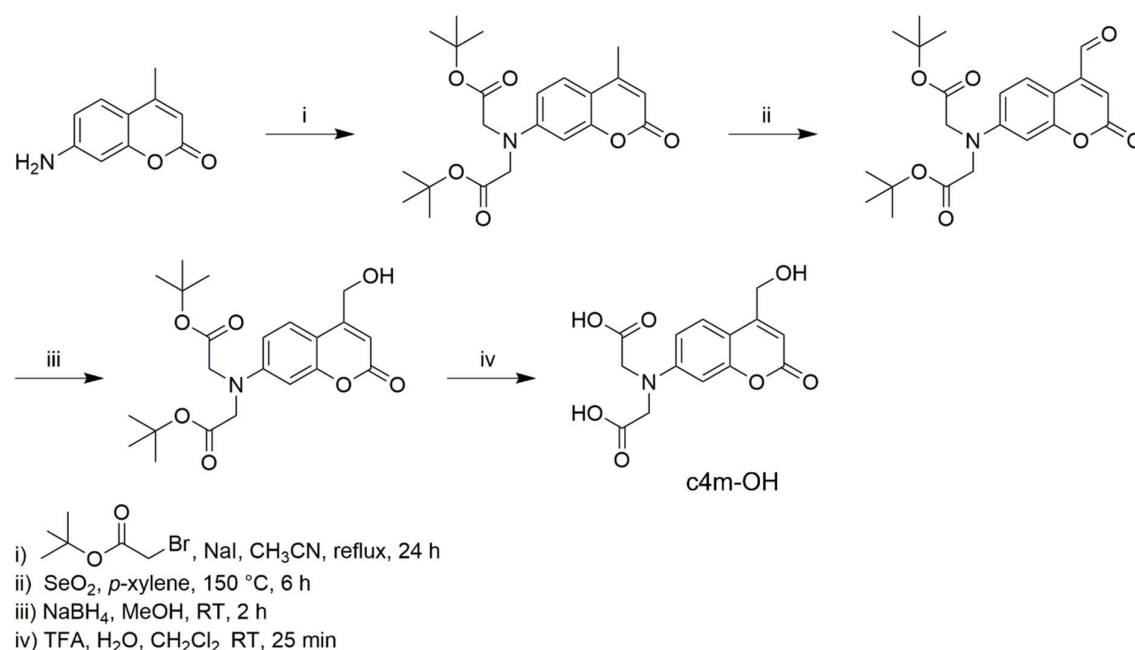
As described before *p*HP PAGs offer many advantages such as good synthetic accessibility, water solubility and appealing quantum yields between 0.03 and 0.65 in aqueous media (Givens *et al.* 2003, Givens *et al.* 2011, Zou *et al.* 2002, Zou *et al.* 2001). However, the low absorption coefficient above 320 nm can be a drawback for biological applications (Pelliccioli *et al.* 2002). To overcome this, current research focusses on the optimization of the *p*HP chromophore to shift its excitation range to higher wavelengths (Barman *et al.* 2016, Conrad *et al.* 2000) and on the exploration of new photoactive core structures like coumarin-4-ylmethyl (c4m) PAGs which can be used up to 500 nm (Givens *et al.* 2012, Hagen *et al.* 2008, Martin *et al.* 2018, Özçoban *et al.* 2015, Schmidt *et al.* 2005). Hence, in the following c4m-based PAGs will be explained in more detail.

3.6.2. Coumarin-4-ylmethyl-based photoacid generators

The research of coumarin-4-ylmethyl (c4m) PAGs commenced with the discovery of the photoactive c4m group by Givens and Matuszewski (1984). The c4m core structure is hereby given in Scheme 8c. Initial limitations of c4m derivatives like the poor water solubility and low quantum yields have been overcome by modifying the coumarin chromophore with amino and carboxylic acid side groups (Givens *et al.* 2012). This led to a new generation of c4ms with good water solubility and highly efficient

photocleavages (Givens *et al.* 2012). Combined with the wide excitation range up to 700 nm and good hydrolytic stabilities (Givens *et al.* 2012), c4ms have gained considerable attention in biochemical research (Hotta *et al.* 2019, Ohtsuki *et al.* 2016) like in cellular process studies (Furuta *et al.* 2004), caging groups for neurotransmitter (Shembekar *et al.* 2005) or the acidification of membrane surfaces (Geißler *et al.* 2005). Furthermore, c4ms were also used in agricultural (Atta *et al.* 2010) and pharmaceutical applications (Al-Wahaibi *et al.* 2018).

Especially Hagen and coworkers contributed to the chemical versatility of c4ms by synthesizing carboxylic acid, alcohol, thioalcohol, and amine c4m derivatives (Hagen *et al.* 2008) (Scheme 11). The general synthesis procedure of c4m derivatives starts by treating 7-amino-4-methylcoumarin with an access of bromoacetic acid *tert*-butyl ester followed by the oxidation of the α-methylen group to the respective aldehyde, which is subsequently reduced with NaBH$_4$ to the primary alcohol (Hagen *et al.* 2005). After removal of the *tert*-butyloxycarbonyl (Boc) protecting groups with trifluoroacetic acid, c4m-OH can be obtained as a valuable precursor for coupling reactions with various nucleophiles, such as acetates to synthesize c4m PAGs.

i) *tert*-butyl bromoacetate, NaI, CH$_3$CN, reflux, 24 h
ii) SeO$_2$, *p*-xylene, 150 °C, 6 h
iii) NaBH$_4$, MeOH, RT, 2 h
iv) TFA, H$_2$O, CH$_2$Cl$_2$, RT, 25 min

Scheme 11: Synthesis of coumarin-4-ylmethyl precursor c4m-OH according to Hagen *et al.* (2005). This precursor can be used for the preparation of coumarin-4-ylmethyl photoacid generators (c4m PAGs) and c4m caged alcohols, thioalcohols and amines (Hagen *et al.* 2008).

To release c4m caged compounds, light between 350 nm and 500 nm is needed (Givens *et al.* 2012) and the underlying photolysis mechanism is demonstrated in

Scheme 12 (Schade *et al.* 1999, Yu *et al.* 2010). After photoexcitation of the c4m species, a heterolysis of the C-O ester bond is induced, which results in a c4m carbocation and a leaving group anion (LG⁻). The latter abstracts a proton from the aqueous solvent to form LG-H. At the same time the remaining hydroxide reacts with the carbocation generating c4m-OH (Schade *et al.* 1999, Yu *et al.* 2010). For c4m carbonate esters, carbamates and thiocarbonates, the photolysis leads to LG-COOH, which can undergo further decarboxylation reactions to LG-H (Yu *et al.* 2010).

R = OMe
LG = OP(O)(OEt)$_2$
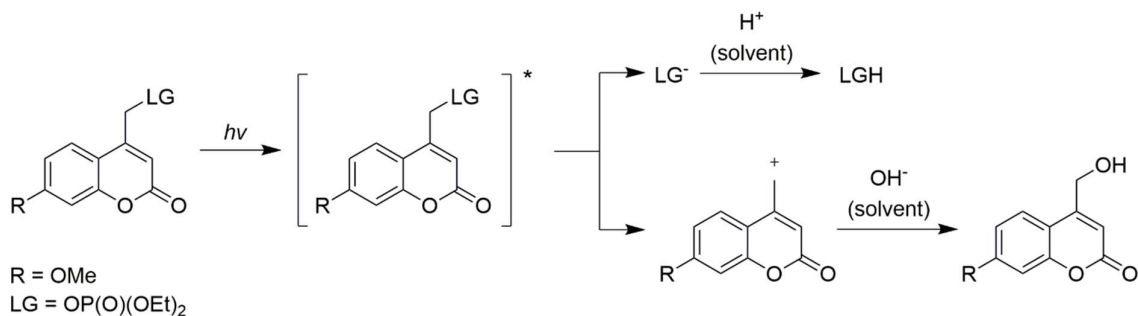
Scheme 12: Photolysis of coumarin-4-ylmethyl (c4m) caged derivatives according to Yu *et al*. (2010).

Taken together, *p*HP and c4m derivatives are attractive PAGs, which are used in various applications. However, compared to other PAGs like diaryliodonium-based PAGs (Feng *et al.* 2015, Schlögl *et al.* 2012) they are rarely used for the modification of the pH value of hydrogel swelling agents. Two interesting swelling agents for hydrogels are water and aqueous carbonate solution, because water is the most frequently used swelling agent for hydrogels and carbonate solutions could lead to new hydrogel foaming strategies similar to Schlögl *et al.* (2012). A good modification reagent for hydrogel swelling agents should therefore be easily accessible, be highly soluble and stable in water and carbonate solution and exhibit an efficient photolysis. Hence, in the last part of my research, I aim to synthesize two novel *p*HP and c4m-based PAGs to ensure high solubility in aqueous media and investigate their photochemical properties.

4. Aim of work and hypotheses

As described in the introduction, hydrogels are used in a broad variety of applications, like in tissue engineering or drug delivery (Hamedi *et al.* 2018, Lee *et al.* 2001). Hence, tailor-made hydrogels, which are specifically modified according to their application, are of growing interest (Singhal *et al.* 2016, Tang *et al.* 2019). There are two basic concepts how hydrogels, which are cross-linked polymer networks in aqueous swelling agents, can be modified: either by modifying the polymer network or through the modification of the swelling agent. For both strategies, appropriate hydrogel modification reagents are needed. Therefore, the aim of this work is the synthesis and characterization of novel hydrogel modification reagents (Figure 9).
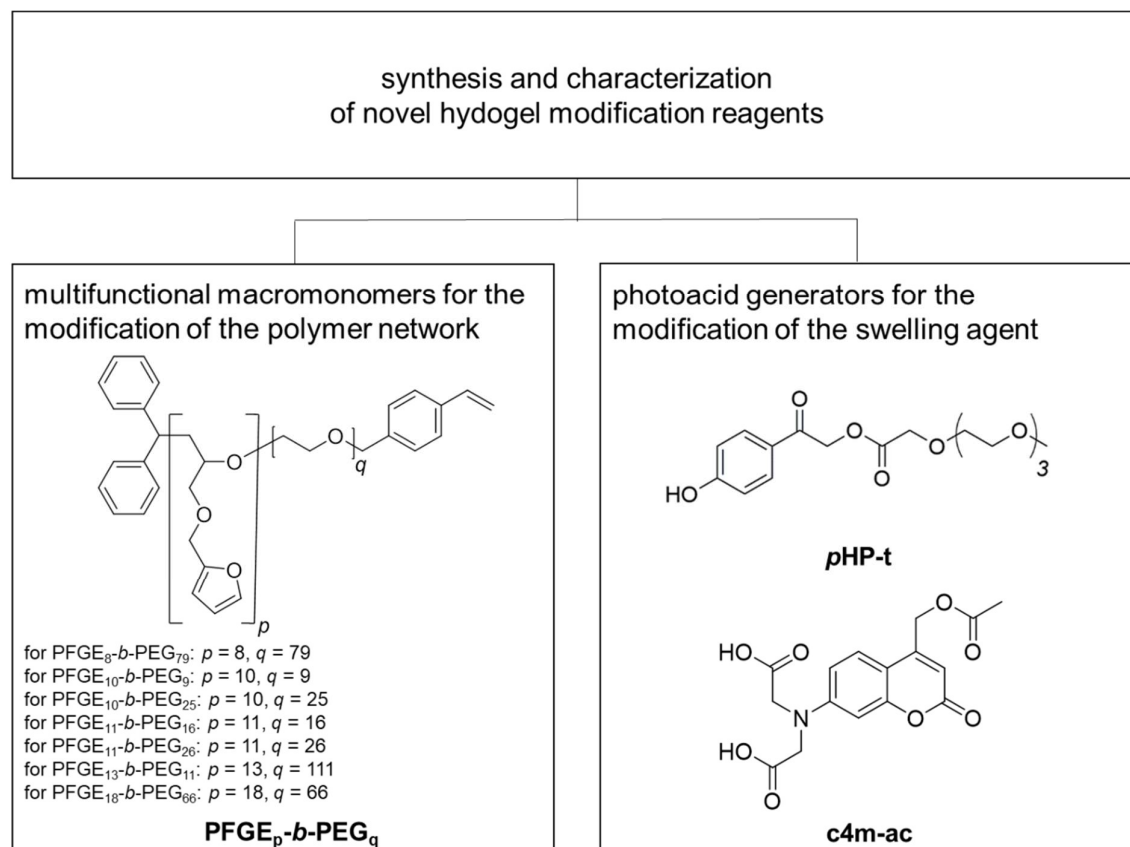
Figure 9: Schematic depiction of the aim of work with focus on the synthesis and characterization of novel hydrogel modification reagents for the modification of the polymer network and the swelling agent of hydrogels.

For the modification of the polymer network, I focus on the synthesis and characterization of multifunctional α-diphenylmethyl-ω-4-vinylbenzyl-poly(furfuryl glycidyl ether)-*block*-poly(ethylene glycol) ($PFGE_p$-*b*-PEG_q) macromonomers and for the potential modification of the swelling agent I synthesize and characterize the two

p-hydroxyphenacyl- (*p*HP) and coumarin-4-ylmethyl (c4m)-based photoacid generators (PAG) *p*HP-t and c4m-ac, which are shown in Figure 9.

In the first part of this work I explore the synthesis and characterization of multifunctional macromonomers for the modification of the polymer networks of radically cross-linked hydrogels. In particular, I aim to investigate the bulk and surface functionalization of radically cross-linked polyacrylamide (p(Aam)) hydrogels with multifunctional macromonomers. I chose PFGE$_p$-*b*-PEG$_q$ macromonomers in Figure 9 as target structure, since it meets all of the three following requirements for an appropriate hydrogel modification reagent as it contains I) a polymerizable unit in order to covalently bind into a radically cross-linked hydrogel; II) a spacer to introduce sufficient water solubility and flexibility and III) multiple functional groups, which are orthogonal to the cross-linking reaction and which can be used as multiple anchor points for post-synthetic modification reactions. Thus, I want to investigate the synthetical approachability, like the end group functionalization degree and the block length adjustability as well as the polymer characteristics, like the molecular weight distribution, the thermal properties and the surface activity of PFGE$_p$-*b*-PEG$_q$ macromonomers. I am also interested in exploring the reactivity of the functional groups of PFGE$_p$-*b*-PEG$_q$ macromonomers in solution and in functionalized p(Aam) hydrogels, to find out whether such functionalized hydrogels can be applied as hydrogel functionalization platform for post-synthetic Diels-Alder reactions.

Therefore, hypothesis I, which will be examined for the modification of the hydrogel network, is:

Hypothesis I:

Well-defined, multifunctional α-diphenylmethyl-ω-4-vinylbenzyl-poly(furfuryl glycidyl ether)-block-poly(ethylene glycol) (PFGE$_p$-b-PEG$_q$) macromonomers can be synthesized via anionic ring opening polymerization and characterized regarding their characteristic polymer properties like their molar mass dispersity (Đ), their glass transition temperature (T$_g$), their melting temperature (T$_m$), their decomposition temperature (T$_d$) and their critical micelle concentration (cmc). PFGE$_p$-b-PEG$_q$ macromonomers can be used for the bulk functionalization of radically cross-linked polyacrylamide (p(Aam)) hydrogels to prepare functional hydrogels with multiple anchor points for post-synthetic Diels-Alder reactions.

Beyond the bulk functionalization of hydrogels, I want to investigate whether $PFGE_p$-b-PEG_q macromonomers can be used for the surface functionalization of hydrogels without functionalizing the hydrogel bulk. To our knowledge no one used multifunctional macromonomers to exclusively functionalize the air-hydrogel interface without functionalizing the hydrogel bulk. Hence, I want to gain knowledge about the film formation ability and the structure-property relations of $PFGE_p$-b-PEG_q macromonomers at the air-water interface to evaluate whether they are suitable surface functionalization reagents. The air-water interface serves as a simplified model of the air-hydrogel precursor solution interface.

So, the hypothesis II, which will be investigated for the hydrogel surface functionalization ability of $PFGE_p$-b-PEG_q macromonomers, is:

Hypothesis II:

Multifunctional $PFGE_p$-b-PEG_q macromonomers are able to form thin films at the air-water interface, whereby the beginning of the film formation correlates with the molecular weight of the macromonomers. The beginning of the film formation is determined by the molecular area of the onset of the surface pressure-area isotherm. The stability of the macromonomer films is dependent on the hydrophilic-lipophilic balance (HLB) value. Furthermore, a molecular mechanism of the $PFGE_p$-b-PEG_q macromonomers at the air-water interface can be proposed, which is in accordance with the film stability and film recovery. $PFGE_p$-b-PEG_q macromonomers are promising functionalization reagents for the functionalization of the air-hydrogel interface of radically cross-linked p(Aam) hydrogels.

Hypotheses I and II are both dedicated to the modification of the polymer network, whereas in the last part of this work I want to explore the synthesis and characterization of novel, water soluble *p*HP- and c4m-based PAGs for the potential modification of hydrogel swelling agents.

As described in the introduction, *p*HPs and c4ms are well known for their excellent photochemical properties and are applied in numerous fields (Givens *et al.* 2012, Hagen *et al.* 2008, Klán *et al.* 2013b). However, in many water-based applications where high PAG concentrations are needed, strong electrolyte PAGs are preferred, even if they are toxic or need additional photosensitizers (Feng *et al.* 2015, Gargava *et al.* 2016, Kovalenko *et al.* 2016, Schlögl *et al.* 2012). This is presumambly based on

the good synthetic approachability and high water solubility of many strong electrolyte PAGs. To give an alternative to such compounds, I aim to design two easily accessible and highly water soluble c4m and pHP-based PAGs, as the substance classes of c4ms and pHPs are well suited for physiological applications and do not need additional sensitizers. Therefore, in this work, I will investigate c4m-ac and pHP-t regarding their synthetic accessibility, their solubility in aqueous media, their stability and photolysis to give a comprehensive insight into the properties of novel c4m and pHP-based PAGs.

So, hypothesis III is focused on the exploration of c4m-ac and pHP-t:

Hypothesis III:

The photoacid generators c4m-ac and pHP-t show good synthetic approachability and high solubility in water and alkaline solutions with maximum solubilities (c_{max}) > 1 mmol L^{-1}. The photochemical properties of c4m-ac and pHP-t, like the absorption maximum (λ_{max}), the maximum molar extinction coefficient (ε_{max}) and the quantum yield (ϕ), are pH dependent. Furthermore, the stability of c4m-ac and pHP-t is pH dependent, in contrast to the photolysis under UV irradiation within the studied conditions.

The three hypotheses regarding the synthesis and characterization of multifunctional macromonomers and photoacid generators for the modification of hydrogels are the core pillar of this work and will be explored and discussed in the following sections.

5. Hydrogels with multiple clickable anchor points: synthesis and characterization of poly(furfuryl glycidyl ether)-*block*-poly(ethylene glycol) macromonomers

Authors: Karishma K. Adatia,[a] Silke Keller,[a] Tobias Götz,[a] Günter E. M. Tovar, [a,b,*] and Alexander Southan [a,*]

[a] Institute of Interfacial Process Engineering and Plasma Technology IGVP, University of Stuttgart, Nobelstraße 12, 70569 Stuttgart, Germany

[b] Fraunhofer Institute for Interfacial Engineering and Biotechnology IGB, Nobelstr. 12, 70569 Stuttgart, Germany

* corresponding authors; E-mail: alexander.southan@igvp.uni-stuttgart.de, guenter.tovar@igvp.uni-stuttgart.de

Own contribution: I conceived and designed the whole research study. I synthesized the macromonomers, performed the SEC, MALDI TOF MS, DSC, TGA, FT-IR and bubble pressure tensiometry measurements and prepared the functionalized and unfunctionalized hydrogels. The ^{1}H and ^{13}C NMRs were recorded at the University of Stuttgart (IOC) and Silke Keller helped me with the LSM experiments. I analyzed and interpreted all the data and wrote the manuscript.

5.1 Abstract

Functional polyacrylamide hydrogels containing multiple furfuryl anchor points for Diels-Alder reactions were prepared employing new macromonomers. For this purpose, α-diphenylmethyl-ω-4-vinylbenzyl-poly(furfuryl glycidyl ether)-*block*-poly(ethylene glycol) (PFGE$_p$-*b*-PEG$_q$) macromonomers were synthesized *via* anionic ring opening polymerization in four different block lengths: PFGE$_{10}$-*b*-PEG$_{25}$, PFGE$_8$-*b*-PEG$_{79}$, PFGE$_{18}$-*b*-PEG$_{66}$ and PFGE$_{13}$-*b*-PEG$_{111}$. These furan containing building blocks were characterized by ^{1}H NMR, ^{13}C NMR and FT-IR spectroscopy, SEC and MALDI TOF MS and revealed low molar mass dispersities between 1.05 and 1.09 and

number average molar masses between 2 330 g mol^{-1} and 6 660 g mol^{-1}. The block lengths of the macromonomers were adjustable *via* the MIR and high end group functionalization degrees between 72 % and 98 % were achieved. The macromonomers were characterized by DSC and TGA regarding their thermal properties (-43 °C ≤ T_g ≤ -32 °, 32 °C ≤ T_m ≤ 45 °C, 369 °C ≤ T_d ≤ 381 °C) and by tensiometry regarding their surface activity, revealing a critical micelle concentration around 0.3 mg mL^{-1} in aqueous solution. The furfuryl groups of the PFGE$_p$-*b*-PEG$_q$ macromonomers were reactive in Diels-Alder reactions in solution as well after their integration into polyacrylamide hydrogels by radical copolymerization, as shown by fluorescence labeling employing a maleimide-functionalized dye. Thus, a new synthetic route is opened up to access functional hydrogels providing clickable anchor points in high density for conjugation of maleimide-functional substrates.

5.2 Introduction

From the beginning of hydrogel science in 1960 when Wichterle and Lim proposed poly(hydroxyethyl methacrylate) hydrogels as materials for contact lenses, hydrogels were considered as functional materials with favorable properties originating from their composition of a hydrophilic network and an aqueous swelling medium (Wichterle *et al.* 1960). Since then, areas of applications for hydrogels have grown tremendously so that today hydrogels can be found in pharmacy (Hamedi *et al.* 2018, Kamoun *et al.* 2017, Klara *et al.* 2018, Qiu *et al.* 2001), biomedicine (Pellá *et al.* 2018, Tavakoli *et al.* 2017), biotechnology (Abd El-Mohdy *et al.* 2008, Ullah *et al.* 2015) tissue engineering (El-Sherbiny *et al.* 2013, Lee *et al.* 2001), cosmetics (Parente *et al.* 2015) agriculture (Guilherme *et al.* 2015), 3D printing (Joas *et al.* 2018, Kraut *et al.* 2017, Li *et al.* 2015) and waste water treatment (Mohammadzadeh Pakdel *et al.* 2018, Ullah *et al.* 2015). Due to the broad range of applications with specific requirements, customized hydrogels with adjustable properties are in the focus of current research (Buwalda *et al.* 2017, Schauenburg *et al.* 2018, Singhal *et al.* 2016, Soontornworajit *et al.* 2010, Wu *et al.* 2018).

A frequently used strategy to introduce tailor-made functionalities into hydrogels is the usage of functional building blocks, which exhibit molecular anchor points for post-synthetic reactions (Altin *et al.* 2010, Baker *et al.* 2017, DeForest *et al.* 2012, Gould *et al.* 2012, Grevesse *et al.* 2013, Grevesse *et al.* 2014, Schauenburg *et al.* 2018, Yilmaz

_et al._ 2011). In chemical and biochemical research, furan building blocks are particularly interesting as they can undergo Diels-Alder click reactions and are often used for bioconjugations (Gandini 2013, Nimmo _et al._ 2011, Smith _et al._ 2018, Steven _et al._ 2008, Tasdelen 2011, Yu _et al._ 2013).

Hence, to create a hydrogel with pendent furan groups for post-synthetic Diels-Alder reactions, a multifunctional building block with three features is needed: I) a polymerizable unit for the covalent incorporation into the hydrogel; II) a spacer for sufficient flexibility and water solubility and III) pendent furan groups as molecular anchor points. Apparently, the higher the number of furan groups per building block, the more anchor points per molecule can be introduced into the hydrogel. We think α-diphenylmethyl-ω-4-vinylbenzyl-poly(furfuryl glycidyl ether)-_block_-poly(ethylene glycol) (PFGE$_p$-_b_-PEG$_q$) macromonomers are fascinating multifunctional building blocks as they fulfill all the above mentioned criteria.

In the last years, intensive research was conducted on the development of furan-containing hydrogels (Baker _et al._ 2017, García-Astrain _et al._ 2013, García-Astrain _et al._ 2014, Smith _et al._ 2018). However, the amount of furan anchor points in the hydrogel was often restricted by using the furans for cross-linking and functionalization reactions simultaneously (García-Astrain _et al._ 2013, García-Astrain _et al._ 2014, Smith _et al._ 2018). Therefore, in the following we will present the synthesis and characterization of multifunctional PFGE$_p$-_b_-PEG$_q$ building blocks with orthogonal cross-linking and post-modification chemistry to establish highly functional hydrogels for post-synthetic Diels-Alder reactions.

5.3 Experimental section

Chemicals. Potassium (98 %), 4-vinylbenzyl chloride (4VBC) (90 %), acrylamide (99 %), _N,N'_-methylenebisacrylamide (MBA) (99 %), α-ketoglutaric acid (99 %), calcium hydride (95 %), naphthalene (99 %), _trans_-2-[3-(4-_tert_-Butylphenyl)-2-methyl-2-propenylidene]-malononitrile (DCTB) (98 %), 3-Phenyl-1-propanol (3PP) (98 %) and petroleum ether (PE) (ACS reagent) were purchased from Sigma Aldrich (Darmstadt, Germany). Diphenylmethane (DPM) (99 %), silica gel 60 with a particle size of 0.063 mm – 0.200 mm and active basic aluminium oxide 66 with a particle size of 0.063 mm – 0.200 mm was bought from Merck KGaA (Darmstadt, Germany). Furfuryl glycidyl ether (FGE) was bought from Acros Organics (Geel, Belgium) and ethylene

oxide (EO) from the Linde group (Dublin, Ireland). Sodium trifluoroacetate was obtained from Fluka Analytical (Munich, Germany).The fluorescence dye Atto 488 maleimide was purchased from Atto-Tec GmbH (Siegen, Germany). Tetrahydrofuran (THF), methanol (MeOH) and diethyl ether were obtained in HPLC grade from VWR chemicals (Radnor, USA). Ethyl acetate (EtOAc) was obtained from J.T. Baker (Phillipsburg, USA). Furfuryl glycidyl ether was purified by column chromatography (silica gel, solvent gradient from EtOAc : PE = 1 : 1 to EtOAc : PE = 3 : 1). THF was dried at least 2 days over calcium hydride and freshly destilled under argon before usage. EO was dried by passing through a column of calcium hydride. 4VBC was flashed over basic aluminum oxide, stirred over calcium hydride for 4 days and destilled under reduced pressure at 50 °C and 10^{-1} mbar. All other chemicals were used as received.

Instrumentation. ^{1}H NMR and ^{13}C NMR spectra were recorded on an "Avance 500" (500 MHz) spectrometer from Bruker (Billierica, USA) with chloroform-d_1 as solvent and tetramethylsilane as internal standard. For size exclusion chromatography (SEC), samples were prepared by dissolving the polymers at a concentration of 2 mg mL^{-1} in THF, mixing them at 40 °C for 24 h and subsequently filtering them through a 0.2 µm PTFE syringe filter. The SEC measurements were performed at 40 °C on a "SECurity System" from PSS GmbH (Darmstadt, Germany) with a PSS SDV precolumn (8 mm x 50 mm) and two PSS SDV 1000 Å (8 mm x 300 mm) columns. For the detection a refractive index (RI) detector was used. The injection volume was 50 µL per run, THF (HPLC grade) was used as solvent, the flow rate was 0.5 mL min^{-1} and the columns were calibrated with polystyrene standards "ReadyCal" from PSS GmbH (Mainz, Germany). The SEC results are shown as abundance mass distributions in order to be able to compare the molar mass distributions with the mass spectrometry data. PSS WinGPC Unichrom software version 8.10 was used for the analysis of the measurements. For matrix assisted laser desorption/ionization time of flight mass spectrometry (MALDI TOF MS), solutions of 2.0 mg mL^{-1} macromonomer, 13.6 mg mL^{-1} sodium triflate and 10.0 mg mL^{-1} *trans*-2-[3-(4-*tert*-Butylphenyl)-2-methyl-2-propenylidene]-malononitrile (DCTB) in THF were prepared and 20 µL of macromonomer solution, 10 µL of the sodium triflate solution and 1 µL of the DCTB solution were mixed. 1 µL of the mixture was placed on a "MTP 384 target plate ground steel TF" target plate from Bruker Daltronik GmbH (Billerica, USA). After the mixture dried on the target plate the measurement was performed using an "Ultraflex II

TOF/TOF" from Bruker Daltronik GmbH (Billerica, USA). $PFGE_{10}$-*b*-PEG_{25}, $PFGE_8$-*b*-PEG_{79} and $PFGE_{18}$-*b*-PEG_{66} were measured in reflective mode and $PFGE_{13}$-*b*-PEG_{111} was measured in linear mode. For all samples the mass range was from 0 Da – 20 000 Da and the laser intensity was 30 %. The analysis was performed with "flexAnalysis 3.3" from Bruker Daltronik GmbH (Billerica, USA). Attenuated total reflection infrared spectra (ATR-IR) were recorded on a FTIR "Equinox 55" from Bruker (Billerica, USA) using a DTGS detector. DSC measurements were performed on a "DSC 200 F3 Maia" from Netzsch Group (Selb, Germany). 15 mg of the sample were measured in an aluminum crucible between -150 °C and 150 °C with a heating/cooling ramp of 10 K min^{-1} under nitrogen atmosphere. The glass transition temperature (T_g) and the melting temperature (T_m) were determined from the second heating curve. TGA was measured under nitrogen flow on a "Jupiter STA 449 F3" from Netzsch Group (Selb, Germany) between 30 °C and 1 000 °C and a heating ramp of 10 K min^{-1}. The decomposition temerature (T_d) was determined by calculating the extrapolated onset temperature. Dynamic surface tensions of polymer solutions were determined using a bubble pressure tensiometer "BP50" from Kruess GmbH (Hamburg, Germany) in the range of 1 500 ms to 12 000 ms at room temperature. The tensiometer was callibrated to the surface tension of water (72.6 mN m^{-1}) at room temperature (21 °C) before usage. Confocal Laser Scanning Microscopy (LSM) measurements were carried out using a Zeiss LSM 710 inverted confocal microscope from Carl Zeiss AG (Oberkochen, Germany). The hydrogels were placed in between two glass cover slips (thickness: 0.13 mm – 0.16 mm). Functionalized polyacrylamide (p(Aam)) hydrogels as well as the respective unfunctionalized control hydrogels were investigated using the objective EC Plan-Neofluar 10x/0.30 M27 from Carl Zeiss AG (Oberkochen, Germany). In order to provide comparability between the two hydrogel types, microscope settings were kept identical. To collect the ATTO 488 signal from the measured hydrogel height, z-stack images were generated using an Argon 488 nm laser for excitation. The acquired 3D data were then projected into a single 2D image (maximum intensity projection) along the z-axis by transfering the brightest pixel (voxel) in each layer into the final 2D image. Image processing was performed using the software ImageJ 1.46r. For the quantification of the fluorescence signal of the fluorescence labeled p(Aam) hydrogels, fluorescence images were first converted into 8-bit grayscale images. The total relative fluorescence intensity *I* was determined from

the corresponding histograms by calculating an abundance-weighted average of the gray scale values g using their respective abundance c_g according to equation (1).

$$I = \frac{\sum_{g=0}^{255}(c_g \cdot g)}{\sum_{g=0}^{255} c_g} \tag{1}$$

Diphenylmethyl potassium synthesis. Based on the procedure described by Duran et al., diphenylmethyl potassium (DPMK) was synthesized in a vacuum dried schlenk flask by dissolving 4.1 g (104.6 mmol, 2.0 eq.) potassium in 75 mL freshly destilled, dry THF and adding a naphthalene solution, containing 6.6 g (51.7 mmol, 1.0 eq.) of sublimated naphthalene and 100 mL freshly distilled, dry THF (Francis et $al.$ 2003). After the mixture turned dark green, 17.4 mL (104.5 mmol, 2.0 eq.) diphenylmethane was added. The dark red DPMK solution was stirred for 8 days at room temperature. The whole synthesis was performed under dry and inert conditions. The DPMK concentration was determined to be 0.8 mol L^{-1} ± 0.1 mol L^{-1} by water free titration. For this, three DPMK aliquots were titrated with dry 3-phenyl-1-propanol under argon until the dark red color of the DPMK solution turned into a slightly yellow solution. DPMK was stored at -20 °C under inert gas.

Macromonomer synthesis. The synthesis of PFGE$_{10}$-b-PEG$_{25}$ is described exemplarily as the other macromonomers PFGE$_8$-b-PEG$_{79}$, PFGE$_{18}$-b-PEG$_{66}$ and PFGE$_{13}$-b-PEG$_{111}$ only differ in their block lenghts. Under dry and inert conditions 2.1 mL DMPK solution (c = 0.8 mol L^{-1}, 1.2 mmol DPMK, 1.0 eq.) were dissolved in 12.0 mL freshly distilled, dry THF. 1.4 mL purified FGE (9.7 mmol, 8.0 eq.) were added quickly to the initator solution and stirred for 41 h at 45 °C. Then the living poly(furfuryl glycidyl ether) (PFGE)-block was cooled to -10 °C in an ice/acetone bath and 1.0 g ethylene oxide (23.6 mmol, 20.0 eq.) were condensed into the flask. The mixture was stirred at 40 °C for 24 h and terminated with 0.9 mL (6.0 mmol, 5.0 eq.) dry 4-vinylbenzyl chloride. After 18 h of stiring at room temperature the solvent was evaporated. PFGE$_{10}$-b-PEG$_{25}$ was purified via column chromatography (silica gel, EtOAc (100%) → EtOAc : MeOH (85% : 15%)) and dried under vacuum, yielding in 2.1 g amber-coloured viscous oil (yield: 72%). PFGE$_8$-b-PEG$_{79}$, PFGE$_{18}$-b-PEG$_{66}$ and PFGE$_{13}$-b-PEG$_{111}$ in contrast were redissolved in 10 mL THF and purified by seven precipitations in diethyl ether, which was cooled with ice. After the solvent was evaporated, the precipitate was dissolved in 2 mL CHCl$_3$ and dialysed against water for 7 days, whereby the water (5 L) was changed twice a day. The moleucular cutoff of

the dialysis membrane "Spectra/Por biotech CE" from spectrum labs was 500 g mol^{-1}. After dyalsis, the macromonomers were lyophylized and PFGE$_{18}$-*b*-PEG$_{66}$ was obtained as amber-coloured highly viscous material in 35% yield. PFGE$_8$-*b*-PEG$_{79}$ and PFGE$_{13}$-*b*-PEG$_{111}$ resulted in a white solid of 55% and 25% yield.

^{1}H NMR (500 MHz, CDCl$_3$): δ [ppm] = 3.22 – 3.72 (m, 150, *a, b, c, h, i*), 4.13 (m, 1 H, *o*), 4.42 – 4.45 (m, 20, *d*), 4.55 (s, 2 H, *j*), 5. 22 – 5.24 (m, 1 H, *n*), 5.72 – 5.75 (m, 1 H, *n*), 6.26 – 6.30 (m, 20, *e, f*), 6.69 – 7.13 (m, 1 H, *m*), 7.12 -7.24 (m, 10 H, *p*), 7.29 -7.30 (m, 4 H, *k*), 7.34 – 7.39 (m, 10 H, *g*). The alphabetical proton assignments refer to Figure 10 and Figure 14 - Figure 17.

^{13}C NMR (500 MHz, CDCl$_3$): δ [ppm] = 152.05, 142.7, 138.03, 137.01, 136.64, 128.59, 128.46, 128.30, 128.03, 127.83, 126.29, 126.12, 113.83, 110.31, 109.25, 78.80, 73.04, 70.65, 70.03, 69.75, 69.49, 65.22, 61.75.

ATR-IR: ṽ [cm^{-1}] = 3118 (w, Ar-H), 2882 (s, C-H), 1465 (m, C-H), 1107 (s, C-O-C).

Determination of the macromonomer yield. The synthesis yield (Y_s) of the macromonomers was determined according to equation (2).

$$Y_s = \frac{m_e}{m_{ini} + m_{FGE} + m_{EO} + m_{4VBC}} \cdot 100\% \qquad (2)$$

Whereby m_e is the experimentally determined mass of the macromonomer, m_{ini} is the mass of the initiatior, m_{FGE} is the mass of FGE, m_{EO} ist the mass of EO and m_{4VBC} is the mass of the 4 vinylbenzyl end group.

Quantification of end group functionalization and block lengths. Quantification of the end group functionalization of the macromonomers was performed by ^{1}H NMR spectroscopy as reported by Semple *et* al. (2016b). The end group functionalization degree (*f*) is given by the ^{1}H NMR integral ratio between the initiator signals (Int_{ini}) caused by n_{ini} protons of the DPM-initiator and the end group signals (Int_{end}) caused by n_{end} protons belonging to the 4 vinylbenzyl end group (equation (3)).

$$f = \frac{n_{ini} \cdot Int_{end}}{n_{end} \cdot Int_{ini}} \cdot 100\% = \frac{j + m + n}{5o} \cdot 100\% \qquad (3)$$

The letters in equation (3) refer to the proton assignments in Figure 10 and Figure 14 - Figure 17. As the aromatic signals of the macromonomers in these NMR spectra were not properly baseline seperated, only the aliphatic signals were used for the end group

quantification. Block lengths of the macromonomers were also determined by ^{1}H NMR spectroscopy. The number of FGE repeating units (p) in the PFGE-block was calculated according to equation (4) relative to Int_{ini}.

$$p = \frac{n_{ini} \cdot Int_{furan}}{n_{furan} \cdot Int_{ini}} = \frac{d + e + f}{4o} \tag{4}$$

Here, Int_{furan} is the combined integral of used furfuryl signals and n_{furan} is the number of contributing protons per FGE repeating unit. The side chain protons c between 3.22 ppm and 3.72 ppm as well as proton g of the furan moiety at 7.39 ppm were not taken into account as they are not baseline separated from other signals. Similarly, the number of EO repeating units (q) in the PEG-block was determined according equation (5):

$$q = \frac{n_{ini}(Int_{BB} - 5p)}{n_{EO} \cdot Int_{ini}} = \frac{a + b + c + h + i - 5p}{4o} \tag{5}$$

In equation (5), Int_{BB} is the signal caused by the macromonomer backbone between 3.47 ppm and 3.74 ppm and n_{EO} is the number of contributing protons per EO repeating unit.

The block length ratio (B) is defined as the ratio of PEG repeating units q to FGE repeating units p:

$$B = \frac{q}{p} \tag{6}$$

Diels-Alder reaction in polymer solution. 21.3 mg (0.004 mmol, 1 eq.) PFGE$_8$-b-PEG$_{79}$ were dissolved in 10 mL MilliQ water and 39.4 mg N-ethylmaleimide (NEM) (0.315 mmol, 79 eq.) were added. The furan to maleimide ratio was 1:10 as PFGE$_8$-b-PEG$_{79}$ contains eight furan moeities in average. The mixture was stirred for 24 h at room temperature and the solvent was evaporated. The conversion of the Diels-Alder reaction (C_{DA}) was determined from the raw product. Similar to Habibi et al. the C_{DA} was quantified via ^{1}H NMR spectroscopy according to equation (7) (Buono et al. 2017).

$$C_{DA} = \frac{\dfrac{Int_p}{n_p}}{\dfrac{Int_e}{n_e} + \dfrac{Int_p}{n_p}} \cdot 100\% = \frac{\dfrac{g' + s'}{3}}{\dfrac{d}{2} + \dfrac{g' + s'}{3}} \cdot 100\% \tag{7}$$

Here, Int_p is the integral of the used Diels-Alder product signals at 5.24 ppm (g') and 1.01 ppm (s') from Figure 25 and n_p is the number of protons of the used Diels-Alder

product signals. Respectively, Int_e is the integral of the educt signal at 4.43 ppm (d) and n_e is the number of protons of the educt signal. Only signals g', s' and d from Figure 25 were used for the quantification because other signals were not clearly baseline separated.

Hydrogel preparation. Functionalized polyacrylamide (p(Aam)) hydrogels were prepared by mixing 15 w% acrylamide, 2 w% *N,N'*-methylenebisacrylamide (MBA), 1 w% α-glutaric acid, 1 w% of the respective macromonomer (PFGE$_8$-*b*-PEG$_{79}$ or PFGE$_{18}$-*b*-PEG$_{66}$ or PFGE$_{13}$-*b*-PEG$_{111}$) and 82 w% water. For unfunctionalized hydrogels extra water instead of macromonomer was added. 200 µL of the mixture was poured into a cylindrical aluminum mold with 150 mm diameter and 1 mm height. The hydrogel precursor solution was covered with a quartz glas pane, which was based on a spacer in order to leave a gap between the glass and the mixture. Then, the hydrogel was cured in a "hartmann.gs UH-H 255" UV chamber from Hartmann Feinwerkbau GmbH (Ober-Moerlen, Germany) for 15 min. The irradiation intensity was approx. 40 mW cm^{-2}.

Equilibrium degree of swelling and gel yield. The equilibrium degree of swelling (*EDS*) of the functionalized and unfunctionalized hydrogels were determined gravimetrically. The *EDS* is defined as follows:

$$EDS = \frac{m_{\text{swollen}} - m_{\text{dry}}}{m_{\text{dry}}} \cdot 100\% \tag{8}$$

Here, m_{swollen} is the mass of the swollen hydrogel after washing it for three days in water and m_{dry} is the mass of the dried hydrogel after washing it for three days and drying it for 24 h at 50 °C and 30 mbar in a vacuum chamber.

The gel yields (Y_g) of the hydrogels were determined gravimetrically according to the following eqation:

$$Y_g = \frac{m_{\text{dry}}}{m_{\text{pol}} \cdot f_{\text{m}}} \cdot 100\% \tag{9}$$

m_{pol} is the the mass of the hydrogel directly after curing, m_{dry} is the mass of the dried hydrogel after washing the hydrogels for 3 days and drying them in the vacuum chamber for 24 h at 50 °C and 30 mbar. The mass fraction (f_{m}) is the sum of monomer, cross-linker and macromonomer fractions in the hydrogel (f_{m} = 0.17 for hydrogels without and f_{m} = 0.18 for hydrogels with macromonomer).

Fluorescence labeling of hydrogels. Polyacrylamide (p(Aam)) hydrogels from 200 µL hydrogel precursor solution were prepared as described before and washed for three days in water, changing the water (20 mL) twice a day. Then one half of the hydrogel was put into 950 µL demineralized water and 50 µL of the fluorescence dye Atto 488 maleimide (1.39 mM in DMSO) were added to the hydrogel. All steps which involve the fluorescent dye were performed under light exclusion. The molecular structure of Atto 488 maleimide is shown in Figure 28. The mixtures were heated to 65 °C for 2 h, before the gels were washed six times by changing the water every 30 minutes in the dark. The fluorescence labeled hydrogels were immediately used for microscopic investigations using the LSM to avoid bleaching of the dye.

Statistical evaluation. OriginPro 9.1 from OriginLab was used for statistical analysis by one-way analysis of variance (ANOVA). An effect was encountered as significant when the differences between individual mean values were significant with $p < 0.05$. The individual mean values were evaluated using the Holm-Bonferroni correction.

5.4 Results and discussion

The fundamental concept for hydrogel functionalization with multiple furan anchor points reactive in Diels-Alder reactions is visualized in Scheme 13. The approach is based on the copolymerization of the monomers acrylamide and MBA with the macromonomer PFGE$_p$-b-PEG$_q$, which exhibits multiple furan side chains for post-synthetic Diels-Alder click reactions.
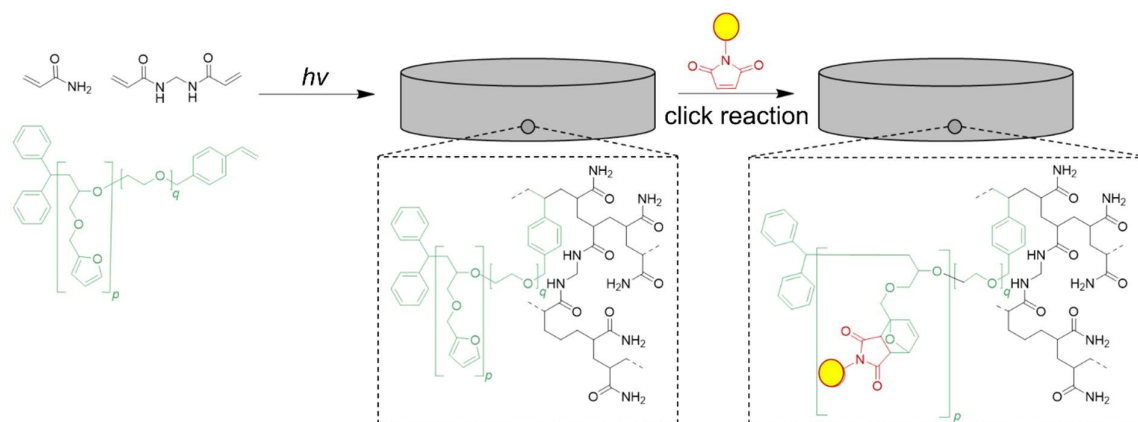

Scheme 13: Schematic representation of the fundamental concept for hydrogel functionalization with multiple clickable anchor points in this study.

Macromonomer synthesis. The macromonomer α-diphenylmethyl-ω-4-vinylbenzyl-poly(furfuryl glycidyl ether)-$block$-poly(ethylene glycol) (PFGE$_p$-b-PEG$_q$) is a promising multifunctional building block since it has a vinylbenzyl end group for radical polymerization and a hydrophilic PEG-block, which is often used in the literature to increase water solubility (Bolourchian et $al.$ 2013, Sill et $al.$ 2017). It is important that the macromonomers are water-soluble, so that they can be used directly in hydrogel formulations. Moreover, the poly(furfuryl glycidyl ether) (PFGE) block exhibits multiple furan side chains for post-synthetic Diels-Alder click reactions with maleimides, which are frequently applied in bioconjugation reactions (Steven et $al.$ 2008, Tasdelen 2011). Additionally, Diels-Alder reactions are orthogonal to radical polymerization reactions (Barthel et $al.$ 2012, Laita et $al.$ 1997, Pramanik et $al.$ 2017).

Based on the pioneering work of the Schubert group on FGE polymerization (Barthel et $al.$ 2012), we developed a synthesis strategy for end group functionalized PFGE$_p$-b-PEG$_q$ macromonomers. Our approach aimed towards the introduction of a polymerizable end group on the hydrophilic PEG-block, which can not be accieved with the synthesis strategy of Barthel et $al.$ (2012). As shown in Scheme 14, we started the

macromonomer synthesis with AROP of FGE and subsequently added EO to it. In the final step the living chain ends were terminated with 4VBC.
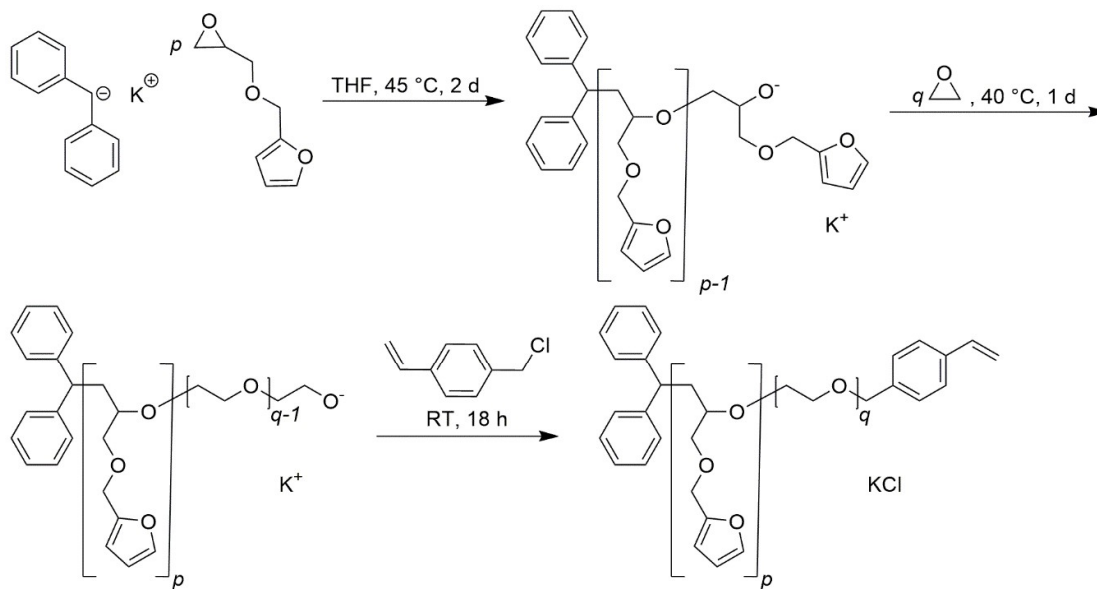
for **PFGE$_{10}$-*b*-PEG$_{25}$**: p = 10, q = 25; 72% yield
for **PFGE$_8$-*b*-PEG$_{79}$**: p = 8, q = 79; 55% yield
for **PFGE$_{18}$-*b*-PEG$_{66}$**: p = 18, q = 66; 35% yield
for **PFGE$_{13}$-*b*-PEG$_{111}$**: p = 13, q = 111; 25% yield

Scheme 14: Synthesis of functional *α*-diphenylmethyl-*ω*-4-vinylbenzyl-poly(furfuryl glycidyl ether)-*block*-poly(ethylene glycol) macromonomers (PFGE$_{10}$-*b*-PEG$_{25}$, PFGE$_8$-*b*-PEG$_{79}$, PFGE$_{18}$-*b*-PEG$_{66}$ and PFGE$_{13}$-*b*-PEG$_{111}$) using sequential living anionic ring opening polymerization.

During optimization of the macromonomer synthesis, first the polymerization of the PFGE-block was investigated similar to Barthel *et al* (2012). In our experiments, PFGE homopolymers with molar masses $M_{n,SEC}$ between 1 022 g mol^{-1} and 3 699 g mol^{-1} and low molar mass dispersities $Đ_{SEC}$ (1.10 ≤ $Đ$ ≤ 1.16) were obtained, which are comparable to Barthel *et al*. (2012). In these cases, the resulting molar masses could be adjusted by the MIR ratio. Upon increasing the MIR, higher number average molar masses $M_{n,SEC}$ up to 14 000 g mol^{-1} could be acchieved, however, with relatively large $Đ$ values around 1.92, probably due to chain transfer reactions (Gatzke 1969). Similar results were found using potassium naphthanelide as an initiator. Interestingly, in contrast to Barthel *et al*. (2012), no conversion was observed with potassium *tert*-butoxide as an initiator. Due to the better storage stability of DPMK solutions compared to potassium naphthanelide solutions, the macromonomer sytheses were carried out using DPMK. Also, targeted molar masses of the PFGE blocks were not higher than 3 000 g mol^{-1} in order to ensure that the majority of the PFGE-chain ends were "alive" when EO was added to the reaction mixture.

Due to the absence of side reactions during AROP of EO in THF (Nagasaki *et al.* 1995), no specific optimization was necessary for the synthesis of the hydrophilic block. Termination of the reaction was carried out either with acryloyl chloride or 4VBC. However, termination with acryloyl chloride resulted in insoluble products, possibly due to a Diels-Alder reaction between the acryloyl group and the furan moieties or auto polymerization (Hiyoshizo *et al.* 1984). On the other hand, termination with 4VBC resulted in products with good solubility in organic solvents like MeOH, THF and $CHCl_3$. In contrast to $PFGE_{10}$-*b*-PEG_{25}, the three macromonomers $PFGE_8$-*b*-PEG_{79}, $PFGE_{18}$-*b*-PEG_{66} and $PFGE_{13}$-*b*-PEG_{111} were soluble in water, which makes them appealing for the usage in hydrogel systems. In summary this approach enabled us to synthesize $PFGE_p$-*b*-PEG_q macromonomers with 25 to 111 EO repeating units and 8 to 18 FGE repeating units, whereby each FGE repeating unit contributes one furfuryl anchor point.

Characterization of macromonomer composition. ^1H NMR and ^{13}C NMR spectra in Figure 10 and Figure 14 - Figure 21 indicated a successful synthesis of $PFGE_p$-*b*-PEG_q macromonomers. The ^1H NMR signals of the furfuryl glycidyl ether at 4.41 ppm and 6.26 ppm as well as the EO repeating units from 3.22 ppm to 3.72 ppm were in accordance with the literature (Barthel *et al.* 2012, Truong *et al.* 2017). Also FT-IR spectroscopy in Figure 27 showed the presence of the furan moieties at 3117 cm^{-1} (Barthel *et al.* 2012, Truong *et al.* 2017). Furthermore, the ^1H NMR spectra in Figure 10 and Figure 14 - Figure 17 proved the absence of remaining monomer because no epoxide signals were detected (Karateev *et al.* 2008). Also signals belonging to the initiator DPMK at 4.13 ppm (o) and 7.12 ppm – 7.24 ppm (p) and to the vinylbenzyl end group at 4.55 ppm (j), 5.22 ppm – 5.24 ppm (n), 5.72 ppm – 5.75 ppm (n) and 6.69 ppm – 7.13 ppm (m) were found.

PEG- and PFGE-block lengths were calculated according to equations (4) and (5) and the following average compositions were obtained: $PFGE_{10}$-*b*-PEG_{25}, $PFGE_8$-*b*-PEG_{79}, $PFGE_{18}$-*b*-PEG_{66} and $PFGE_{13}$-*b*-PEG_{111}. These block lengths were quite close to the targeted values (Table 4), showing the good control over molar masses and block length ratios by tuning the MIR. Reasons for divergence between the targeted and synthesized macromonomers might be found in uncertainties during the titration of the initiator concentration or the handling of small monomer amounts (especially EO) under dry conditions.

To be able to use the macromonomers as multifunctional building block for hydrogel functionalization, a high end group functionalization is of crucial importance. The end group functionalization degree f was calculated according to equation (3) from the ^{1}H NMR spectra in Figure 10 and Figure 14 - Figure 17. Resulting f values were rather high with 98 % for PFGE$_{18}$-b-PEG$_{66}$, 92 % for both PFGE$_{10}$-b-PEG$_{25}$ and PFGE$_{13}$-b-PEG$_{111}$, and 72 % for PFGE$_8$-b-PEG$_{79}$ (Table 2). Schlaad et $al.$ determined end group functionalizations of their $α,ω$-bifunctional PEGs between 80% - 100%, which is in the range of our results (Schlaad et $al.$ 2001). This indicates that the macromonomer synthesis generally proceeded in a controlled, living way with an efficient termination reaction using 4VBC.
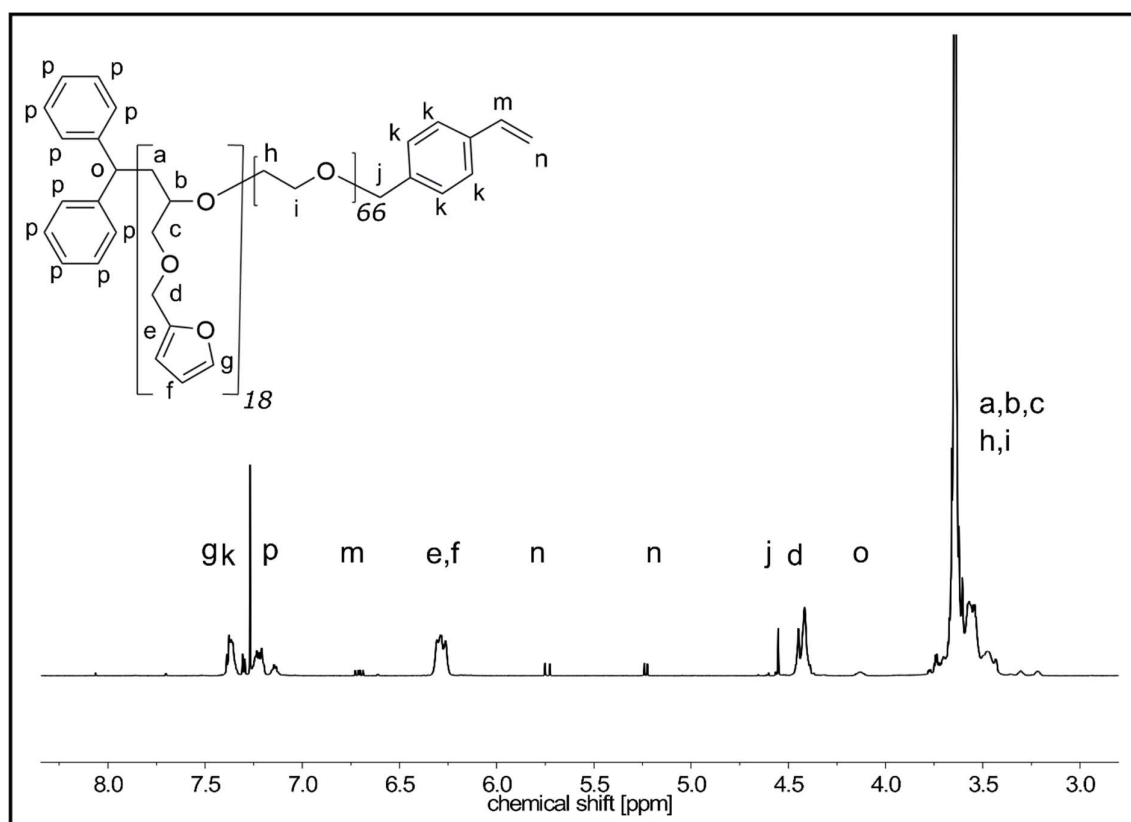

Figure 10: ^{1}H NMR spectrum of macromonomer PFGE$_{18}$-b-PEG$_{66}$.

In order to further shed light into the outcome of the macromonomer synthesis, the molar mass distributions (MMD) were analyzed by SEC and MALDI TOF MS (Figure 11and Figure 22). The SEC measurements showed that all four macromonomers had a monomodal and narrowly distributed MMD with a $Đ_{SEC}$ of 1.05 – 1.09 (Figure 11), similar as reported before FGE-based block copolymers (Barthel et $al.$ 2012). The number average molar masses $M_{n,SEC}$ were in the same range of the number average

molar masses $M_{n,NMR}$ determined by ^{1}H NMR spectroscopy (Table 2). Similar results were obtained by MALDI TOF MS (Figure 11b, Figure 22 and Table 2), with lower masses compared to SEC probably caused by mass discrimination during the MALDI TOF MS measurements or due to the relative molar masses obtained by SEC (Mori *et al.* 2013, Nielen 1999, Wu *et al.* 1998). MALDI TOF MS furthermore confirmed the absence of lower molar mass homopolymers which would show a distinct spacing between individual signals corresponding to the mass of the repeating units (154.06 Da for FGE and 44.03 Da for EO) (Barthel *et al.* 2012). In summary, the NMR, SEC and MALDI TOF MS data confirm the successful synthesis of well-defined vinylbenzyl terminated poly(furfuryl glycidyl ether)-*block*-poly(ethylene glycol) macromonomers in different block lengths, making them suitable multifunctional building blocks for hydrogel functionalization.
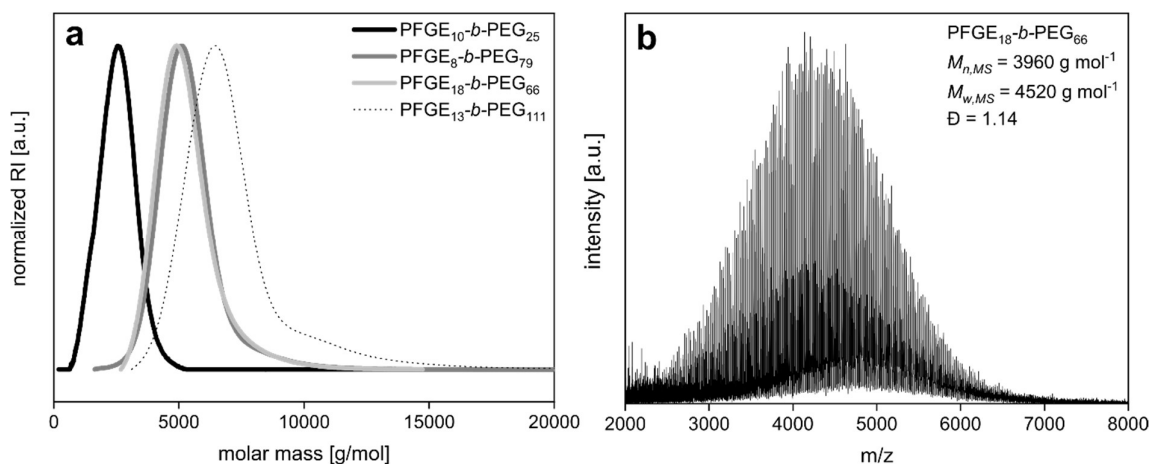

Figure 11: a) SEC traces of the studied macromonomers from Table 2 and b) MALDI TOF MS spectrum of PFGE$_{18}$-*b*-PEG$_{66}$. The MALDI TOF MS spectra from PFGE$_{10}$-*b*-PEG$_{25,}$ PFGE$_8$-*b*-PEG$_{79}$ and PFGE$_{13}$-*b*-PEG$_{111}$ are given in Figure 22.

To deepen the knowledge of the structure-property relations of the synthesized macromonomers, the thermal properties were investigated. For this, the thermal properties of the macromonomers were characterized by DSC and TGA as shown in Figure 24 and are summarized in Table 3. Glass transition temperatures T_g were determined to be between -43 °C and -32 °C and melting temperatures between 32 °C and 45 °C.

Only one distinct T_g was observed for all macromonomers which can be attributed to the PFGE-segments. The T_g of PFGE homopolymers was previously reported to be at -40 °C (Barthel *et al.* 2013b, Roos *et al.* 2016). In this study, no second T_g at -79 °C

was observed in contrast to a report on PFGE-*b*-PEG (PFGE$_{10}$-*b*-PEG$_{330}$ and PFGE$_{20}$-*b*-PEG$_{330}$) block copolymers (Barthel *et al.* 2013b). The presence of two separated T_g values was interpreted as a hint for phase separation (Barthel *et al.* 2013b). The present macromonomers therefore might not show similar phase separation due to lower molar masses (2 927 g mol^{-1} – 7 177 g mol^{-1}) than the reported ones (16 000 g mol^{-1} – 17 600 g mol^{-1}) (Barthel *et al.* 2013b). However, then one would expect a shift of T_g to lower temperatures with higher PEG content as described for example for statistic poly(furfuryl glycidyl ether)-*co*-poly(propylene oxide) copolymers (Roos *et al.* 2016). Therefore, we rather tend to the conclusion that the T_g signal during DSC analysis is too shallow to be analyzed as is often observed for PEG (Faucher *et al.* 1966). This reasoning is further supported by the pronounced melting peaks in the DSC at a melting temperature T_m around 40 °C which were attributed to the PEG segments, as PEG (molar mass ~ 4,000 g mol-1) has a T_m of 56 °C and the homopolymer PFGE$_{55}$ does not exhibit a melting temperature between -100 °C and 125 °C (Barthel *et al.* 2013b, Lloyd *et al.* 1997). The melting enthalpy (ΔH_m) increased from 0.16 g J^{-1} for PFGE$_{10}$-*b*-PEG$_{25}$ to 75.04 g J^{-1} to PFGE$_{13}$-*b*-PEG$_{111}$ with growing PEG-block length (Table 3).This is in line with reports from the Zhou group, who also measured higher ΔH_m values for their poly(ethylene 2,5-furandicarboxylate)-*block*-poly(ethylene glycol) block copolymers with increasing PEG content (Wang *et al.* 2017).

Table 2: Number average molar masses (M_n) and mass average molar masses (M_w), molar mass dispersity (*Đ*) and end group functionalization degree (*f*) of the PFGE$_p$-*b*-PEG$_q$ macromonomers in this study. The indices refer to the determination method: NMR = nuclear magnetic resonance spectroscopy, SEC = size exclusion chromatography and MS = MALDI TOF mass spectrometry.

sample	$M_{n,NMR}$ [g mol^{-1}]	$M_{n,SEC}$ [g mol^{-1}]	$M_{w,SEC}$ [g mol^{-1}]	$Đ_{SEC}$	$M_{n,MS}$ [g mol^{-1}]	$M_{w,MS}$ [g mol^{-1}]	$Đ_{MS}$	*f* [%]
PFGE$_{10}$-*b*-PEG$_{25}$	2 930	2 320	2 550	1.09	1 950	2 150	1.10	92
PFGE$_8$-*b*-PEG$_{79}$	5 000	5 140	5 450	1.06	3 760	4 260	1.13	72
PFGE$_{18}$-*b*-PEG$_{66}$	5 970	5 110	5 430	1.06	3 960	4 520	1.14	98
PFGE$_{13}$-*b*-PEG$_{111}$	7 180	6 660	7 300	1.09	5 590	6 480	1.16	92

Thermal properties of macromonomers. Additionally, the macromonomer decomposition temperatures T_d were determined by TGA (Figure 23b). The macromonomers showed T_d values between 369 °C and 381 °C and a thermal stability of approximately 330 °C under nitrogen. This fits very well to the reported thermal

stability of 335 °C for PFGE-*b*-PEG block copolymers (Barthel *et al.* 2013b), revealing that the end group functionalization has a minor effect on the thermal properties. Our macromonomers exhibit excellent thermal stability under nitrogen atmosphere with decomposition temperatures at 5% mass loss ($T_{d,5}$) over 355 °C compared to other very stable PEG based block copolymers with $T_{d,5}$ of 300 °C (Table 3) (Wang *et al.* 2017).

Surface activity of macromonomers. Due to their amphiphilic structure with on the one hand a hydrophilic PEG-block end functionalized with a hydrophobic vinylbenzyl group and on the other hand a hydrophobic PFGE block, the surface activity of the macromonomers was analyzed by tensiometry. One key value for surface active substances is their cmc, which defines the surfactant concentration above which the surface is saturated with surfactant molecules and micelles are formed. Similar to Schramm and Green (1992), the surface tension of aqueous macromonomer solutions was measured at different concentrations between 0.08 mg mL^{-1} and 5.00 mg mL^{-1}. As demonstrated in Figure 12 the surface tension decreased with increasing macromonomer concentration until a plateau was reached at approximately 52 mN m^{-1}. The cmc values were obtained at the intersection between the extrapolated line of the concentration dependent region and the line passing through the plateau (Patist *et al.* 2000). Cmc values were determined to be 0.25 mg mL^{-1} (0.04 mM) for PFGE$_{18}$-*b*-PEG$_{66}$, 0.32 mg mL^{-1} (0.06 mM) for PFGE$_8$-*b*-PEG$_{79}$ and 0.33 mg mL^{-1} (0.05 mM) for PFGE$_{13}$-*b*-PEG$_{111}$ (Table 3).

For PFGE$_{10}$-*b*-PEG$_{25}$ a cmc could not be measured due to lacking solubility in water caused by the relatively short PEG-block. The cmc values of the other three water soluble macromonomers fit into the cmc range of non-ionic PEG-based block copolymers like Pluronic P85 (PEO$_{26}$-PPO$_{40}$-PEO$_{26}$, molar mass = 4 600 g mol^{-1}) with a cmc of 0.06 mM (Kabanov *et al.* 2002).

Owen *et al.* (2012) explained that for block copolymers an increase of the hydrophobic chain length correlates with an increased micelle stability and therefore reduces the cmc values. As the macromonomers did not have a constant hydrophilic block length, the cmc dependency was evaluated regarding the hydrophilic to hydrophobic block length ratio *B* (equation(6)).
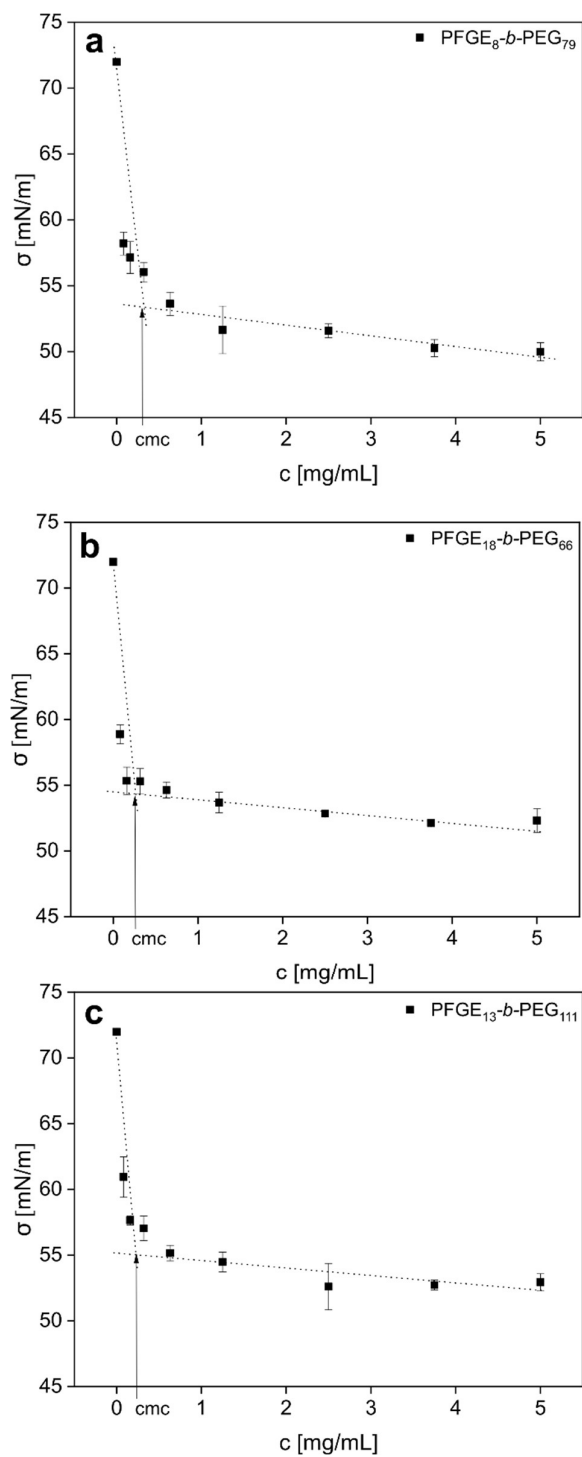
Figure 12: Surface tension (σ) of aqueous macromonomer solutions at different concentrations (c). The critical micelle concentration (cmc) of macromonomers a) PFGE$_8$-b-PEG$_{79}$, b) PFGE$_{18}$-b-PEG$_{66}$ and c) PFGE$_{13}$-b-PEG$_{111}$ was determined at the intersection between the extrapolated line of the concentration dependent region and the line passing through the concentration plateau. The cmc is marked with an arrow.

For B (PFGE$_{18}$-b-PEG$_{66}$) = 3.5 the cmc was 0.04 mM, for B (PFGE$_{13}$-b-PEG$_{111}$) = 8.1 the cmc was 0.05 mM and for B (PFGE$_8$-b-PEG$_{79}$) = 8.6 the cmc was 0.06 mM, which

means that with increasing B the cmc increases. Therefore, our observations fit to the conclusions of Owen *et al.* (2012). Similar observations were reported by Adams and Kwon *et al.* (2002, 2003a) for poly(ethylene oxide)-*block*-poly(*N*-hexyl-L-aspartamide)-acyl copolymers and by Gaucher *et al.* (2005) for polyvinylpyrrolidone-*block*-poly(D,L-lactide)-*block*-polyvinylpyrrolidon.

Table 3: Glass transition temperature (T_g), melting temperature (T_m), melting enthalpy (ΔH_m), decomposition temperature (T_d), decomposition temperature at 5 % mass loss ($T_{d,5}$) and critical micelle concentration (cmc) of the studied PFGE$_p$-*b*-PEG$_q$ macromonomers. T_g, T_m and ΔH_m were determined by differential scanning calorimetry. T_d and $T_{d,5}$ were measured by thermogravimetric analysis and the cmc was obtained using bubble pressure tensiometry.

sample	T_g [°C]	T_m [°C]	ΔH_m [J g^{-1}]	T_d [°C]	$T_{d,5}$ [°C]	cmc [mg mL^{-1}]	cmc [mM]
PFGE$_{10}$-*b*-PEG$_{25}$	-43	44	0.16	369	355	/	/
PFGE$_8$-*b*-PEG$_{79}$	-33	43	74.06	381	365	0.32	0.06
PFGE$_{18}$-*b*-PEG$_{66}$	-32	32	47.25	377	380	0.25	0.04
PFGE$_{13}$-*b*-PEG$_{111}$	-33	45	75.04	377	372	0.33	0.05

Hydrogel functionalization. In order to create functional hydrogels with multiple furan anchor points, we need to ensure that all functionalities of our multifunctional PFGE$_p$-*b*-PEG$_q$ building blocks are reactive and accessible. In particular, the furan groups of our macromonomer need to be able to undergo Diels-Alder click reactions and the 4-vinylbenzyl end group has to covalently bind to hydrogels.

To investigate the first, we observed the Diels-Alder reaction of the block copolymer PFGE$_8$-*b*-PEG$_{79}$ with the model substrate *N*-ethylmaleimide (NEM) *via* ^{1}H NMR spectroscopy. After 24 h at room temperature we obtained a conversion of the Diels-Alder reaction C_{DA} of 75 %, whereby the newly emerged Diels-Alder product signals at 2.83 ppm, 2.91 ppm and 5.24 ppm in Figure 25 are in accordance with the literature (Elter *et al.* 2018). The conversion C_{DA} is similar to Habibi *et al.* who published a C_{DA} of 71 % for their furan-maleimide based Diels-Alder reaction (Buono *et al.* 2017). We could increase C_{DA} from 31 % to 75 % by using water instead of THF as solvent. The supporting effect of water during Diels-Alder reactions due to hydrogen bond interactions and solvatophobic effects is intensively discussed in the literature (Chiappe *et al.* 2010, Rideout *et al.* 1980). This makes it especially interesting to use the Diels-Alder reaction for post-synthetic modification reactions in hydrogels. In

conclusion we could proof that the furan side chains of our macromonomers provide the desired reactivity and accessibility for Diels-Alder reactions.

In the next step we examined the reactivity of the 4-vinylbenzyl group by polymerizing the macromonomers into radically cross-linked p(Aam) hydrogels with MBA as cross-linker. The functionalized p(Aam) hydrogels contained 1 w % macromonomer in contrast to unfunctionalized hydrogels, where the macromonomer was substituted by water. ATR-IR measurements in Figure 27 of the functionalized and unfunctionalized p(Aam) hydrogels revealed that the functionalized hydrogels showed two new vibrational bands at $2\,870$ cm^{-1} and $1\,110$ cm^{-1} compared to the unfunctionalized p(Aam) hydrogels. The vibrational band at $2\,870$ cm^{-1} can be assigned to the CH stretching mode of the PEG backbone (Shinzawa *et al.* 2017) and the signal increase at $1\,110$ cm^{-1} is attributed to asymmetric ether stretching vibration of PEG backbone of the macromonomers (McCullough *et al.* 2013). The furan signal of the macromonomer at $3\,120$ cm^{-1} from Figure 23 could not be detected because of the strong overlapping CH and NH vibration bands between $2\,980$ cm^{-1} and $3\,660$ cm^{-1} of the p(Aam) hydrogel (Murugan *et al.* 1998). Furthermore, there is an optical difference after drying between the yellowish functionalized and colorless unfunctionalized hydrogels as shown in Figure 26. The yellow color is most probably based on aging processes of the furans, which were studied intensively by Taher and Cates (Taher *et al.* 1974). In conclusion, the appearance of two new IR bands and the color difference of the functionalized hydrogels compared to the unfunctionalized hydrogel indicate that the macromonomers were covalently incorporated into the p(Aam) hydrogels, which confirms that the 4-vinylbenzyl end group can be used as polymerizable unit of the macromonomers.

The functionalized and unfunctionalized p(Aam) hydrogels were furthermore characterized regarding their gel yield (Y_g) and their equilibrium swelling degree (EDS). As shown in Figure 30, Y_g of all hydrogels are roughly in the same region between 111 % ± 2 % and 121 % ± 5 %. The Y_g of the unfunctionalized p(Aam) hydrogel is significantly higher (Y_g = 121 % ± 5 %) compared to the functionalized hydrogels (Y_g = 111 % ± 2 % -113 % ± 0 %) but still in the same range. This means that the photo polymerizations of the p(Aam) hydrogels were successful and the hydrogels are comparable among each other. The range of the Y_g is in accordance with the literature, where gel yields between 105 % - 125 % are reported for p(Aam) hydrogels with 0.2 %

to 1.0 % MBA (Götz *et al.* 2018). As explained in the literature gravimetrically determined gel yields above 100 % are a result of remaining water in the hydrogels after drying because of the strong hydrogen bonds with the amide groups in the polymer network (Götz *et al.* 2018, Zhang *et al.* 2015). Moreover, the EDS of the unfunctionalized p(Aam) hydrogels with 432 % ± 7 % is significantly higher than the EDS of functionalized hydrogels with EDS values between 393 % ± 1 % and 402 % ± 7 %. The literature shows the higher the MBA content, the higher the cross-linking rate and therefore the lower the EDS of the respective p(Aam) hydrogel (Götz *et al.* 2018) For example for p(Aam) hydrogels with 1 % MBA the EDS is around 1 100 % and for 0.2 % MBA the EDS increases to roughly 1 700 %.(Götz *et al.* 2018) Hence, our EDS values around 400 % seem reasonable for p(Aam) hydrogels with 2 % MBA. All Y_g and EDS are summarized in Table 5.

After confirming the reactivity of our multifunctional $PFGE_p$-*b*-PEG_q building blocks, we investigated whether the furan groups are still intact and accessible within the hydrogels. Therefore we incubated the functionalized and unfunctionalized hydrogels with the fluorescence dye Atto 488 maleimide, so that the maleimides of the dye could react in a Diels-Alder reaction with the furan groups of the hydrogel bound macromonomers (Diels *et al.* 1926). The molecular structure of Atto 488 maleimide and the reaction of the fluorescent dye with our macromonomers are shown in Figure 28 - Figure 29. The labeled gels were washed five times to minimize unspecific binding and subsequently analyzed with confocal LSM. In Figure 13a – Figure 13d the maximum intensity projections of the functionalized and unfunctionalized p(Aam) hydrogels are shown.

The functionalized hydrogels in Figure 13a – Figure 13c exhibit much stronger green fluorescence signals than their unfunctionalized counterpart in Figure 13d. To quantify the fluorescence signal of the fluorescence labeled hydrogels the histograms of the maximum intensity projection from Figure 32 were converted according equation (1). The results of the fluorescence quantification are summarized in Figure 13e, which demonstrates fluorescence intensities *I* between 71 ± 1 and 79 ± 5 for hydrogels with macromonomer and a significantly lower *I* of 6 ± 1 for the unfunctionalized hydrogels. The remaining fluorescence signal of the negative control is most probably due to unspecific interactions of the fluorescence marker and the hydrogel network. The significantly higher *I* of the functionalized hydrogels proof that the fluorescent dye binds

specifically to the furan side chains of the macromonomer and therefore leaves the hydrogel containing no macromonomer almost unlabeled. The experiments also confirm that the macromonomers can covalently bind to the hydrogels as the gels were washed for three days, changing the water twice a day, to remove unpolymerized material. Hynd *et al.* (2007) also used fluorescence labeling to verify the covalent incorporation of streptavidin-acrylamide into p(Aam) hydrogels and concluded ligand specific binding between their streptavidin-functionalized hydrogel and their biotin-linked fluorescent marker as their functionalized hydrogel showed a significant higher fluorescence signal compared to the unfunctionalized hydrogel.
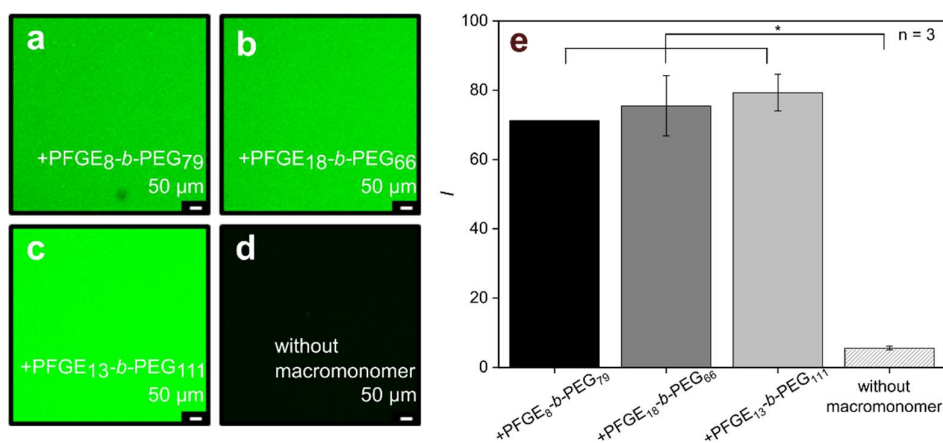
Figure 13: Maximum intensity projection (MIP) of light scanning microscopy (LSM) measurements from fluorescence labeled polyacrylamide (p(Aam)) hydrogels with macromonomers a) PFGE$_8$-*b*-PEG$_{79}$, b) PFGE$_{18}$-*b*-PEG$_{66}$, c) PFGE$_{13}$-*b*-PEG$_{111}$ compared to fluorescence labeled p(Aam) without macromonomer. E) Fluorescence intensity (*I*) of fluorescence labeled p(Aam) with and without macromonomers.

In summary, the fluorescence experiments showed that the macromonomers are able to bind covalently into p(Aam) hydrogels and that the water-soluble macromonomers are attractive multifunctional building blocks for the development of functional hydrogels with multiple clickable anchor points. Based on the fluorescence labeling experiments with the maleimide-functionalized dye, these multifunctional PFGE$_p$-*b*-PEG$_q$ building blocks open up the way to conjugate any molecule possessing maleimide groups onto the functional hydrogel using Diels-Alder reactions.

5.5 Conclusions

We developed functional hydrogels with multiple clickable anchor points for post-synthetic Diels-Alder reactions by using multifunctional PFGE$_p$-*b*-PEG$_q$ building blocks. For this, PFGE$_p$-*b*-PEG$_q$ macromonomers were synthesized *via* anionic ring opening

polymerization with in average 8 to 18 anchor points per building block. ^{1}H NMR analysis showed that the block lengths of our macromonomers are well adjustable and that a high end group functionalization degree f with 4-vinylbenzyl end groups between 72 % and 98 % could be achieved. This is important for the covalent incorporation of the macromonomers into the hydrogel. Furthermore, the macromonomer properties were measured by SEC, MALDI TOF MS, DSC, TGA and bubble pressure tensiometry to deepen the knowledge of the molecular structure and to understand the structure-property relations of the macromonomers. Beyond the polymer characterization, we demonstrated the intact reactivity and accessibility of the functional groups of the macromonomers in solution, as well as in hydrogel bound macromonomers. Fluorescence labeling experiments with a maleimide-functionalized dye proved that it was not only possible to functionalize polyacrylamide hydrogels with the PFGE$_p$-b-PEG$_q$ macromonomers, but that the furan groups also participate in post-synthetic Diels-Alder reactions. Hence, this elegant hydrogel functionalization strategy based on multifunctional furan building blocks might open up the way to conjugate any molecule possessing maleimide groups to the hydrogel using Diels-Alder click reactions.

5.6 Acknowledgements

Conflicts of interest. The authors declare no conflict of interest.

5.7 Supporting information
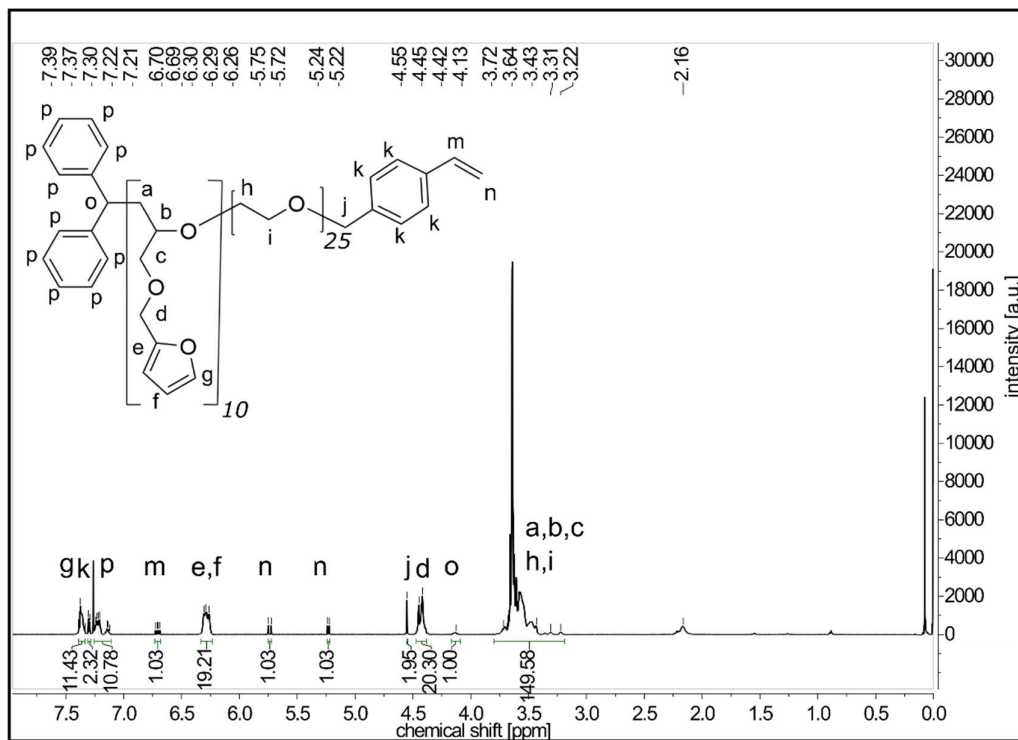
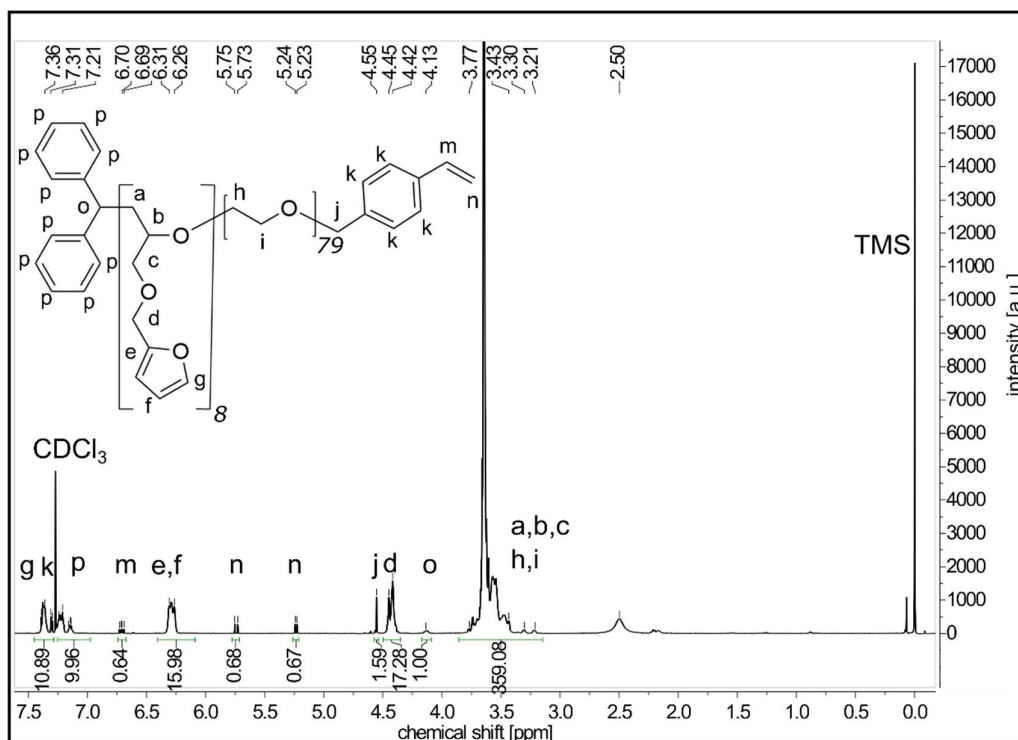Figure 14: ^{1}H NMR spectrum of macromonomer PFGE$_{10}$-*b*-PEG$_{25}$.

Figure 15: ^{1}H NMR spectrum of macromonomer PFGE$_8$-*b*-PEG$_{79}$.
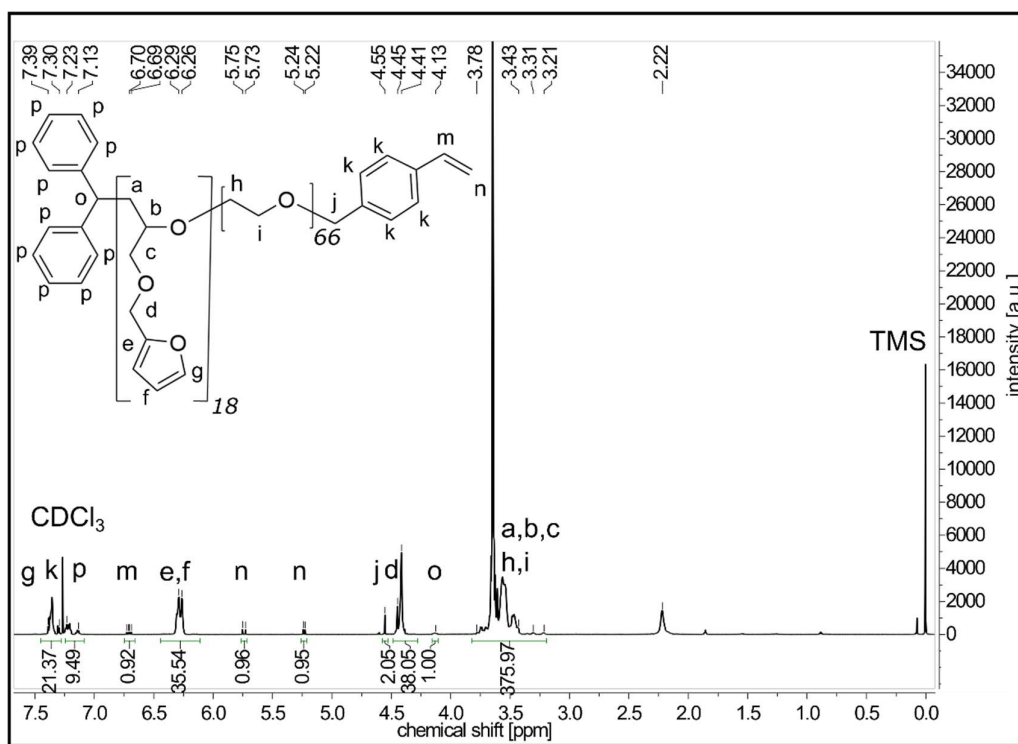
Figure 16: ^{1}H NMR spectrum of macromonomer PFGE$_{18}$-*b*-PEG$_{66}$.
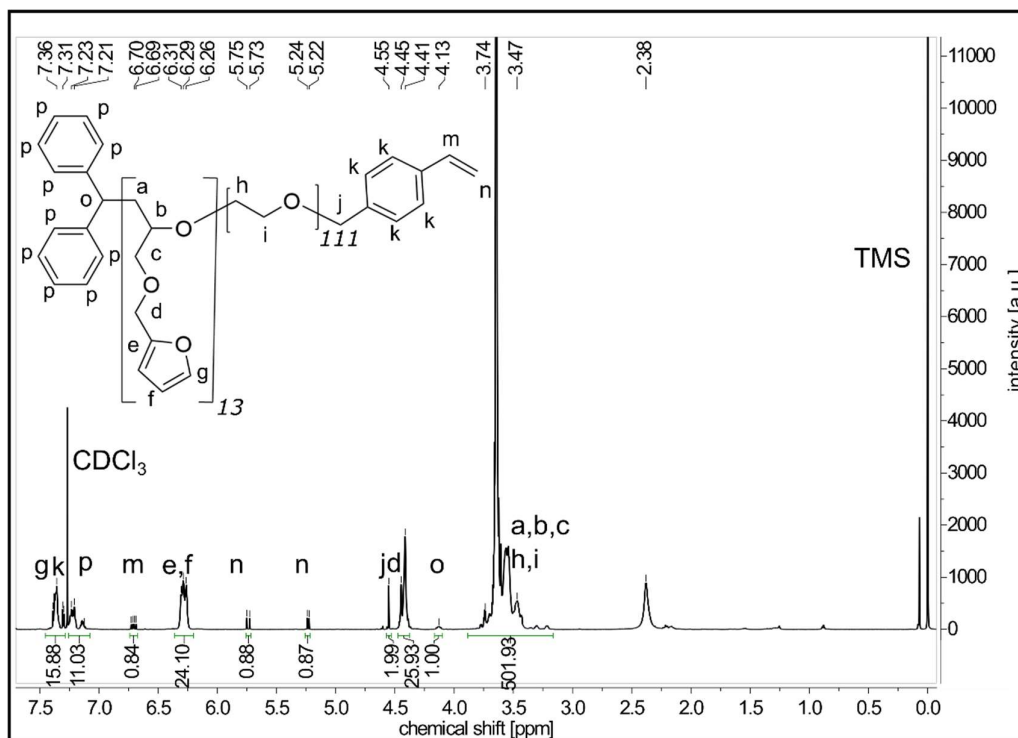
Figure 17: ^{1}H NMR spectrum of macromonomer PFGE$_{13}$-*b*-PEG$_{111}$.
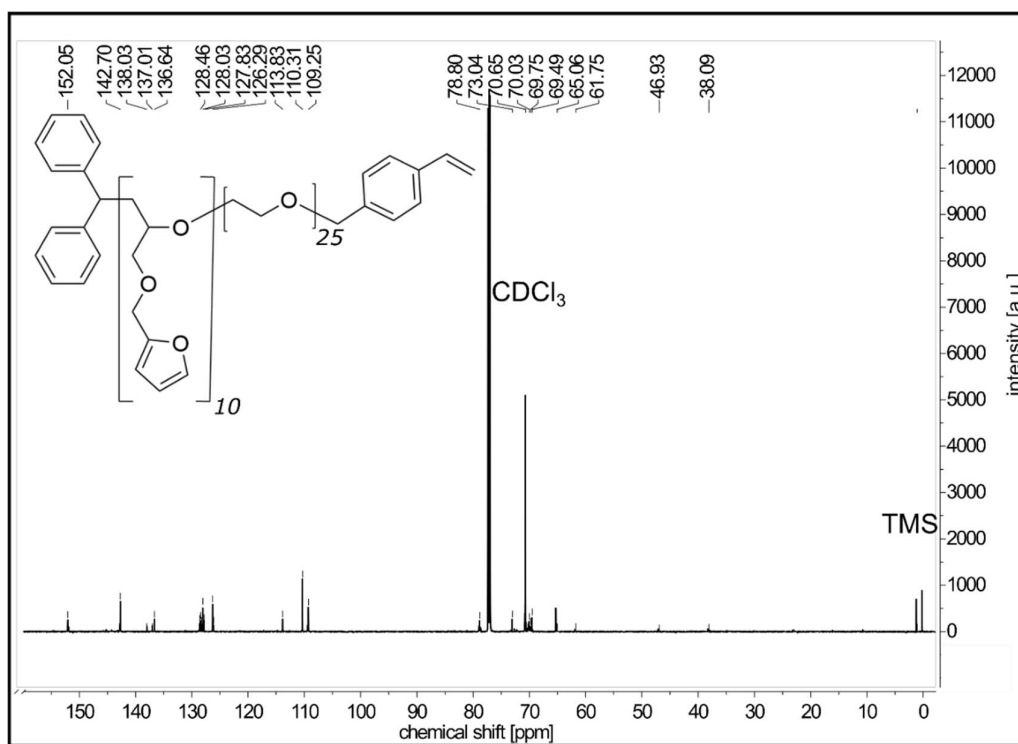
Figure 18: ^{13}C NMR spectrum of macromonomer PFGE$_{10}$-*b*-PEG$_{25}$.
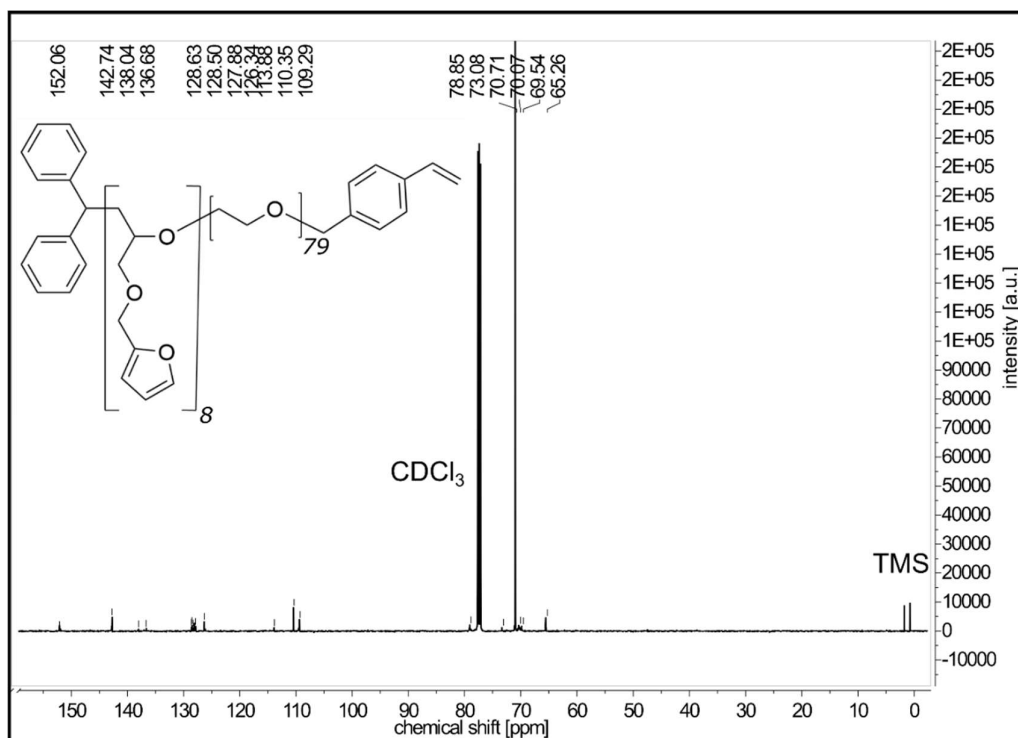
Figure 19: ^{13}C NMR spectrum of macromonomer PFGE$_8$-*b*-PEG$_{79}$.
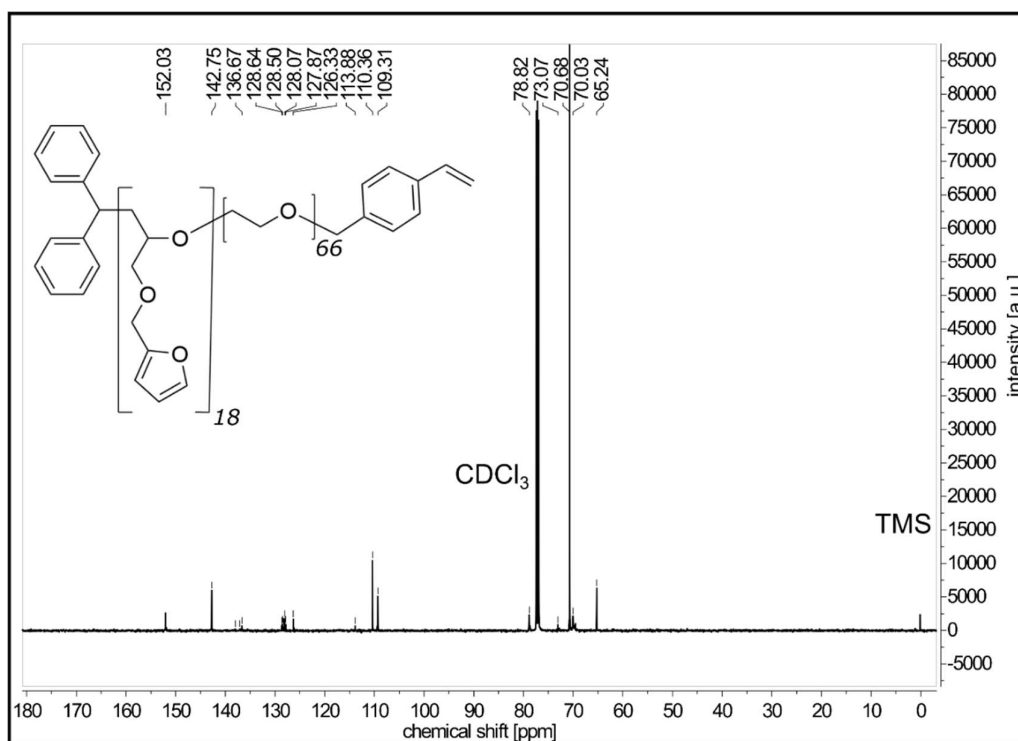
Figure 20: ^{13}C NMR spectrum of macromonomer PFGE$_{18}$-*b*-PEG$_{66}$.
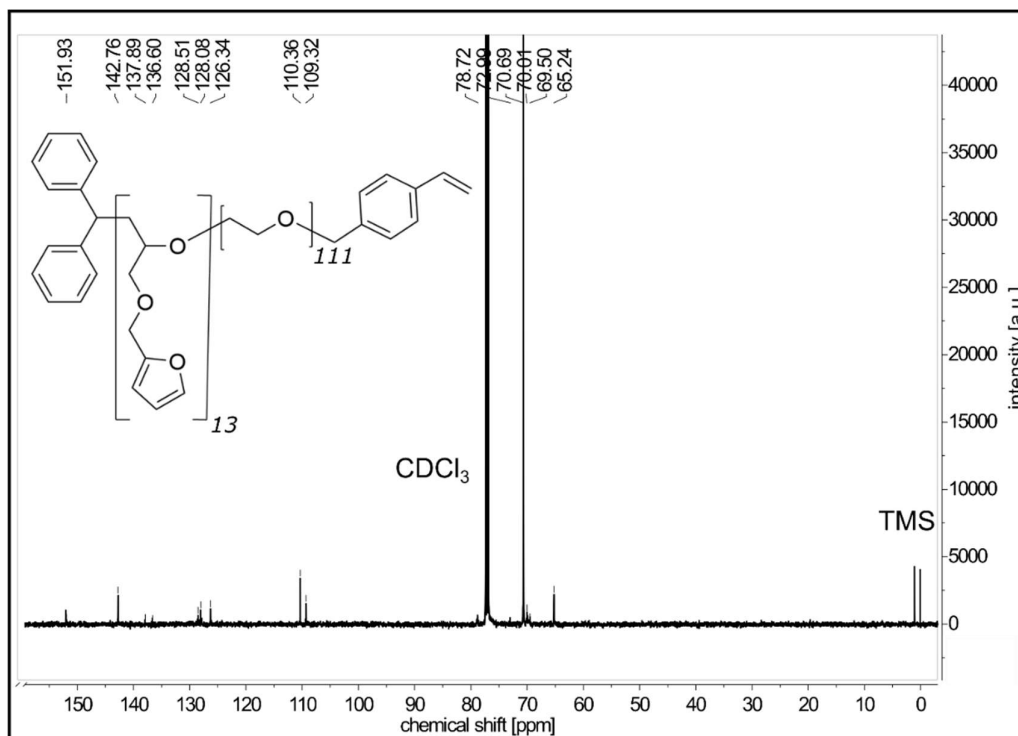

Figure 21: ^{13}C NMR spectrum of macromonomer PFGE$_{13}$-*b*-PEG$_{111}$.

Table 4: Number of poly(furfuryl glycidyl ether) repeating units (p), poly(ethylene oxide) repeating units (q) and block length ratio (B) determined by ^{1}H NMR. Targeted parameters are marked with the subscript "t" and experimentally obtained parameters are labeled with a subscripted "e". "Δ" indicates the difference between the targeted and the experimentally obtained parameters.

sample	p_t	p_e	Δp [%]	q_t	q_e	Δq [%]	B_t	B_e	ΔB [%]
PFGE$_{10}$-b-PEG$_{25}$	8	10	25	20	25	25	2.5	2.5	0
PFGE$_8$-b-PEG$_{79}$	8	8	0	69	79	15	9.9	8.6	13
PFGE$_{18}$-b-PEG$_{66}$	15	18	20	52	66	27	3.7	3.5	5
PFGE$_{13}$-b-PEG$_{111}$	15	13	13	121	111	8	8.5	8.1	5
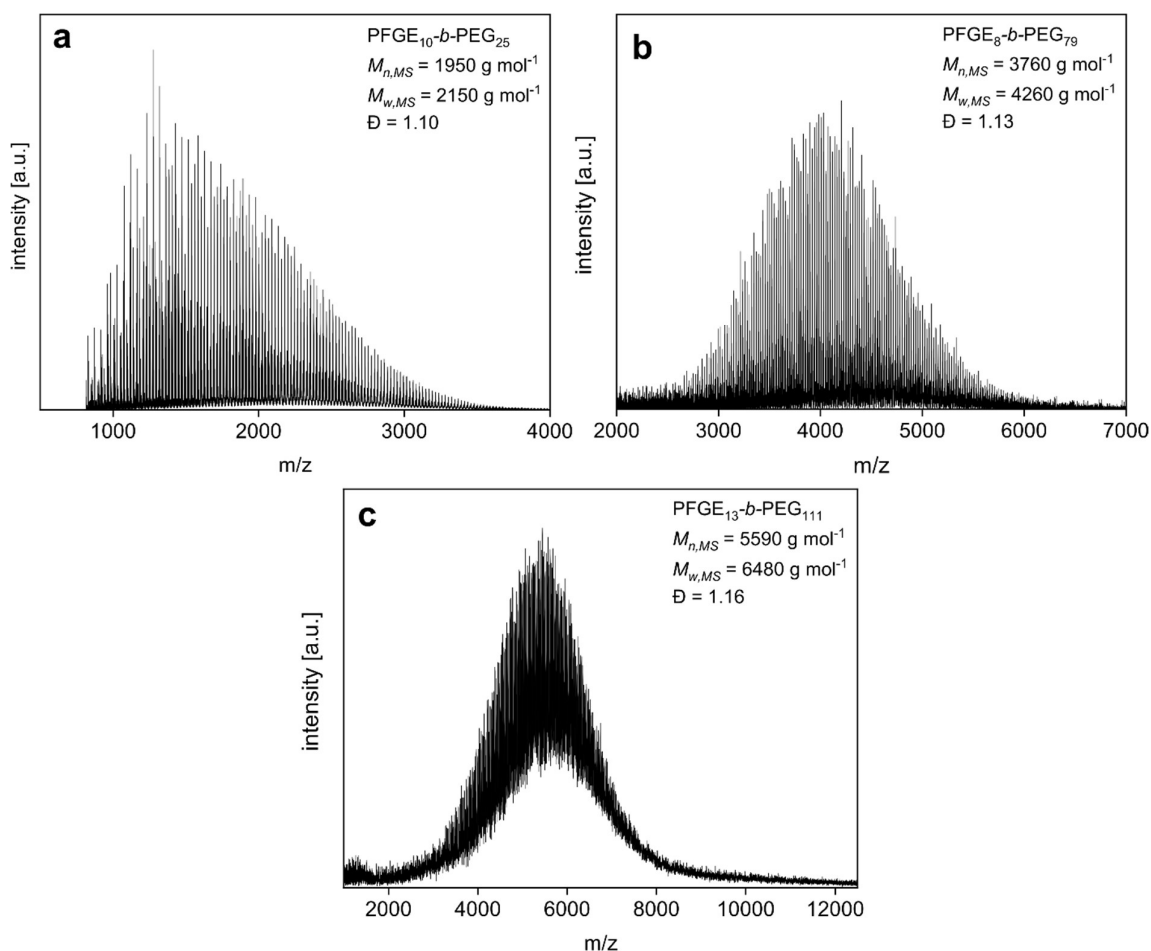
Figure 22: MALDI TOF MS spectra of macromonomers a) PFGE$_{10}$-b-PEG$_{25}$, b) PFGE$_8$-b-PEG$_{79}$ and c) PFGE$_{13}$-b-PEG$_{111}$.
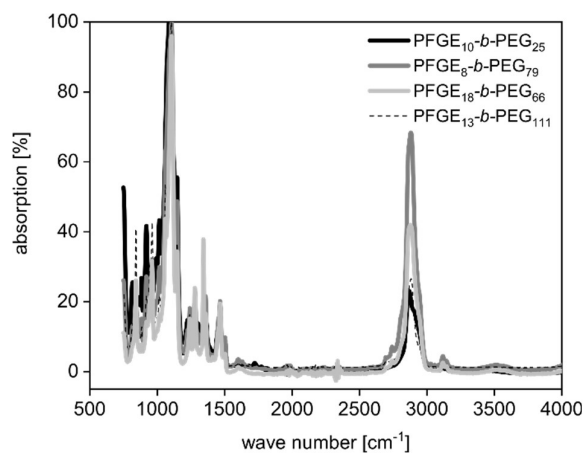
Figure 23: ATR-IR spectra of macromonomers PFGE$_{10}$-*b*-PEG$_{25}$, PFGE$_8$-*b*-PEG$_{79}$, PFGE$_{18}$-*b*-PEG$_{66}$ and PFGE$_{13}$-*b*-PEG$_{111}$.
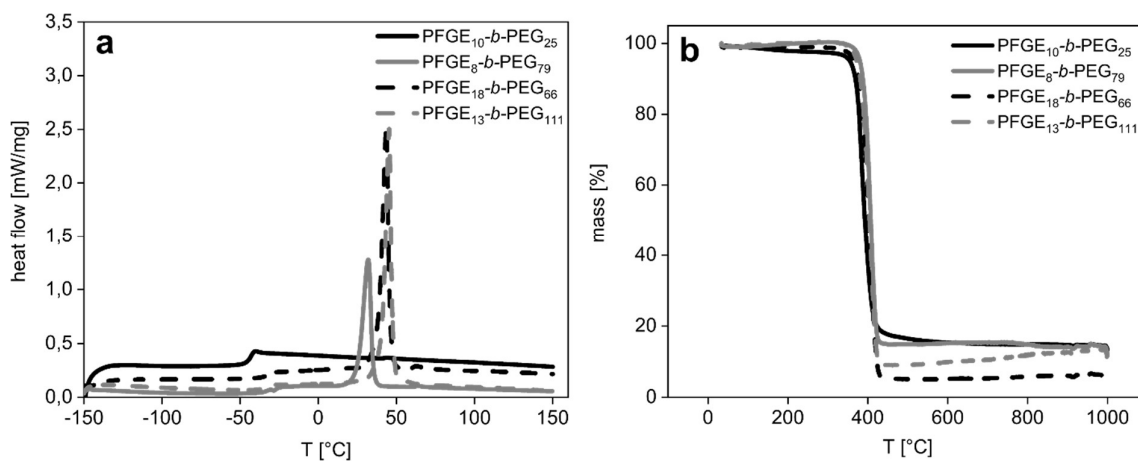
Figure 24: a) DSC thermograms and b) TGA measurements under nitrogen of macromonomers PFGE$_{10}$-*b*-PEG$_{25}$, PFGE$_8$-*b*-PEG$_{79}$, PFGE$_{18}$-*b*-PEG$_{66}$ and PFGE$_{13}$-*b*-PEG$_{111}$.

Figure 25: ^{1}H NMR spectrum of the Diels-Alder reaction between macromonomer PFGE$_8$-*b*-PEG$_{79}$ and *N*-ethylmaleimide (NEM).
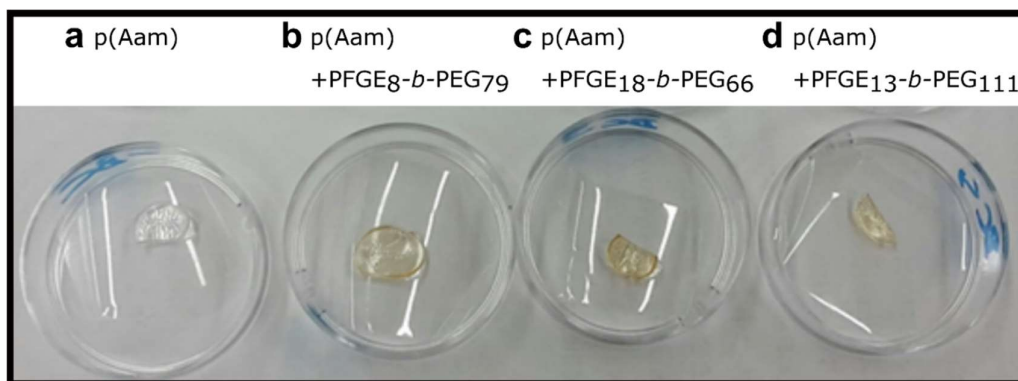
Figure 26: Photograph of dried a) unfunctionalized and functionalized polyacrylamide (p(Aam)) hydrogels with macromonomers b) PFGE$_8$-*b*-PEG$_{79}$ c) PFGE$_{18}$-*b*-PEG$_{66}$ and d) PFGE$_{13}$-*b*-PEG$_{111}$.

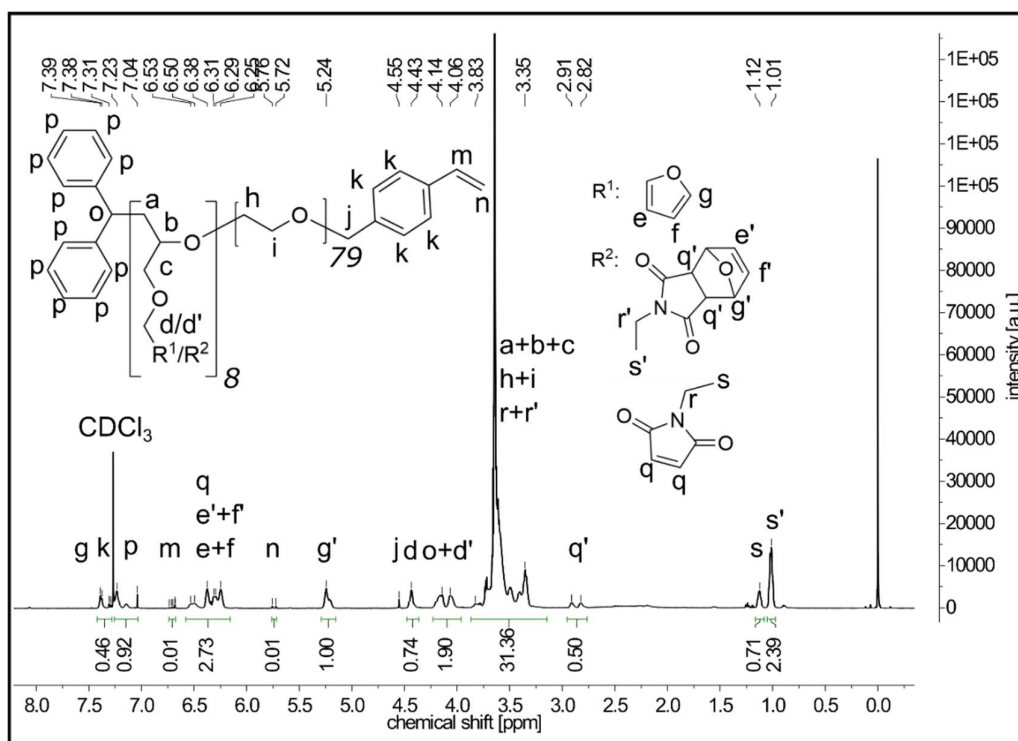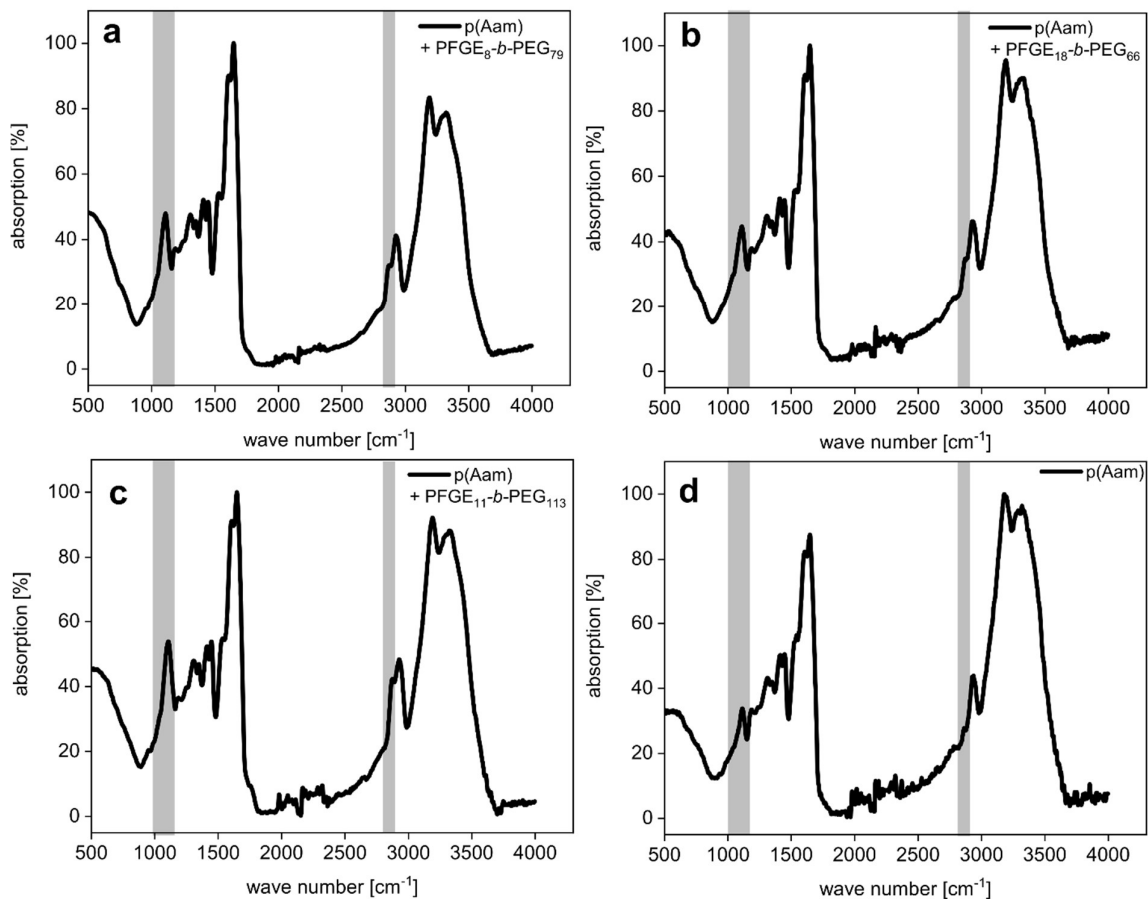Figure 27: ATR-IR spectra of functionalized polyacrylamide (p(Aam)) hydrogels with macromonomers a) $PFGE_8$-b-PEG_{79} b) $PFGE_{18}$-b-PEG_{66} and c) $PFGE_{13}$-b-PEG_{111}. in comparison to d) unfunctionalized p(Aam). The ether stretching vibration at 1 100 cm^{-1} and the CH stretching vibration at 2 870 cm^{-1} of the macromonomer back bone are highlighted in gray.
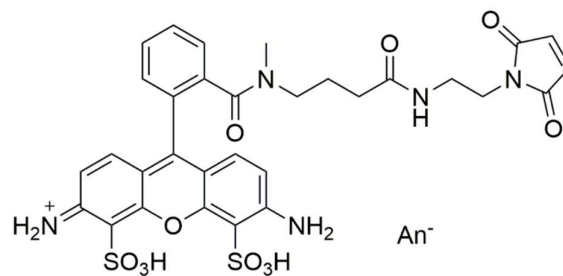
Figure 28: Molecular structure of the fluorescent dye Atto 488 maleimide.
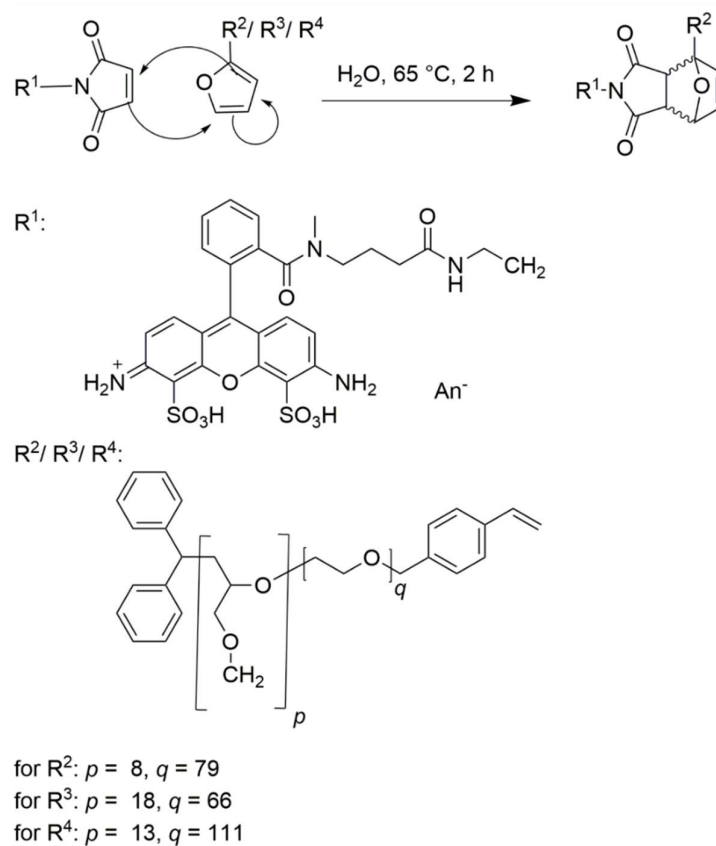
Figure 29: Diels-Alder reaction of the fluorescent dye Atto 488 maleimide and the macromonomers PFGE$_8$-*b*-PEG$_{79}$, PFGE$_{18}$-*b*-PEG$_{66}$ and PFGE$_{13}$-*b*-PEG$_{111}$.
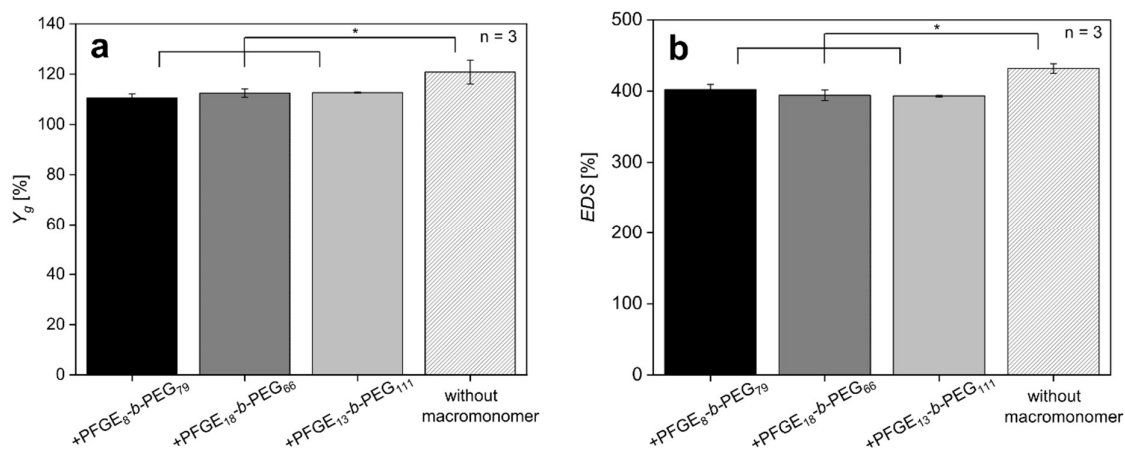
Figure 30: Gel yield (Y_g) and equilibrium degree of swelling (*EDS*) of functionalized polyacrylamide (p(Aam)) hydrogels with macromonomers PFGE$_8$-*b*-PEG$_{79}$, PFGE$_{18}$-*b*-PEG$_{66}$ and PFGE$_{13}$-*b*-PEG$_{111}$ in comparison to unfunctionalized p(Aam) hydrogels without macromonomer. * = p < 0.05.

_____

Table 5: Gel yield (Y_g) and equilibrium degree of swelling (*EDS*) of functionalized polyacrylamide (p(Aam)) hydrogels with macromonomers $PFGE_8$-*b*-PEG_{79}, $PFGE_{18}$-*b*-PEG_{66} and $PFGE_{13}$-*b*-PEG_{111} in comparison to unfunctionalized p(Aam) hydrogels without macromonomer. All experiments were repeated three times (n = 3). The figures are given as mean values ± standard deviation.

sample	Y_g [%]	*EDS* [%]
+ $PFGE_8$-*b*-PEG_{79}	111 ± 2	402 ± 1
+ $PFGE_{18}$-*b*-PEG_{66}	112 ± 2	394 ± 7
+ $PFGE_{13}$-*b*-PEG_{111}	113 ± 0	393 ± 1
without macromonomer	121 ± 5	432 ± 7
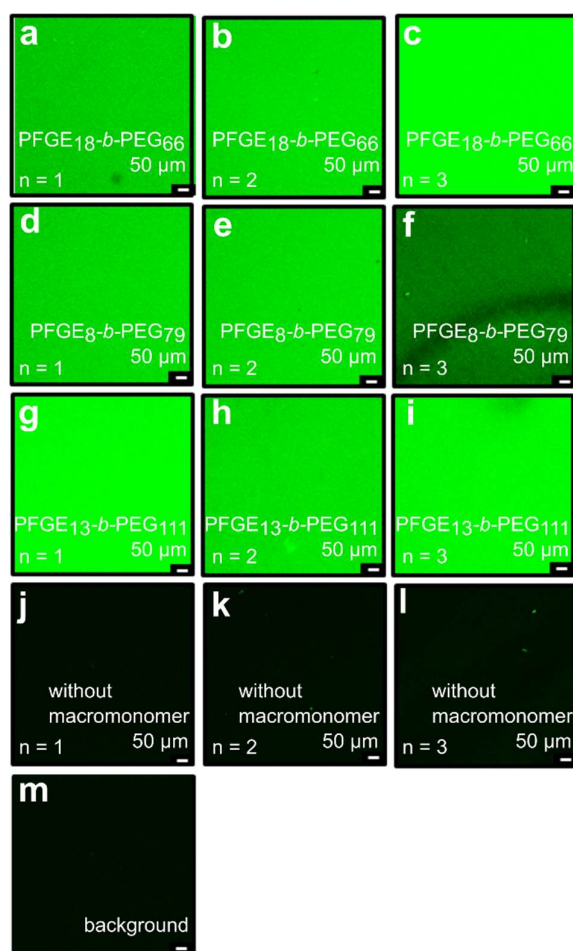
Figure 31: Maximum intensity projection (MIP) of fluorescence labeled polyacrylamide ((p(Aam)) hydrogels with macromonomers a – c) $PFGE_{18}$-*b*-PEG_{66}, d – f) $PFGE_8$-*b*-PEG_{79}, g – i) $PFGE_{13}$-*b*-PEG_{111} and j – l) p(Aam) hydrogels without macromonomer in comparison to m) the background signal.
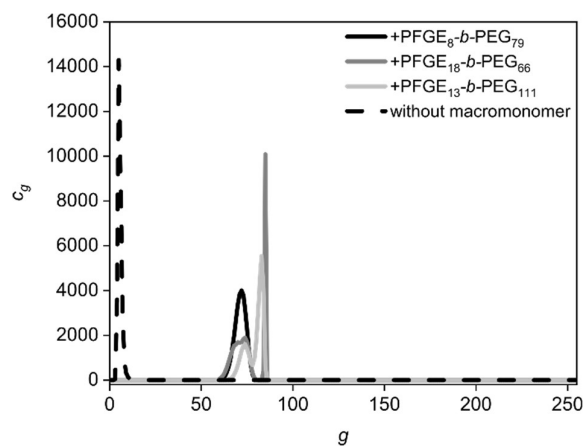
Figure 32: Histogram of fluorescence labeled polyacrylamide (p(Aam)) hydrogels with macromonomers PFGE$_8$-b-PEG$_{79}$, PFGE$_{18}$-b-PEG$_{66}$ and PFGE$_{13}$-b-PEG$_{111}$ compared to fluorescence labeled p(Aam) hydrogels without macromonomer.

6. Structure-property relations of amphiphilic poly(furfuryl glycidyl ether)-*block*-poly(ethylene glycol) macromonomers at the air-water interface

Authors: Karishma K. Adatia,[a,b] Alexander Holm,[b] Alexander Southan,[a*] Curtis W. Frank,[b*] and Günter E.M. Tovar[a,c*]

[a] Institute of Interfacial Process Engineering and Plasma Technology IGVP, University of Stuttgart, Nobelstr.12, D-70569 Stuttgart, Germany.

[b] Department of Chemical Engineering, Stanford University, Stanford, CA 94305, USA.

[c] Fraunhofer Institute for Interfacial Engineering and Biotechnology IGB, Nobelstr. 12, D-70569 Stuttgart, Germany.

* Corresponding authors: guenter.tovar@igvp.uni-stuttgart.de, cwfrank@stanford.edu, alexander.southan@igvp.uni-stuttgart.de.

Own contribution: I designed and conceived the whole research study. I performed all the experiments in this manuscript, such as the synthesis of the macromonomers, the characterization and the measurement of the Langmuir film balance experiments. The ^{1}H NMRs were recorded at the University of Stuttgart (IOC). I analyzed and interpreted all the data and wrote the manuscript.

6.1 Abstract

To deepen our knowledge of the film formation and the structure-property relations of poly(furfuryl glycidyl ether)-*block*-poly(ethylene glycol) ($PFGE_p$-*b*-PEG_q) macromonomers at the air-water interface, we synthesized $PFGE_p$-*b*-PEG_q in six different block lengths. The molar mass of the $PFGE_p$-*b*-PEG_q macromonomers varied from ~2 000 g mol^{-1} to ~7 000 g mol^{-1} and included a wide range of HLB values between 3.6 and 13.9. The π-A isotherms of these amphiphilic macromonomers revealed that the block lengths and the molar mass influence the isotherm shape and

onset. Smaller, more hydrophobic macromonomers (HLB < 8) showed a steeper surface pressure increase in the liquid condensed phase compared to larger, more hydrophilic macromonomers with HLB > 8. The molecular area for isotherm onsets increased almost linearly with growing molar mass of the macromonomers. Static and dynamic film stability measurements demonstrated limited stability of all macromonomer monolayers at the air-water interface. The more hydrophilic macromonomers $PFGE_8$-b-PEG_{79}, $PFGE_{18}$-b-PEG_{66} and $PFGE_{13}$-b-PEG_{111} (HLB > 8) showed higher film stability compared to the more hydrophobic macromonomers (HLB < 8). Hysteresis experiments displayed an almost linear increase of the film degradation with rising HLB values of the macromonomers. Due to partial film recovery of our macromonomers, we propose an interplay between a reversible folding and an irreversible submersion mechanism for the macromonomer monolayers at the air-water interface. The molecular structure and the film forming ability of the macromonomers at the air-water interface indicate that they are promising surface functionalization reagents for materials formed from aqueous solutions, such as hydrogels. In this regard, $PFGE_{10}$-b-PEG_9 is the most promising hydrogel surface functionalization reagent, because it can introduce the highest number of functional groups per surface area.

6.2 Introduction

The Langmuir film balance technique is a highly valuable method for the preparation and characterization of monolayers formed by amphiphilic molecules at the air-water interface (Brugger *et al.* 2010, Dynarowicz-Łątka *et al.* 2001, Langmuir 1917, Nutting *et al.* 1939, Shimizu *et al.* 2015).

In the last 100 years it has been applied to a broad range of substances such as small molecules (Fazio *et al.* 1998, Komitov *et al.* 1994, Modlińska *et al.* 2011), polymers (Faure *et al.* 1998, Miñones *et al.* 2009), particles (Holm *et al.* 2019), metal complexes (Liu *et al.* 1997, Yoo *et al.* 1999) and supra-molecular assemblies (Culp *et al.* 2002, Ni *et al.* 2004) to explore monolayer formation, molecular area per amphiphile, interfacial organization and film stability (Dynarowicz-Łątka *et al.* 2001).

In particular, amphiphilic macromolecules based on PEG, such as PEG-based poly(benzyl ether) monodendrons (Kampf *et al.* 1999), poly(ethylene glycol)-*block*-polystyrene (PEG-*b*-PS) (Da Silva *et al.* 1996, Faure *et al.* 1998, Fauré *et al.* 1999)

and PEGylated-lipomers (Baekmark *et al.* 1995) have been intensively investigated to broaden the knowledge of their molecular features at the air-water interface (Bijsterbosch *et al.* 1995, Cardenas-Valera *et al.* 1993, Joncheray *et al.* 2006, Malzert *et al.* 2001, Napoli *et al.* 2002). Kampf *et al.* (1999) for example demonstrated that the molecular area of PEG-based poly(benzyl ether) monodendrons grew linearly with the molar mass and that a longer hydrophilic tail improved the film stability. Furthermore, PEG-containing macromolecules often display conformational changes from pancake-like to mushroom-like to brush-like structures during monolayer compression (Baekmark *et al.* 1995). However, this model is not applicable to all PEG-containing polymers, as shown by Faure *et al.* for PEG-*b*-PS block copolymers (Faure *et al.* 1998). This indicates that the surface characteristics of PEG-based macromolecules are diverse, and each molecular composition may need individual exploration.

In the case of PFGE$_p$-*b*-PEG$_q$ macromonomers, there is almost no knowledge available regarding their behavior at the air-water interface. In fact, only the micelle formation in water of poly(furfuryl glycidyl ether)-*block*-poly(ethylene glycol) block copolymers and the critical micelle concentration of PFGE$_p$-*b*-PEG$_q$ macromonomers has been reported (Adatia *et al.* 2019, Barthel *et al.* 2012). In previous work, we used PFGE$_p$-*b*-PEG$_q$ macromonomers for hydrogel functionalization with multiple, clickable anchor points. The terminal 4-vinylbenzyl moiety of the macromonomer was utilized as a polymerizable unit for the covalent immobilization of the macromonomer in the hydrogel bulk and the furan side chains served as molecular anchor points for post-synthetic Diels-Alder reactions (Adatia *et al.* 2019). To explore whether PFGE$_p$-*b*-PEG$_q$ macromonomers are not only able to functionalize the hydrogel bulk, but also could self-assemble to form monolayers at the surface of aqueous solutions and thus result in hydrogel surface functionalization after curing, further knowledge about the film forming properties and the monolayer stability is needed. Surface functionalized hydrogels are especially attractive for tissue engineering (Brynda *et al.* 2009), drug delivery (Hu *et al.* 2016, Sajeesh *et al.* 2010) and biochemical applications (Hynd *et al.* 2007).

Therefore, PFGE$_p$-*b*-PEG$_q$ macromonomers with different average molar masses and block ratios were synthesized and characterized with the Langmuir film balance technique. This will contribute to a deeper understanding of the structure-property relations of PFGE$_p$-*b*-PEG$_q$ macromonomers at the air-water interface and facilitate an

evaluation of PFGE$_p$-*b*-PEG$_q$ macromonomers as potential hydrogel surface functionalization reagents.

6.3 Experimental section

Materials. Potassium (98%), 4-vinylbenzyl chloride (4VBC) (90%), and calcium hydride (95%), were purchased from Sigma Aldrich (Darmstadt, Germany) and ethylene oxide (EO) from the Linde group (Dublin, Ireland). Diphenylmethane (DPM) (99%), silica gel 60 with a particle size of 0.063 mm – 0.200 mm and active basic aluminium oxide 66 with a particle size of 0.063 mm – 0.200 mm were bought from Merck KGaA (Darmstadt, Germany). Furfuryl glycidyl ether (FGE) was obtained from Acros organics (Geel, Belgium) and purified by column chromatography (silica gel, solvent gradient from EtOAc : PE = 1 : 1 to EtOAc : PE = 3 : 1). Tetrahydrofuran (THF), isopropanol (*i*PrOH), ethanol (EtOH), methanol (MeOH), chloroform (CHCl$_3$) and diethylether were purchased in HPLC grade from VWR chemicals (Radnor, USA) and ethyl acetate (EtOAc) was obtained from J.T. Baker (Phillipsburg, USA). For the macromonomer synthesis, THF was dried at least 2 days over calcium hydride and freshly distilled under argon before use. EO was dried by passing through a column of calcium hydride. 4VBC was flashed over basic aluminium oxide, stirred over calcium hydride for 4 days and distilled under vacuum at 50 °C and 10^{-1} mbar. If not further explained, all chemicals were used as received.

Synthesis. PFGE$_p$-*b*-PEG$_q$ macromonomers were synthesized *via* anionic polymerization as described previously (Adatia *et al.* 2019). Briefly, DPMK was used as an initiator for the polymerization of FGE. Then EO was added to the living PFGE chains to form the second block. The living chain ends were terminated with 4VBC for vinylbenzyl end groups. For hydroxyl end groups, the termination was performed with MeOH. The block lengths were determined *via* ^{1}H NMR spectroscopy by calculating the ratio between the integral of the initiator protons and the integral of the protons of the respective repeating unit (Adatia *et al.* 2019).
^{1}H NMR (500 MHz, CDCl$_3$): δ [ppm] = 3.22 – 3.72 (m, 150, *a, b, c, h, i*), 4.13 (m, 1 H, *o*), 4.42 – 4.45 (m, 20, *d*), 4.55 (s, 2 H, *j*), 5. 22 – 5.24 (m, 1 H, *n*), 5.72 – 5.75 (m, 1 H, *n*), 6.26 – 6.30 (m, 20, *e, f*), 6.69 – 7.13 (m, 1 H, *m*), 7.12 -7.24 (m, 10 H, *p*), 7.29 -7.30

(m, 4 H, *k*), 7.34 – 7.39 (m, 10 H, *g*). The alphabetical proton assignments refer to Figure 37 - Figure 40.

Polymer characterization. ^{1}H NMR spectra were recorded on an "Avance 500" (500 MHz) spectrometer from Bruker (Billierica, USA). Chloroform-d_1 was used as solvent and tetramethylsilane as internal standard. For SEC the macromonomers were dissolved in THF for 24 h through a 0.2 µm poly(tetrafluoroethylene) syringe filter before injecting 50 µL of the sample into a "SECurity System" from PSS GmbH (Darmstadt, Germany). The system had a PSS SDV precolumn (8 mm x 50 mm), two PSS SDV 1000 Å (8 mm x 300 mm) columns and a RI detector. THF (HPLC grade) was used as solvent, the flow rate was 0.5 mL min^{-1} and the columns were calibrated with polystyrene standards "ReadyCal" from PSS GmbH (Darmstadt, Germany). For the analysis of the measurements PSS WinGPC Unichrom software version 8.10 was used.

Langmuir film balance experiments. For Langmuir film balance experiments a KSV-5 000 Nima Langmuir-Blodgett trough with the dimensions 150 mm x 580 mm from Biolin Scientific Holding AB (Stockholm, Sweden) was used. Before each experiment the barriers and the trough were cleaned carefully with a soft brush and then rinsed three times with deionized (DI) water, ethanol and finally again with DI water. About 1 300 mL ultrapure MilliQ water from a Millipore system was used as subphase. After an equilibration time of 30 minutes to 21.7 °C (± 0.2 °C), the barriers were compressed with a constant speed of 50 mm min^{-1} to a trough area A_t of 100 cm² so that the surface could be cleaned by aspirating 50 mL from the surface. Then the barriers were expanded to the maximum A_t and few microliters of a 1 mg mL^{-1} macromonomer solution in CHCl$_3$ (HPLC grade) were spread carefully on the surface using a microsyringe. The compression for the film isotherm experiments started at a A_t of 780 cm² and ended at 100 cm². The amounts of the macromonomers were chosen in such a way that the isotherm onset appeared around 700 cm² (± 50 cm²) trough area. The exact amount of block polymer used in each experiment is given in the supporting information (Table 8). All glassware for the preparation of the macromonomer solutions were cleaned in a base bath containing 8 L *i*PrOH, 2 L DI water and 500 g potassium hydroxide and rinsed numerous times with DI and MillQ water before it was dried in the oven at 120 °C. After a waiting period of 20 minutes for solvent evaporation, the

experiments were performed with a constant barrier speed of 10 mm min^{-1} (0.5 cm² s^{-1}). π is defined as the difference between the surface tension γ_0 of pure water and the surface tension γ of water with surfactant:

$$\pi = \gamma_o - \gamma \tag{10}$$

π was measured using a rinsed Wilhelmy plate connected to a highly sensitive film balance. The Wilhelmy plate method has an experimental error of approximately 0.1 mN m^{-1} (Adatia *et al.* 2019, Kampf *et al.* 1999). For the Langmuir isotherms the barriers were compressed to a trough area of $A = 100$ cm². For the hysteresis and recovery experiments, the barriers were immediately expanded to the maximum trough area after compression. Compressions and expansions were carried out at the same constant barrier speed of 10 mm min^{-1} (0.5 cm² s^{-1}). The isotherm onset was defined at $\pi = 0.3$ mN m^{-1}. In the film stability experiments, the macromonomer film was compressed to a starting surface pressure (π_0) of 5 mN m^{-1} and then the barriers stayed at that position for 1 h so that the surface pressure drop $\Delta\pi_d$ could be measured.

Characteristic polymer values. In addition to their molar masss and molar mass dispersities, polymers were categorized by their HLB value (Adatia *et al.* 2019, Griffin 1954, Griffin 1949):

$$HLB = 20 \cdot \left(1 - \frac{M_l}{M_{n,}}\right) \tag{11}$$

The molecular structure of the PFGE$_p$-*b*-PEG$_q$ macromonomers is shown in Figure 33 and the HLB values were calculated by using the molar mass of the lipophilic moiety (M_l) and M_n, which were both determined by NMR (Table 6). In particular, the lipophilic part of the macromonomers comprises the PFGE-block and the 4-vinylbenzyl end group, whereas the hydrophilic part is given by the PEG-block (Figure 33, Table 6).

Furthermore, the amount surface coverage factor Θ_n and the mass surface coverage factor Θ_m were calculated according to equation (12) and (13) to quantify how much polymer per area are needed to cause the onset surface pressure of $\pi = 0.3$ mN m^{-1}.

$$\theta_n = \frac{n}{a_0} \tag{12}$$

$$\theta_m = \frac{n \cdot M_n}{a_0} = \theta_n \cdot M_n \tag{13}$$

Here, n is the amount of macromonomers used in the specific experiment and a_o is the trough area at the isotherm onset.

Derived from Θ_n the surface functionality factor S can be calculated by multiplication with p, which is the number of repeating units of the PFGE-block.

$$S = \frac{n \cdot p}{a_o} = \theta_n \cdot p \qquad (14)$$

In theory, each FGE repeating unit exhibits a furan moiety, which is available for post-synthetic modification reactions (Adatia *et al.* 2019). In contrast to the surface coverage factor Θ_n, the surface functionalization factor S expresses how many functional furan groups per area are available through our macromonomers.

Furthermore, the recovery of the macromonomers to the air-water interface after five hysteresis cycles was measured by the surface pressure difference $\Delta\pi$ between the hysteresis maximum of the recovery cycle ($\pi_{HM,r}$) and the hysteresis maximum of the fifth hysteresis cycle ($\pi_{HM,5}$) (equation (15)). For normalized values the surface pressure of the hysteresis maximum of the first hysteresis cycle ($\pi_{HM,1}$) was set to 100%.

$$\Delta\pi = \pi_{HM,r} - \pi_{HM,5} \qquad (15)$$

Statistical data evaluation. The statistical analysis was performed by one-way analysis of variance (ANOVA) using the Holm-Bonferroni post-hoc test with the software OriginPro 9.1 from OriginLab Corporation (Northampton, USA). An effect was judged significant when the differences between individual mean values were significant with $p < 0.05$.

6.4 Results and discussion

Macromonomer synthesis. The aim of this work is to deepen the knowledge of film formation and structure-property relations of poly(furfuryl glycidyl ether)-*block*-poly(ethylene glycol) macromonomers at the air-water interface and to evaluate them as potential hydrogel surface functionalization reagents. Therefore, we synthesized six different *α*-diphenylmethyl-*ω*-4-vinylbenzyl-poly(furfuryl glycidyl ether)-*block*-poly(ethylene glycol) macromonomers, which are abbreviated with PFGE$_p$-*b*-PEG$_q$, whereby p is the number of repeating units in the PFGE-block and q is the numer of repeating units in the PEG-block (Figure 33). The PFGE-block lengths varied from

p = 8 – 18 and the PEG-block contained 9 to 111 repeating units. This led to number average molar masses $M_{n,NMR}$ from 2 220 g mol^{-1} to 7 180 g mol^{-1} and a broad range of HLB values between 3.6 and 13.9 (Table 6). Furthermore, the macromonomer PFGE$_{11}$-b-PEG$_{26}$ was synthesized with a hydrophobic 4-vinylbenzyl end group (like all the other macromonomers) and with a hydrophilic hydroxy end group (PFGE$_{11}$-b-PEG$_{26}$H) to explore the influence of the end group at the air-water interface. The molecular structures and a matrix depiction of all macromonomers are shown in Figure 33. Additionally, the number average molar masses and the HLB values are summarized in Table 6.
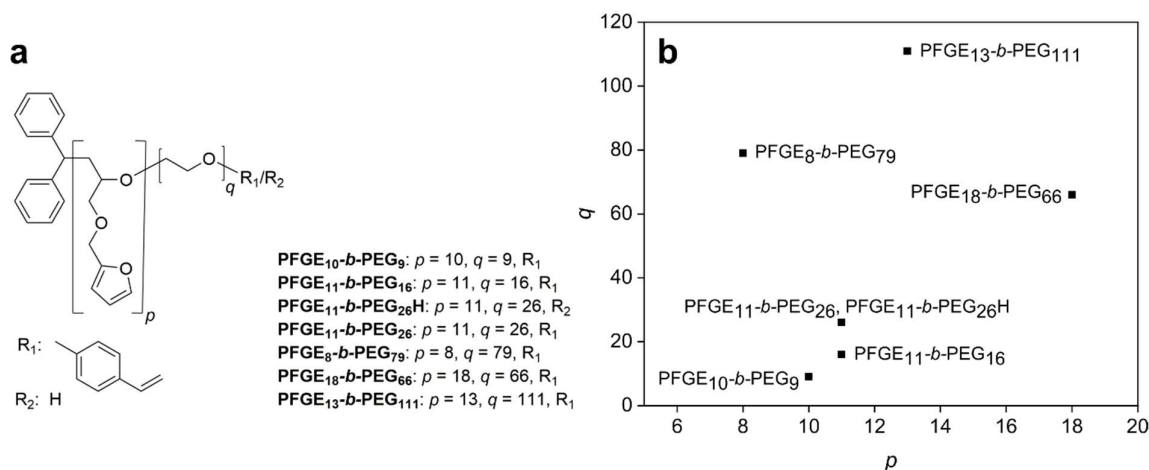

Figure 33: a) Molecular structure and b) matrix depiction of α-diphenylmethyl-ω-4-vinylbenzyl-poly(furfuryl glycidyl ether)-$block$-poly(ethylene glycol) (PFGE$_p$-b-PEG$_q$) macromonomers. p is the number of repeating units in the PFGE-block and q is the numer of repeating units in the PEG-block of the respective macromonomer.

^{1}H NMR spectra (Figure 37 - Figure 40) confirmed the successful synthesis of all macromonomers described in Figure 33, since the proton signals are in accordance with the literature. Additionally, SEC traces showed narrow, monomodal molar mass distributions with low molar mass dispersities (Figure 41). Overall, the molar masses determined by ^{1}H NMR ($M_{n,NMR}$) and SEC ($M_{n,SEC}$) in Table 6 were in good agreement. All macromonomers from Table 6 showed good solubility in organic solvents like THF, CHCl$_3$ and MeOH. In addition, the three previously published macromonomers PFGE$_8$-b-PEG$_{79}$, PFGE$_{18}$-b-PEG$_{66}$ and PFGE$_{13}$-b-PEG$_{111}$ were soluble in water because of their comparatively long PEG-block (Adatia $et\ al.$ 2019, Bolourchian $et\ al.$ 2013, Sill $et\ al.$ 2017).

Table 6: Overview of number average molar mass (M_n), average molar mass of the lipophilic polymer moiety (M_l), average molar mass of the hydrophilic polymer moiety (M_h), weight average molar mass (M_w), molar mass dispersity ($Đ_{SEC}$) and hydrophilic-lipophilic balance (HLB) values of macromonomers

used in this study. The molar masses and molar mass dispersities were determined by nuclear magnetic resonance spectroscopy (NMR) or size exclusion chromatography (SEC), which is indicated by the subscript.

sample	$M_{n,NMR}$ [g mol^{-1}]	$M_{l,NMR}$ [g mol^{-1}]	$M_{h,NMR}$ [g mol^{-1}]	$M_{n,SEC}$ [g mol^{-1}]	$M_{w,SEC}$ [g mol^{-1}]	$Đ_{SEC}$	HLB
PFGE$_{10}$-b-PEG$_9$	2 220	1 830	400	4 530	4 950	1.09	3.6
PFGE$_{11}$-b-PEG$_{16}$	2 690	1 980	710	2 650	2 960	1.12	5.2
PFGE$_{11}$-b-PEG$_{26}$H	3 010	1 870	1 150	3 000	3 260	1.09	7.6
PFGE$_{11}$-b-PEG$_{26}$	3 130	1 980	1 150	3 140	3 390	1.08	7.3
PFGE$_8$-b-PEG$_{79}$	5 000	1 520	3 480	5 020	5 260	1.05	13.9
PFGE$_{18}$-b-PEG$_{66}$	5 970	3 060	2 910	5 190	5 440	1.05	9.7
PFGE$_{13}$-b-PEG$_{111}$	7 180	2 290	4 890	6 660	7 250	1.09	13.6

π-A Isotherms. Film formation at the air-water interface of all macromonomers from Table 6 was assessed by the Langmuir technique. The good reproducibility of our π-A isotherm experiments, especially for PFGE$_{11}$-b-PEG$_{16}$, is shown in Figure 42. Furthermore, the π-A isotherm onsets did not significantly change upon varying the barrier speed in the range of 10 mm min^{-1} to 50 mm min^{-1} (Figure 43 and Figure 44), which is in line with π-A isotherms of other amphiphiles like ytterbium bisphthalocyanine or arachidic acid (Angelova et $al.$ 1996, Dhanabalan et $al.$ 1999). We chose a barrier speed of 10 mm min^{-1} for our further experiments, which is frequently used in the literature, to give the system as much time as possible to equilibrate and to avoid kinetic effects (Angelova et $al.$ 1996, Constantino et $al.$ 1999, Dhanabalan et $al.$ 1999, Kampf et $al.$ 1999).

As shown in Figure 34, all macromonomers caused an increase of surface pressure π when compressed to smaller areas per molecule A, which demonstrates that the macromonomers were present at the air-water interface. This is a clear proof of their surface activity, which is in accordance with previous surface activity measurements via bubble pressure tensiometry of the water-soluble macromonomers PFGE$_8$-b-PEG$_{79}$, PFGE$_{18}$-b-PEG$_{66}$ and PFGE$_{13}$-b-PEG$_{111}$. The tensiometry measurements revealed π up to 18 mN m^{-1} for PFGE$_{13}$-b-PEG$_{111}$, 19 mN m^{-1} for PFGE$_{18}$-b-PEG$_{66}$ and 21 mN m^{-1} for PFGE$_8$-b-PEG$_{79}$ when the polymer concentration was increased above the critical micelle concentration of roughly 0.3 mg mL^{-1} (Adatia et $al.$ 2019).
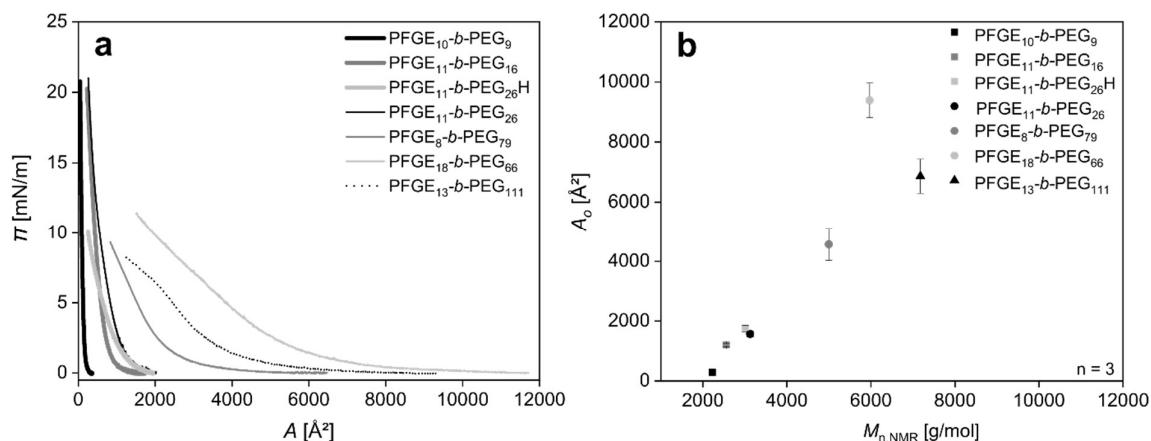
Figure 34: a) Surface pressure-area (π-A) isotherms and b) correlation of the area per molecule at the onset (A_o) with the molar mass ($M_{n,NMR}$) of the macromonomers from Table 6. A_o was defined at $\pi = 0.3$ mN m^{-1}. For the rather hydrophobic macromonomers PFGE$_{10}$-b-PEG$_9$, PFGE$_{11}$-b-PEG$_{16}$, PFGE$_{11}$-b-PEG$_{26}$H and PFGE$_{11}$-b-PEG$_{26}$ the error bars of the standard deviation are roughly the same size as the symbols.

π-A isotherms (Figure 34a) of the macromonomers (Figure 33a and Table 6) revealed the influence of block lengths and molar masses on the isotherm shape and onset. All macromonomers started in the gas phase with a low π and transferred into the liquid-expanded state with a steeper slope during compression. The larger the amphiphile, the more the course of the π-A isotherm was shifted to larger areas per molecule A. This is in line with Kampf et al., who reported a π-A isotherm shift to a growing A with increasing monodendron size (Kampf et al. 1999). Moreover, the smaller, more hydrophobic macromonomers (HLB < 8) showed a steeper ascent in the liquid condensed phase compared to larger, more hydrophilic macromonomers with HLB > 8. A similar trend was described for PEG-based monodendrons with growing PEG-tails (Kampf et al. 1999).

The change in slope of the π-A isotherm for the macromonomer PFGE$_{13}$-b-PEG$_{111}$ around 6 mN m^{-1} may suggest a transition from pancake-like structure to a mushroom-like or brush-like structure of the PEG chains at the water air interface, as observed by Yang et al. for fluoroalkyl-terminated PEGs (Yang et al. 2009). Similar transitions of PEG-based polymers were also reported by Fauré et al. (1998), Baekmark et al. (1995) and Wiesenthal et al. (1999). We did not observe a transition state for the other macromonomers, presumably due to the shorter PEG-chains, which is in line with Clop et al. who explained that a certain chain length is necessary for a transition state to occur (Clop et al. 2016).

We further investigated the structure-property relations of the macromonomers at the air-water interface and found that the area per molecule at the isotherm onset (A_0) correlates with the number average molar mass $M_{n,NMR}$ of the macromonomers (Figure 34b). Hereby, $M_{n,NMR}$ of our macromonomers were between 2 220 g mol^{-1} and 7 180 g mol^{-1} and the measured A_0 varied between 279 Å² and 9 386 Å². Figure 34b shows that an increase of $M_{n,NMR}$ correlates in an almost linear way with A_0, whereby the mean values of A_0 differ significantly from each other with $p < 0.01$. Except for PFGE$_{18}$-b-PEG$_{66}$, the higher the $M_{n,NMR}$ of the macromonomer, the more area each polymer occupies at the air-water interface. A similar trend was also published by Clop et al. (2016) for PEG-grafted dipalmitoyl phosphatidylethanolamines, in which A_0 increased from 660 Å² to 6 000 Å² when the molar mass of the PEG-block grew from 350 g mol^{-1} to 5 000 g mol^{-1}. Also Kampf et al. (1999) observed a linear correlation of the molar mass with the molecular area of their monodendrons at the air-water interface.

Moreover, we examined whether the hydrophobic 4-vinylbenzyl unit at the end of the hydrophilic PEG-block has an influence on the surface coverage at the air-water interface. Therefore, we synthesized two analogous block copolymers PFGE$_{11}$-b-PEG$_{26}$ and PFGE$_{11}$-b-PEG$_{26}$H, which only differ in their end group (Figure 33). PFGE$_{11}$-b-PEG$_{26}$ was terminated with a hydrophobic 4-vinylbenzyl end group (like all of our other macromonomers) and PFGE$_{11}$-b-PEG$_{26}$H ends with a hydrophilic hydroxyl moiety. According to equation (12), PFGE$_{11}$-b-PEG$_{26}$ shows a higher amount surface coverage factor Θ_n with 25 pmol cm^{-2} ± 7 pmol cm^{-2} compared to PFGE$_{11}$-b-PEG$_{26}$H with Θ_n = 22 pmol cm^{-2} ± 4 pmol cm^{-2} (Table 9). The mass surface coverage factor Θ_m from equation (13) is also higher for PFGE$_{11}$-b-PEG$_{26}$ with Θ_m = 79 ng cm^{-2} ± 22 ng cm^{-2} than for PFGE$_{11}$-b-PEG$_{26}$H with Θ_m = 65 ng cm^{-2} ± 1 ng cm^{-2} (Table 9). Though we measured small differences of Θ_n and Θ_m between the two differently terminated polymers, these differences are not significant with $p > 0.05$. Kyeremateng et al. in contrast described a change in the surface activity resulting from perfluorination of the end group of their poly(propylene)-$block$-poly(isopropylidene glycerol methacrylate) block copolymer, but did not mention the significance (Kyeremateng et al. 2008). They explained that the increase in hydrophobicity resulted in a different allocation of their polymer at the surface (Kyeremateng et al. 2008). In fact, the new fluoro-end group with $M_{n,NMR}$ = 600 g mol^{-1} increased the molar mass of the poly(propylene) block with $M_{n,NMR}$ = 1 570 g mol^{-1} up to 38 %, whereas our

4-vinylbenzyl end group ($M_{n,NMR}$ = 117 g mol^{-1}) caused a weight increase of only 10 % of the PEG-block ($M_{n,NMR}$ = 1 150 g mol^{-1}). Hence, we conclude that the relatively small structural change through the end group of our macromonomer caused very little differences in the conformation at the air-water interface and therefore did not influence the surface coverage significantly. This is advantageous for the synthesis, because the implementation of a more polar polymerizable unit in form of an acryloyl moiety led to auto polymerization (Adatia *et al.* 2019).

Overall, the *π-A* isotherms revealed that all macromonomers are able to localize at the air-water interface and show film formation, which is a fundamental prerequisite for the application as surface-functionalization reagent for materials prepared from aqueous solution such as hydrogels. Compared to the end group, the molar mass of the macromonomers have a much stronger influence on the surface properties like the isotherm shape and onset. In fact, we observed an almost linear growth of the isotherm onsets with growing molar mass of the macromonomers.

Film stability. Since we found that all PFGE$_p$-*b*-PEG$_q$ macromonomers are able to form Langmuir monolayers at the air-water interface, we were interested in the film stability under static and dynamic conditions. For static investigations we used a very similar approach to Deschênes *et al.* (2015), as we monitored the *π* over time (*t*) at a starting surface pressure $π_0$ of 5 mN m^{-1} and then kept the trough barriers at a constant area (A_c).

Figure 35 shows that the *π* of all macromonomer films dropped over time and the jagged lines indicate a dynamic process at the air-water interface (Ramírez *et al.* 2011). Since *π* is defined in equation (10) as the difference between the surface tension of water $γ_0$ and the surface tension of water with surfactant *γ*, a surface pressure drop $Δπ_d$ indicates a decreasing amount of macromonomers at the surface (McNaught *et al.* 1997).
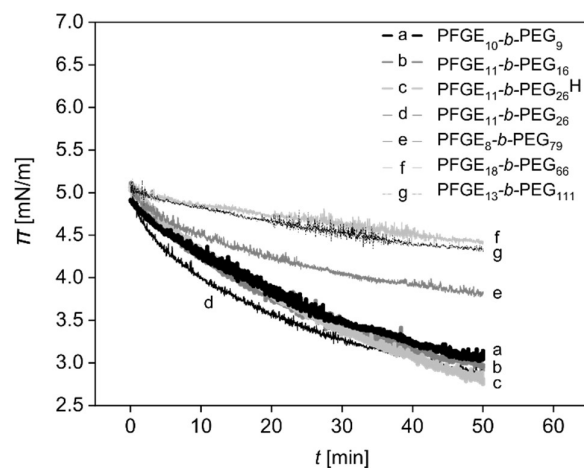
Figure 35: Film stability of the macromonomer films from Table 6 determined by measuring the surface pressure (π) over time (t) at constant trough area (A_c) with a starting surface pressure (π_0) of 5 mN m^{-1}.

During 50 minutes, we observed a surface pressure drop $\Delta\pi_d$ for the more hydrophilic macromonomers PFGE$_8$-b-PEG$_{79}$, PFGE$_{18}$-b-PEG$_{66}$ and PFGE$_{13}$-b-PEG$_{111}$ between 0.5 mN m^{-1} and 1.25 mN m^{-1} and a $\Delta\pi_d$ for the more hydrophobic macromonomers PFGE$_{10}$-b-PEG$_9$, PFGE$_{11}$-b-PEG$_{16}$, PFGE$_{11}$-b-PEG$_{26}$H and PFGE$_{11}$-b-PEG$_{26}$ between 1.8 mN m^{-1} and 2.2 mN m^{-1} (Figure 35 and Figure 45). This demonstrates that the hydrophilic macromonomer films with HLB values > 8, are more stable compared to the hydrophobic films with HLB values < 8. We attribute this to the anchoring effect of the PEG-block at the air-water interface, which was analyzed previously by Kampf *et al*. (1999).

To explain the surface pressure decrease over time, there are two possibilities in the literature how amphiphiles can leave a film at the air-water interface: Either they immerse to the subphase, or the molecules transfer from a two dimensional (2D) film to a three dimensional (3D) formation (Barentin *et al.* 1998, Goto *et al.* 2013). Both options seem reasonable for our macromonomers. Regarding the first, a submersion was observed for many PEG-based polymers before and PFGE-b-PEG block copolymers are additionally known to form micelles in the subphase (Barentin *et al.* 1998, Barthel *et al.* 2012). Regarding the latter, it is likely that the asymmetric nature of our macromonomers induce monolayer bending which leads to a 2D-3D transition as it was described for multiple amphiphiles (Diamant *et al.* 2001, Gopal *et al.* 2001, Lee 2008, Safran *et al.* 1996, Ybert *et al.* 2002). Therefore, we believe that a combination of both mechanisms is likely.

We furthermore investigated the monolayer stability under dynamic conditions, for which we measured five hysteresis cycles of each macromonomer (Figure 46). For all macromonomers the surface pressures of the hysteresis maxima (π_{HM}) decreased with ongoing hysteresis cycles. Moreover, the hysteresis loops, which display the difference between compression and expansion cycle, shrank with increasing number of cycles. This indicates that the system was approaching an equilibrium state. There are different processes in the literature that explain hysteresis loops of a monolayer (Ivanova *et al.* 1991): I) the Marangoni effect, which describes mass transfer along the interface of two fluids due to a gradient of the surface tension ; II) conformation and relaxation processes in the monolayer; III) a collapse of the monolayer into a 3D phase and IV) interchange of molecules between the soluble monolayer and the subphase. We think that our hysteresis loops are most probably a result of an interplay of all these four points. Concerning point I, our macromonomers are exposed to the Marangoni effect, since the movable barriers, which have a different deformation effect on the subphase compared to the film, lead to a surface pressure gradient (Ivanova *et al.* 1991). Regarding point II and III it was described that folded regions can coexist with the 2D monolayer, whereby further compression changes the fraction of the monolayer in the folds relative to the 2D regions (Lee 2008, Lipp *et al.* 1998). Such an ongoing 3D fold formation of our macromonomers could explain the successive surface pressure decrease per hysteresis cycle. Additionally, an equilibrium between our macromonomers at the interface and macromonomer micelles is very likely based on the ability of PFGE-*b*-PEG block copolymers to form micelles (point IV) (Barthel *et al.* 2012).

To quantify the surface pressure decrease during the hysteresis experiment, we fitted the surface pressures of the hysteresis maxima π_{HM} per cycle and looked at the absolute value of the slope (s_{HM}). An overview of the linear fits and the coefficients of determination (R^2) are given in Figure 47 and Table 10. If s_{HM} is big, it indicates a high hysteresis decline, which means more molecules left the air-water interface during each compression-expansion cycle. The mean values of s_{HM} reach from 1.0 to 4.0 and differ significantly from each other with $p < 0.01$. In Figure 36a, the correlation of the surface pressure declines and the HLB value is presented. It shows that with rising HLB values of the macromonomer, s_{HM} decreases. For example, the most hydrophobic macromonomer PFGE$_{10}$-*b*-PEG$_9$ has the steepest slope ($s_{HM} = 3.7$) and the most hydrophilic macromonomer PFGE$_8$-*b*-PEG$_{79}$ shows the lowest slope ($s_{HM} = 1.4$).

Furthermore, the surface pressure of the more hydrophobic macromonomer films of PFGE$_{10}$-*b*-PEG$_9$, PFGE$_{11}$-*b*-PEG$_{16}$, PFGE$_{11}$-*b*-PEG$_{26}$H and PFGE$_{11}$-*b*-PEG$_{26}$ decreased stronger during the hysteresis experiment compared to the more hydrophilic macromonomers PFGE$_{18}$-*b*-PEG$_{66}$, PFGE$_8$-*b*-PEG$_{79}$ and PFGE$_{13}$-*b*-PEG$_{111}$. This is in line with the static stability experiments in Figure 35.

Besides that, we exposed the macromonomers to compression and expansion forces for 45 min, 90 min and 225 minutes to investigate the effect of the force exposure time. We kept the number of hysteresis cycles constant at five cycles as we know from the hysteresis experiment that a higher number of hysteresis cycles leads to more decline of the macromonomer films. In Figure 43 and Figure 44, we showed that the barrier speed has no significant influence on the π-*A* isotherm of the macromonomers. This enables us to investigate the time dependent hysteresis decline at a constant number of hysteresis cycles by varying the barrier speed from 10 mm min^{-1} to 50 mm min^{-1}. Five hysteresis cycles at a barrier speed of 50 mm min^{-1}, 25 mm min^{-1} and 10 mm min^{-1} resulted in a force exposure time of 45 min, 90 min and 225 min. Figure 48 shows that the film decline is higher when the macromonomer is exposed to compression and expansion forces for longer time.

In conclusion, all macromonomers showed limited film stability under static and dynamic conditions, whereby the films of the more hydrophobic macromonomers (HLB < 8) were less stable compared to the films of the more hydrophilic macromonomers (HLB > 8). This might be critical for the application as hydrogel surface functionalization reagents, but since the film decline is time-dependent, a rapid immobilization of the macromonomers could help to circumvent this obstacle.

Monolayer recovery and molecular mechanism. After finding out, that our macromonomers were leaving the 2D monolayer over time, we were curious whether they are able to recover to the air-water interface if they have enough time and space. Therefore, we measured five hysteresis cycles, then expanded the barriers of the Langmuir-Blodgett trough to the maximum trough area A_t of 780 cm² and analyzed the surface pressure π after 12 hours. The hysteresis and recovery cycles of PFGE$_8$-*b*-PEG$_{79}$ are shown in Figure 36b. The analogous experiments of the other macromonomers are demonstrated in Figure 49. As described before, the π of the macromonomer films declined with ongoing hysteresis cycles, but after 12 hours, we

could measure higher π during the recovery cycle, which indicates the recovery of macromonomers to the air-water interface.

To quantify the recovery, we normalized the π_{HM} of the first hysteresis cycle to 100 % and calculated the π of the other hysteresis and recovery maxima accordingly (equation (15)). For all macromonomers we measured a higher surface pressure of the hysteresis maximum in the recovery cycle ($\pi_{HM,r}$) compared to the surface pressure of the fifth hysteresis cycle ($\pi_{HM,5}$), which is shown in Figure 36c. This is significant with $p < 0.05$ for PFGE$_{11}$-*b*-PEG$_{26}$H, PFGE$_{10}$-*b*-PEG$_9$, PFGE$_{18}$-*b*-PEG$_{66}$, PFGE$_8$-*b*-PEG$_{79}$ and PFGE$_{13}$-*b*-PEG$_{111}$. PFGE$_{11}$-*b*-PEG$_{16}$ and PFGE$_{11}$-*b*-PEG$_{26}$ do not exhibit significantly higher $\pi_{HM,r}$ compared to $\pi_{HM,5}$, but still follow the same trend (Figure 36c).

The recovery ability of the macromonomers to the air-water interface after five hysteresis cycles was quantified by the surface pressure difference ($\Delta\pi$) between the hysteresis maximum of the recovery cycle ($\pi_{HM,r}$) and the hysteresis maximum of the fifth hysteresis cycle ($\pi_{HM,5}$) (equation (15)). This normalized recovery ability of the studied macromonomers is shown in Figure 36. The mean values of the $\Delta\pi$ are between 14 % and 45 % and do not differ significantly with $p > 0.05$ from each other, which means the surface pressure recovery ability of the macromonomers is indistinguishable from each other. This is probably based on the fact that the macromonomer recovery cannot be attributed to a single factor such as the molar mass or the HLB value, but is rather an interplay of various factors like the molecular structure, the rate of compression and molecule entrapments (Baoukina *et al.* 2008, Goto *et al.* 2013, Ries Jr *et al.* 1987). This multi-factor dependency of the recovery process also explains the relatively high standard deviations in our recovery experiment (Figure 36d).
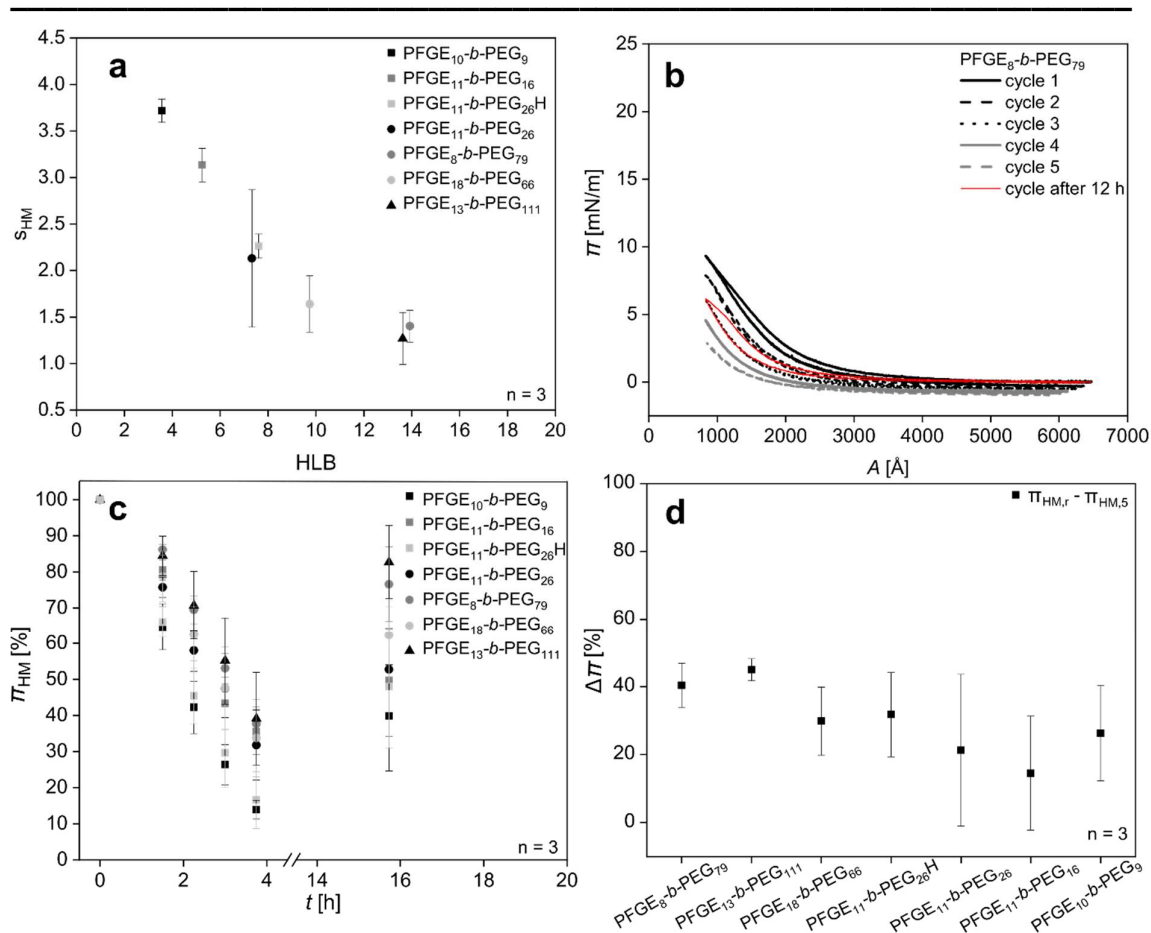
Figure 36: Hysteresis and recovery cycles of PFGE$_8$-b-PEG$_{79}$. Analogous hysteresis and recovery cycles of PFGE$_{10}$-b-PEG$_9$ – PFGE$_{13}$-b-PEG$_{111}$ are given in Figure 46 and Figure 49. b) Normalized surface pressure of the hysteresis maxima (π_{HM}) over time (t) and c) correlation of hysteresis decline with the hydrophilic-lipophilic balance (HLB) value of the macromonomers. s$_{HM}$ is the slope of the linear hysteresis maxima fit from Table 10 and represents the hysteresis decline. d) Normalized recovery ability of the studied macromonomers demonstrated by the surface pressure difference ($\Delta\pi$) between the surface pressure of the hysteresis maxima of the recovery cycle ($\pi_{HM,r}$) and the surface pressure of hysteresis maxima of the fifth hysteresis cycle ($\pi_{HM,5}$) (equation (15)).

The ability of the macromonomers to recover to the air-water interface is a strong indication for a folding mechanism as its reversibility was frequently described in the literature (Baoukina *et al.* 2008, Ding *et al.* 2001, Takamoto *et al.* 2001). Solubilization and multilayer collapse processes in contrast are encountered as irreversible (Lee 2008, Ries Jr *et al.* 1987). We rather exclude a mechanism which is mainly based on the collapse to multilayers, as we did not observe a collapse pressure, which is typical for multilayer formations (Yang *et al.* 2009). Additionally a multilayer collapse mostly occurs at very high π, when the amphiphiles are compressed beyond their stability limit (Goto *et al.* 2013). Collapse pressures are often in the range of 50 mN m^{-1} to 60 mN m^{-1}, such as 50 mN m^{-1} for PEG-based azo dyes (Rivera *et al.* 2007), around 50 mN m^{-1} for β-sheet peptides (Maget-Dana 1999) and 60 mN m^{-1} of fatty acid films

(Das *et al.* 2016). In contrast our macromonomers were studied at relatively low π between 0 mN m^{-1} and 23 mN m^{-1}, which is why we don't think our macromonomers collapsed to multilayers.

Since the declined macromonomers did only recover partly, we suggest an interplay between a folding and a submerge mechanism for our macromonomer films. Basically, the folding mechanism explains the recovery of the macronomomers to the air-water interface and the submerge mechanism, which was also discussed during the stability measurements, clarifies why the macromonomers do not recover quantitatively.

Overall, the recovery experiments played an important role to give further insights into the molecular mechanisms of the studied macromonomer monolayers at the air-water interface.

Evaluation of the macromonomers as potential surface functionalization reagents of hydrogels. Hydrogel surface functionalization reagents have to fulfill three major criteria: I) they need a functional unit which participates in the material curing reaction for covalent immobilization of the functional groups on the hydrogel surface, II) they should contain functional groups which can serve as molecular anchor points for post-synthetic modification reactions after the curing reaction and III) they should be able to form stable films at the air-water interface to specifically functionalize the material surface. The studied macromonomers fully fulfill the first two requirements. The macromonomers contain a polymerizable 4-vinylbenzyl unit for covalent incorporation into radically cross-linkable hydrogels and the furan side chains can react in post-synthetic Diels-Alder reactions (Adatia *et al.* 2019). This work shows that all the studied macromonomers were able to form films at the air-water interface, but only with limited stability. Therefore, the third criteria is only partially fulfilled. To overcome this obstacle, we recommend a fast hydrogel curing process for the preparation of surface functionalized hydrogels. Once the macromonomers are covalently bound to the material, they are immobilized and the film stability becomes irrelevant. Hence, we believe our macromonomers are suitable hydrogel surface functionalization reagents.

To identify which macromonomer is the most favorable hydrogel surface functionalization reagent, we ranked them according to the surface functionalization factor S (equation (14)). S quantifies how many functional groups per area are available at the air-water interface. For our macromonomers, S focuses on the furan

groups per area. An overview of the surface functionalization factor and the surface functionality ranking (SFR) of the examined macromonomers are given in Table 7 .

According to the surface functionalization factors the hydrophobic macromonomers PFGE$_{10}$-*b*-PEG$_9$, PFGE$_{11}$-*b*-PEG$_{16}$ and PFGE$_{11}$-*b*-PEG$_{26}$ with HLB < 8 are more favorable surface functionalization reagents compared to the hydrophilic macromonomers PFGE$_8$-*b*-PEG$_{79}$, PFGE$_{18}$-*b*-PEG$_{66}$ and PFGE$_{13}$-*b*-PEG$_{111}$ with HLB < 8. The macromonomer PFGE$_{10}$-*b*-PEG$_9$ is the most promising hydrogel surface functionalization reagent, because it can introduce the highest number of functional groups (11.9 x 10^{-10} mol cm^{-2}) per surface area (Table 7).

Table 7: Surface functionality factor (*S*) and surface functionality ranking (SFR) of the macromonomers used in this study.

sample	S [10^{-10} mol cm^{-2}]	SFR
PFGE$_{10}$-*b*-PEG$_9$	11.9 ± 1.4	1
PFGE$_{11}$-*b*-PEG$_{16}$	3.1 ± 0.1	2
PFGE$_{11}$-*b*-PEG$_{26}$	2.8 ± 0.8	3
PFGE$_{11}$-*b*-PEG$_{26}$H	2.4 ± 0.4	4
PFGE$_{13}$-*b*-PEG$_{111}$	0.8 ± 0.1	5
PFGE$_{18}$-*b*-PEG$_{66}$	0.8 ± 0.1	5
PFGE$_8$-*b*-PEG$_{79}$	0.7 ± 0.1	6

6.5 Conclusions

In summary, we could show the film formation of all six PFGE$_p$-*b*-PEG$_q$ macromonomers and give more insight into the structure-property relations at the air-water interface by highlighting the influence of the molar mass $M_{n,NMR}$ and the HLB values on the surface properties. *π-A* isotherms of the macromonomers revealed that compared to the end group, the molar mass of the macromonomers have a much stronger influence on the surface properties like the isotherm shape and onset. Smaller, more hydrophobic macromonomers (HLB < 8) showed a steeper surface pressure increase in the liquid condensed phase compared to larger, more hydrophilic macromonomers with HLB > 8. Additionally, the isotherm onsets shifted to larger molecular areas in an almost linear way with growing molar mass of the macromonomers. Furthermore, stability experiments of our macromonomers under static and dynamic conditions revealed limited stability of the macromonomer monolayers at the air-water interface. In fact, the macromonomer films with HLB

values > 8 were more stable than the hydrophobic ones with HLB < 8, which we attributed to the anchoring effect of the PEG-tail at the air-water interface. Moreover, the film degradation during hysteresis experiments increased almost linearly with rising HLB values of the macromonomers. Based on the partial film recovery, we propose an interplay between a reversible folding and an irreversible submersion mechanism for the macromonomer monolayers at the air-water interface. As our macromonomers provide a polymerizable unit for covalent attachment, have several furan moieties, which can be used for post-synthetic Diels-Alder reactions and are able to form monolayers at the air-water interface, we believe they are promising surface functionalization reagents of hydrogels, even if the macromonomer films show limited stability. According to our surface functionality ranking, $PFGE_{10}$-b-PEG_9 is the most promising hydrogel surface functionalization reagent among our macromonomers, because it can introduce the highest number of functional groups per surface area.

6.6 Acknowledgements

Conflicts of interest. The authors declare no conflict of interest.

6.7 Supporting information

Table 8: Macromolecules used in the Langmuir film balance experiments. Vs is the spreaded volume of a 1 mg mL^{-1} macromonomer stock solution in $CHCl_3$ and n ist he amount of macromonomers.

sample	V_s [µL]	n [nmol]
$PFGE_{10}$-b-PEG_9	80	36
$PFGE_{11}$-b-PEG_{16}	20	7.45
$PFGE_{11}$-b-$PEG_{26}H$	20	6.65
$PFGE_{11}$-b-PEG_{26}	20	6.40
$PFGE_8$-b-PEG_{79}	10	2.00
$PFGE_{18}$-b-PEG_{66}	7	1.11
$PFGE_{13}$-b-PEG_{111}	10	1.39
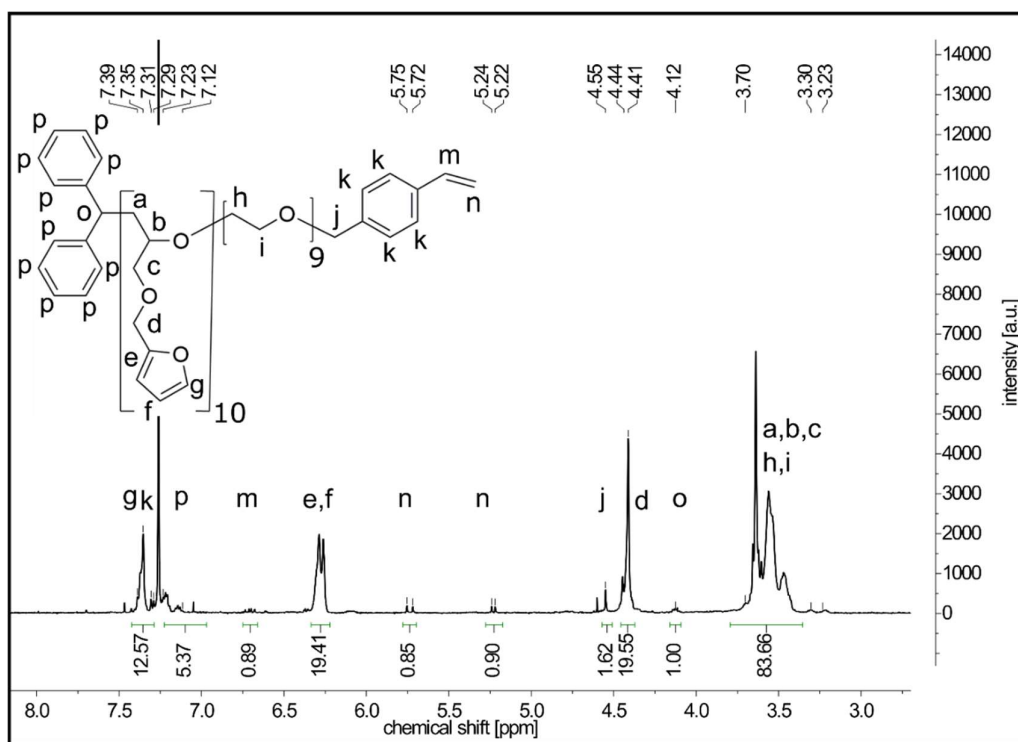
Figure 37: ^{1}H NMR spectrum of macromonomer PFGE$_{10}$-*b*-PEG$_9$.
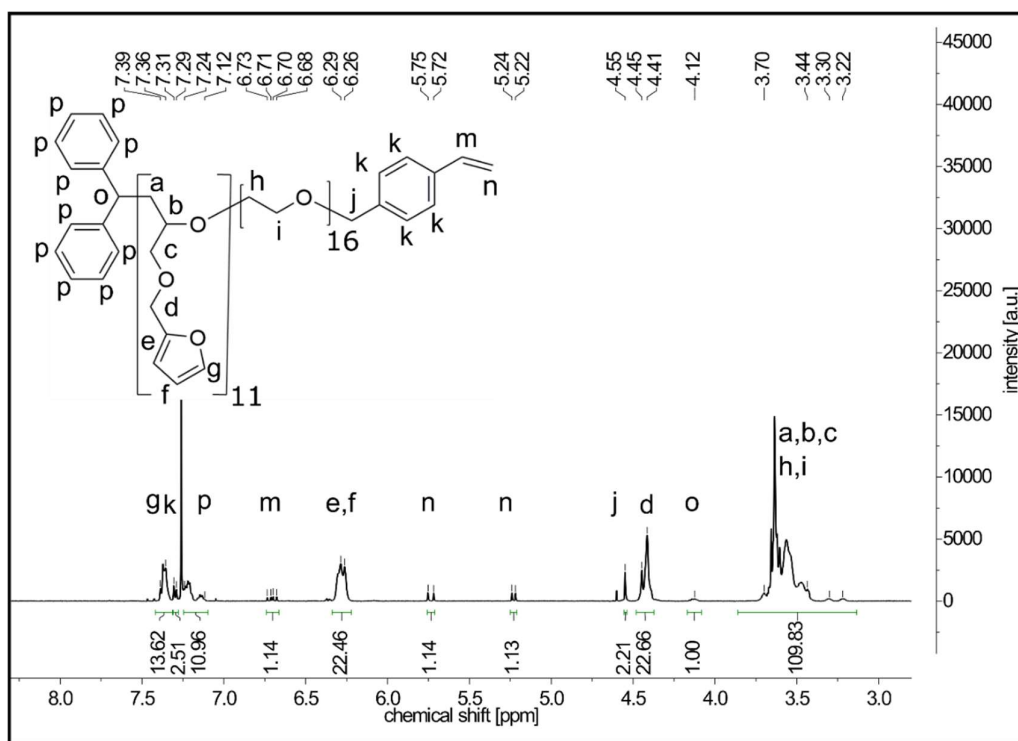
Figure 38: ^{1}H NMR spectrum of macromonomer PFGE$_{11}$-*b*-PEG$_{16}$.
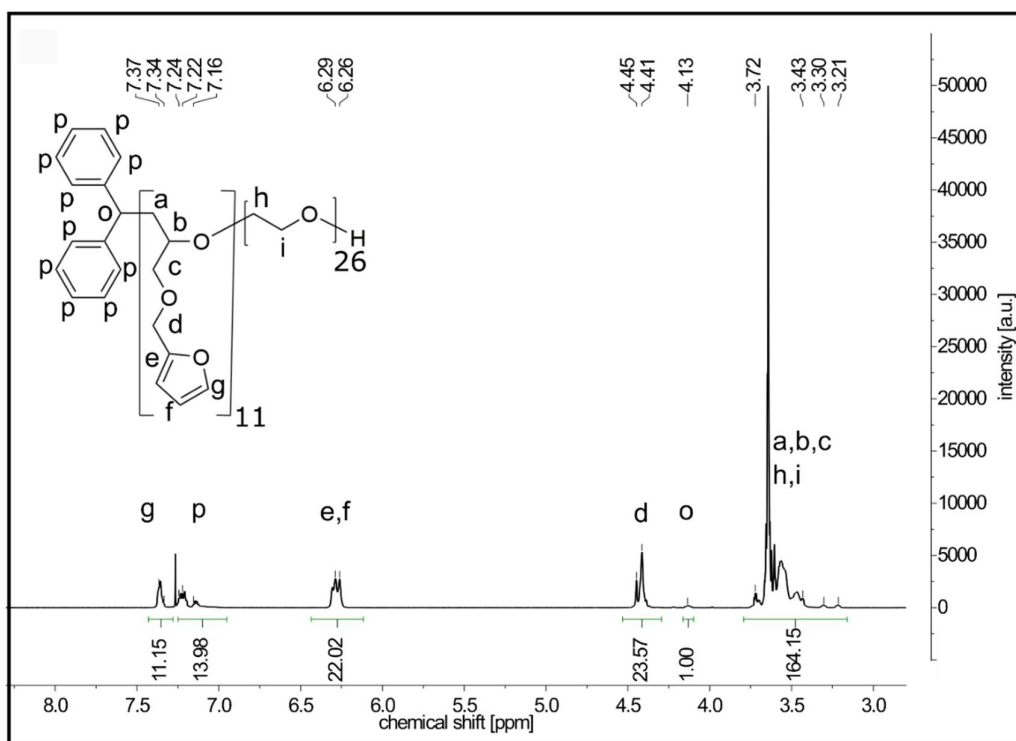
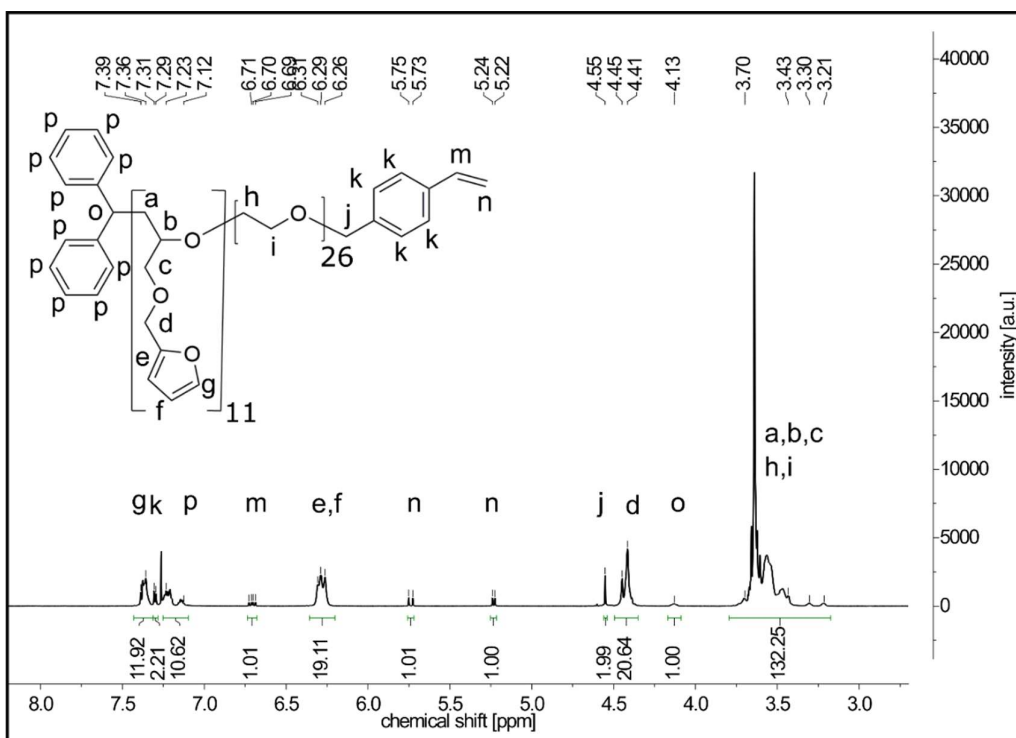Figure 39: ^{1}H NMR spectrum of PFGE$_{11}$-*b*-PEG$_{26}$H.

Figure 40: ^{1}H NMR spectrum of macromonomer PFGE$_{11}$-*b*-PEG$_{26}$.
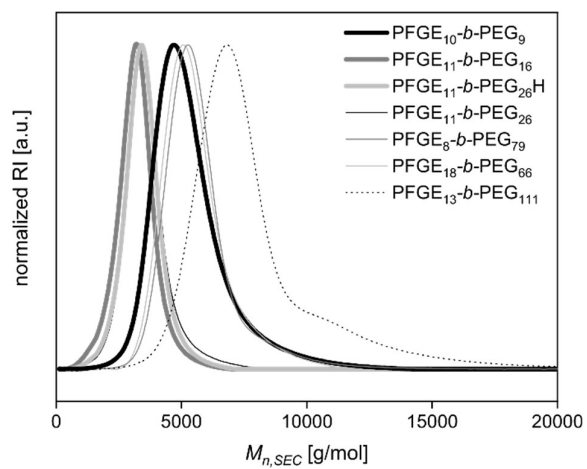
Figure 41: Size exclusion chromatography traces of all studied macromonomers. PFEG$_8$-*b*-PEG$_{79}$, PFEG$_{18}$-*b*-PEG$_{66}$ and PFGE$_{13}$-*b*-PEG$_{111}$ were already published (Adatia *et al.* 2019). The number average molecular weights ($M_{n,SEC}$), the weight average molecular weights ($M_{w,SEC}$) and the molar mass dispersity ($Đ_{SEC}$) of the macromonomers determined by SEC are summarized in Table 6.

Figure 42: Reproducibility of π-A isotherms of the studied macromonomers.

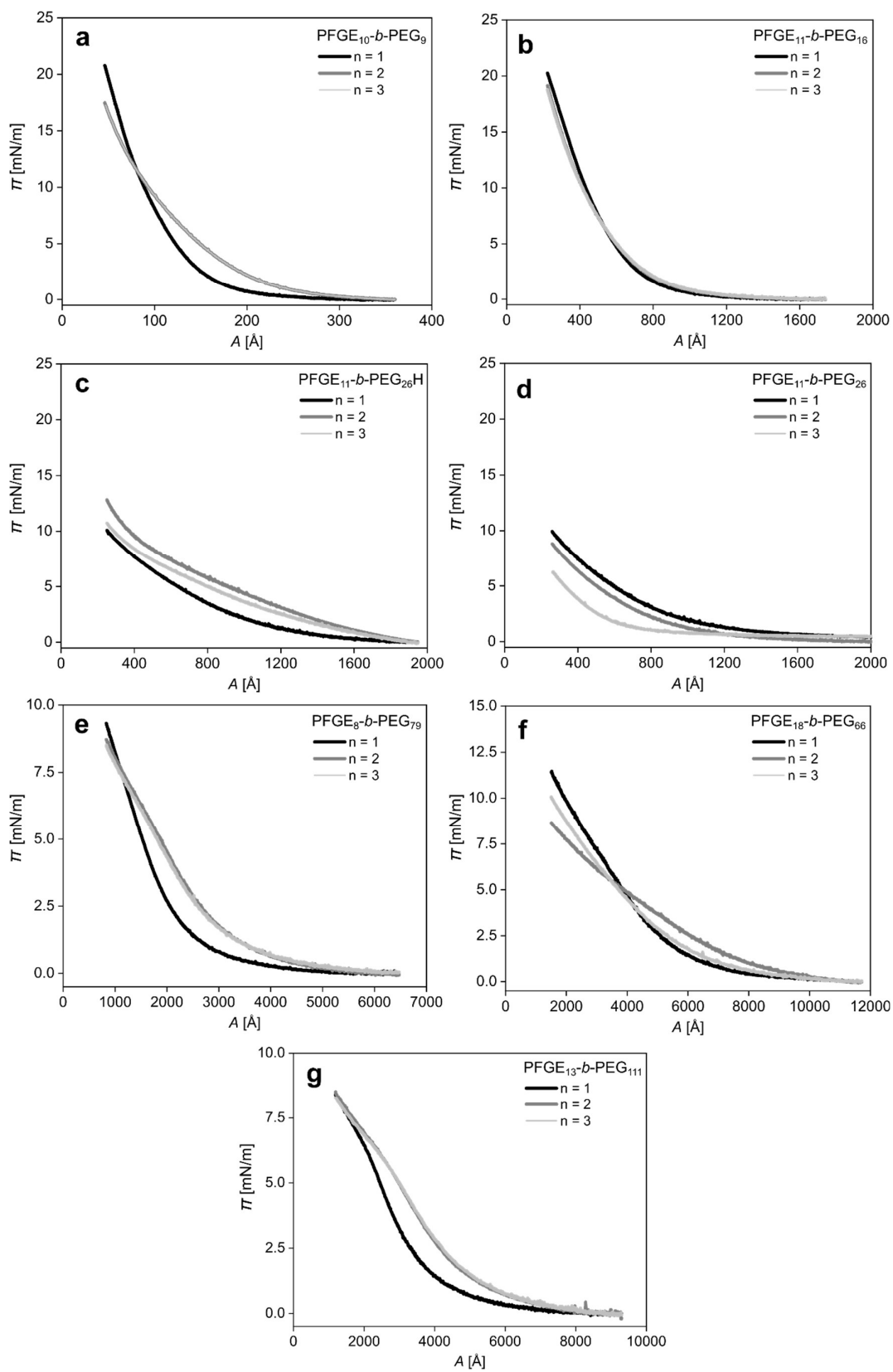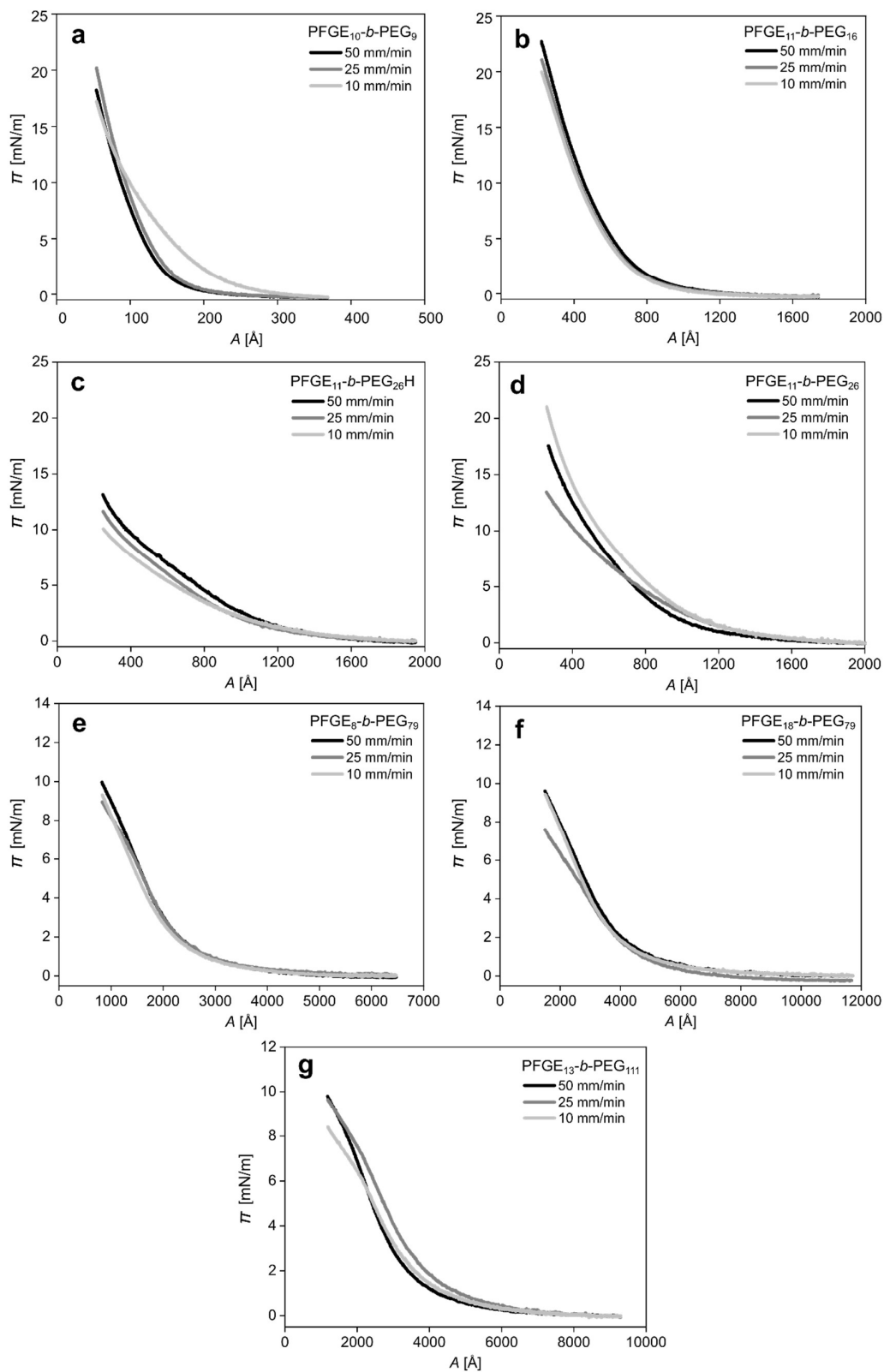Figure 43: π-A isotherms of the studied macromonomers at different barrier speeds from 10 mm min^{-1} to 50 mm min^{-1}.
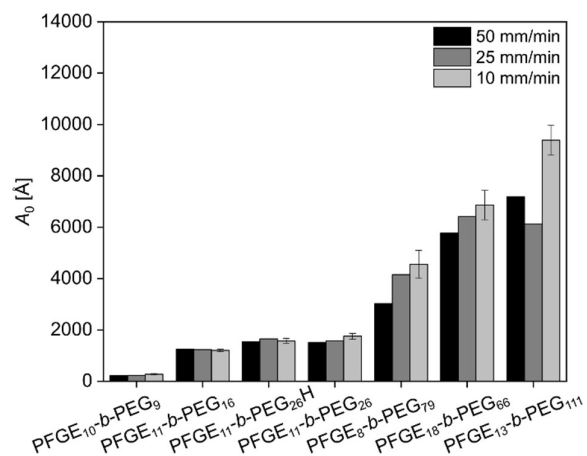
Figure 44: Area at the π-A-isotherm onsets (A_0) of the studied macromonomers at different barrier speeds from 10 mm min^{-1} to 50 mm min^{-1}.

Table 9: Amount surface coverage factor (Θ_n) and mass surface coverage factor (Θ_m) of the macromonomers used in this study.

sample	Θ_n [pmol cm^{-2}]	Θ_m [ng cm^{-2}]
PFGE$_{10}$-b-PEG$_9$	119 ± 14	266 ± 31
PFGE$_{11}$-b-PEG$_{16}$	28 ± 1	75 ± 1
PFGE$_{11}$-b-PEG$_{26}$H	22 ± 4	65 ± 12
PFGE$_{11}$-b-PEG$_{26}$	25 ± 7	79 ± 22
PFGE$_8$-b-PEG$_{79}$	10 ± 1	48 ± 5
PFGE$_{18}$-b-PEG$_{66}$	10 ± 1	26 ± 1
PFGE$_{13}$-b-PEG$_{111}$	6 ± 1	43 ± 5

Figure 45: Surface pressure drop ($\Delta\pi_d$) after 50 minutes of the studied macromonomers at constant trough area (A_c) with a starting surface pressure (π_0) of 5 mN m^{-1}.

Figure 46: Hysteresis cycles of the studied macromonomers.
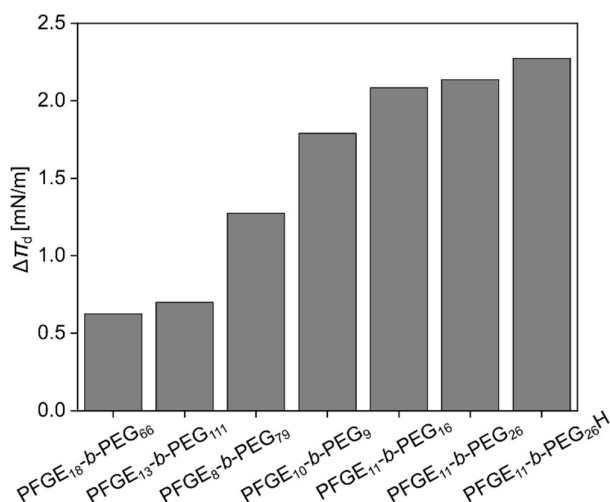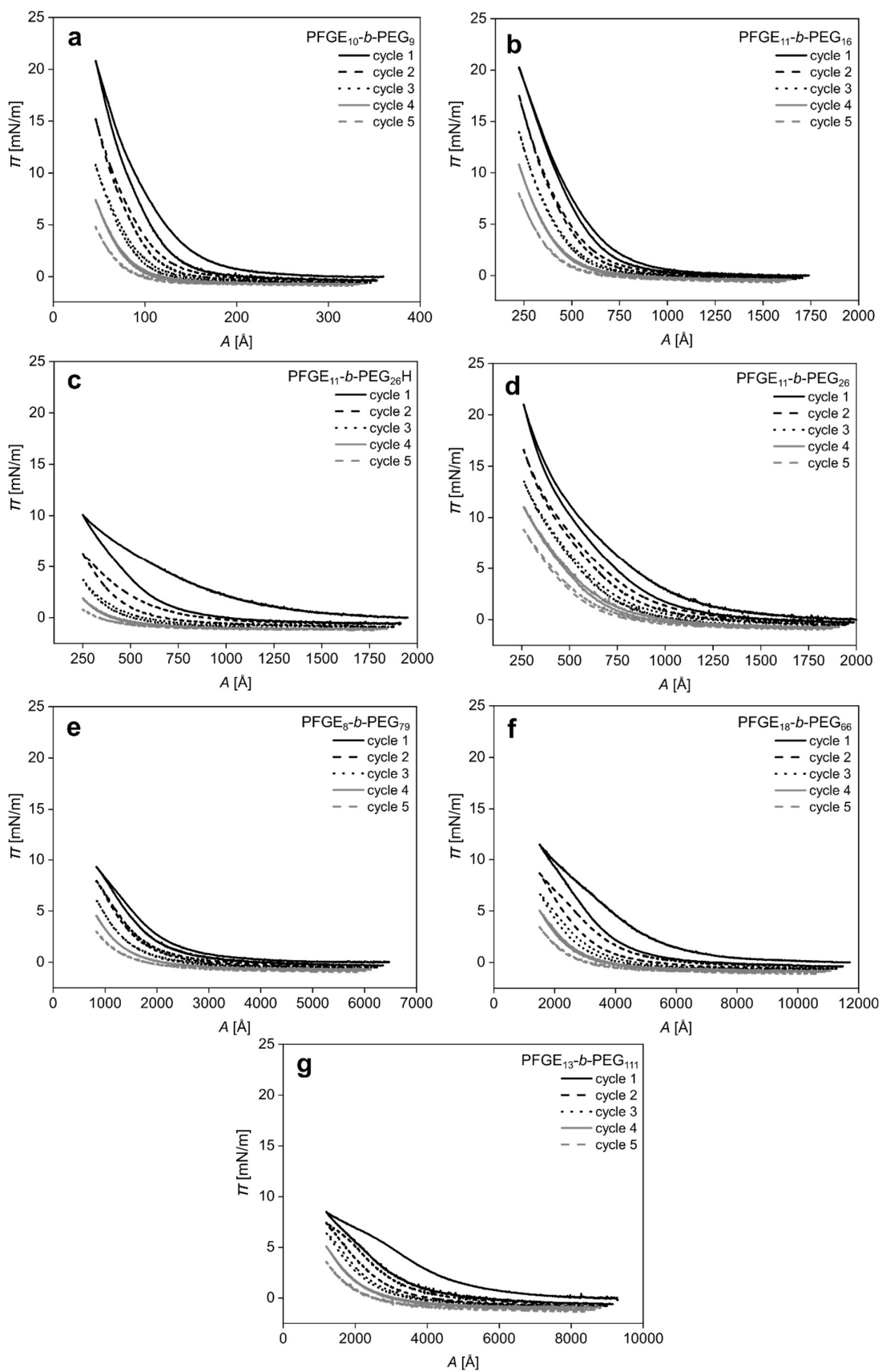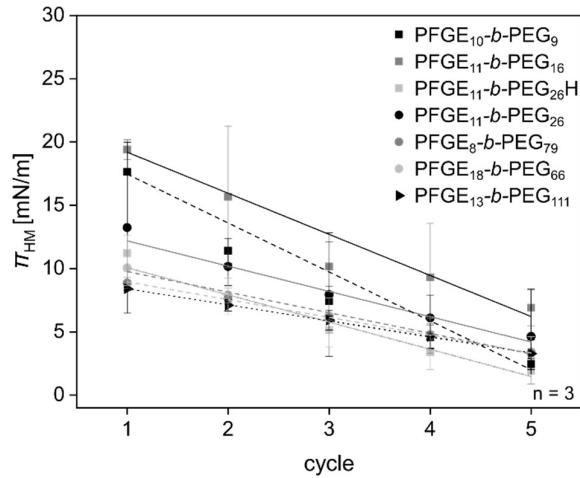
Figure 47: Linear fit of the hysteresis maxima surface pressures (π_{HM}) during hysteresis cycles of the studied macromonomers.

Table 10: Linear fit of the hysteresis maxima surface pressures (π_{HM}) during hysteresis cycles (c_H) of the studied macromonomers, absolute value of the respective slope (s_{HM}) and coefficient of determination (R^2).

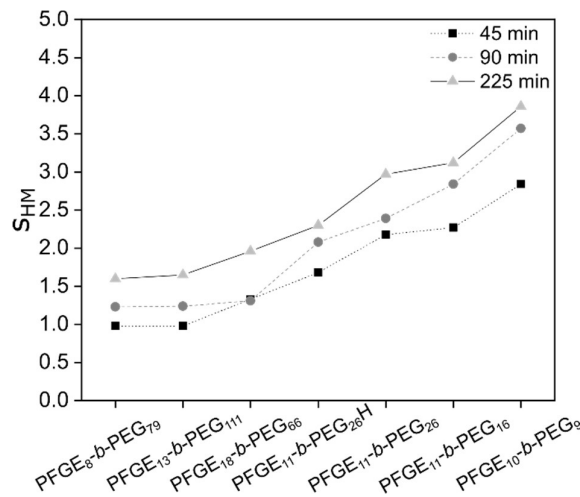| sample	linear fit	s_{HM}	R^2
PFGE$_{10}$-*b*-PEG$_9$	$\pi_{HM} = -3.87 c_H + 21.33$	3.87	0.98873
PFGE$_{11}$-*b*-PEG$_{16}$	$\pi_{HM} = -2.25\ c_H + 22.44$	2.25	0.97180
PFGE$_{11}$-*b*-PEG$_{26}$H	$\pi_{HM} = -2.15\ c_H + 12.22$	2.15	0.96029
PFGE$_{11}$-*b*-PEG$_{26}$	$\pi_{HM} = -2.00\ c_H + 14.19$	2.00	0.99039
PFGE$_8$-*b*-PEG$_{79}$	$\pi_{HM} = -1.40\ c_H + 10.35$	1.40	0.99926
PFGE$_{18}$-*b*-PEG$_{66}$	$\pi_{HM} = -1.63\ c_H + 11.39$	1.63	0.99264
PFGE$_{13}$-*b*-PEG$_{111}$	$\pi_{HM} = -1.27\ c_H + 9.67$	1.27	0.99965

Figure 48: Correlation of hysteresis decline with exposure time to compression and expansion forces of the studied macromonomers. s_{HM} is the slope of the surface pressure hysteresis maxima fit from Table 10. The lines are only for the guidance of the eyes.
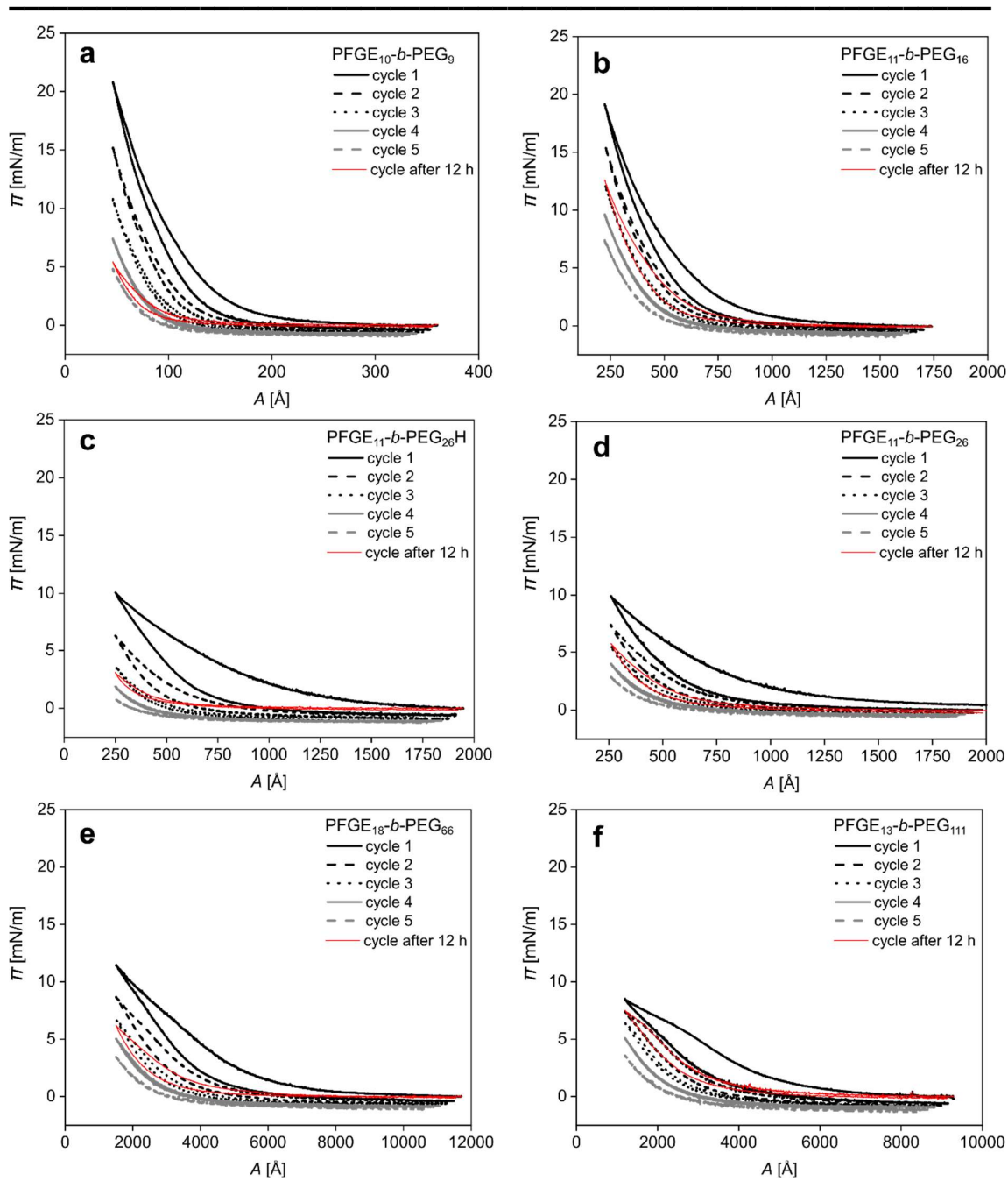
Figure 49: Hysteresis and recovery cycles of the studied macromonomers.

7. Investigation of the surface functionalization of polyacrylamide hydrogels with poly(furfuryl glycidyl ether)-*block*-poly(ethylene glycol) macromonomers

As described in section 5, it could be proven that our multifunctional macromonomers are able to functionalize the hydrogel bulk above their cmc and provide multiple anchor points for post-synthetic modification reactions. Furthermore, it was shown in section 6.that the macromonomers align at the air-water interface below their cmc. This raises the question whether the macromonomers can be used for the specific surface functionalization of hydrogels, without functionalizing the hydrogel bulk. To our knowledge, no one used multifunctional macromonomers to exclusively functionalize the air-hydrogel interface without functionalizing the hydrogel bulk. Therefore, in the following the surface functionalization of polyacrylamid (p(Aam)) hydrogels with $PFGE_p$-*b*-PEG_q macromonomers will be investigated *via* fluorescence labeling experiments.

7.1 Materials

Chemicals. Acrylamide (99 %), *N,N'*-methylenebisacrylamide (MBA) (99 %) and α-ketoglutaric acid (99 %) were purchased from Sigma Aldrich (Darmstadt, Germany). Isopropanol (*i*PrOH), ethanol (EtOH), chloroform ($CHCl_3$) and xylene were purchased in HPLC grade from VWR chemicals (Radnor, USA). $PFGE_{13}$-*b*-PEG_{111} was synthesized as described previously in section 5.

Hydrogel preparation. Functionalized p(Aam) hydrogels were prepared by mixing 15 w% acrylamide, 2 w% *N,N'*-methylenebisacrylamide, 1 w% α-glutaric acid and 82 w% water. 200 µL of the hydrogel precursor solution was poured into a cylindrical aluminum mold with 150 mm diameter and 1 mm height and placed in a "hartmann.gs UH-H 255" UV chamber from Hartmann Feinwerkbau GmbH (Ober-Moerlen, Germany). Then 7 µL of a $PFGE_{13}$-*b*-PEG_{111} solution in $CHCl_3$ (1 mg mL^{-1}) was spread carefully on top of the hydrogel precursor solution using a 10 µL Hamilton syringe. For unfunctionalized hydrogels, the macromonomer solution was replaced by pure solvent (without macromonomer). After an evaporation time of 15 min, a quartz glas plate based on a spacer was set on top of the mold. Then the hydrogel was cured for 15 min

in the UV chamber. The distance between UV source and mold was 7.5 cm and the irradiation intensity was approx. 40 mW cm^{-2}. The cured hydrogels were washed 3 days in 8 mL MilliQ water, changing the water twice a day. Hereby it is important that the upper side of the hydrogel did not touch any other surfaces to prevent damages of the potentially functionalized hydrogel surface.

Hydrogel preparation under argon atmosphere. To polymerize hydrogels under argon atmosphere the polymerization equipment in Figure 50 was developed. Herefore a cylindrical aluminum mold of 150 mm diameter and 1 mm height and two attached spacers was placed in a polypropylene (PP) plastic bag. The bag was sealed with gaffa tape and a 5 cm polytetrafluoroethylene (PTFE) tube was incorporated in one corner. The tube was oped and closed with gaffa tape as needed. The tube was used to link the polymerizaiton equipment with a schlenk line to be able to evacuate and flood the construction with argon 3 times. The construction was placed in a "hartmann.gs UH-H 255" UV chamber from Hartmann Feinwerkbau GmbH where it was not moved until curing. 200 µL of the above described hydrogel precursor solution were poured into the mold under argon flooding using the feed whole. Subsequently, 7 µL of a 1 mg mL^{-1} PFGE$_{13}$-*b*-PEG$_{111}$ solution in CHCl$_3$ were spread on top of the hydrogel precursor solution and the feed whole was sealed with gaffa tape. Unfunctionalized hydrogels were prepared by replacing the macromonomer solution through solvent. After 20 min evaporation time, the hydogel was cured for 15 min under UV irradiation. The cured gels were washed 3 days in 8 mL MilliQ water, changing the water twice a day without touching the hydrogel surface.
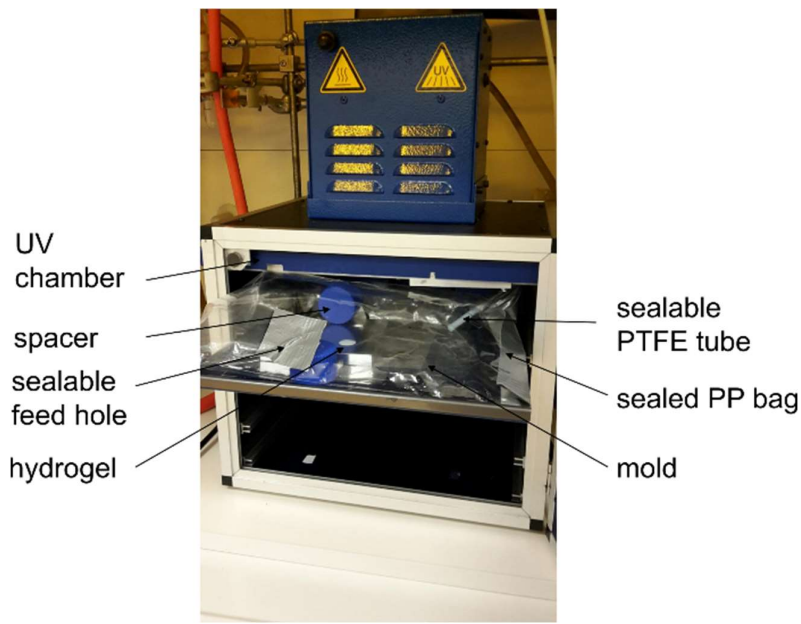
Figure 50: Polymerization equipment for the preparation of surface functionalized hydrogels under argon atmosphere.

Fluorescence labeling and fluorescence measurements. One half of the functionalized/ unfunctionalized hydrogel was put into 950 µL demineralized water and 50 µL of the fluorescence dye Atto 488 maleimide (1.39 mM in DMSO) were added. All steps which involve using the fluorescent dye were performed under light exclusion. The mixture was heated to 65 °C for 2 h, before the gels were washed 6 times by changing the water every 30 minutes in the dark. These fluorescence labeled hydrogels were then used for microscopic investigations. For all steps, the handling of the hydrogel was performed with highest precaution to avoid defects of the hydrogel surface. The labeled hydrogels were analyzed with confocal laser scanning microscopy (LSM) or fluorescence microscopy. The hydrogels were put in between two glass cover slips (thickness: 0.13 mm – 0.16 mm). LSM measurements were carried out using a Zeiss LSM 710 inverted confocal microscope from Carl Zeiss AG with a EC Plan-Neofluar 10x/0.30 M27 objective. Fluorescence microscopy spectra were recorded using a KEYENCE Biorevo BZ-9000 fluorescence spectrometer with a twofold magnification lens NA0.1 WD8.5 and a hard-coated GFP BP filter with an excitation wave length of 473 nm and emission wave lengths of 520 nm. The fluorescence signals were not quantified, because the jelly-like consistency of the

hydrogel did not allow a reproducible positioning of the hydrogel surface area towards the detector.

7.2 Results and Discussion

To investigate whether $PFGE_p$-b-PEG_q macromonomers can be exclusively functionalized the air-hydrogel interface, two types of p(Aam)-based hydrogels were prepared: (a) with $PFGE_p$-b-PEG_q macromonomers for functionalized p(Aam) hydrogels and (b) without $PFGE_p$-b-PEG_q macromonomers for unfunctionalized p(Aam) hydrogels. For the functionalized p(Aam) hydrogels, a macromonomer solution containing $PFGE_{13}$-b-PEG_{111} was spread on the hydrogel precursor solution before curing. $PFGE_{13}$-b-PEG_{111} was used as model macromonomer, as it showed the highest fluorescence intensity during the fluorescence labeling experiments of bulk functionalized p(Aam) hydrogels (Figure 13). The spreading process was inspired by the Langmuir-trough experiments at the air-water interface discussed in section 6 since the goal was to create a functional macromonomer layer at the hydrogel-air interface. After the hydrogels were cured, they were washed 3 days to remove non-polymerized material and then labeled with the fluorescence marker Atto 488 maleimide. The molecular structure of Atto 488 maleimide and the reaction mechanism of the Diels-Alder reaction between our macromonomer and the fluorescence marker is given in Figure 28 and Figure 29. The LSM images of surface functionalized and unfunctionalized, fluorescence labeled p(Aam) hydrogels are shown in Figure 51. After the surface functionalized and unfunctionalized hydrogels were washed for 1 day, they both exhibited a green fluorescent surface and a non-fluorescent hydrogel bulk. As two different polymerization setups for the preparation of functionalized and unfunctionalized hydrogels were used, macromonomer contaminations of the negative control can be excluded. This indicates that the fluorescence signal is not based on specific binding of the fluorescence dye to $PFGE_{13}$-b-PEG_{111}. Furthermore, the fluorescence microscopy images of surface functionalized and unfunctionalized p(Aam) hydrogels without fluorescence marker did not reveal any fluorescence signal, so optical scattering effects can be ruled out. Therefore, the fluorescence signal is most probably due to unspecific binding of Atto 488 maleimide to the hydrogel.
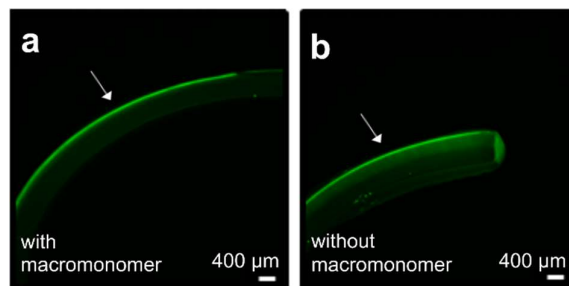
Figure 51: Light scanning microscopy (LSM) images of fluorescence labeled polyacrylamide (p(Aam)) hydrogels a) with macromonomer $PFGE_{13}$-b-PEG_{111} and b) without macromonomer after 1 day washing. The white arrow indicates the hydrogel-air interface during curing.

It was investigated whether the fluorescence signal can be reduced by extending the washing process from 1 day to 1 week and by using different washing solutions. Figure 52 shows that even after 1 week of washing in water the functionalized and unfunctionalized hydrogels show comparable fluorescence intensities of the hydrogel surface. Furthermore the fluorescence labeled hydrogels in Figure 52 were exposed to a washing solution gradient from polar to unpolar solvents by washing the hydrogels in water, EtOH : H_2O = 70 % : 30 %, EtOH : H_2O = 90 % : 10 %, EtOH : H_2O = 96 % : 4 %, isopropanol (iPrOH), iPrOH : xylene = 50 % : 50 % and xylene for 15 min each.
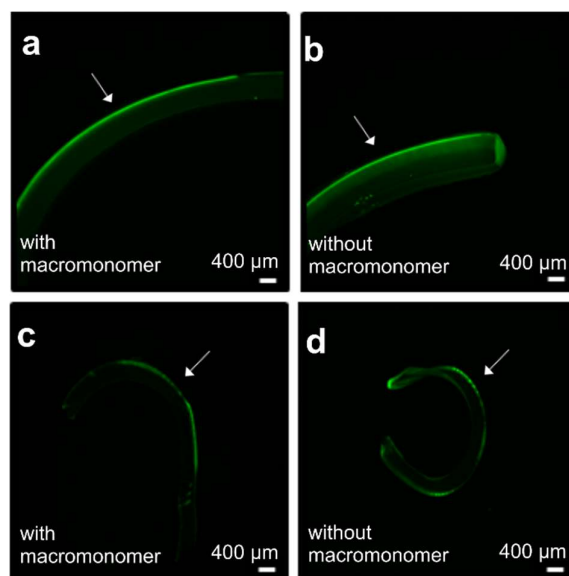
Figure 52: Fluorescence microscopy images of fluorescence labeled polyacrylamide (p(Aam)) hydrogels a, c) with macromonomer $PFGE_{13}$-b-PEG_{111} and b, d) without macromonomer. The p(Aam) hydrogels in a, b) were washed for 1 week in water and the p(Aam) hydrogels in c, d) were washed in a solvent gradient with increasing organic solvent ratio. The white arrow indicates the hydrogel-air interface during curing.

The shriveled appearance of the hydrogels in Figure 52 is due the restricted swelling ability of hydrogels in organic solvents. Figure 52 demonstrates that the fluorescence

signals of surface functionalized and unfunctionalized hydrogels are still in the same range.

Taken together the washing time and the washing solution did not cause a reduction of the fluorescence signal of the negative control compared to the surface functionalized hydrogels.

Interestingly, only the upper hydrogel surface at the hydrogel-air interface is fluorescent and the bottom surface at the hydrogel-mold interface is not. There are two main differences between the upper and the bottom surface of p(Aam) hydrogels: I) the macromonomer solution was only spread on the upper surface of the hydrogel and II) only the upper hydrogel surface was in contact with air during the UV curing process. Hence, in the following both factors will be examined.

To investigate the influence of the spreading process, hydrogels with and without spreading process were compared. For the hydrogel with spreading process, PFGE$_{13}$-b-PEG$_{111}$ was dissolved in CHCl$_3$ and spread on the hydrogel surface before curing as described before. CHCl$_3$ was chosen as solvent because it was often used in the literature to prepare monolayers at the air-water interface (Bijsterbosch et $al.$ 1995, Kampf et $al.$ 1999) and previously showed good results for the preparation of PFGE$_p$-b-PEG$_q$ monolayers (section 6.. For the negative control, the spreading step was skipped, which usually contains the spreading of solvent without macromonomer. Figure 53 demonstrates that both hydrogels regardless of the spreading step exhibit a fluorescent hydrogel surface. This clearly shows that the spreading process itself does not cause the fluorescence at the hydrogel surface.
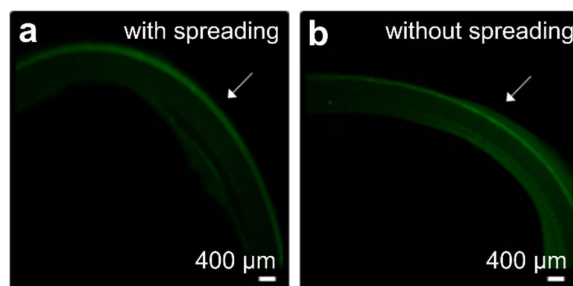
Figure 53: Fluorescence microscopy images of fluorescence labeled polyacrylamide (p(Aam)) hydrogels a) with spreading of PFGE$_{13}$-b-PEG$_{111}$ solution in CHCl$_3$ at the hydrogel surface and b) without spreading. The white arrow indicates the hydrogel-air interface during curing.

Apart from chloroform, other spreading solvents like dichloromethane (DCM) and water were tested to confirm that the spreading solvent has also no effect on the fluorescence

of the hydrogel surface. DCM was chosen because it is eligible to solubilize our macromonomer and it is not miscible with water, which enhances the desired phase separation at the air-water interface. Additionally, DCM evaporates quickly at room temperature (boiling point: 39.6 °C), which should support the immobilization of the macromonomer at the air-water interface. As counterweight to this suitable spreading solvent, water was used, which should not enhance the surface functionalization of hydrogels because it is miscible with the hydrogel precursor solution. For the negative control, hydrogels without macromonomer were prepared by spreading the respective solvent (DCM or water) on the hydrogel surface.
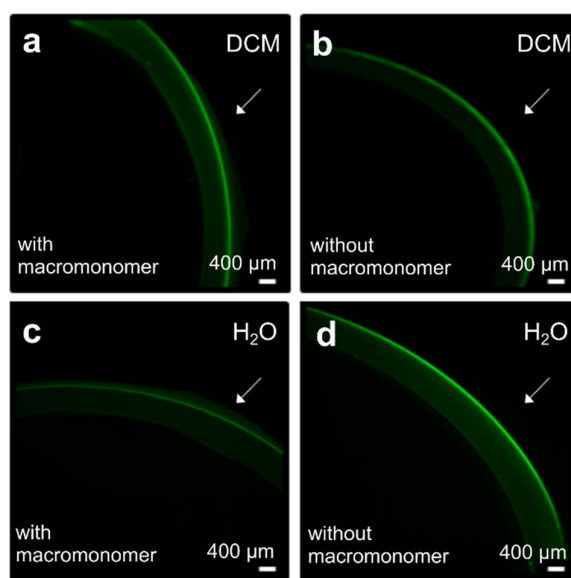
Figure 54: Fluorescence microscopy images of fluorescence labeled polyacrylamide (p(Aam)) hydrogels a, c) with PFGE$_{13}$-b-PEG$_{111}$ and b, d) without macromonomer. The spreading process was performed with a, b) dichloromethane (DCM) and c, d) water. The white arrow indicates the hydrogel-air interface during curing.

Figure 54 demonstrates that regardless of the spreading solvent, the hydrogel surface of functionalized and unfunctionalized hydrogels is fluorescent. So, neither the spreading process itself, nor the spreading solvent are responsible for the fluorescent hydrogel surface.

The second point, which needs to be investigated, is the effect of the surrounding air during the hydrogel curing, because only the upper surface of the hydrogel, which was fluorescent, was in contact with air. The bottom hydrogel surface in contrary was touching the mold and did not show fluorescence. This phenomenon was observed without exception for more than 20 p(Aam) hydrogels. Therefore, surface functionalized and unfunctionalized p(Aam) hydrogels were prepared under argon

atmosphere, labeled with the fluorescent dye Atto 488 maleimide, washed and analyzed with fluorescence microscopy. In contrast to hydrogels which were prepared under air (Figure 51), the hydrogels prepared under argon (Figure 55) are not fluorescent. In fact, neither the hydrogel upper surface nor the hydrogel bottom surface are fluorescent, regardless whether they were surface functionalized or not. One possible explanation is that the oxygen in the air inhibits the radical polymerization during the hydrogel curing due to its biradical nature. The inhibitory effect of oxygen in radical polymerizations is widely reported in the literature (Decker *et al.* 1985, Gauthier *et al.* 2005, Studer *et al.* 2003). The incomplete polymerization at the hydrogel-air interface might be the reason for an altered surface chemistry of the hydrogel-air interface, which could lead to more hydrogel interactions with the fluorescence dye or entrapments. Recently, Kascholke *et al*. (2017) also observed a fluorescent hydrogel-air surface of their functionalized and unfunctionalized hydrogels, which were radically polymerized under air. Unfortunately they did not explain their observation. Taken together, the hydrogel curing experiments under argon strongly indicate that the surrounding environment of the hydrogel has an impact on the surface fluorescence, but further research is needed to explain the exact underlying mechanism.
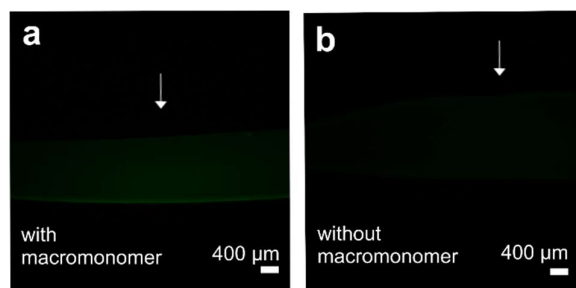
Figure 55: Fluorescence microscopy images of fluorescence labeled polyacrylamide (p(Aam)) hydrogels, which were cured under argon a) with macromonomer PFGE$_{13}$-*b*-PEG$_{111}$ and b) without macromonomer. The white arrow indicates the hydrogel-argon interface during curing.

In conclusion, it was not yet possible to functionalize the air-hydrogel interface of p(Aam) hydrogels exclusively, but we could demonstrate that p(Aam) hydrogels regardless of their functionalization showed a fluorescent air-hydrogel interface. This was overcome by polymerizing the hydrogels under argon atmosphere. The two most evident reasons why the surface functionalization of hydrogels did not work, are, that either the macromonomers did not covalently bind to the hydrogel surface, or that the macromonomer amount on the hydrogel surface was too little for detection. Until now we only know, that the macromonomers can covalently bind into the p(Aam) hydrogel

bulk (Figure 13) and that they are able to form thin films at the air-water interface (Figure 34). As surface chemistry can differ dramatically from bulk chemistry, further research is needed to evaluate whether the macromonomers are able to covalently bind to hydrogel surfaces.

To tackle this, it could be helpful to reduce the complexity of hydrogel surfaces by investigating whether the macromonomer in the first step can bind to a solid surface. A reasonable model substrate therefore is a self-assembled monolayer of 3-methacryloylpropyl trimethoxysilane on a silicon wafer as described by Bialk *et al.* (2002). After extensive washing, the success of the macromonomer immobilization on the solid surface can be analyzed with atomic force microscopy (AFM). If the macromonomer immobilization and detection is successful, the experiment should be repeated with the same macromonomer concentration as in the surface functionalization experiments to find out whether the macromonomer is also detectable with fluorescence microscopy. This will answer the question whether the applied macromonomer amount in the hydrogel surface functionalization experiments was below the fluorescence microscopy detection limit. An alternative approach is based on the work of Tylor *et al.* (2016), who utilized time-of-flight secondary-ion mass spectrometry (TOF-SIMS) for the 3D mapping of functionalized poly(2-hydroxyethyl methacrylate) p(HEMA) hydrogels. TOF-SIMS might also be applicable for the detection of surface functionalized p(Aam) hydrogels. Taken together, we could show that our macromolecules are promising hydrogel functionalization reagents, but further research is needed to fulfil the ambitious task of exclusively functionalizing the air-hydrogel interface.

8. Coumarin-4-ylmethyl and *p*-hydroxyphenacyl-based photoacid generators with high solubility in aqueous media: synthesis, stability and photolysis

Authors: Karishma K. Adatia,[a] Thomas Halbritter,[b] Matiss Reinfelds,[b] Andre Michele,[a,c] Michael Tran,[a,c] Sabine Laschat,[c] Alexander Heckel,[b] Günter E.M. Tovar,[a,d]* and Alexander Southan,[a]*

[a] Institute of Interfacial Process Engineering and Plasma Technology IGVP, University of Stuttgart, Nobelstr.12, 70569 Stuttgart, Germany.

[b] Institute for Organic Chemistry and Chemical Biology, Goethe University Frankfurt, Max-von-Laue-Str. 7, 60438 Frankfurt/Main, Germany

[c] Institute of Organic Chemistry IOC, University of Stuttgart, Pfaffenwaldring 55, 70569, Stuttgart, Germany

[d] Fraunhofer Institute for Interfacial Engineering and Biotechnology IGB, Nobelstr. 12, 70569 Stuttgart, Germany

* Correspondence: alexander.southan@igvp.uni-stuttgart.de, guenter.tovar@igvp.uni-stuttgart.de

Own contribution: I designed the whole project and supervised the students Andre Michele and Michael Tran, who synthesized the *p*HP derivatives and measured the solubility, stability, photochemical behavior and the photolysis. I initiated and fostered the cooperation with Dr. Thomas Halbritter, Dr. Matiss Reinfelds and Prof. Dr. Alexander Heckel, who provided us with c4m-ac. I assisted Dr. Matiss Reinfelds with the quantum yield measurments. I analyzed and interpreted all the data and wrote the manuscript.

8.1 Abstract

(Coumarin-4-yl)methyl (c4m) and *p*-hydroxyphenacyl (*p*HP)-based compounds are well known for their highly efficient photoreactions, but often show limited solubility in aqueous media. To circumvent this, we synthesized and characterized the two new c4m and *p*HP-based photoacid generators (PAGs) 7-[bis(carboxymethyl)amino]-4-(acetoxymethyl)coumarin (c4m-ac) and *p*-hydroxyphenacyl-2,5,8,11-tetraoxatridecan-13-oate (*p*HP-t) and determined their solubilities, stabilities and photolysis in aqueous media. The two compounds showed high solubilities in water of 2.77 mmol L^{-1} ± 0.07 mmol L^{-1} (c4m-ac) and 124.66 mmol L^{-1} ± 2.1 mmol L^{-1} (*p*HP-t). In basic conditions at pH 9, solubility increased for c4m-ac to 646.46 mmol L^{-1} ± 0.63 mmol L^{-1}, for *p*HP-t it decreased to 34.68 mmol L^{-1} ± 0.62 mmol L^{-1}. Photochemical properties of the two PAGs such as the absorption maxima, the maximum molar absorption coefficients and the quantum yields were found to be strongly pH-dependent. Both PAGs showed high stabilities s_{24h} ≥ 95% in water for 24 h, but decreasing stability with increasing pH due to hydrolysis. The present study contributes to a clearer insight into the synthesis, solubilities, stabilities, and photolysis of c4m-ac and *p*HP-based PAGs for further photochemical applications when high PAG-concentrations are required such as in polymeric foaming.

8.2 Introduction

(Coumarin-4-yl)methyl (c4m) and *p*-hydroxyphenacyl (*p*HP)-based compounds are well known for their excellent photochemical properties such as their clean and highly efficient photo cleavage (Du *et al.* 2001, Givens *et al.* 2008, Givens *et al.* 1984, Givens *et al.* 1996, Givens *et al.* 2012, Klán *et al.* 2013b, Schmidt *et al.* 2005). This was highlighted in an excellent review article by Givens *et al.*, who pointed out that c4m and *p*HP derivatives are especially well suited for time-resolved biochemical and physiological applications (Givens *et al.* 2012). Furthermore, these two chromophores are easy to access synthetically, cover a wide range of excitation wavelengths from 250 nm to 450 nm by adjusting their substituents and can be used without sensitizer (Du *et al.* 2001, Givens *et al.* 2012, Givens *et al.* 2011, Givens *et al.* 2000, Hagen *et al.* 2008, Hagen *et al.* 2005, Klán *et al.* 2013b, Pelliccioli *et al.* 2002, Schmidt *et al.* 2005, Shembekar *et al.* 2007). Therefore, c4m and *p*HP-based compounds have gained considerable attention in biochemical (Geibel *et al.* 2000, Givens *et al.* 1996,

Givens *et al.* 2000, Hotta *et al.* 2019, Ohtsuki *et al.* 2016), agricultural (Atta *et al.* 2012b, Atta *et al.* 2010) and pharmaceutical applications (Barman *et al.* 2016, Buckup *et al.* 2010, Kandler *et al.* 1998). They have been used for neurotransmitter release (Kandler *et al.* 1998), enzyme catalysis (Geibel *et al.* 2000), membrane acidification (Geißler *et al.* 2005) or for drug delivery of anticancer agents (Al-Wahaibi *et al.* 2018). Barman *et al.* for instance used *p*HP–benzothiazole–chlorambucil conjugates as a photoregulated drug delivery system due to its fast photocleavage and high biocompatibility (Barman *et al.* 2016). Morover, c4m esters were employed to study proton migration in biological systems such as lipid bilayers (Geißler *et al.* 2005, Serowy *et al.* 2003).

They were also used as photoacid generators (PAGs) to release acidic compounds under UV irradiation in aqueous media (Hagen *et al.* 2008, Pelliccioli *et al.* 2002). However, in many water-based applications where high PAG concentrations are required, like in the field of bioinspired hydrogels (Cornwell *et al.* 2015, Gargava *et al.* 2016), hydrogel modification reactions (Feng *et al.* 2015) or foaming of polymeric materials (Kovalenko *et al.* 2016, Schlögl *et al.* 2012), strong electrolyte PAGs are preferred compared to weak electrolyte PAGs like c4ms or *p*HPs. For such applications, diphenyliodonium compounds are often used as strong electrolyte PAGs, which were discovered by Crivello *et al.* in 1977 (Crivello *et al.* 1977). However, many diphenyliodonium-based PAGs like diphenyliodonium nitrate or dipheyliodonium antimonate are toxic, which significantly limits their application (Shirai *et al.* 1996). In fact, such PAGs cannot be implemented into biological, physiological and medical applications. Nevertheless, Gargava *et al.* used diphenyliodonium nitrate as PAG to regulate the pH-dependent pore size of bioinspired hydrogel valves (Gargava *et al.* 2016). Also Feng *et al.* applied diphenyliodonium nitrate as PAG to trigger light controlled shape memory hydrogels (Feng *et al.* 2015). The process involved shape retention through coordination interaction between the imidazole groups of the poly(acrylamide-co-*N*-vinylimidazole) hydrogel and dissolved metal ions in the aqueous swelling agent (Feng *et al.* 2015). Shape recovery of the hydrogel was acchieved by switching off the complexation *via* PAG photolysis reaction due to the protonation of imidazole groups (Feng *et al.* 2015). Diphenyliodonium nitrate was also used to phototrigger the self assembly of a 1,3:2,4-dibenzylidene-D-sorbitol hydrogel in a controlled way when the pH was lowered (Cornwell *et al.* 2015). There are approaches to circumvent the toxicity of diphenyliodonium nitrate by using other photoacid generators like diaryliodonium tetrakis (pentafluorophenyl) borate or

diphenyliodonium hexafluorophosphate, but they frequently need additional photosensitzers (Kovalenko *et al.* 2016, Schlögl *et al.* 2012). Kovalenko *et al.* for instance applied commercially available diaryliodonium tetrakis (pentafluorophenyl) borate (Silcolease UV Cata211) with low toxicity, but needed 2-isopropylthioxanthone as photosensitizer to tailor the porous structure of polydimethylsiloxane foams (Kovalenko *et al.* 2016). A further example where strong electrolyte PAGs were favoured was published by Schlögl *et al.* for the foaming of 3D printed polyacrylate films (Schlögl *et al.* 2012). In particular, they utilized diphenyliodonium hexafluorophosphate as PAG and a toxic anthracene photosensitizer in combination with carbonate particles to generate CO_2 as foaming agent (Schlögl *et al.* 2012). The implementation of PAGs enabled them to simultaneously foam and cure their 3D printed polymers (Schlögl *et al.* 2012). Such 3D printed porous materials are subject to current research (Kankala *et al.* 2018, Schuster *et al.* 2019, Schuster *et al.* 2017). Especially in the above described fields of hydrogel research and polymeric foaming, c4m- and *p*HP-based PAG could be benefical, since they do not exhibit a cationic core structure which often limits biocomtability. However, c4m- and *p*HP-based PAG are rarely used, presumably due to the restricted or undetermined solubility of c4m and *p*HP-based PAGs aqueous solutions. In some publications, a water solubility of c4m and *p*HP derivatives was reported (Givens *et al.* 1996, Givens *et al.* 2011, Hagen *et al.* 2008, Hagen *et al.* 2005, Hagen *et al.* 2010), but a solubility in aqueous media was not yet quantified, which is a crucial parameter for the PAG selection process.

Thus, to develop PAGs that would be usable in aqueous media in high concentration, we designed a c4m and a *p*HP derivative where a bis(carboxymethyl)amino moiety or a tri(ethylene glycol) moiety, respectively, should ensure high water solubility. The synthesis of 7-[bis(carboxymethyl)amino]-4-(acetoxymethyl)coumarin (c4m-ac) and *p*-hydroxyphenacyl-2,5,8,11-tetraoxatridecan-13-oate (*p*HP-t) (Scheme 15) is described and the solubility in aqueous media is quantified. We aimed to synthesize c4m and *p*HP-based PAGs with solubilities well above 1 mM in aqueous media, which are referred to as good in the c4m and *p*HP literature (Givens *et al.* 1996, Givens *et al.* 2011, Hagen *et al.* 2008, Hagen *et al.* 2005, Hagen *et al.* 2010). We furthermore characterized these new c4m and *p*HP-based PAGs and determined their photochemical properties, their pH dependent stability and photolysis in aqueous media. We envision that our studies will contribute to an increased applicability of c4m

and *p*HP-based PAG in aqueous media, where high PAG concentrations are needed, like in hydrogel research or the field of polymeric foaming.

8.3 Experimental section

Materials. 2-Bromo-4-hydroxyacetophenone, 4-dimethylamino-pyridine (4-DMAP), 1-ethyl-3-(3-dimethylaminopropyl)-carbodiimide (EDC) and dichloromethane were purchased at TCI Germany GmbH (Eschborn, Germany). Ammonium chloride, hydrogen chloride, potassium permanganate, sodium hydride (60% dispersion in methanol), 7-amino-4-methylcoumarin, bromoacetic acid *tert*-butyl ester, sodium iodide, selenium dioxide, *p*-xylene, sodium borohydride, *N,N*-dimethylformamide (DMF) and sodium sulfate were obtained from Sigma-Aldrich Chemicals GmbH (Darmstadt, Germany). Ethyl bromoacetate was purchased from Alpha Aesar (Ward hill, USA), sodium acetate (NaOAc) from Merck Chemicals GmbH (Darmstadt, Germany) and phenylalanine from Acros Organics (Geel, Belgium). Tri(ethylene glycol) monomethyl ether and sodium hydroxide were bought from Fluka Analytical (Munich, Germany). Diethylether and magnesium sulfate were purchased from AppliChem GmbH (Darmstadt, Germany). Acetic acid (AcOH), sodium chloride, sodium hydrogencarbonate and trifluoroacetic acid (TFA) were bought from Carl Roth GmbH + Co. KG (Karlsruhe, Germany). The solvents ethanol (EtOH), ethyl acetate (EtOAc), methanol (MeOH) and *n*-hexane were bought from VWR chemicals (Radnor, USA). Acetonitrile (MeCN) and tetrahydrofuran (THF) were obtained from J.T. Baker (Phillipsburg, USA). All chemicals and solvents were of the highest grade commercially available and were used without further purification. Thin-layer chromatography (TLC) analyses were performed on aluminum plates coated with silica gel 60 F 254 by Merck Chemicals GmbH (Darmstadt, Germany) and Nano-Silica gel RP-18W by Fluka Analytical (Munich, Germany). For flash chromatography, silica gel 60 by Macherey-Nagel or silica gel 60 (0.063 – 0.200 mm) and LiChroprep RP-18 (40-63 µm) by Merck Chemicals GmbH (Darmstadt, Germany) were used. Water was purified with a TKA X-CAD Milli-Q system from Thermo Fischer Scientific (Waltham, USA).

Instrumentation. The NMR spectra of the c4m-based compounds were recorded on a Bruker AVIII-HD 500 MHz instrument from Bruker (Billerica, USA) equipped with a N_2 cooled cryogenic probe head using DMSO-d^6. The NMR spectra of the *p*HP-based compounds were recorded on a Bruker Avance 500 from Bruker (Billerica, USA) with

$CDCl_3$ as solvent. Mass spectrometry was performed on an ESI-MS Bruker MicroTOFQ from Bruker (Billerica, USA) under nitrogen atmosphere.

For the measurement of the pH value an InLab 1 022 pH electrode from Mettler Toledo (Columbus, USA) in combination with a Lab 850 pH meter was used. Photolysis experiments were performed in an UV-H 255 UV chamber from Hartmann Feinwerkbau GmbH (Ober-Moerlen, Germany) with an irradiation intensity of approx. 40 mW cm^{-2} between 300 nm and 450 nm (Figure 74). The emission spectrum was determined with an Ocean Optics USB 2 000+ spectrometer from Ocean Optics Germany GmbH (Ostfieldern, Germany). The distance between the bottom of the sample and the UV source in the UV chamber was 8.5 cm. UV-vis spectra were recorded in a two beam UV-vis spectrometer UV-2450 from Shimadzu (Kyoto, Japan) with quartz cuvettes of 1 cm path length and a cross-sectional area of 1 cm².

For quantum yield determinations c4m-ac was irradiated with a M365L2 LED from Thorlabs at 365 nm. For the irradiation of *p*HP-t and *p*HP-ac a M310L3 LED from Thorlabs (Newton, USA) at 310 nm was used. Both were operated by a DC4100 LED driver from Thorlabs (Newton, USA). The decay of c4m-ac was analyzed with a 1 260 Infinity HPLC from Agilent Technologies Germany GmbH (Waldbronn, Germany), equipped with a diode array detector. Separation was done using MultoKrom® 100-5 C18 column (250 x 4.6 mm) from CS-Chromatographie Service GmbH (Langerwehe, Germany). Chromatograms were analyzed with ChemStation software from Agilent Technologies Germany GmbH (Waldbronn, Germany).

For stability and photolysis determinations, HPLC measurements were performed using an analytical CBM-20A/20Alite HPLC from Shimadzu (Kyoto, Japan) with a Superspher 100 RP-18 (125 mm x 4.0 mm) column from Merck Chemicals GmbH (Darmstadt, Germany) and a SPD-M20A photodiode detector from Shimadzu (Kyoto, Japan). For c4m-ac a mixture of ACN : H_2O = 15 % : 85 %, for *p*HP-t a mixture of ACN : H_2O = 17 % : 83 % and for *p*HP-ac a mixture of ACN : H_2O = 10 % : 90 % was used for eluation. Trifluoroacetic acid (0.1%) was added to the HPLC solvent for *p*HP-t and *p*HP-ac. The flow rate was 1.0 mL min^{-1}. The HPLC chromatograms were analyzed with LCsolution software from Shimadzu (Kyoto, Japan).

Synthesis and characterization. C4m-ac was synthesized by altering Hagen *et al.*'s synthesis route for c4m-based photoacid generators (Hagen *et al.* 2005). The

compound *p*HP-t and the reference substance *p*-hydroxyphenacyl acetate (*p*HP-ac) were synthesized by modifying the synthesis from the literature (Kaila *et al.* 2007, Le *et al.* 2016).

Di-*tert*-butyl 2,2'-((4-methyl-2-oxo-*2H*-chromen-7-yl)-azanediyl)diacetate (1a): 7-Amino-4-methylcoumarin (**1**) (5.26 g, 30 mmol, 1.0 eq), bromoacetic acid *tert*-butyl ester (29.56 mL, 200 mmol, 6.7 eq), diisopropylethylamine (20.54 mL, 120 mmol, 4.0 eq) and NaI (4.5 g, 30 mmol, 1.0 eq) were dissolved in acetonitrile (90 mL) and stirred at 80 °C for 10 days. The mixture was cooled to room temperature (RT), filtered, and the solvent was removed under reduced pressure. The residue was dissolved in EtOAc (250 mL), washed with brine (3 × 50 mL), dried over Na_2SO_4 and the solvent was removed under reduced pressure. Purification *via* flash chromatography (silica, EtOAc : *n*-hexane = 1:4) afforded di-*tert*-butyl 2,2'-((4-methyl-2-oxo-2*H*-chromen-7-yl)azanediyl)diacetate (**1a**) (5.08 g, 12.60 mmol, 42 %) as a yellow oil.

^{1}H NMR (500 MHz, DMSO-d$_6$): δ [ppm] = 7.55 (d, *J* = 9.0 Hz, 1H), 6.57 (dd, *J* = 9.0 Hz, 2.5 Hz, 1H), 6.42 (d, *J* = 2.5 Hz, 1H), 6.03 (s, 1H), 4.18 (s, 4H), 2.50 (s, 3H), 1.42 (s, 18H).

^{13}C NMR (125 MHz, DMSO-d$_6$): δ [ppm] = 168.9, 160.5, 154.9, 153.5, 151.2, 126.0, 110.0, 109.1, 108.9, 98.0, 81.0, 53.5, 27.7, 17.9.

ESI-MS (+): m/z: $[M+H]^+$ 404.19.

Di-*tert*-butyl 2,2'-((4-formyl-2-oxo-*2H*-chromen-7-yl)-azanediyl)diacetate (1b): Di-*tert*-butyl 2,2'-((4-methyl-2-oxo-2*H*-chromen-7-yl)azanediyl)diacetate (**1a**) (4.03 g, 10 mmol, 1.0 eq) was dissolved in 50 mL *p*-xylene by heating, selenium dioxide (2.21 g, 20 mmol, 2.0 eq) was added, and the mixture was refluxed for 24 h. The mixture was filtered hot to remove black selenium, and the filtrate was concentrated under reduced pressure. The resulting precipitate afforded di-*tert*-butyl 2,2'-((4-formyl-2-oxo-2*H*-chromen-7-yl)azanediyl)diacetate (**1b**) (3.41 g, 8 mmol, 80 %) as orange-red powder.

^{1}H NMR (500 MHz, DMSO-d$_6$): δ [ppm] = 10.08 (s, 1H), 8.23 (d, *J* = 9.1 Hz, 1H), 6.76 (s, 1H), 6.64 (dd, *J* = 9.1 Hz, 2.6 Hz, 1H), 6.52 (d, *J* = 2.6 Hz, 1H), 4.21 (s, 4H), 1.42 (s, 18H).

^{13}C NMR (125 MHz, DMSO-d$_6$): δ [ppm] = 194.0, 168.7 160.9, 156.1, 151.5, 143.7, 126.4, 118.1, 109.8, 105.0, 98.4, 81.2, 53.5, 27.7.

ESI-MS (+): m/z: [M-H]$^+$ 416.20.

Di-*tert*-butyl-2,2'-((4-(hydroxymethyl)-2-oxo-*2H*-chromen-7-yl)azanediyl)-diacetate (1c): Di-*tert*-butyl 2,2'-((4-formyl-2-oxo-*2H*-chromen-7-yl)azanediyl)-diacetate (**1b**) (2.00 g, 5 mmol, 1.0 eq) was dissolved in MeOH (100 mL) and NaBH$_4$ (0.23 g, 6 mmol, 1.3 eq) was slowly added. The mixture was stirred at RT for 2 hours, diluted with H$_2$O (40 mL), acidified (pH 5) with 0.1 N HCl and extracted with CH$_2$Cl$_2$ (30 mL, 3x). The combined organic layers were washed with H$_2$O and brine, dried over Na$_2$SO$_4$ and the solvent was removed under reduced pressure. Purification by flash chromatography (hexane : EtOAc = 2 : 1) afforded di-*tert*-butyl 2,2'-((4-(hydroxy-methyl)-2-oxo-*2H*-chromen-7-yl)azanediyl)diacetate (**1c**) (1.6 g, 4 mmol, 74 %) as yellow solid.

^{1}H NMR (500 MHz, DMSO-d$_6$): δ [ppm] = 7.48 (d, J = 9.0 Hz, 1H), 6.54 (dd, J = 9.0 Hz, 2.6 Hz, 1H), 6.43 (d, J = 2.6 Hz, 1H), 6.15 (t, J = 1.4 Hz, 1H), 5.54 (t, J = 10 Hz, 1H), 4.68 (d, J = 3.0 Hz, 2H), 4.18 (s, 4H), 1.42 (s, 18H).

^{13}C NMR (125 MHz, DMSO-d$_6$): δ [ppm] = 168.9, 160.9, 156.8, 154.9, 151.1, 124.9, 108.9, 107.4, 105.3, 98.1, 81.1, 59.0, 53.5, 27.7.

ESI-MS (+): m/z: [M+H]$^+$ 420.19.

2,2'-((4-(Hydroxymethyl)-2-oxo-*2H*-chromen-7-yl)azanediyl)diacetic acid (1d): Di-*tert*-butyl 2,2'-((4-(hydroxymethyl)-2-oxo-2H-chromen-7-yl)azanediyl)diacetate (**1c**) (0.50 g, 1 mmol) was stirred in a mixture of TFA/ H$_2$O/ CH$_2$Cl$_2$ (74 : 1 : 25) (20 mL) at RT for 25 min. The solvent was removed under reduced pressure and coevaporated with Et$_2$O (2x), dissolved in a acetonitrile-water mixture, lyophilized and afforded 2,2'-((4-(hydroxymethyl)-2-oxo-*2H*-chromen-7-yl)azanediyl)diacetic acid (**1d**) (0.37 g, 1 mmol) quantitatively.

^{1}H NMR (500 MHz, DMSO-d$_6$): δ [ppm] = 7.47 (d, J = 9.0 Hz, 1H), 6.56 (dd, J = 9.0, 2.6 Hz, 1H), 6.45 (d, J = 2.6 Hz, 1H), 6.14 (t, J = 1.4 Hz, 1H), 4.68 (d, J = 1.0 Hz, 2H), 4.21 (s, 4H).

^{13}C NMR (125 MHz, DMSO-d$_6$): δ [ppm] = 171.4, 160.9, 156.8, 154.9, 151.1, 125.0, 108.9, 107.3, 105.2, 98.0, 59.0, 52.8.

ESI-MS (+): m/z: [M+H]$^+$ 308.15.

7-[bis(carboxymethyl)amino]-4-(acetoxymethyl)coumarin (c4m-ac): 2,2'-((4-(Hydroxymethyl)-2-oxo-*2H*-chromen-7-yl)azanediyl)diacetic acid (**1d**) (0.10 g, 0.3 mmol, 1.0 eq), 4-DMAP (0.12 g, 1 mmol, 3.0 eq), EDC (0.17 g, 1 mmol, 3.0 eq) and AcOH (51 μL, 1 mmol, 3.0 eq) were dissolved in DMF (5 mL) and stirred at RT for 12 hours. The solvent was removed under reduced pressure. Purification *via* RP-HPLC afforded 7-[bis(carboxymethyl)amino]-4-(acetoxymethyl)coumarin (0.07 g, 0.2 mmol, 63 %) (c4m-ac) as yellow solid.

^{1}H NMR (500 MHz, DMSO-d$_6$): δ [ppm] =12.85 (s, 2H), 7.51 (d, *J* = 9.0 Hz, 1H), 6.60 (dd, *J* = 9.0 Hz, 2.3 Hz, 1H), 6.48 (d, *J* = 2.3 Hz, 1H), 6.10 (s, 1H), 5.28 (s, 2H), 4.23 (s, 4H), 2.16 (s, 3H).

^{13}C NMR (125 MHz, DMSO-d$_6$): δ [ppm] = 171.4, 170.0, 160.4, 155.1, 151.5, 150.6, 125.4, 109.2, 106.9, 106.6, 98.1, 61.1, 52.8, 20.5.

ESI-MS (+): m/z: [M+H]$^+$ 350.13.

Ethyl-2,5,8,11-tetraoxatridecan-13-oate (2a): Under nitrogen atmosphere tri(ethylene glycol) monomethyl ether (**2**) (5.54 g, 34 mmol, 1.0 eq) and sodium hydride (1.62 g, 67 mmol, 2.0 eq) were dissolved in anhydrous THF (100 mL) at 0 °C. Ethyl bromoacetate (14.09 g, 84 mmol, 2.5 eq) was added at RT, stirred for two hours and filtrated. The white residue was dissolved in NH$_4$Cl solution at 0 °C and the aqueous phase was extracted with EtOAc. The combined organic phases were washed with water and dried over MgSO$_4$. The solvent and the excess of ethyl bromoacetate were removed under reduced pressure to afford ethyl-2,5,8,11-tetraoxatridecan-13-oate (**2a**) (4.37 g, 17 mmol, 52 %) as a colorless oil.

^{1}H-NMR (500 MHz, CDCl$_3$): δ [ppm] = 4.22 (q, *J* = 7.2 Hz, 2H), 4.15 (s, 2H), 3.64-3.75 (m, 10H), 3.54-3.56 (m, 2H), 3.38 (s, 3H), 1.29 (t, *J* = 6.9 Hz, 3H).

^{13}C NMR (125 MHz, CDCl$_3$): δ [ppm] = 170.5, 71.9, 70.9-70.6, 68.7, 60.8, 59.0, 14.2.

ESI-MS (+): m/z: [M+Na]$^+$ 273.13 Da.

2,5,8,11-Tetraoxatridecan-13-oic acid (2b): The ester **2a** (0.98 g, 4 mmol, 1.0 eq) was dissolved in a 1 M methanolic solution of sodium hydroxide (22.00 mL, 20 mmol, 5.0 eq) and stirred for 72 h at RT. The solution was adjusted to a pH value of 3 by adding aqueous HCl solution. The solvent was removed under reduced pressure and the residue was dissolved in diethylether. Unsoluble solid was separated through filtration and the organic phase was washed with water. By evaporating the solvents 2,5,8,11-tetraoxatridecan-13-oic acid (**2b**) (0.75 g, 3 mmol, 86 %) could be obtained as colorless oil.

^{1}H NMR (500 MHz, CDCl$_3$): δ [ppm] = 8.33 (s, 1H), 4.17 (s, 2H), 3.77-3.75 (m, 2H) 3.70-3.64 (m, 8H), 3.59-3.57 (m, 2H), 3.39 (s, 3H).

^{13}C NMR (125 MHz, CDCl$_3$): δ [ppm] = 172.8, 71.9-70.32, 68.9, 58.9.

ESI-MS (-): m/z: [M-H]$^-$ 221.1 Da.

_p_-Hydroxyphenacyl-2,5,8,11-tetraoxatridecan-13-oate (_p_HP-t): 2,5,8,11-tetraoxa-tridecan-13-oic acid (**2b**) (0.76 g, 3 mmol, 2.0 eq) were added to a 0.5 M aqueous sodium hydroxide solution (4.2 mL, 2 mmol, 1.1 eq) and stirred at RT for 10 minutes. 2-Brom-4-hydroxyacetophenone (0.36 g, 2 mmol, 1.0 eq) were dissolved in EtOH (15 mL) and heated under reflux conditions for 2 hours. After removing the solvent under reduced pressure the oily residue was dissolved in water and adjusted to a pH 8 by adding saturated sodium hydrogencarbonate solution (3.5 mL). The aqueous phases were extracted with dichloromethane and the combined organic phases were washed with brine and dried over sodium sulfate. The solvent was evaporated under reduced pressure and the raw product was purified _via_ column chromatography (silica, _n_-hexane : EtOAc = 1 : 2, EtOAc, EtOAC : MeOH = 1 : 9). The solvent was removed under reduced pressure to afford _p_-hydroxyphenacyl-2,5,8,11-tetraoxatridecan-13-oate (_p_HP-t) (0.29 g, (1 mmol, 49 %) as colorless oil.

^{1}H NMR (500 MHz, CDCl$_3$): δ [ppm] = 7.80 (dt, _J_ = 8.8 Hz, 2.7 Hz, 2H), 6.91 (dt, _J_ = 8.8 Hz, 2.7 Hz, 2H), 5.32 (s, 2H), 4.30 (s, 2H), 3.76–3.75 (m, 2H), 3.70–3.64 (m, 8H), 3.57–3.55 (m, 2H), 3.37 (s, 3H).

^{13}C NMR (125 MHz, CDCl$_3$): δ [ppm] = 190.3, 170.2, 161.6, 130.4, 126.6, 115.8, 71.9, 70.9–70.4, 68.5, 66.1, 59.0.

ESI-MS (-): m/z: [M-H]$^-$ 355.15 Da.

***p*-Hydroxyphenacylacetate (*p*HP-ac):** 2-Bromo-4-hydroxyacetophenone (1.48 g, 7 mmol, 1.0 eq) were dissolved in EtOH and a mixture of sodium acetate (1.12 g, 8 mmol, 1.2 eq) and AcOH (0.36 mL, 6 mmol, 0.9 eq) in water (3.6 mL) was added dropwise. The solution was heated for 3h at 90 °C under reflux conditions. The solvent was removed under reduced pressure and the remaining oily residue was dissolved in aqueous sodium carbonate solution. The aqueous phase was extracted with EtOAc and the combined organic phases were washed with brine and dried over sodium sulfate. After evaporation of the solvent, the raw product was recrystallized from EtOAc and purified by a column chromatography (*n*-hexane : EtOAc = 7 : 3). *p*-hydroxyphenacylacetate (*p*HP-ac) (0.97 g, 5 mmol, 73 %) was obtained as a white solid.

^{1}H NMR (500 MHz, CDCl$_3$): δ [ppm] = 7.83 (dt, *J* = 8.8 Hz, 2.8 Hz, 2H), 6.89 (dt, *J* = 8.8 Hz, 2.8 Hz, 2H), 6.19 (s, 1H), 5.30 (s, 2H), 2.24 (s, 3H).

^{13}C-NMR (125 MHz, CDCl$_3$): δ [ppm] = 190.8, 170.9, 160.9, 130.4, 127.1, 115.7, 65.8, 20.7.

ESI-MS (-): m/z: [M-H]$^-$ 193.03 Da.

Solubility determination. The solubilities of c4m-ac, *p*HP-t and *p*HP-ac were determined photometrically in water and alkaline solution (3M KHCO$_3$ solution, pH 9). For the determination of the solubility in water $c_{max,w}$ and the solubility in alkaline solution $c_{max,a}$ a calibration curve was prepared by measuring the UV-vis absorption spectra of the PAGs at four different concentrations in water and in basic solution (Figure 69).

The concentrations were selected in such a way that the absorbance maxima were spread over the linear absorbance range (A_λ = 0.1 - 0.9) of the Beer's law (Beer 1852):

$$A_\lambda = \varepsilon_\lambda \cdot c \cdot d \tag{16}$$

In this equation, A_λ is the absorbance at a specific wavelength λ, ε_λ is the molar absorption coefficient at the wavelength λ, c is the concentration and *d* is the path length. The calibration curve was used to determine the molar absorption coefficient ε_λ of the PAG in the respective media. Three saturated PAG solutions were prepared and diluted until the absorbance maxima were in the linear absorbance range. To calculate the concentration of the diluted sample (c_d) the previously determined molar absorption

coefficient ε_λ was used. As shown in equation (17), the solubility in water $c_{max,w}$ can be quantified by multiplying the concentration of the diluted PAG solution c_d with the dilution factor d_f.

$$c_{max,w} = \frac{A_\lambda}{\varepsilon_\lambda \cdot d} \cdot d_f = c_d \cdot d_f \tag{17}$$

The solubility in alkaline solution $c_{max,a}$ is determined respectively by using A_λ, ε_λ and d_f of the alkaline solution. The solubility determination was performed in triplicates.

Quantum Yield determination. All measurements were performed in 1 cm quartz fluorescence cuvette from Hellma GmbH (Müllheim, Germany). For irradiation of c4m-ac, a M365L2 LED from Thorlabs at 365 nm was used and for *p*HP-t and *p*HP-ac, an M310L3 LED from Thorlabs (Newton, USA) at 310 nm was applied. Both were operated by a DC4100 LED driver from Thorlabs (Newton, USA). Light sources were calibrated using iron (III) ferrioxalate actinometry, following the literature procedure (Hatchard *et al.* 1956). The photo reaction of c4m-ac was followed by HPLC and of *p*HP-t and *p*HP-ac by UV-vis spectroscopy. All quantum yields Φ were measured in triplicates and calculated as previously described (Reinfelds *et al.* 2018).

For the Φ determination of c4m-ac, an aqueous sample of c4m-ac containing the internal standard phenylalanine was irradiated at 365 nm and the conversion was analyzed *via* HPLC. The conversion change (in %) of c4m-ac was plotted against irradiation time (t_{irr}). The plot was fitted using following exponential decay function (equation (18)), where A_1 and t_1 are fit parameters and y_0 is a constant (Reinfelds *et al.* 2018).

$$y = A_1 e^{\frac{t_{irr}}{t_1}} + y_0 \tag{18}$$

The initial rate of the concentration change (y') at the beginning of the irradiation can be calculated by deriving equation (19) and inserting the corresponding fit parameters for $t_{irr} = 0$ (Reinfelds *et al.* 2018):

$$y' = -\frac{A_1 e^{\frac{-t_{irr}}{t_1}}}{t_1} \tag{19}$$

For c4m-ac, Φ is then calculated by equation (20), where c is the concentration of the irradiated solution, V is the volume of the irradiated sample, y' is the change in concentration, n_p is the photon flux of the light source determined by actinometry and

_____

A_λ is the absorbance of the PAG solution at the irradiation wavelength (Reinfelds *et al.* 2018).

$$\Phi = \frac{c \cdot V \cdot y'}{n_p \cdot (1 - 10^{-A_\lambda})} \tag{20}$$

In contrast to c4m-ac, Φ of *p*HP-t and *p*HP-ac was determined by UV-vis spectroscopy. Therefore, *p*HP-t and *p*HP-ac samples with a high absorption ($A_\lambda > 3$) at 310 nm were used to ensure complete absorption of radiant flux. The *p*HP-based PAGs were irradiated and the change of absorption was measured simultaneously using a photodiode array detector. A plot of the absorption change against irradiation time was prepared choosing a suitable wavelength with $A_\lambda < 1$. The decrease of the absorption in the initial phase of the reaction (conversion < 10 %) was fitted by a linear regression. Φ of *p*HP-t and *p*HP-ac was calculated using equation (21):

$$\Phi = \frac{-k\, V}{d \cdot \varepsilon_\lambda \cdot n_p} \tag{21}$$

Here, k is the slope from the linear regression, V is the volume of the irradiated sample, d is the pathlength of the cuvette, ε_λ is the molar absorption coefficient of the wavelength used for the reaction control (here at 321 nm) and n_p is the photon flux of the light source.

Stability determination. C4m-ac, *p*HP-t and *p*HP-ac were dissolved in water at a concentration of 0.2 g L^{-1}, which led to pH 3 for c4m-ac, pH 6 for *p*HP-t and pH 5 for *p*HP-ac. Aliquots of these PAG solutions were adjusted to pH 7 and pH 8 with 0.01 M NaOH. The samples were stored under light exclusion at RT for 1 h, 3 h and 24 h. After filtration, they were measured *via* HPLC. The elution time (t_{elu}) of c4m-ac was 6.3 min, of *p*HP-t 9.0 min and of *p*HP-ac 9.5 min. The PAG stability (s) was calculated according equation (22), where $P_{t=0}$ is the peak area of the PAG immediately after preparation ($t = 0$) and P_t is the respective peak area after a storage time t_s.

$$s = \frac{P_t}{P_{t=0}} \tag{22}$$

Photolysis. An aqueous solution of c4m-ac, *p*HP-t and *p*HP-ac was prepared with a concentration of 0.2 mg mL^{-1}. This led to a solution of pH 3 for c4m-ac, of pH 6 for *p*HP-t and of pH 5 for *p*HP-ac, respectively. An aliquot of each PAG solution was adjusted to pH 7 and to pH 8 using 0.01 M NaOH. 1 mL samples of the PAG solutions were irradiated in a quartz glass cuvette using a hartmann.gs UV-H 255 UV chamber.

The irradiation time t_{irr} was adjusted to the photolysis speed of the compound. The photolysis of c4m-ac for instance was measured after 0.5 min, 1 min, 1.5 min, 2 min, 3 min, 4 min, 6 min and 8 min UV irradiation. For pHP-t, the photolysis was measured every two minutes for the first 10 minutes and then every 5 minutes. After 30 min, pHP-t was analyzed every 10 minutes until an overall t_{irr} of 60 minutes. For pHP-ac, the concentration was measured every minute in the first 10 minutes and afterwards every five minutes up to 80 minutes.

8.4 Results and discussion

Synthesis of c4m and pHP-based PAGs. The synthesis route and the molecular structures of the c4m and pHP-based PAGs, namely 7-[bis(carboxymethyl)amino]-4-(acetoxymethyl)coumarin (c4m-ac) and p-hydroxyphenacyl-2,5,8,11-tetraoxatridecan-13-oate (pHP-t), are shown in Scheme 15.

The synthesis of c4m-ac is based on previous work by Hagen *et al.* (Hagen *et al.* 2005) and started with the alkylation of 7-amino-4-methylcoumarin (**1**) with bromoacetic acid *tert*-butyl ester, followed by oxidation with SeO_2 to the corresponding aldehyde **1b** which was subsequently reduced with $NaBH_4$ to the primary alcohol **1c**. Deprotection of the carboxyl groups with trifluoroacetic acid yielded **1d** which was acetylated with acetic acid in the presence of 4-dimethylaminopyridine (4-DMAP) and 1-ethyl-3-(3-dimethyl-aminopropyl) carbodiimide (EDC) to form c4m-ac. The ^{1}H NMR and ^{13}C NMR spectra of c4m-ac and its intermediates are given in Figure 60 - Figure 64.

The synthesis of pHP-t was derived from Kaila *et al.*, whereby 3,6,9,12-tetraoxatridecanoic acid (**2b**) was used as nucleophile instead of acetic acid (Scheme 15) (Kaila *et al.* 2007). We used a two-step synthesis to generate **2b** according to Le *et al. via* Williamson ether synthesis of tri(ethylene glycol) monomethyl ether (**2**) with ethyl bromoacetate and subsequent saponification reaction (Le *et al.* 2016, Williamson 1850). The nucleophilic substitution of 2-bromo-4-hydroxy-acetophenone (**3**) with **2b** led to pHP-t. The ^{1}H NMR and ^{13}C NMR spectra of pHP-t and its intermediates are given in Figure 65 - Figure 68. Furthermore, p-hydroxyphenacylacetate (pHP-ac) was synthesized as reference substance according to Kaila *et al.* (2007) (Scheme 9). Figure 68 shows the ^{1}H NMR and ^{13}C NMR spectra of pHP-ac.
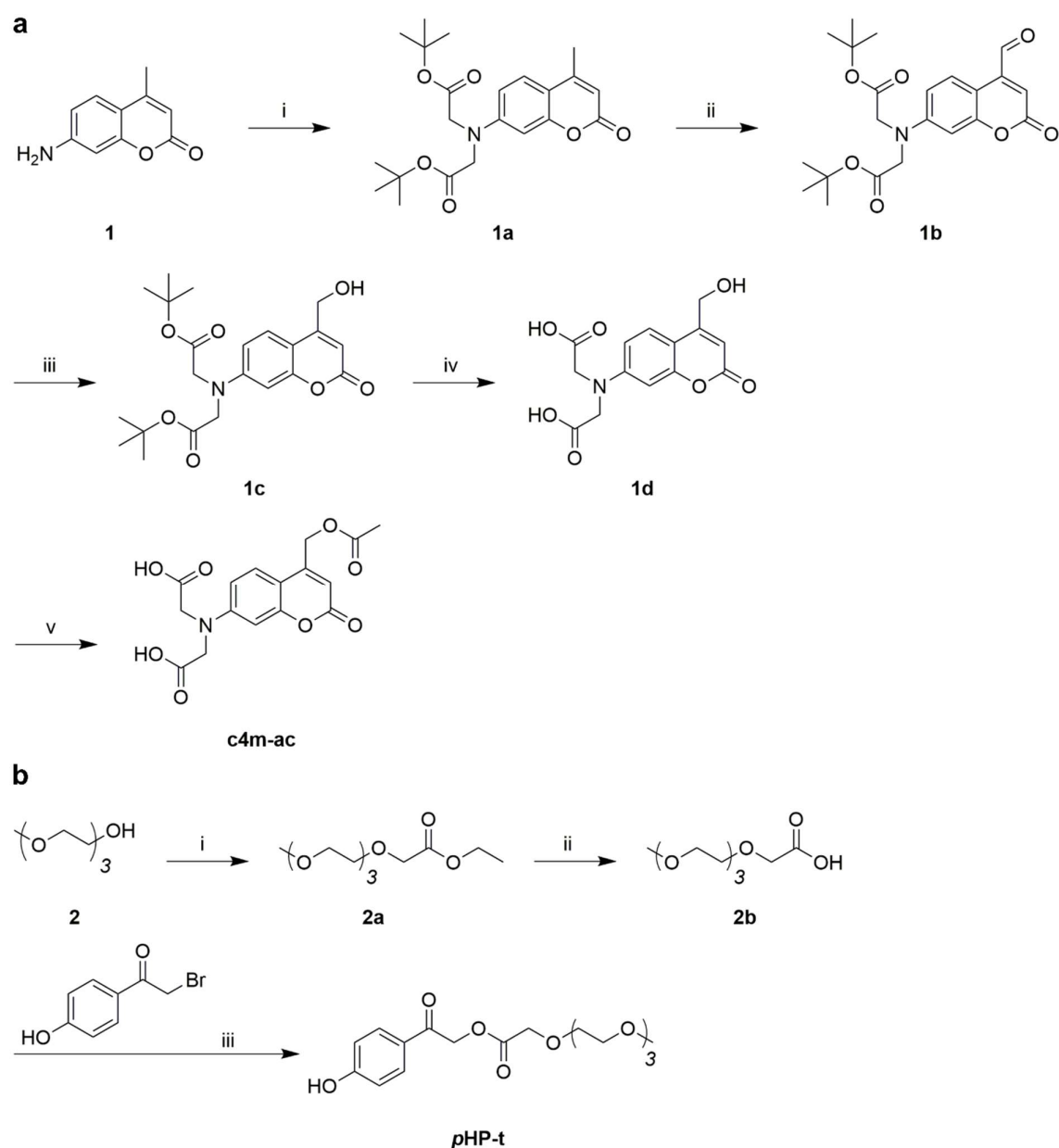
Scheme 15: Synthesis of a) 7-[bis(carboxymethyl)amino]-4-(acetoxy-methyl)coumarin (c4m-ac) over 5 steps with i) bromoacetic acid *tert*-butyl ester, NaI, ACN, 80 °C, 10 d, 43 %; ii) SeO$_2$, *p*-xylene, 150 °C, 24 h, 80 %; iii) NaBH$_4$, MeOH, RT, 2 h, 74 %; iv) TFA, H$_2$O, CH$_2$Cl$_2$, RT, 25 min, 100 %; v) 4-DMAP, EDC, AcOH, DMF, RT, 12 h, 63 %. Synthesis of b) *p*-hydroxyphenacyl-2,5,8,11-tetraoxatridecan-13-oate (*p*HP-t) over 3 steps with i) NaH, bromoacetic acid ethyl ester, THF, RT, 3 h, 52 %. ii) NaOH, MeOH, RT, 72 h, 86 %. iii) NaOH, EtOH, 115 °C, 2 h, 49 %.

Generally, all characterization data indicate that the syntheses yielded c4m-ac, *p*HP-t and *p*HP-ac in sufficient purity for further characterization as described below.

Solubility determination. As the solubility of many c4m- and *p*HP-based derivatives were only estimated roughly in previous studies (Givens *et al.* 1996, Givens *et al.* 2011,

Hagen *et al.* 2008, Hagen *et al.* 2005, Hagen *et al.* 2010), we wanted to quantify the solubilities $c_{max,w}$ and $c_{max,a}$ of c4m-ac and *p*HP-t in water and alkaline solution, respectively. Solubilities were determined photometrically by diluting saturated solutions of the compounds to diluted concentrations c_d. The value of c_d was determined by applying appropriate UV-vis calibrations for c4m-ac and *p*HP-t (Table 13, Figure 69). The solubilities $c_{max,w}$ and $c_{max,a}$ were then calculated with equation (17) using the dilution factor.
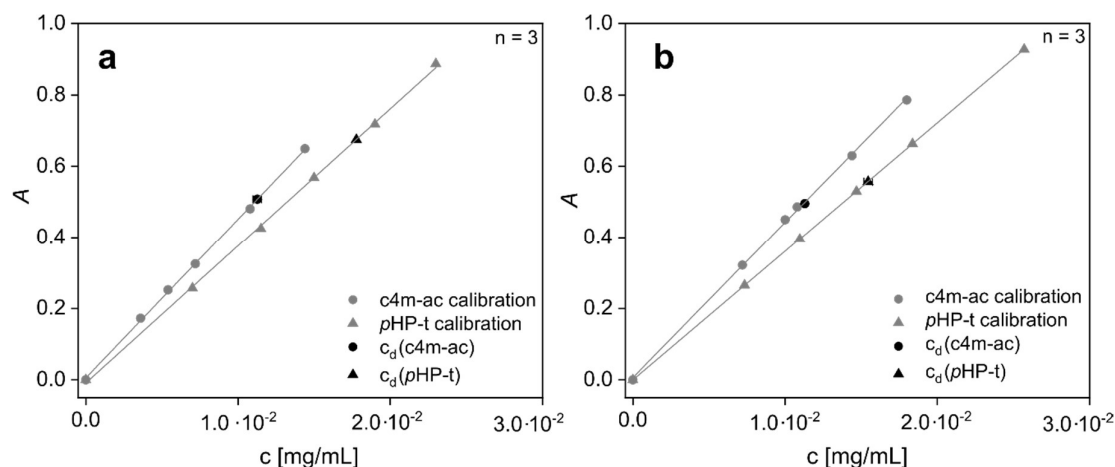

Figure 56: Absorbance *A* of c4m-ac and *p*HP-t solutions at different concentrations c for the photometric determination of the solubility in a) water and in b) alkaline solution at pH 9. The standard deviation of c_d is in the range of the symbol size.

Figure 56 demonstrates the absorbance of c4m-ac and *p*HP-t at different concentrations as well as at c_d at the wavelength λ_{max} of maximum absorbance in water and basic medium. In water, λ_{max} of c4m-ac is at 366 nm and of *p*HP-t at 281 nm (Table 12). In alkaline solution, λ_{max} of c4m-ac shifts to 377 nm and of *p*HP-t to 327 nm (Table 12). Resulting values for c_d are listed Table 13 and $c_{max,w}$ and $c_{max,a}$ are shown in Table 11. The compound c4m-ac shows a solubility $c_{max,w}$ in water of 2.77 mmol L^{-1} ± 0.07 mmol L^{-1} and a solubility $c_{max,a}$ in alkaline solution of 646.46 mmol L^{-1} ± 0.63 mmol L^{-1}. For *p*HP-t, a $c_{max,w}$ of 124.66 ± 2.19 mmol L^{-1} and a $c_{max,a}$ of 34.68 ± 0.62 mmol L^{-1} were found. Since PAG solubilities above 1 mmol L^{-1} in aqueous solutions were referred to as good (Hagen *et al.* 2008, Pella 2012), c4m-ac and *p*HP-t exhibit excellent solubility in water and basic solution. For comparison purposes, the solubilities of the reference substance *p*HP-ac were determined to be 14.40 ± 0.40 mmol L^{-1} ($c_{max,w}$) and 21.46 ± 8.58 mmol L^{-1} ($c_{max,a}$) (Figure 70).

In water, it becomes evident that the additional, hydrophilic tri(ethylene glycol) moiety present in pHP-t increased the solubility by a factor of 8.7 compared to pHP-ac, and thus the solubility enhancing effect of the tri(ethylene glycol) residue was clearly identified. In these conditions, the phenolic hydroxy group present in both pHP-t- and pHP-ac can be expected to be in its neutral form. Similarly, in c4m-ac the carboxylic acid groups will be partly protonated, resulting in a relatively low solubility in water.

In contrast, the solubility of c4m-ac in alkaline solution is boosted by a factor of 233 to the highest solubility observed in this study which can be explained by the more complete deprotonation of both carboxylic groups. A similar effect was observed for pHP-ac, however with only a moderate solubility increase by a factor of 1.5 due to the higher pK_a value of the phenolic hydoxy group compared to carboxylic acid groups. Interestingly, for pHP-t the solubility decreased in alkaline conditions although one could expect that also its phenolic group is deprotonated to a similar extent like in pHP-ac. We tend to explain this observation with a disruption of the hydrogen bonds between water and the tri(ethylene glycol) residue of pHP-t in salt-containing alkaline solution. Similar salting-out effects were reported by Brunchi et al., who measured a decreasing solubility of poly(ethylene glycol) (PEG) in aqueous solution when adding electrolytes (Brunchi et $al.$ 2013). However, the solubility of pHP-t still was 1.6-fold higher in alkaline conditions than of pHP-ac.

Overall, pHP-t showed the highest solubility in water ($c_{max,w}$ = 124.66 ± 2.19 mmol L^{-1}) and c4m-ac demonstrated the highest solubility in basic solution ($c_{max,a}$ = 646.46 mmol L^{-1} ± 0.63 mmol L^{-1}) among the studied PAGs (Table 11).·

Table 11: Solubility in water ($c_{max,w}$) and in alkaline solution ($c_{max,a}$) at pH 9 of the photoacid generators (PAGs) c4m-ac, pHP-t and pHP-ac.

PAG	$c_{max,w}$ [mmol L^{-1}]	$c_{max,w}$ [g L^{-1}]	$c_{max,a}$ [mmol L^{-1}]	$c_{max,a}$ [g L^{-1}]
c4m-ac	2.77 ± 0.07	0.97 ± 0.02	646.46 ± 0.63	225.80 ± 0.22
pHP-t	124.66 ± 2.19	44.43 ± 0.78	34.68 ± 0.62	12.36 ± 0.02

Stability in solution. As all PAGs investigated in this study contain at least one ester bond, hydrolysis may occur in aqueous solution. In order to quantify the influence of hydrolysis, the pH dependent stabilities (s) of c4m-ac, pHP-t and the reference compound pHP-ac in aqueous solution were investigated via HPLC. For this purpose,

aqueous c4m-ac, *p*HP-t and *p*HP-ac solutions at pH 7, pH 8 and pH 9 were prepared and the PAG concentrations were measured after 1 h, 3 h, and 24 h storage time t_s under light exclusion at room temperature. Additionally, the stabilities of c4m-ac, *p*HP-t, and *p*HP-ac in water without pH adjustment after dissolution leading to pH 3, pH 6, and pH 5, respectively, were investigated. PAG stabilities were calculated according to equation (22). The resulting pH dependent stabilities are shown in Figure 57 (c4m-ac, *p*HP-t) and Figure 71 (*p*HP-ac) and are summarized in Table 14.

Generally, the studied PAGs showed high stabilities (s_{24h} ≥ 95 %) for 24 h in slightly acidic solution as obtained without pH adjustment. At pH 7, c4m-ac showed the highest stability after 24 h (s_{24h} = 99 %), whereas *p*HP-t showed only limited stability (s_{24h} = 85 %) under the same conditions, compared to an s_{24h} value of 94 % for *p*HP-ac. Upon increasing the pH value, stabilities generally decreased. At pH 8, c4m-ac still showed s_{24h} ≥ 95 %, whereas for *p*HP-t s_{24h} dropped to 48 % compared to an unaltered value of 94 % for *p*HP-ac. At pH 9, all PAGs were significantly degraded with remaining concentrations of 11 % (c4m-ac), 0 % (*p*HP-t), and 53 % (*p*HP-ac). Summarizing, the PAGs showed decreasing stability with increasing pH and time. Because in all PAGs in this study, an ester bond is present, these observations can be ascribed to the faster ester bond hydrolysis under more alkaline conditions. For example, increasing hydrolysis rates were published for *p*HP-based esters at higher pH (> 9), which is in line with our measurements (Table 14) (Givens *et al.* 2012).
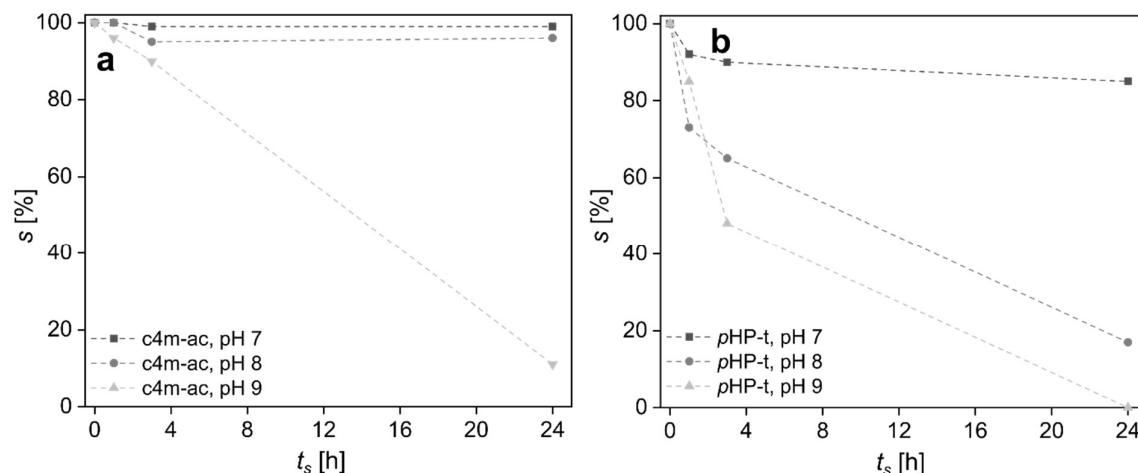

Figure 57: Stabilities (*s*) of the photoacid generators c4m-ac and *p*HP-t after a storage time t_s of 1 h, 3 h and 24 h at pH 7, pH 8 and pH 9. The stabilities were determined *via* HPLC and calculated according to equation (22). The dashed lines are only for the guidance of the eye.

The results demonstrate that at neutral to moderately alkaline conditions (pH ≤ 8), c4m-ac is most resistant towards hydrolytic degradation. The stability of c4m-ac is in the range of other c4m-caged esters and amines from Hagen *et al*. (2008), which are described to be highly resistant to spontaneous hydrolysis at pH 7. In contrast, Hagen *et al.* also reported hydrolysis of c4m-caged aryl alcohols, thioaryl alcohol and carbamates up to 10 % at pH 7 during 24 h, which demonstrates the high stability of c4m-ac with less than 1 % hydrolysis under comparable conditions (Hagen *et al.* 2008, Hagen *et al.* 2010).

As far as the stability of *p*HP derivatives is concerned, our results show that the leaving group present in the PAG influences its stability. At all pH values tested, *p*HP-t- showed faster hydrolysis than *p*HP-ac. Rather fast hydrolysis of esters neighboring an oligo(ethylene glycol) moiety were reported before by Claaßen *et al.* (2018) and can presumably be explained by the negative inductive effect of the tri(ethylene glycol) residue, resulting in a better carboxylate leaving group. The influence of the leaving group on *p*HP-based compounds can also be found in the literature: On the one hand, quantitative stabilities were reported for *p*HP esters and other *p*HP derivatives like *p*HP-adenosine triphosphate (ATP) in TRIS buffer at pH 7 after 24 h (Givens *et al.* 1996, Park *et al.* 1997). On the other hand, *p*HP esters similar to *p*HP-t showed reduced stability (Givens *et al.* 2011, Givens *et al.* 2000). The di-alanine (Ala-Ala) *p*HP derivative *p*HP-Ala-Ala for instance hydrolyzed to 50 % in TRIS buffer at pH 7 in less than 4 h (Givens *et al.* 2000).

In summary, hydrolysis is relevant for all PAGs studied, and has to be taken into account when considering to use these compounds in aqueous solution. Hydrolysis separates the acid from the chromophore, and therefore destroys the PAG functionality. Additionally, (unwanted) hydrolysis cannot be triggered and stopped as easily as (wanted) photolysis, and thus is a continuous process accompanying photolysis. Hence, photolysis conditions need to be chosen in such a way that hydrolysis plays only a minor role. For this reason, the photochemical properties of the PAGs are described in detail below.

Photochemical properties. The reaction pathways for photolysis of c4m and *p*HP based compounds are well known as they were extensively investigated by Hagen *et al.* (2008) and Givens *et al*. (2008), respectively. Hagen *et al.* (2008) showed that c4m derivatives with the same coumarin group like in this study photolyse to

7-[bis(carboxymethyl) amino]-4-(hydroxymethyl)coumarin (c4m-OH) and the respective caged molecule. The photolysis of pHP derivatives in contrast is based on the Favorskii-rearrangement, which leads to p-hydroxy-phenylacetic acid and the corresponding caged compound, like acetic acid for pHP-ac (Givens *et al.* 2008).
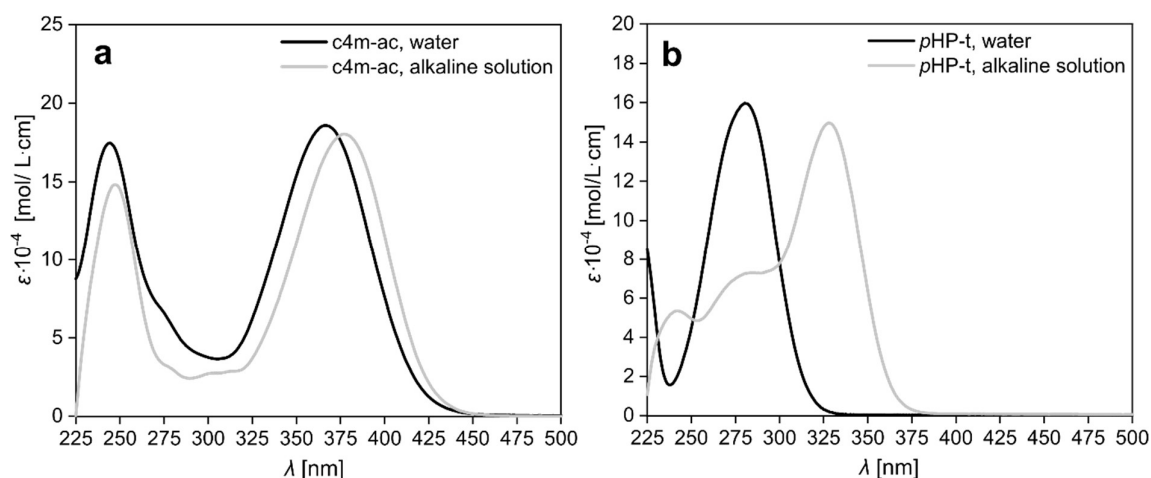

Figure 58: UV-vis spectra of a) c4m-ac and b) pHP-t in water and alkaline solution at pH 9.

However, the efficiency of the photolysis reaction depends on the exact molecular structure and the solvent, which define the absorption coefficients and the quantum yields. Therefore, as a first step to assess the photochemical properties of c4m-ac and pHP-t as well as the reference compound pHP-ac, their UV-vis absorption spectra both in water as well as alkaline solution were measured directly after dissolution (Figure 58 and Figure 72). All studied PAGs contain acidic groups, so it can be expected that their absorption spectrum is pH dependent. In order to assess if this was the case, the wavelength λ_{max} at maximum absorption and the molar absorption coefficients ε_{max} at λ_{max} were extracted from the spectra (Table 12).

Table 12: Wavelength at maximum absorption (λ_{max}), molar absorption coefficient (ε_{max}) at λ_{max} and quantum yield Φ at the wavelength λ_Φ given in parentheses. Tested solvents were water (w) and alkaline solution (a) at pH 9.

PAG	solvent	λ_{max} [nm]	ε_{max} [L mol^{-1} cm^{-1}]	Φ (λ_Φ)	ε_Φ [L mol^{-1} cm^{-1}]	$\Phi\varepsilon_\Phi$ [L mol^{-1} cm^{-1}]
c4m-ac	w	366	15 800	0.02 (365 nm)	15 800	320
c4m-ac	a	377	15 300	0.02 (365 nm)	13 900	280
pHP-t	w	281	13 500	0.69 (310 nm)	2 500	1700
pHP-t	a	327	12 900	0.07 (310 nm)	8 900	620
pHP-ac	w	281	11 600	0.46 (310 nm)	2 200	1000
pHP-ac	a	327	20 400	0.02 (310 nm)	15 300	300

In water, the compound c4m-ac absorbed light up to 450 nm with a λ_{max} at 366 nm and an ε_{max} of 15 800 L mol^{-1} cm^{-1} (Table 12). This was in the range of other c4m-based compounds like c4m thioalcohol derivatives, which exhibited similar UV-vis absorption properties with λ_{max} between 376 nm and 383 nm as well as ε_{max} between 18 300 L mol^{-1} cm^{-1} and 20 000 L mol^{-1} cm^{-1} in hydroxyethyl piperazineethanesulfonic acid (HEPES) buffer at pH 7 (Hagen *et al.* 2008). In alkaline solution, the absorption band of c4m-ac shifted to longer wavelengths with a λ_{max} of 377 nm and an ε_{max} of 15 300 L mol^{-1} cm^{-1}. This bathochromic shift was based on solvatochromic effects in alkaline solution, since the polarity of the alkaline solution was higher compared to water. Similar observations were reported from Liu and co-workers (2013), who described a red shift of the UV-vis spectra of 7-aminocoumarins in more polar solvents. Also Nad and Pal (2001) published a λ_{max} shift of 7-amino-4-trifluoromethylcoumarin from 347 nm to 378 nm by increasing the solvent polarity from hexane to methanol. Both explained that the higher the polarity of the solvent, the more intermolecular interactions between the coumarin moiety and the solvent can evolve, which stabilizes the ground state and shifts the UV-vis absorption to lower excitations energies (Liu *et al.* 2013, Nad *et al.* 2001).

Compared to the two strong absorption bands of c4m-ac around 245 nm and 366 nm, *p*HP-t showed only one prominent π-π* absorption band from 240 nm to 320 nm with a λ_{max} at 281 nm and an ε_{max} of 13 500 L mol^{-1} cm^{-1} in water (Table 12). The λ_{max} of *p*HP-t shifted from 281 nm in water to 327 nm under basic conditions due to deprotonation of the phenol moiety. This phenoxide species contains an enlarged π-electron system, which leads to a bathochromic shift of the λ_{max} in alkaline solution. This is in accordance with multiple *p*HP derivatives published by Givens *et al*. (2011). Similar to c4m-ac, ε_{max} of *p*HP-t slightly decreased from 13 500 L mol^{-1} cm^{-1} in water to 12 900 L mol^{-1} cm^{-1} in alkaline solution (Table 12). For *p*HP derivatives this is quite unusal as most reported *p*HP phenoxide derivatives show significantly higher ε_{max} than their protonated counterparts (Givens *et al.* 2011). The measurements on *p*HP-ac with an ε_{max} of 11 600 L mol^{-1} cm^{-1} in water and an ε_{max} of 20 400 L mol^{-1} cm^{-1} in basic solution confirmed the trend in the literature (Figure 72, Table 12) (Givens *et al.* 2011).

Apart from the molar absorption coefficients, quantum yields (Φ) are equally important in defining the rate of a photolysis reaction, as the rate is determined by the product of Φ and ε. Therefore, the photolysis quantum yields were measured at wavelengths near

λ_{max}, *i.e.* 310 nm for *p*HP derivatives and 365 nm for c4m-ac (Table 12). This way, a high Φ value of 0.69 was found for *p*HP-t in water. In alkaline solution, Φ of *p*HP-t decreased to 0.07. Similarly, Φ of *p*HP-ac decreased from 0.46 in water to 0.02 in alkaline solution. The results for the two *p*HP-based compounds thus are in a similar range of other *p*HP-caged compounds with Φ values between 0.03 and 0.65 in water (Givens *et al.* 2003, Givens *et al.* 2011, Zou *et al.* 2002, Zou *et al.* 2001). Also the reduction of the quantum efficiency is in line with previous reports, where it was described that the conjugated phenoxide base has a much lower quantum yield than the protonated species (Givens *et al.* 2011, Zou *et al.* 2001). This was attributed to a decreased intersystem crossing efficiency or competing nonproductive pathways (Givens *et al.* 2011, Zou *et al.* 2001).

The Φ of c4m-ac in contrast was not influenced by the pH and stayed at a relatively low value of 0.02 in water and basic solution, as the two carboxylic acid groups of c4m-ac were not part of the conjugated π-electron system. The Φ values of c4m-ac were in the range of other c4m-caged compounds reported by Hagen *et al.* with Φ between 0.01 and 0.30 in ACN/ HEPES-mixtures at pH 7.2 (Hagen *et al.* 2008, Hagen *et al.* 2005).

A comparison of the different photolysis efficiencies is now possible by comparing the product of Φ and the molar absorption coefficient ε_Φ at the wavelength where the quantum yield was measured (Table 12). It becomes evident that the two *p*HP-based compounds showed higher photolysis rates than c4m-ac when irradiated during the quantum yield measurements. The fastest photoreaction was observed for *p*HP-t, which under such 'ideal' photolysis conditions is the most efficient PAG. The difference in photolysis rates could probably be further enhanced by irradiating closer to the respective λ_{max} values, assuming that the quantum yields at these wavelengths are similar to the measured ones.

Photolysis with broadband light source. The data on molar absorption coefficients and quantum yields in the previous section give insight into photolysis rates when using monochromatic light sources or light sources with a narrow emission spectrum such as lasers and LEDs. However, broadband light sources are common in non-photochemical laboratories when rather short irradiation wavelengths are needed like for the *p*HP based compounds. This is especially true in the fields of PAG application described in the introduction such as polymer chemistry, hydrogel curing, and 3D

printing (Adatia *et al.* 2019, Hiller *et al.* 2017). To evaluate which of the studied PAGs are favorable under such circumstances, we investigated the photolysis of c4m-ac, *p*HP-t, and *p*HP-ac at three different pH values using a standard broadband light source by HPLC (see Figure 75 for an exemplary HPLC dataset). The emission spectrum of the light source ranged between wavelengths of 300 nm and 450 nm (Figure 74). The resulting PAG concentrations c against irradiation time t_{irr} of c4m-ac and *p*HP-t are shown in Figure 59, the respective data of the reference substance *p*HP-ac in Figure 73.

Generally, all PAGs disappeared completely during irradiation (Figure 75). The photolysis kinetics seem to follow a monoexponential decay of PAG concentrations. However, a correct physicochemical model describing the entire photolysis reaction will be more complex and the data were not fitted with a monoexponential function. Nevertheless, in order to compare the photolysis kinetics, the value of t_{irr}, which corresponds to a decrease of the concentration to half of the initial concentration, was determined. For c4m-ac, this was the case after 1 min to 2 min, for *p*HP-t after about 6 min, and for *p*HP-ac after about 15 min. These values were independent of the pH value of the solution. Interestingly, these results seem to contradict the results found in the previous sections because 1) *p*HP-t was previously identified to show the most efficient photolysis reaction, and 2) absorption spectra and/ or quantum yields were found to depend on pH.

These findings can be explained by an interplay between the spectral overlap of the emission spectrum of the light source and the corresponding quantum yields. For c4m-ac, the absorption spectrum overlaps to a great extent with the lamp spectrum both in water as well as in alkaline conditions. Therefore, although the quantum yields were measured to be quite low, the photolysis proceeded rapidly in both conditions. In contrast, both *p*HP-t and *p*HP-ac absorption spectra in water overlap only to a minor extent with the lamp spectrum. Therefore, although quantum yields were measured to be much larger than for c4m-ac, photolysis was slower than for c4m-ac. The red shift of *p*HP-t and *p*HP-ac absorption spectra in alkaline conditions improves the overlap with the lamp spectrum, but concomitantly the quantum yields decreased drastically. These opposing effects obviously cancel each other out, so that no overall change of photolysis rates were observed upon changing the pH value.

In fact, the stable photolysis rates with various pH values simplify the usage of c4m-ac and *p*HP-t. This way, is possible to tune the pH value according to other experimental prerequisites without having to worry about the photolysis rate, given that the pH value is in a range where hydrolysis is not predominant. For prospective polymeric foaming experiments under these irradiation conditions, c4m-ac seems most advantageous compared to *p*HP-t due to the favorable absorption properties, the higher pH stability and the faster photolysis.
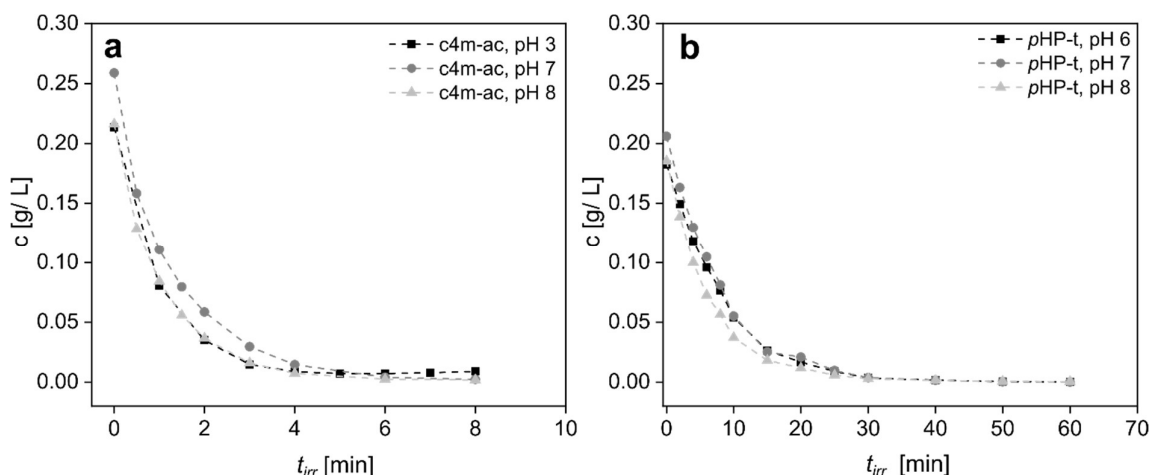

Figure 59: HPLC determined photolysis of c4m-ac and *p*HP-t in water, neutral (pH 7) and alkaline conditions (pH 8) during UV irradiation (300 nm - 450 nm, ~ 40 mW cm^{-2}, UV light emission spectrum is given in Figure 74). For the photolysis measurements in water the pH was not adjusted, which lead to pH 3 for c4m-ac and to pH 6 for *p*HP-t at a concentration of c = 0.2 mg mL^{-1}. The photolysis is given by the decay of c during the irradiation time (t_{irr}). The lines are only for the guidance of the eye.

8.5 Conclusions

Our studies contribute to a comprehensive understanding of the synthesis, solubility, stability and photolysis of two highly water soluble c4m and *p*HP-based PAGs. This could help to satisfy the growing demand for water soluble PAGs especially in the field of hydrogel research and polymeric foaming. Yet, in such applications many strong electrolyte PAGs like diphenyliodonium salts are used, even if they are toxic or need additional sensitizer. This is mainly due to their good accessibility and high water solubility. With this work, we provided an alternative approach to such compounds by designing two easily accessible and highly water soluble c4m and *p*HP-based PAGs, as the substance classes of c4ms and *p*HPs are well suited for physiological applications and do not need additional sensitizers (Givens *et al.* 2012).

The successful synthesis of c4m-ac and *p*HP-t showed their accessibility and the introduction of the hydrophilic groups did not interfere with the excellent photochemical properties of c4m and *p*HP-based PAGs. We also investigated other key parameters like the stability and the photolysis of these PAGs, which confirmed that c4m-ac and *p*HP-t are fairly stable and well photo cleavable in aqueous media under varying pH conditions.

These properties should enable the use of c4m-ac and *p*HP-t for polymeric foaming, e.g. by using an alkaline carbonate solution and the *in situ* generated acid as foaming agent. We presume that c4m-ac and *p*HP-t are cytocomptible which would make them interesting candidates as PAGs e.g. for the production of 3D printed hydrogel foams as polymer scaffolds in tissue engineering. The question of cytocompatibility has to be addressed further in future studies.

8.6 Acknowledgements

Conflict of interest: The authors declare no conflict of interest.

8.7 Supporting information
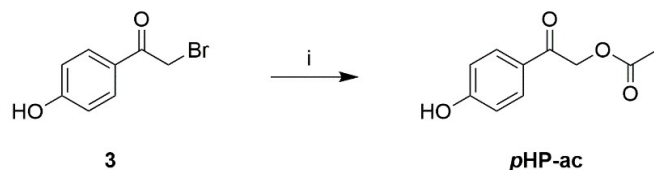
Scheme 16: Synthesis of *p*-hydroxyphenacylacetate (*p*HP-ac) according to Kaila *et al*. (2007). i) AcOH, NaOAc, H2O, 90 °C, 3 h, 73 %.
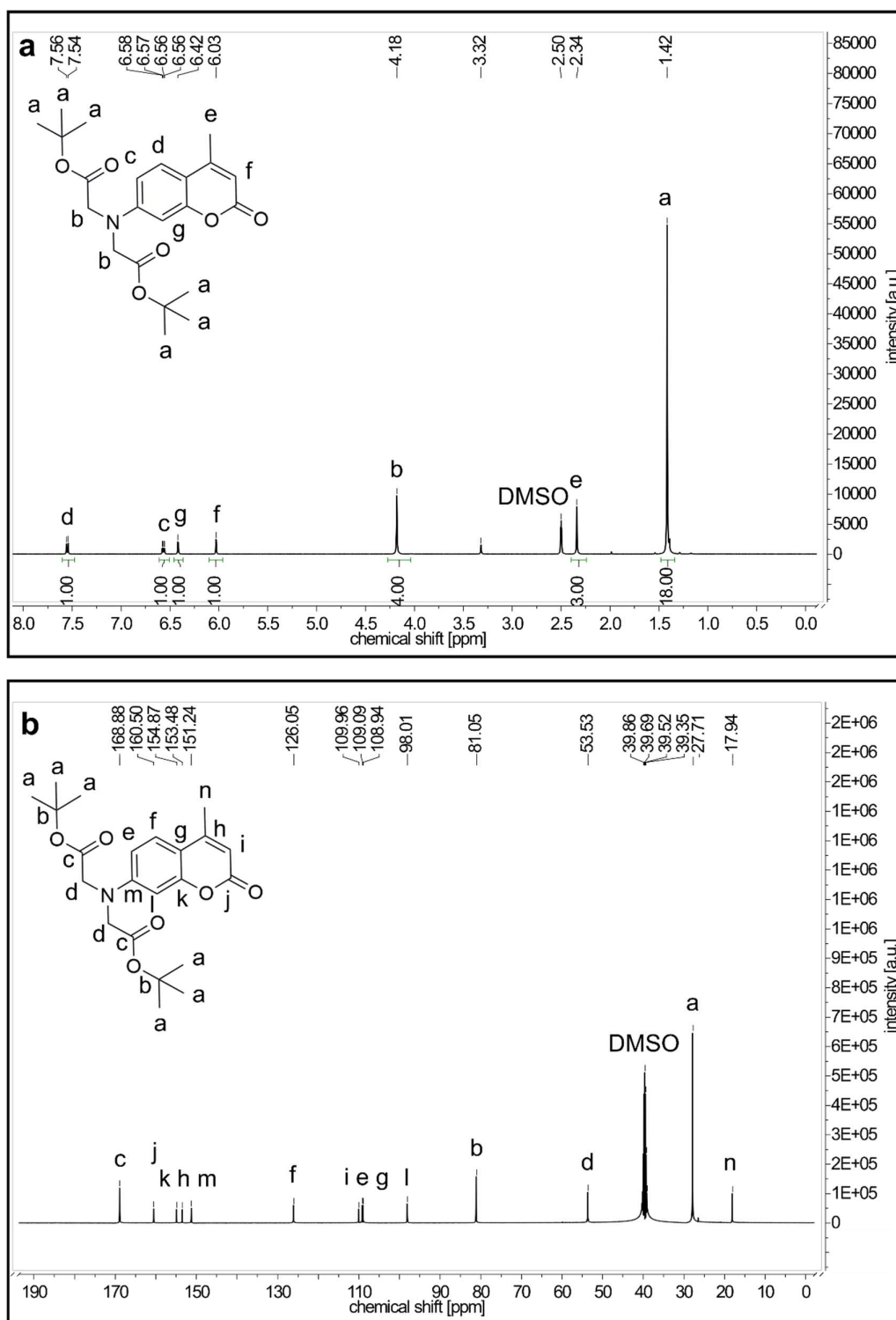
Figure 60: a) ^{1}H NMR spectrum and b) ^{13}C NMR spectrum of 7-[bis(*tert*-butylcarboxymethyl)amino]-4-(methyl)coumarin (**1a**).
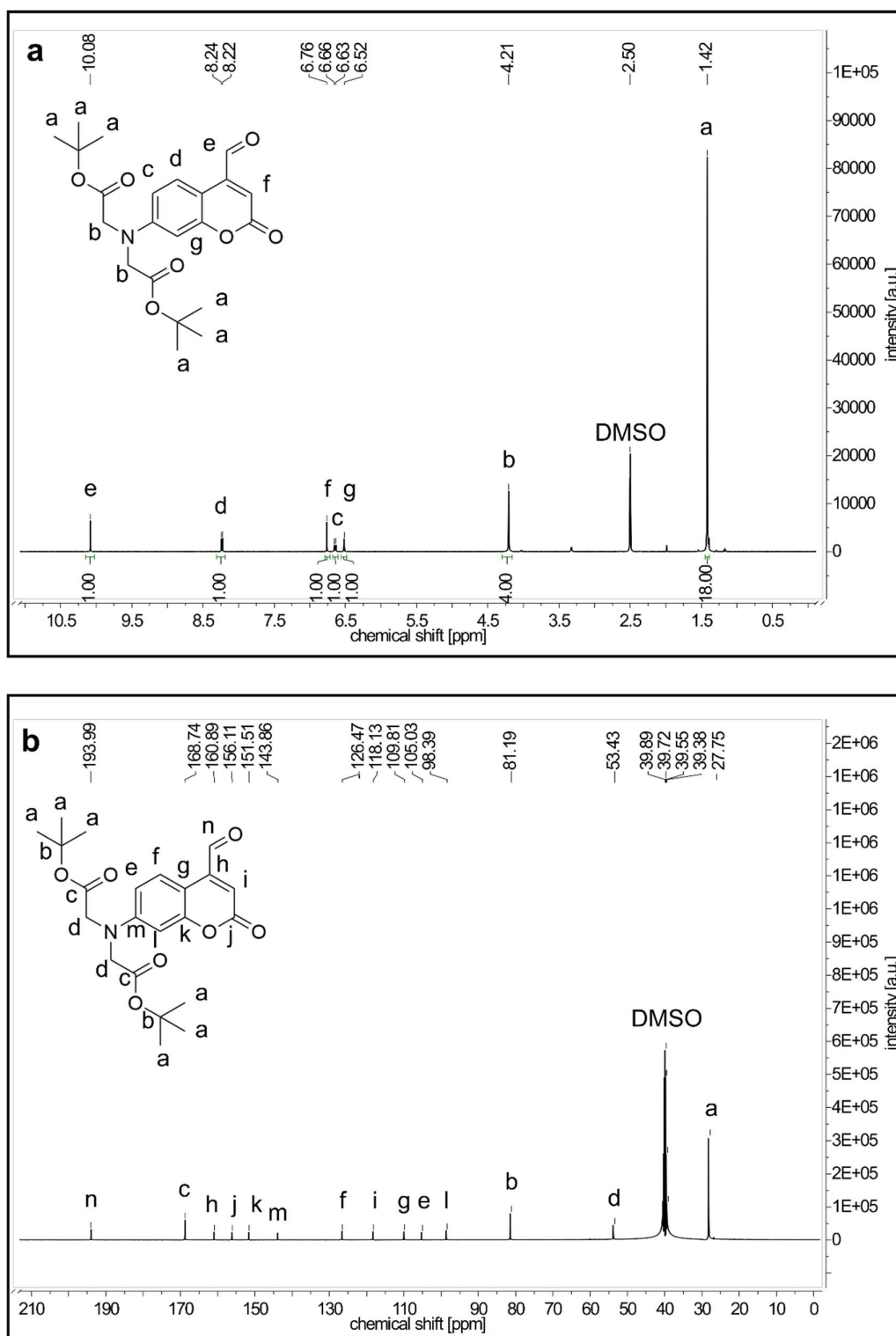
Figure 61: a) ^{1}H NMR spectrum and b) ^{13}C NMR spectrum of 7-[bis(*tert*-butylcarboxymethyl)amino]-4-(formylmethyl)coumarin (**1b**).
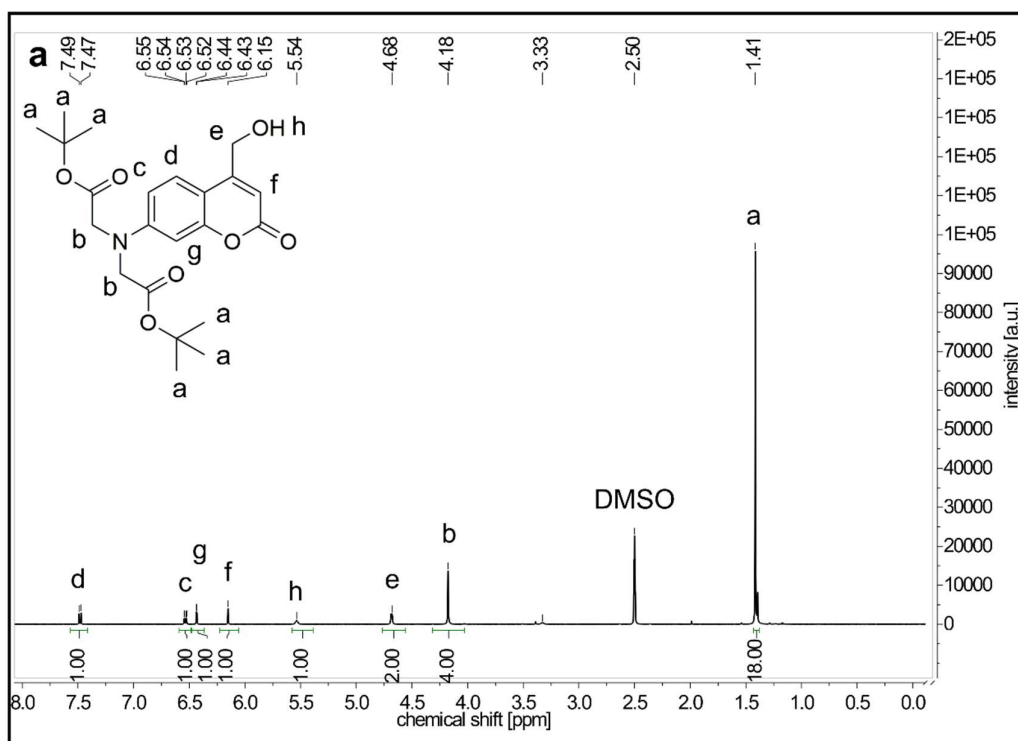
Figure 62: a) ^{1}H NMR spectrum and b) ^{13}C NMR spectrum of 7-[bis(*tert*-butylcarboxymethyl)amino]-4-(hydroxymethyl)coumarin (**1c**).
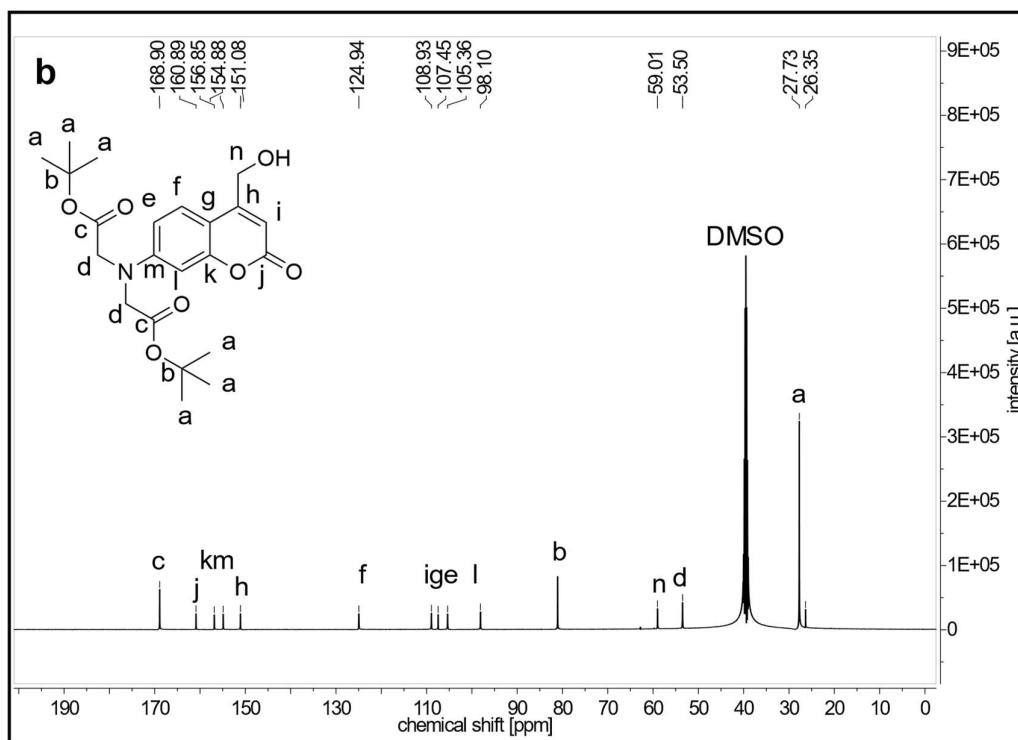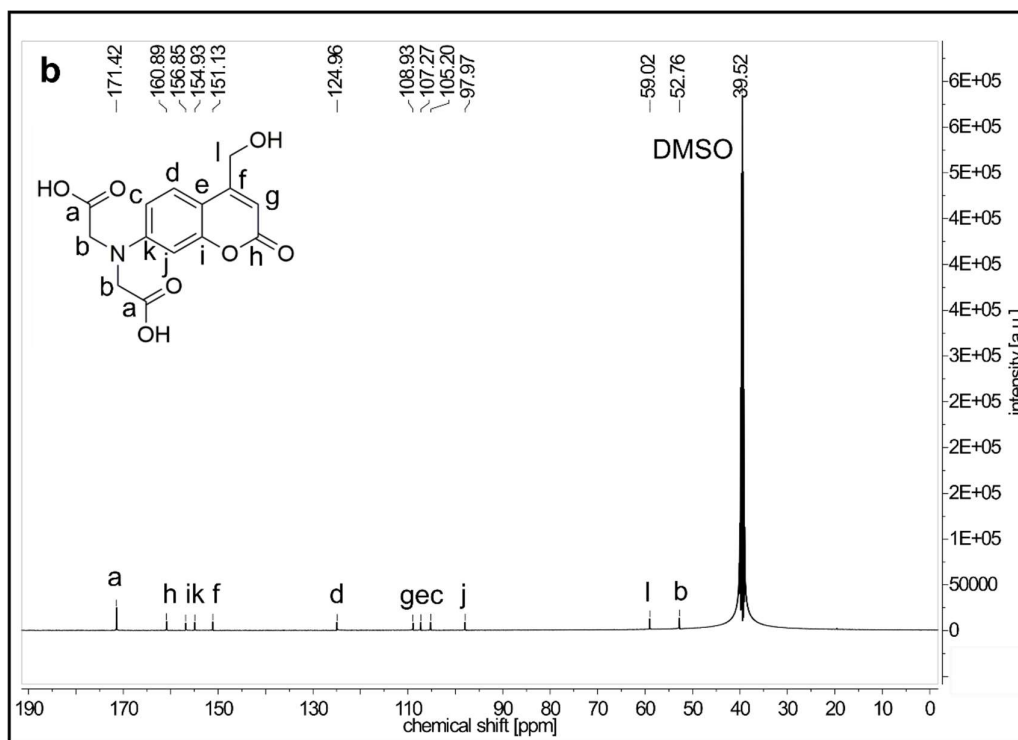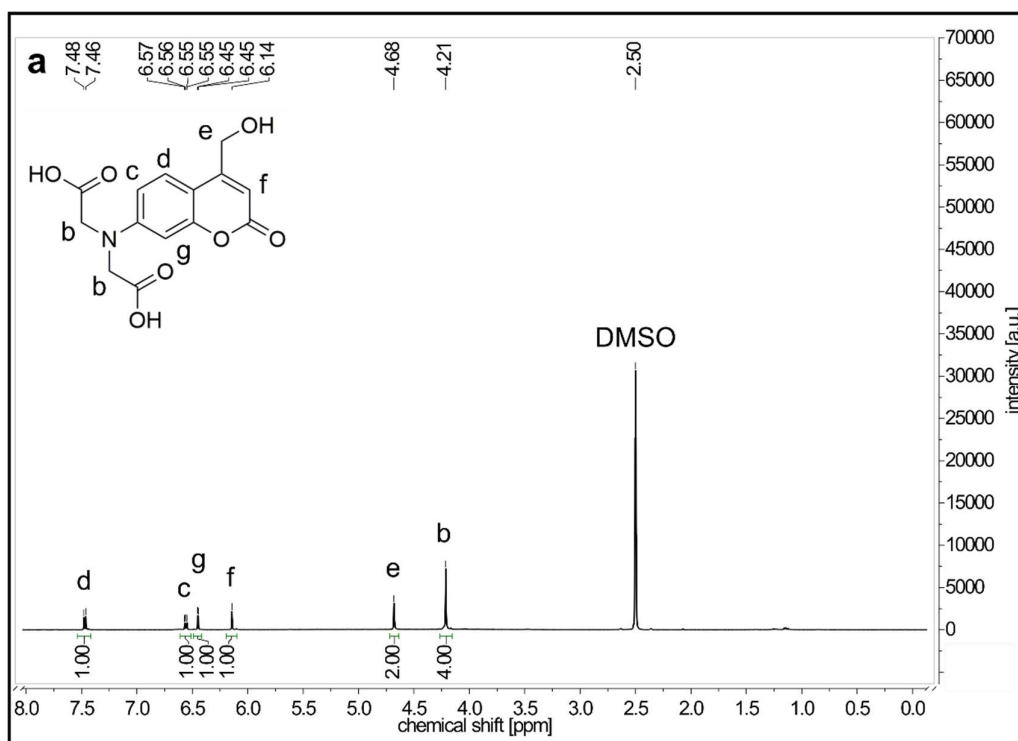
Figure 63: a) ^{1}H NMR spectrum and b) ^{13}C NMR spectrum of 7-[bis(carboxymethyl)amino]-4-(hydroxymethyl)coumarin (**1d**).
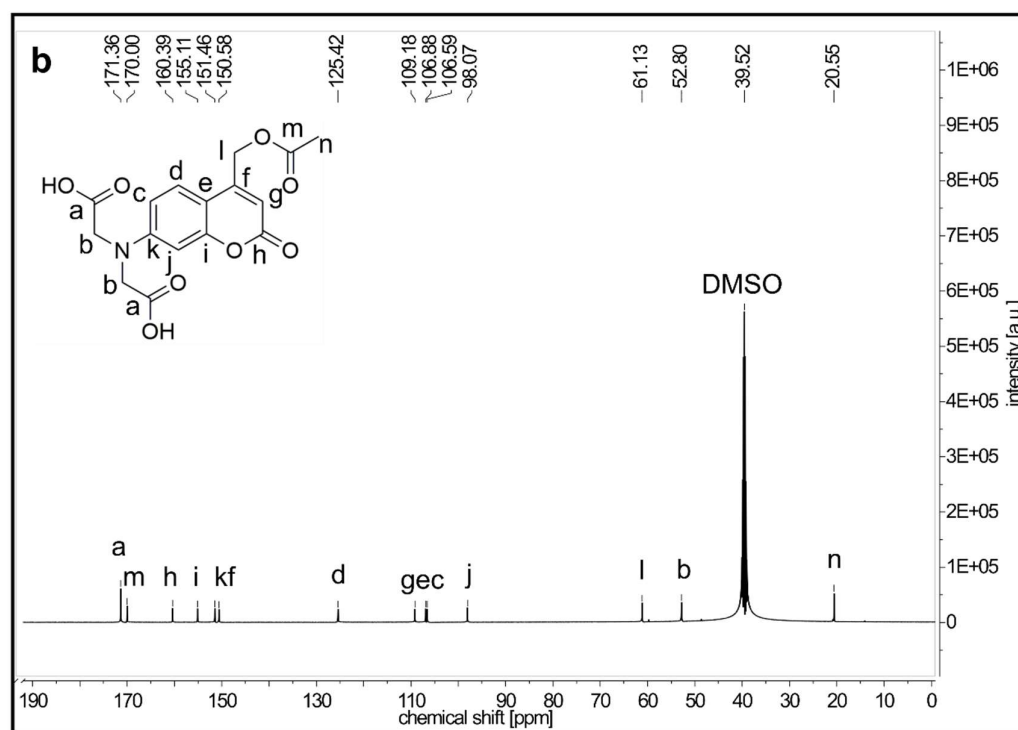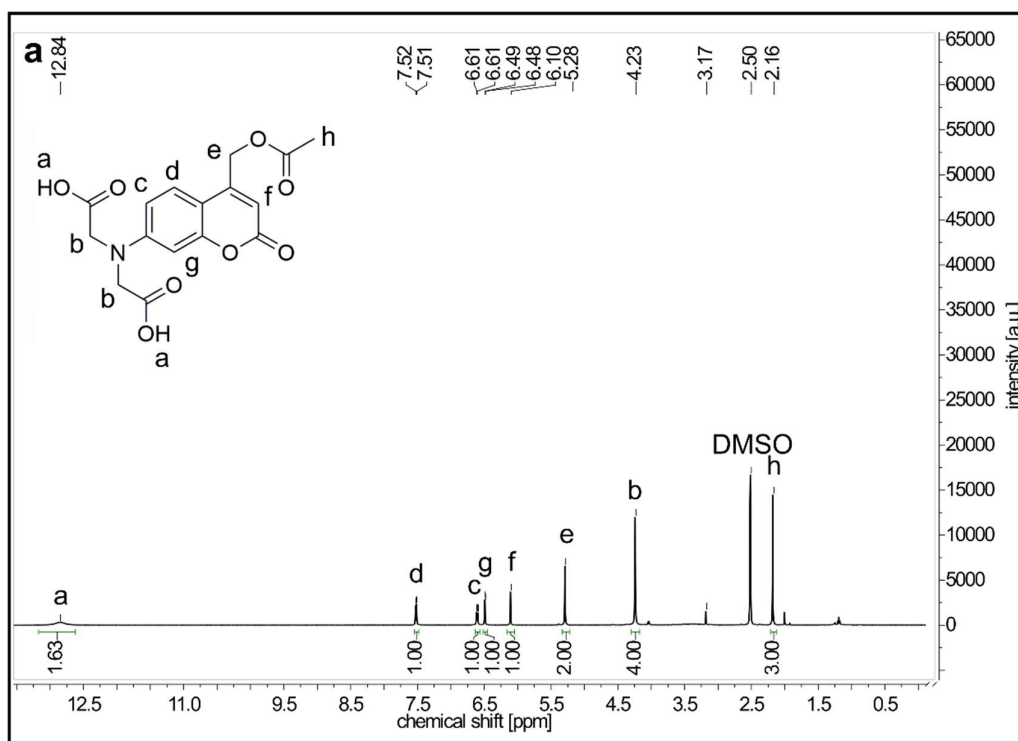
Figure 64: a) ^{1}H NMR spectrum and b) ^{13}C NMR spectrum of 7-[bis(carboxymethyl)amino]-4-(acetoxymethyl)coumarin (c4m-ac).
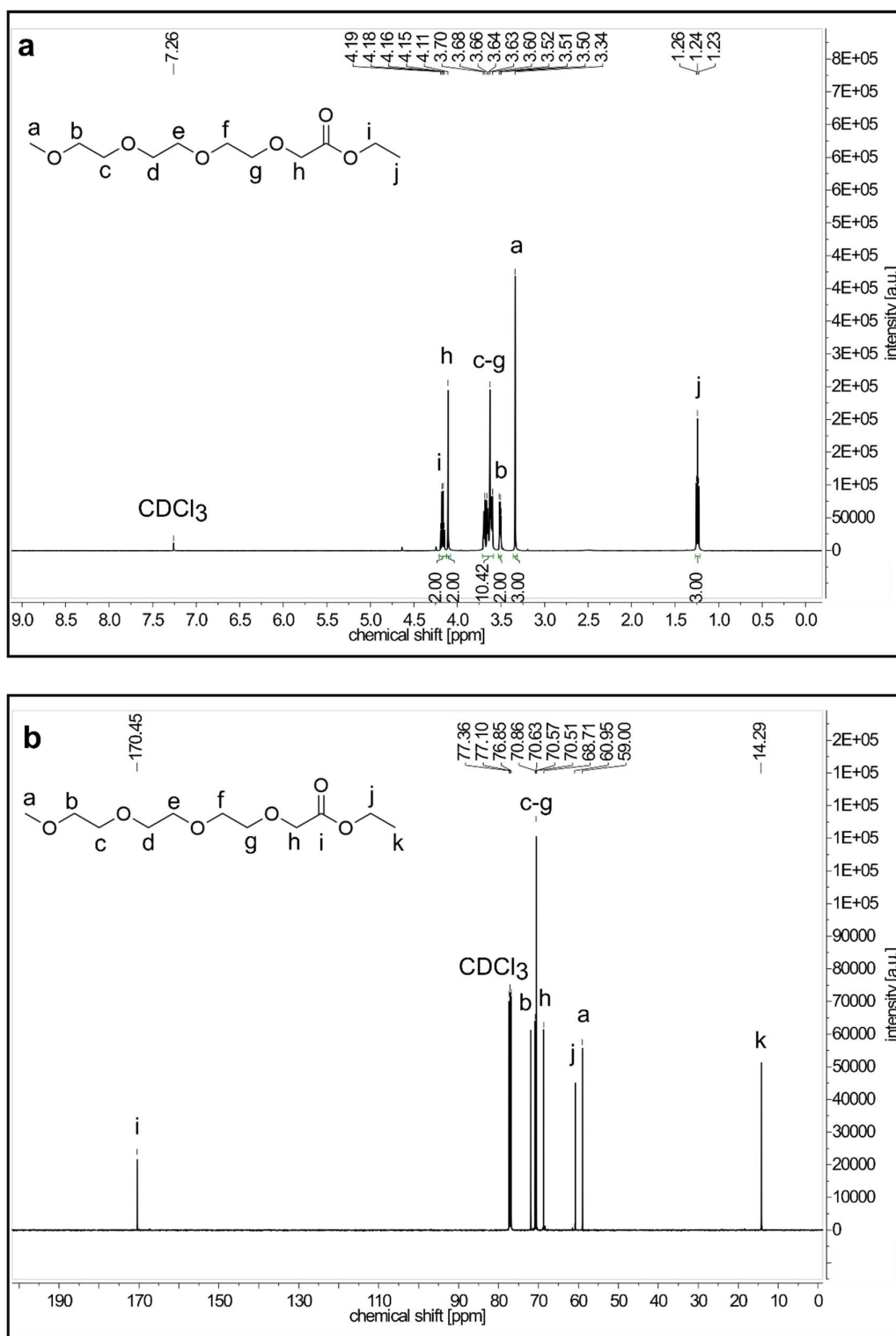
Figure 65: ^{1}H NMR spectrum and b) ^{13}C NMR spectrum of ethyl-2,5,8,11-tetraoxatridecan-13-oate (**2a**).
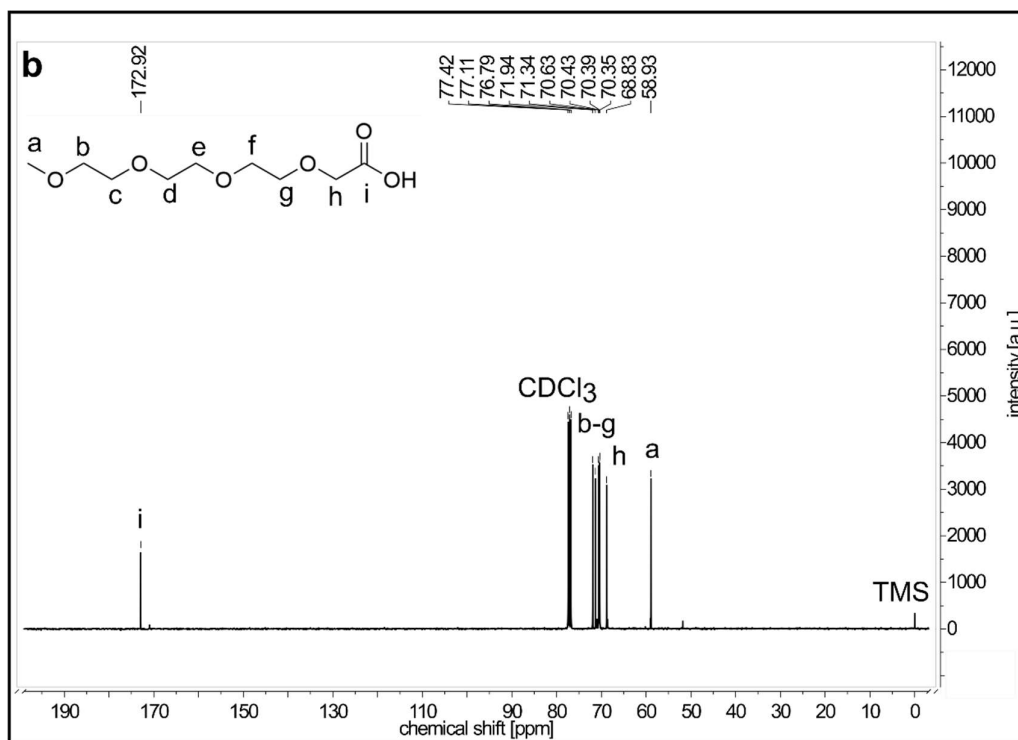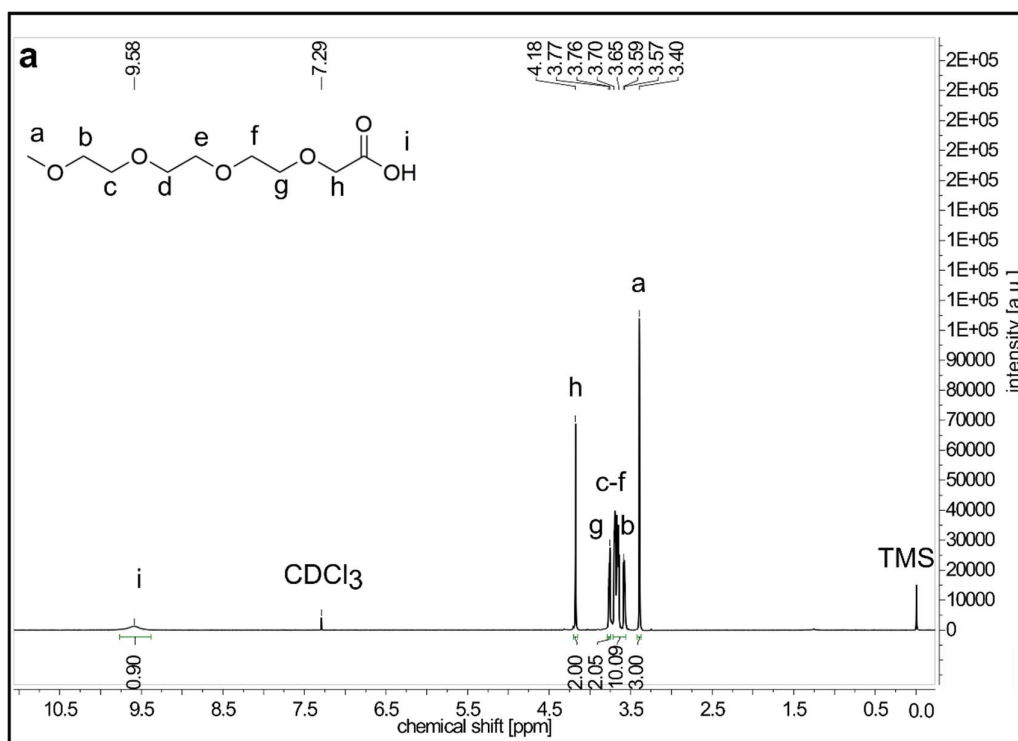
Figure 66: ^{1}H NMR spectrum and b) ^{13}C NMR spectrum of 2,5,8,11-tetraoxatridecan-13-oic acid (**2b**).
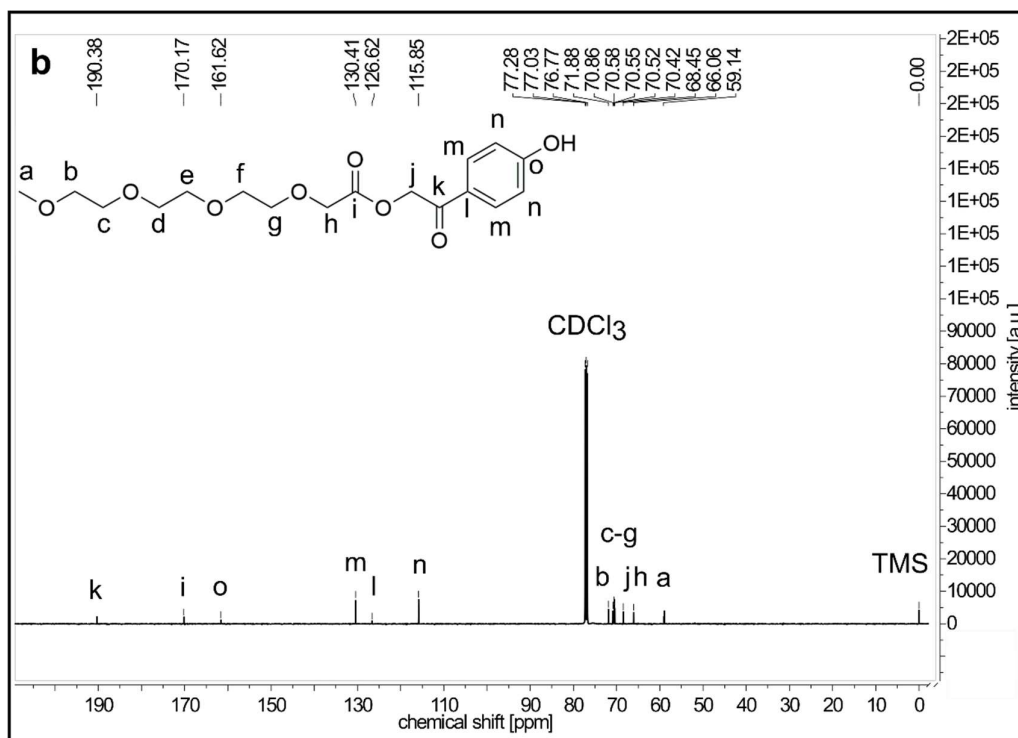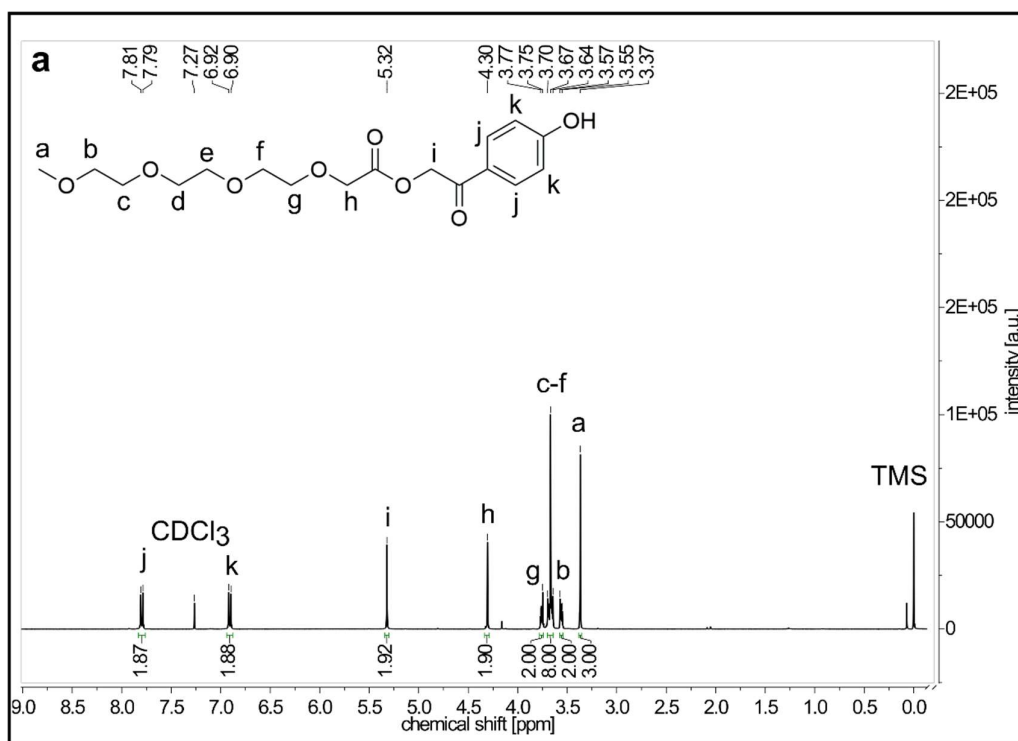
Figure 67: a) ^{1}H NMR spectrum and b) ^{13}C NMR spectrum of 2-(4-hydroxyphenyl)-2-oxoethyl-2,5,8,11-tetraoxatridecan-13-oate (pHP-t).
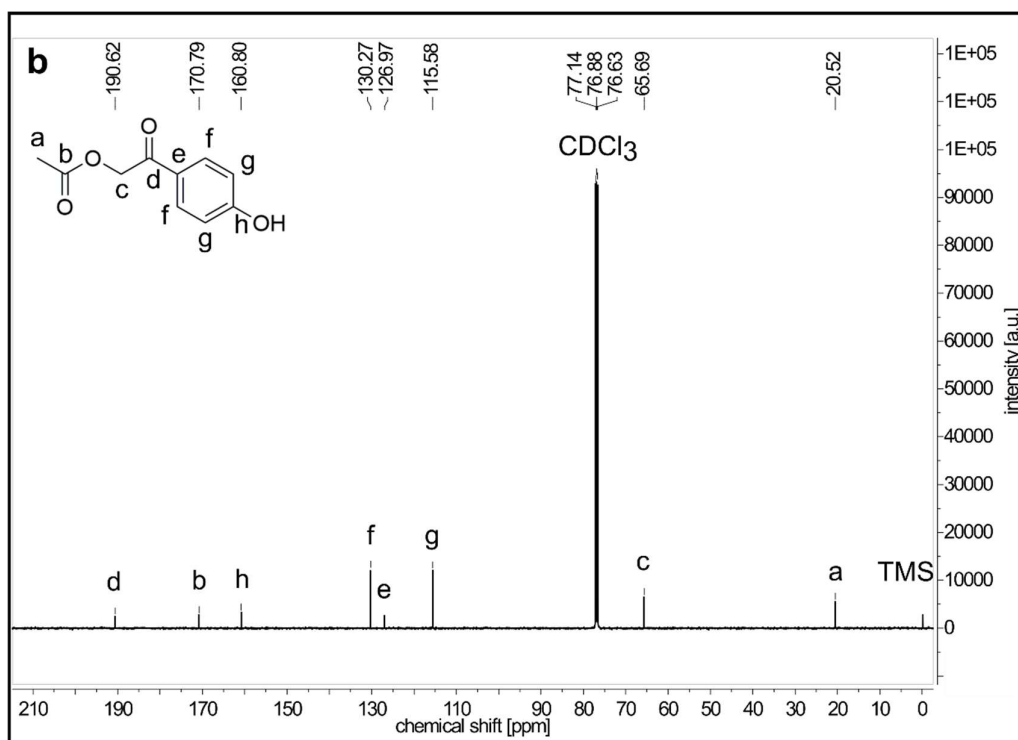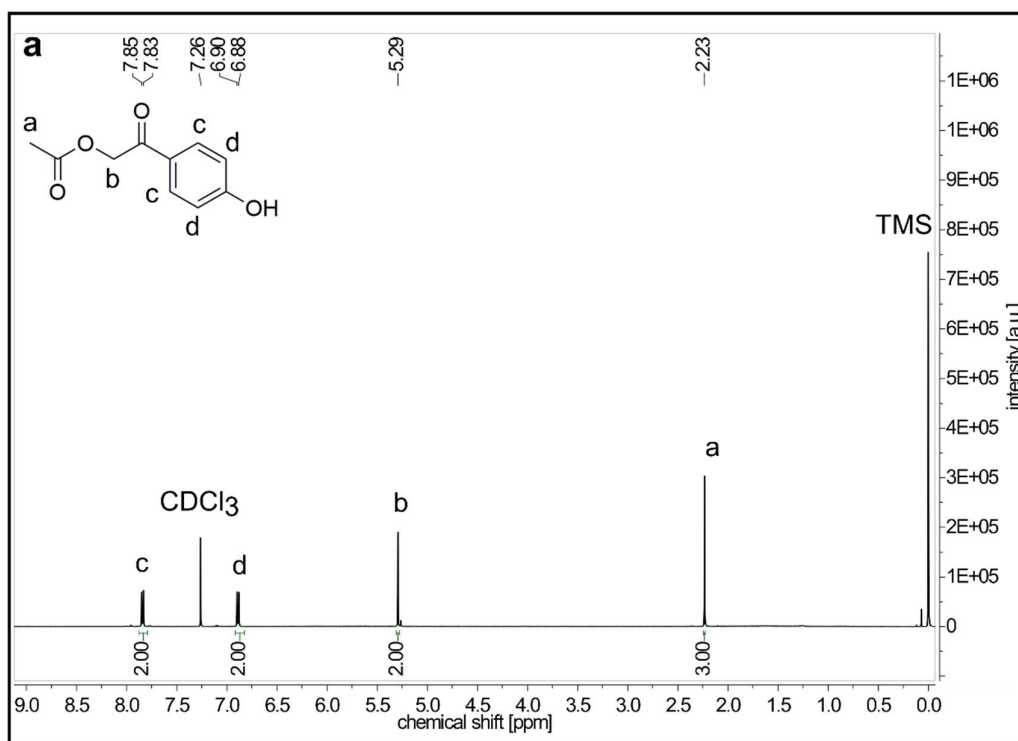
Figure 68: a) ^{1}H NMR spectrum and b) ^{13}C NMR spectrum of *p*-hydroxyphenacylacetate (*p*HP-ac). The labile phenoxide proton is not always visible in the ^{1}H NMR spectrum.
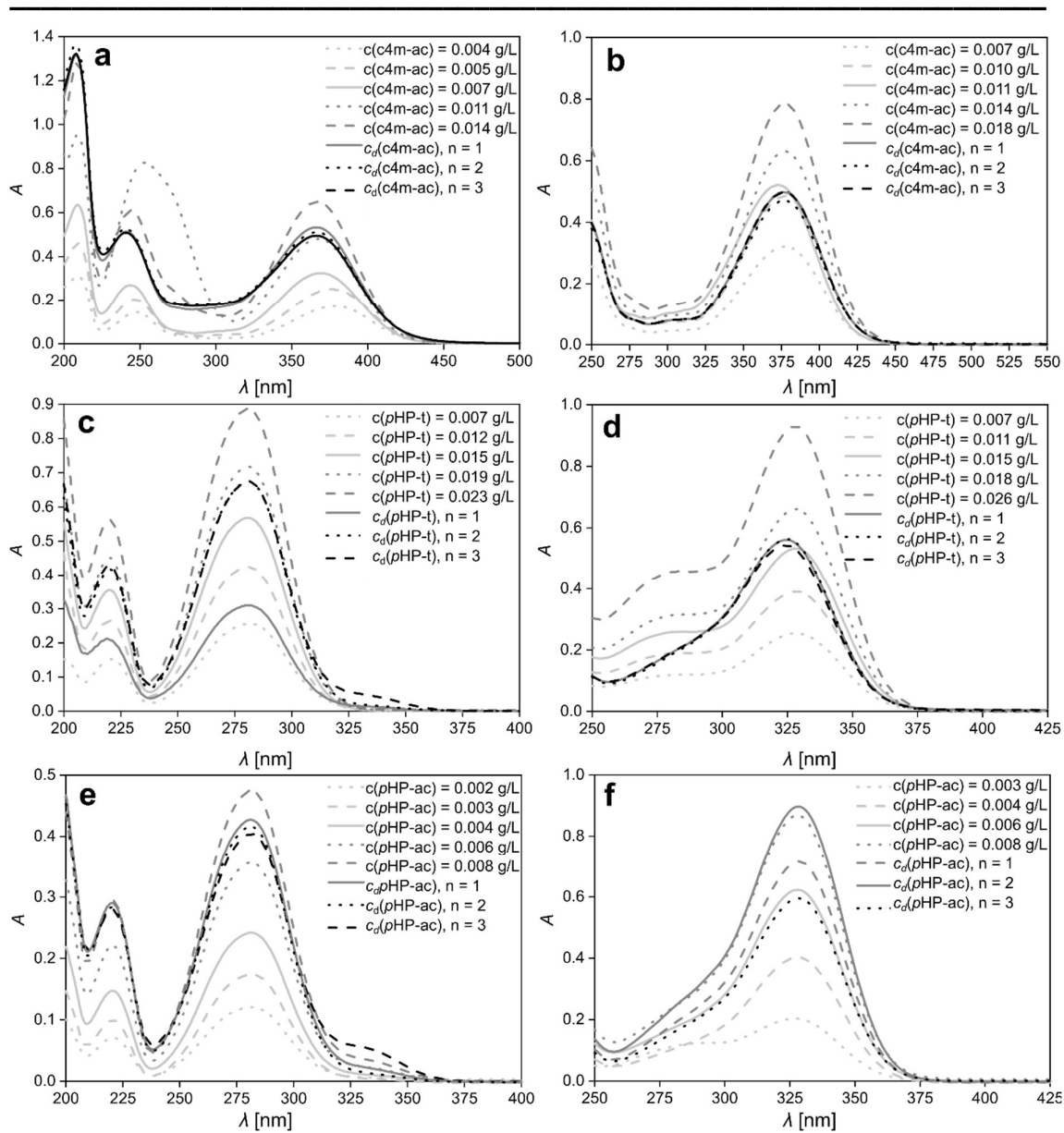
Figure 69: UV Vis spectra for the calibration and determination of the maximum solubility of c4m-ac, *p*HP-t and *p*HP-ac in a), c), e) water as well as in b), d), f) alkaline solution. The diluted samples for the determination of maximum solubility (c_d) were measured in triplicates (n = 3).
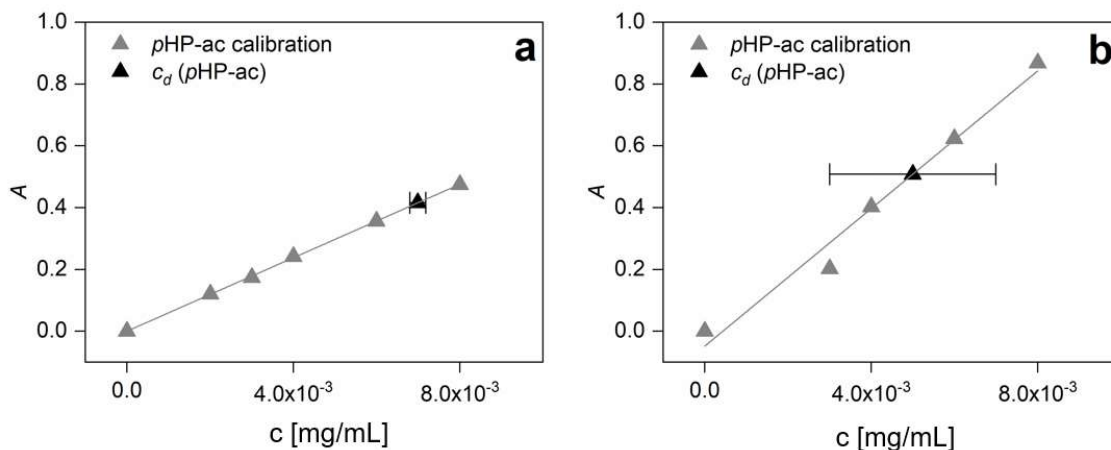
Figure 70: Photometric determination of the solubility (c_{max}) of pHP-ac in a) water as well as in b) alkaline solution at pH 9. c_{max} is calculated according to equation (17). The diluted concentration (c_d) with the respective dilution factor (d_f) are summarized in Table 13.

Table 13: Diluted concentrations c_d and dilution factor d_f of the photoacid generators c4m-ac, pHP-t and pHP-ac. The subscript 'w' indicates measurements in water and 'a' refers to alkaline solution.

PAG	$d_{f,w}$	$c_{d,w}$ [g L^{-1}]	$d_{f,a}$	$c_{d,a}$ [g L^{-1}]
c4m-ac	86	0.01	20 000	0.01
pHP-t	2 500	0.02	800	0.02
pHP-ac	400	0.01	833	0.01

Table 14: Stabilities (s) of the photoacid generators (PAG) c4m-ac, pHP-t and pHP-ac after 1 h (s_{1h}), 3 h (s_{3h}) and 24 h (s_{24h}) at pH 7, pH 8, and pH 9, as well as in water without pH adjustment after dissolution. The stabilities were determined *via* HPLC. n.d. = not determined.

PAG	pH	s_{1h} [%]	s_{3h} [%]	s_{24h} [%]
c4m-ac	3	100	100	100
c4m-ac	7	100	99	99
c4m-ac	8	100	95	96
c4m-ac	9	96	90	11
pHP-t	6	97	96	95
pHP-t	7	92	90	85
pHP-t	8	73	65	48
pHP-t	9	56	17	0
pHP-ac	5	100	100	99
pHP-ac	7	100	99	94
pHP-ac	8	99	99	94
pHP-ac	9	100	n.d.	53
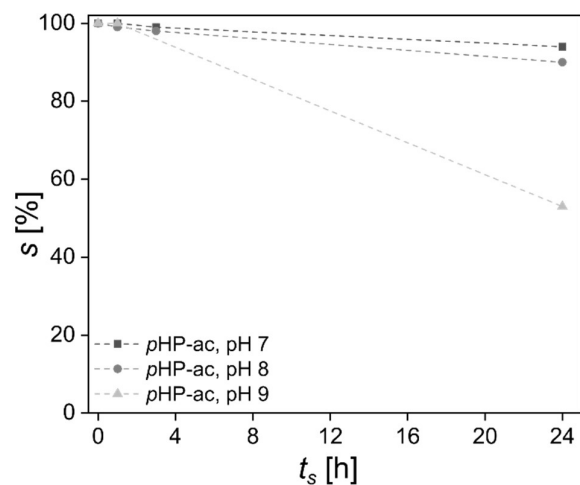
Figure 71: HPLC determined stabilities (*s*) of *p*HP-ac after a storage time (t_s) of 1 h, 3 h and 24 h at pH 7, pH 8 and pH 9.. The lines are only for the guidance of the eye.
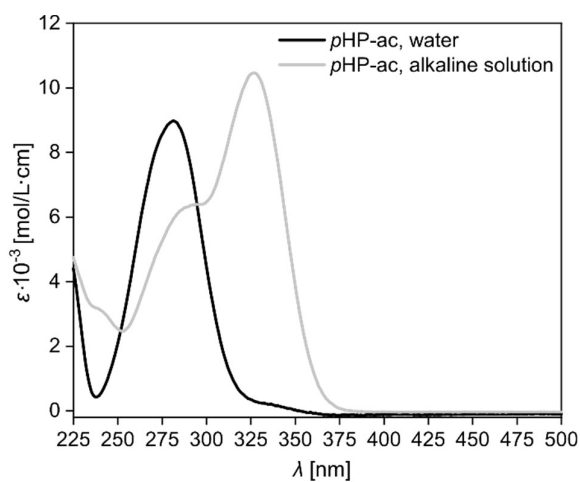
Figure 72: UV-vis spectra of *p*HP-ac in water and alkaline solution at pH 9.
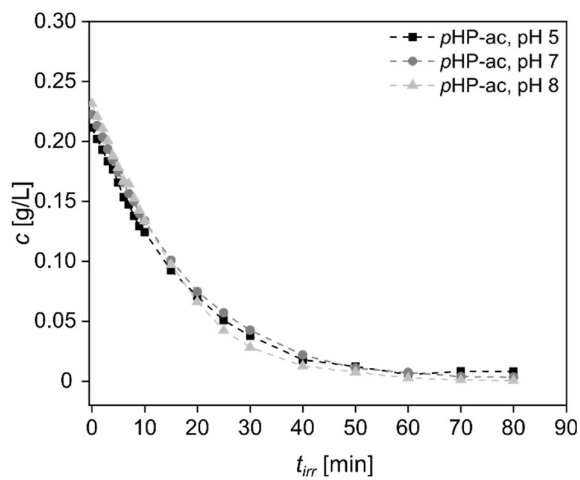
Figure 73: Photolysis under UV irradiation of *p*HP-ac in water (pH 5), neutral (pH 7) and alkaline conditions (pH 8). The lines are only for the guidance of the eye.
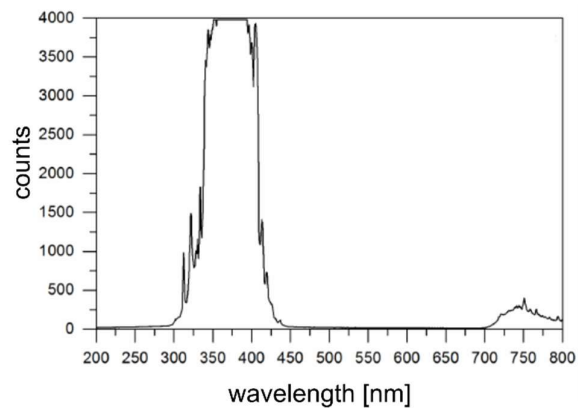
Figure 74: Emission spectrum of a UV-H 255 UV chamber from Hartmann Feinwerkbau GmbH for the photolysis experiments.
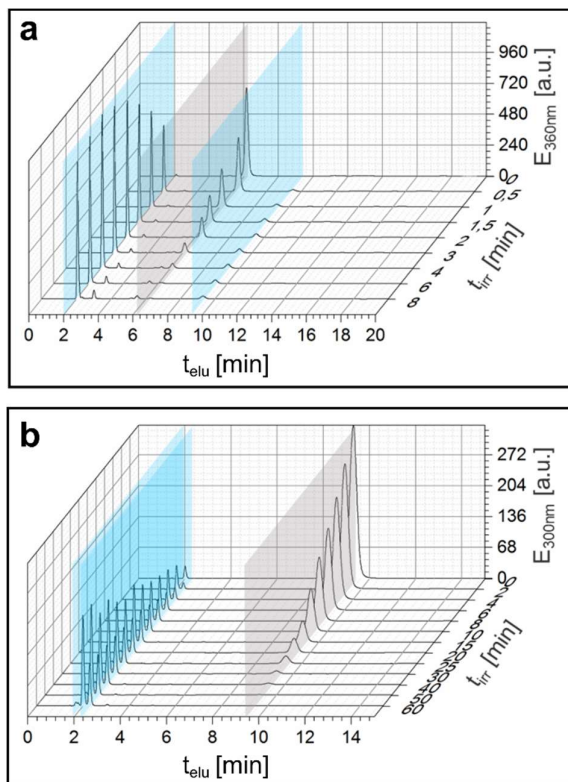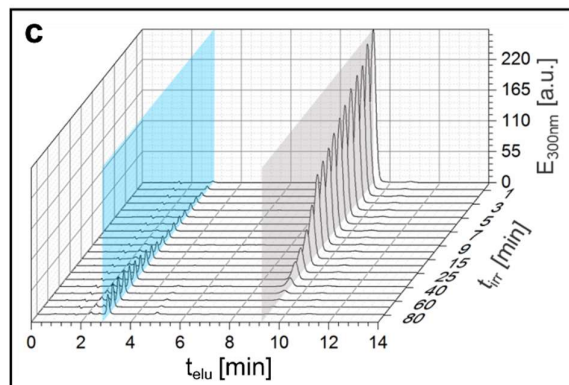
Figure 75: HPLC monitored photolysis of a) c4m-ac, b) *p*HP-t and c) *p*HP-ac under UV irradiation. t_{elu} is the elution time during the HPLC measurement, t_{irr} is the irradiation time under UV light and A is the absorbance at the respective wavelength. The absorbance of c4m-ac is shown at 360 nm and of *p*HP-t and *p*HP-ac at 300 nm. The photoacid generator is marked in gray and the photolysis products are marked in blue.

9.   Discussion of the hypotheses

This thesis on synthesis and characterization of multifunctional macromonomers and photoacid generators for the modification of hydrogels is structured by three hypotheses (hypothesis I, II and III, section 4). The exploration and results of each hypothesis led to a manuscript, which is either already published or in the publication process. In the following, the main results, which were explained comprehensively in section 5, will be discussed briefly to proof or disproof these hypotheses.

Hypothesis I:

Well-defined, multifunctional α-diphenylmethyl-ω-4-vinylbenzyl-poly(furfuryl glycidyl ether)-block-poly(ethylene glycol) (PFGE$_p$-b-PEG$_q$) macromonomers can be synthesized via anionic ring opening polymerization and characterized regarding their characteristic polymer properties like their molar mass dispersity (Đ), their glass transition temperature (T$_g$), their melting temperature (T$_m$), their decomposition temperature (T$_d$) and their critical micelle concentration (cmc). PFGE$_p$-b-PEG$_q$ macromonomers can be used for the bulk functionalization of radically cross-linked polyacrylamide (p(Aam)) hydrogels to prepare functional hydrogels with multiple anchor points for post-synthetic Diels-Alder reactions.

In our publication "Hydrogels with multiple clickable anchor points: synthesis and characterization of poly(furfuryl glycidyl ether)-*block*-poly(ethylene glycol) macromonomers" (section 5), we described the synthesis of α-diphenylmethyl-ω-4-vinylbenzyl-poly(furfuryl glycidyl ether)-*block*-poly(ethylene glycol) (PFGE$_p$-*b*-PEG$_q$) macromonomers *via* subsequent anionic ring opening polymerization of furfuryl glycidyl ether (FGE) and ethylene oxide (EO). The termination of the living chain ends was performed with 4-vinylbenzyl chloride (4-VBC) to introduce the polymerizable unit at the hydrophilic chain end. The successful synthesis of the macromonomers was proven by ^{1}H NMR, ^{13}C NMR and FT-IR spectroscopy, SEC and MALDI TOF mass spectrometry and revealed low Đ between 1.05 and 1.09 as well as number average molar masses between 2 330 g mol^{-1} and 6 660 g mol^{-1}. The block lengths of the macromonomers were adjustable *via* the MIR ratio and high end group functionalization degrees between 72 % and 98 % were achieved. DSC and TGA measurements displayed -43 °C ≤ T_g ≤ -32, 32 °C ≤ T_m ≤ 45 °C and 369 °C ≤ T_d ≤ 381 °C. The cmc of the water soluble macromonomers PFGE$_8$-*b*-PEG$_{79}$,

PFGE$_{18}$-*b*-PEG$_{66}$ and PFGE$_{13}$-*b*-PEG$_{111}$ was determined by bubble pressure tensiometry and resulted for all three compounds in almost the same value of 0.3 mg mL^{-1}. This shows that the cmc is rather influenced by the mass per volume of the macromonomers instead by the number of molecules. Similar observations were made in the Langmuir film balance experiments at the air-water interface, where the isotherm onset shifts to larger areas per molecule when the molecular weight of the macromonomer grows. Furthermore, I was able to immobilize PFGE$_{p}$-*b*-PEG$_{q}$ macromonomers into p(Aam) hydrogels by radical copolymzeriation and labeled the pending furan groups of the macromonomers with a maleimide-functionalized fluorescence dye. As the fluorescence intensity of fluorescence labeled p(Aam) with and without PFGE$_{p}$-*b*-PEG$_{q}$ macromonomers was significantly different in our laser scanning microscopy (LSM) measurements, we could demonstrate that the furan groups of our macromonomers can undergo post-synthetic Diels-Alder reactions. Thus, our macromonomers can be used to access functional hydrogels providing clickable anchor points in high density for conjugation of maleimide-functional substrates.

Taken together, our results from ^{1}H NMR, ^{13}C NMR, FT-IR spectroscopy, SEC, MALDI TOF mass spectrometry, DSC, TGA, bubble pressure tensiometry and LSM measurements clearly confirm hypothesis I.

Beyond the bulk functionalization of hydrogels, I wanted to explore whether PFGE$_{p}$-*b*-PEG$_{q}$ macromonomers can be used to exclusively functionalize the air-hydrogel interface without functionalizing the hydrogel bulk. Therefore, knowledge about the film formation ability and the structure-property relations of PFGE$_{p}$-*b*-PEG$_{q}$ macromonomers at the air-water interface was needed. For these experiments the air-water interface served as a simplified model of the air-hydrogel precursor solution interface.

So the second hypothesis focuses on the investigation of PFGE$_{p}$-*b*-PEG$_{q}$ macromonomers at the air-water interface, to evaluate whether they are promising functionalization reagents for the air-hydrogel interface.

Hypothesis II:

Multifunctional PFGE$_{p}$-b-PEG$_{q}$ macromonomers are able to form thin films at the air-water interface, whereby the beginning of the film formation correlates with the

molecular weight of the macromonomers. The beginning of the film formation is determined by the molecular area of the onset of the surface pressure-area isotherm. The stability of the macromonomer films is dependent on the hydrophilic-lipophilic balance (HLB) value. Furthermore, a molecular mechanism of the PFGE$_p$-b-PEG$_q$ macromonomers at the air-water interface can be proposed, which is in accordance with the film stability and film recovery. PFGE$_p$-b-PEG$_q$ macromonomers are promising functionalization reagents for the functionalization of the air-hydrogel interface of radically cross-linked p(Aam) hydrogels.

Hypothesis II was explored in our manuscript „structure-property relations of amphiphilic poly(furfuryl glycidyl ether)-*block*-poly(ethylene glycol) macromonomers at the air-water interface" (section 6) and in preliminary hydrogel surface functionalization experiments described in section 7. We could demonstrate the film formation ability of our PFGE$_p$-*b*-PEG$_q$ macromonomers by measuring surface pressure-area (π-A) isotherms at the air-water interface. The surface pressure π increase during compression is a clear sign for the surface activity of our macromonomers and their presence at the air-water interface. The π-A isotherms revealed that the block lengths and the molar mass of the macromonomers influenced the isotherm shape and onset. Smaller, more hydrophobic macromonomers (HLB < 8) showed a steeper surface pressure increase in the liquid condensed phase of the π-A isotherms if compared to larger, more hydrophilic macromonomers with HLB > 8. The molecular area for isotherm onsets increased almost linearly with growing molar mass of the macromonomers, which shows that the beginning of the film formation correlates with the molecular weight of the macromonomers.

Static and dynamic film stability measurements demonstrated limited stability of all macromonomer monolayers at the air-water interface. The more hydrophilic macromonomers PFGE$_8$-*b*-PEG$_{79}$, PFGE$_{18}$-*b*-PEG$_{66}$ and PFGE$_{13}$-*b*-PEG$_{111}$ (HLB > 8) showed higher film stability compared to the more hydrophobic macromonomers (HLB < 8). Hysteresis experiments displayed an almost linear increase of the film degradation with rising HLB values of the macromonomers. This shows that the film stability is correlated with the HLB value of our PFGE$_p$-*b*-PEG$_q$ macromonomers.

Moreover, we could measure partial film recovery of our macromonomer films at the air-water interface after 5 hysteresis cycles and 12 h recovery time in an expanded Langmuir trough. The ability of the macromonomers to recover to the air-water

interface is a strong indication for a folding mechanism as its reversibility was frequently described in the literature (Baoukina *et al.* 2008, Ding *et al.* 2001, Takamoto *et al.* 2001). As the macromonomers do not recover fully to the air-water interface, it is likely that some molecules are trapped in irreversible processes like submersion or multilayer collapse (Lee 2008, Ries Jr *et al.* 1987). We rather exclude a collapse to multilayers, as we did not observe a collapse pressure, which is typical for multilayer formations (Yang *et al.* 2009). Additionally, a multilayer collapse mostly occurs at very high π, when the amphiphiles are compressed beyond their stability limit, which is often over 50 mN m^{-1} (Das *et al.* 2016, Goto *et al.* 2013, Maget-Dana 1999, Rivera *et al.* 2007). In contrast, in our study the macromonomers were compressed applying relatively low film pressures with 0 mN m^{-1} ≤ π ≤ 23 mN m^{-1}, which should not yet lead to multilayer collapse. A submersion to the subphase seems to be much more likely for our macromonomers, as this was frequently reported for other PEG-based amphiphiles (Barentin *et al.* 1998). It also fits to the micelle formation ability of PFGE-*b*-PEG block copolymers in water (Barthel *et al.* 2012) and explains the limited stability of our macomonomer monolayers. Hence, the combined analysis of the film stability and film recovery measurements indicates an interplay between a reversible folding and an irreversible submersion mechanism for the macromonomer monolayers at the air-water interface.

We propose that the PFGE$_p$-*b*-PEG$_q$ macromonomers will be efficient functionalization reagents of the air-hydrogel air interface. This statement is based on the nature of their molecular structure, containing a polymerizable unit, an amphiphilic core structure and multiple furan groups for post-synthetic modification reactions, as well as their film forming ability at the air-water interface. In this regard, PFGE$_{10}$-*b*-PEG$_9$ seems to be the most promising hydrogel surface functionalization reagent because it can introduce the highest number of functional groups per surface area.

In our preliminary experiments, we could not yet prove the functionalization of the air-hydrogel interface *via* fluorescence labeling, which was used to confirm bulk functionalization previously (section 5). The p(Aam) hydrogels exhibited a fluorescent air-hydrogel interface regardless of their functionalization. We could overcome this by polymerizing the hydrogels under argon atmosphere. The two most evident reasons why the surface functionalization of hydrogels did not work yet, are, that either the macromonomers did not covalently bind to the hydrogel surface, or that the

macromonomer amount on the hydrogel surface was too low for detection. Regarding the first assumption, it could be helpful to reduce the complexity of hydrogel surface by investigating whether the macromonomers can bind to a solid surface such as a self-assembled monolayer of 3-methacryloylpropyl trimethoxysilane on a silicon wafer (Bialk *et al.* 2002). Regarding the second assumption, another detection method than fluorescence spectroscopy like TOF-SIMS could be used, which was reported by Tylor *et al.* (2016) for the 3D mapping of functionalized p(HEMA) hydrogels. This shows that our macromonomers are promising hydrogel functionalization reagents, but further research is needed to fulfil the ambitious task of exclusively functionalizing the air-hydrogel interface.

In conclusion, the Langmuir film balance measurements and the hydrogel functionalization experiments show the potential of PFGE$_p$-*b*-PEG$_q$ macromonomers as functionalization reagents for the air-hydrogel interface, even if we could not prove this yet. However, hypothesis II is confirmed.

Hypotheses I and II are both dedicated to the modification of the polymer network, whereas hypothesis III is focused on the exploration of the synthesis and characterization of novel, water soluble *p*HP- and c4m-based PAGs for the potential modification of hydrogel swelling agents.

The substance class of *p*HPs and c4ms are well known for their excellent photochemical properties and are applied in numerous fields (Givens *et al.* 2012, Hagen *et al.* 2008, Klán *et al.* 2013b). Yet, in many water-based applications where high PAG concentrations are needed, like in hydrogel modification strategies or foaming of polymeric materials, strong electrolyte PAGs are preferred, even if they are toxic or need additional photosensitizers (Feng *et al.* 2015, Gargava *et al.* 2016, Kovalenko *et al.* 2016, Schlögl *et al.* 2012). This is maily due to their good synthetic approachability and their high water solubility. To provide an alternative approach to such compounds, I synthesized the two novel c4m- and *p*HP-based PAGs c4m-ac and *p*HP-t (Figure 9), which are in the center of hypothesis III.

<u>Hypothesis III</u>:

The photoacid generators c4m-ac and pHP-t show good synthetic approachability and high solubility in water and alkaline solutions with maximum solubilities $c_{max} > 1$ mmol L^{-1}. The photochemical properties of c4m-ac and pHP-t, like the absorption maximum (λ_{max}), the maximum molar extinction coefficient (ε_{max}) and the quantum yield (ϕ), are pH dependent. Furthermore, the stability of c4m-ac and pHP-t is pH dependent, in contrast to the photolysis under UV irradiation within the studied conditions.

As described in the manuscript "Coumarin-4-ylmethyl and *p*-hydroxyphenacyl-based photoacid generators with high solubility in aqueous media: synthesis, stability and photolysis" (section 8), c4m-ac and *p*HP-t show good synthetic approachability, since c4m-ac was synthesized in 5 steps with an overall yield of 16 % and *p*HP-t was synthesized in 3 steps with an overall yield of 22 %. The success of the synthesis was confirmed with ^{1}H NMR, ^{13}C NMR and mass spectrometry.

Moreover, we measured excellent maximum solubilities in water ($c_{max,w}$) of 2.77 mmol L^{-1} ± 0.07 mmol L^{-1} for c4m-ac and 124.66 mmol L^{-1} ± 2.1 mmol L^{-1} for *p*HP-t. Under basic conditions at pH 9 c_{max} of c4m-ac increased 230-fold to 646.46 mmol L^{-1} ± 0.63 mmol L^{-1} due to deprotonation of the two carboxylic acid groups, whereas the solubility of *p*HP-t decreased 3-fold to 34.68 mmol L^{-1} ± 0.62 mmol L^{-1} in alkaline solution due to salting out effects. All determined solubilities are well above 1 mmol L^{-1}, which is referred as good for coumarin-4-ylmethyl and *p*-hydroxyphenacyl-based compounds in the literature (Hagen *et al.* 2008, Pella 2012).

The photochemical properties of c4m-ac and *p*HP-t were pH-dependent, as they showed a bathochromic shift of the absorption maxima λ_{max} and a reduction of the maximum molar extinction coefficients ε_{max} in alkaline solution compared to water. For c4m-ac, the quantum yield ϕ stayed at 0.02 regardless of the pH, whereas the relatively high ϕ of *p*HP-t at 0.69 in water dropped to 0.07 at pH 9.

The compounds c4m-ac and *p*HP-t showed high stabilities ($s_{24h} \geq 95\%$) in water for 24 h, but decreasing stability with increasing pH due to hydrolysis. Our HPLC measurements revealed that c4m-ac is far more stable than *p*HP-t in water as well as in basic solution.

Under UV irradiation, a complete photolysis (> 99 %) of c4m-ac was reached within 5 min and of pHP-t in 20 min, whereby the pH did not change the photolysis time significantly. For fast applications (< 1h) in water, pHP-t is favorable because of its high solubility ($c_{max,w}$ = 124.66 mmol L^{-1} ± 2.19 mmol L^{-1}) and quantum yield (ϕ = 0.69). For longer applications (< 24h) under basic conditions, the usage of c4m-ac is advantageous, since it shows high solubility ($c_{max,a}$ = 646.46 mmol L^{-1} ± 0.63 mmol L^{-1}), good stabilities (s_{24h} ≥ 96 % up to pH 8) and the fast photolysis.

The synthesis and characterization experiments of c4m-ac and pHP-t clearly confirm hypothesis III. Therefore, we envision that c4m-ac and pHP-t are promising PAGs for the modification of hydrogel swelling agents in the future.

Overall, I could prove all three hypotheses of this work.

10. Conclusions and outlook

Hydrogels are applied in a broad variety of fields such as tissue engineering (Lee *et al.* 2001), drug delivery (Hamedi *et al.* 2018) or waste water treatment (Mohammadzadeh Pakdel *et al.* 2018, Ullah *et al.* 2015). Therefore, tailor-made hydrogels, which are specifically modified according to their application, are subject of current research (Singhal *et al.* 2016, Tang *et al.* 2019). The two basic hydrogel modification concepts are based on the modification of the polymer network or the modification of the hydrogel swelling agent. For both strategies, appropriate hydrogel modification reagents are needed. Hence, this work is dedicated to the synthesis and characterization of multifunctional macromonomers and photoacid generators for the modification of hydrogels.

In the first part of this work, I established the synthesis of α-diphenylmethyl-ω-4-vinylbenzyl-poly(furfuryl glycidyl ether)-*block*-poly(ethylene glycol) ($PFGE_p$-*b*-PEG_q) macromonomers to functionalize the polymer network of p(Aam) hydrogels with multiple clickable anchor points for post-synthetic Diels-Alder reactions (Figure 76).
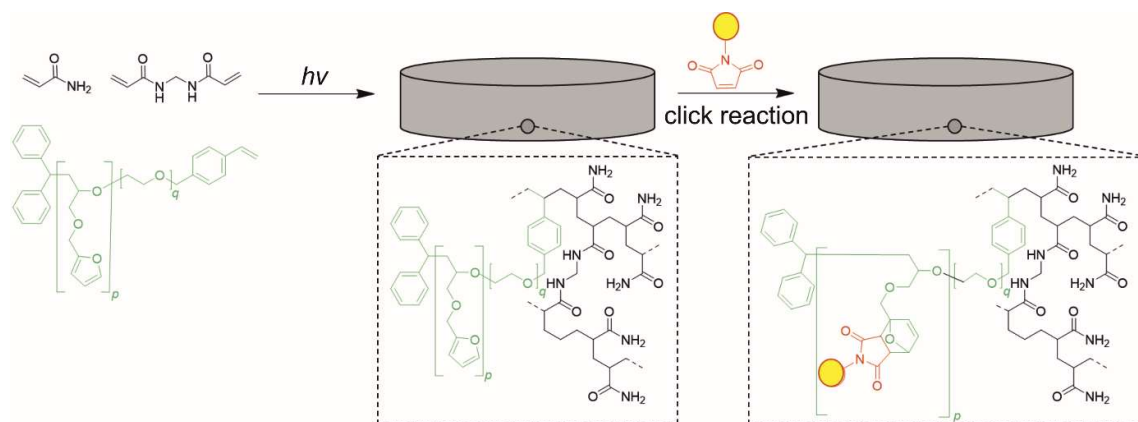
Figure 76: Schematic representation of the hydrogel modification approach based on the functionalization of the hydrogel network with multifunctional macromonomers.

These $PFGE_p$-*b*-PEG_q macromonomers were synthesized in different block length ratios *via* AROP of FGE, followed by EO and terminated with 4-VBC. The successful synthesis of well-defined macromonomers was proven by ^{1}H NMR, ^{13}C NMR and FT-IR spectroscopy. Furthermore, SEC and MALDI TOF mass spectrometry revealed low Đ between 1.05 and 1.12 and number average molar masses between 2 330 g mol^{-1} and 6 660 g mol^{-1}. The block lengths of the macromonomers were adjustable *via* the MIR ratio and high end group functionalization degrees between 72 % and 98 % were

achieved. The macromonomers were immobilized into p(Aam) hydrogels by radical copolymzeriation and the pending furan groups of the macromonomers were labeled with a maleimide-functionalized fluorescence dye. As the fluorescence intensity of fluorescence labeled p(Aam) with and without $PFGE_p$-*b*-PEG_q macromonomers was significantly different in our laser scanning microscopy (LSM) measurements, we could prove that the furan groups of our macromonomers are able to undergo post-synthetic Diels-Alder reactions.

This in conclusion demonstrates that our $PFGE_p$-*b*-PEG_q macromonomers can be used for the modification of a hydrogel network providing clickable anchor points in high density for conjugation of maleimide-functional substrates. These results led to the publication "hydrogels with multiple clickable anchor points: synthesis and characterization of poly(furfuryl glycidyl ether)-*block*-poly(ethylene glycol) macromonomers", which was published in the journal *Polymer Chemistry* (RSC).

Beyond the bulk functionalization of hydrogels, I explored whether $PFGE_p$-*b*-PEG_q macromonomers can be used to exclusively functionalize the air-hydrogel interface without functionalizing the hydrogel bulk. To evaluate whether $PFGE_p$-*b*-PEG_q macromonomers are suitable functionalization reagents for the air-hydrogel interface, knowledge about the film formation ability and the structure-property relations of $PFGE_p$-*b*-PEG_q macromonomers at the air-water interface was needed. Therefore, Langmuir film measurements were performed at the air-water interface, which served as a simplified model of the air-hydrogel precursor solution interface. The general research approach based on Langmuir measurements of $PFGE_p$-*b*-PEG_q macromonomers at the air-water interface, leading to the elucidation of the structure-property, film stability and a potential film mechanism, is shown in Figure 77.
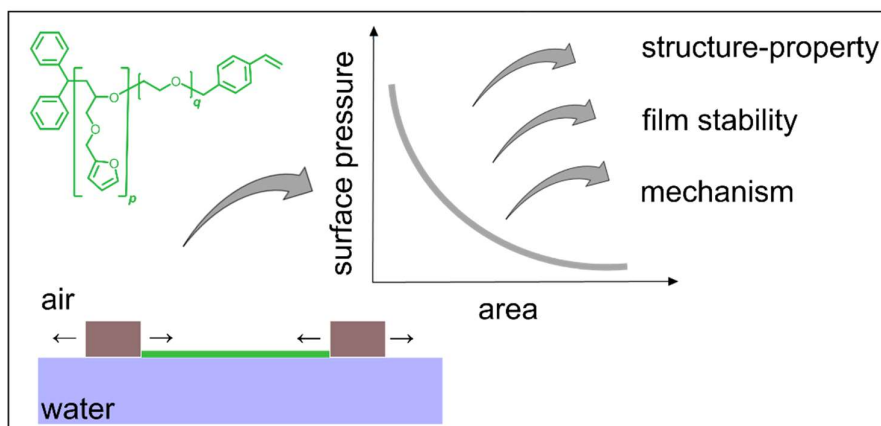
Figure 77: Schematic research approach for the investigation of structure-property, film stability and film mechanim of PFGE$_p$-b-PEG$_q$ macromonomers at the air-water interface.

Using Langmuir surface pressure-area (π-A) isotherms, I could prove the film formation ability of our PFGE$_p$-b-PEG$_q$ macromonomers at the air-water interface as the surface pressure (π) increase during compression is a clear sign for their surface activity. By analyzing the π-A isotherms, I could also elucidate structure-property relations of the macromonomers at the air-water interface. It was shown that the block lengths and the molar masses of the macromonomers influenced the isotherm shape and onset. Smaller, more hydrophobic macromonomers (HLB < 8) showed a steeper surface pressure increase in the liquid condensed phase of the π-A isotherms compared to larger, more hydrophilic macromonomers with HLB > 8. Moreover, the molecular area for isotherm onsets increased almost linearly with growing molar mass of the macromonomers, which shows that the beginning of the film formation correlates with the molar mass of the macromonomers.

I also investigated the film stability of the macomonomers at the air-water interface, since this is an important feature for future functionalization experiments at the air-hydrogel interface. Static and dynamic film stability measurements demonstrated limited stability of all macromonomer monolayers at the air-water interface. Hereby, the more hydrophilic macromonomers with HLB > 8, showed higher film stability compared to the more hydrophobic macromonomers (HLB < 8). Also, hysteresis experiments displayed an almost linear increase of the film degradation with rising HLB values of the macromonomers. This shows that the film stability correlates with the HLB value of our PFGE$_p$-b-PEG$_q$ macromonomers. This in conclusion means, that a fast immobilization process (around 5 min) is recommendable for functionalization experiments at the air-hydrogel interface, because the film stability is limited.

To get more insights into the film mechanism of our macromonomers at the air-water interface, I investigated the film recovery after film degradation. In fact, I could measure partial film recovery to the air-water interface of degraded macromonomer films after 12 h in an expanded Langmuir trough. The ability of the macromonomers to recover to the air-water interface is a strong indication for a folding mechanism as its reversibility was frequently described in the literature (Baoukina *et al.* 2008, Ding *et al.* 2001, Takamoto *et al.* 2001). However, as the macromonomers do not recover fully to the air-water interface, it is likely that some molecules are trapped in irreversible processes like submersion or multilayer collapse (Lee 2008, Ries Jr *et al.* 1987). We rather exclude a collapse to multilayers, since we did not observe a collapse pressure, which is typical for multilayer formations (Yang *et al.* 2009). Such multilayer collapses mostly occur at very high π, when the amphiphiles are compressed beyond their stability limit, which is often over 50 mN m^{-1} (Das *et al.* 2016, Goto *et al.* 2013, Maget-Dana 1999, Rivera *et al.* 2007). Our macromonomers in contrast, were studied at relatively low π between 0 mN m^{-1} and 23 mN m^{-1}, which is why we exclude a multilayer collapse of our macromonomers. A submersion to the subphase is much more likely for our macromonomers, as this was reported for other PEG-based amphiphiles (Barentin *et al.* 1998). It also fits to the micelle formation ability of PFGE-*b*-PEG block copolymers in water (Barthel *et al.* 2012) and explains the observation of the limited stability of our macomonomer monolayers. Hence, the combined analysis of the film stability and film recovery measurements indicates an interplay between a reversible folding and an irreversible submersion mechanism for the macromonomer monolayers at the air-water interface.

Taken together, we believe PFGE$_p$-*b*-PEG$_q$ macromonomers are promising hydrogel surface functionalization reagents, because of their film forming ability at the air-water interface and their molecular structure, consisting of a polymerizable unit, an amphiphilic core structure and multiple furan groups for post-synthetic modification reactions. According to our surface functionalization ranking, PFGE$_{10}$-*b*-PEG$_9$ is the most promising hydrogel surface functionalization reagent, because it can introduce the highest number of functional groups per surface area. All these results regarding the structure-property relations, the film stability and film mechanism of PFGE$_p$-*b*-PEG$_q$ macromonomers at the air-water interface are published as the article „structure-property relations of amphiphilic poly(furfuryl glycidyl ether)-*block*-poly(ethylene glycol) macromonomers at the air-water interface" inth journal *Polymer Chemistry* (RSC).

However, we could not show an exclusively functionalized air-hydrogel interface yet, as the air-hydrogel interface of our p(Aam) hydrogels was fluorescent regardless of its functionalization. The two most evident reasons why the functionalization of the air-hydrogel interface did not work yet, are, that either the macromonomers did not covalently bind to the air-hydrogel interface, or that the macromonomer amount at the hydrogel interface was too little for detection. In the future one should reduce the complexity of the hydrogel interface by investigating whether the macromonomers can bind to a solid surface such as e.g. a self-assembled monolayer of 3-methacryloyl-propyl trimethoxysilane on a silicon wafer (Bialk *et al.* 2002). Furthermore, another detection method than fluorescence spectroscopy like time-of-flight secondary-ion mass spectrometry (TOF-SIMS) should be tested, which was reported by Tylor *et al.* (2016) for the 3D mapping of functionalized p(HEMA) hydrogels. Overall it seems, that our macromonomers are promising hydrogel functionalization reagents, but further research is needed to fulfil the ambitious task of exclusively functionalizing the air-hydrogel interface.

In the future it is interesting to investigate whether our PFGE$_p$-*b*-PEG$_q$ macromonomers can be applied for the improvement of polymer scaffolds in tissue engineering. At present, many polymer scaffolds which are used for the construction of functional tissue, cannot provide sufficient cell attachment or maturation due to lacking cell recognition sites (Tallawi *et al.* 2015). PFGE$_p$-*b*-PEG$_q$ macromonomers could contribute to overcome this obstacle by providing a functionalization platform for post-synthetic modification reactions with e.g. growth factors (De Witte *et al.* 2018), RGD-sequences (Zhang *et al.* 2014) or other required signaling substances (Ullah *et al.* 2015). Similar to Mann *et al.* (2001) cell proliferation experiments between such post-functionalized hydrogels and unfunctionalized hydrogels could help to assess the potential of PFGE$_p$-*b*-PEG$_q$ macromonomers. Especially hydrogels with an exclusively functionalized air-hydrogel interface could be highly interesting for tissue engineering applications, since tailor-made surface characteristics could be introduced without changing the hydrogel bulk properties.

Beyond the hydrogel modification of the polymer network, I also investigated novel hydrogel modification reagents for the potential modification of hydrogel swelling agents, which targets the second hydrogel modification strategy. Until now, many strong electrolyte PAGs like diphenyliodonium salts are used for the modification of

hydrogel swelling agents, even if they are toxic or need additional sensitizer. This is mainly due to their good accessibility and high water solubility. With this research I want to show an alternative approach to such strong electrolyte PAGs by designing two easily accessible and highly water soluble c4m and pHP-based PAGs, as the substance classes of c4ms and pHPs are well suited for physiological applications and do not need additional sensitizers (Givens *et al.* 2012). Hence, I explored the synthesis, solubility, stability and photolysis of two novel c4m and pHP-based PAGs, in particular c4m-ac and pHP-t. These compounds were synthetically well accessible as proven by ^{1}H NMR, ^{13}C NMR and mass spectrometry. Furthermore, they demonstrated high solubility in water with a maximum solubility of $c_{max,w}$(c4m-ac) = 2.77 mmol L^{-1} ± 0.07 mmol L^{-1}, $c_{max,w}$(pHP-t) = 124.66 mmol L^{-1} ± 2.10 mmol L^{-1} and high solubility under basic conditions at pH 9 with a maximum solubility in alkaline solution of $c_{max,a}$(c4m-ac) = 646.46 mmol L^{-1} ± 0.63 mmol L^{-1}, $c_{max,a}$(pHP t) = 34.68 mmol L^{-1} ± 0.62 mmol L^{-1}. These solubilities are well above 1 mmol L^{-1}, which is referred to as good in the c4m and pHP literature (Givens *et al.* 1996, Givens *et al.* 2011, Hagen *et al.* 2008). Moreover, the photochemical properties of both PAGs, like the absorption maxima and maximum molar absorption coefficients, were pH-dependent in contrast to their quantum yields Φ. The Φ of c4m-ac at 365 nm stayed at 0.02 regardless of the pH, whereas the relatively high Φ at 310 nm of pHP-t at 0.69 in water dropped to 0.07 at pH 9. The compounds c4m-ac and pHP-t showed high stabilities (s_{24h} ≥ 95%) in water for 24 h, but decreasing stability with increasing pH to hydrolysis. Overall, our studies contributed to a comprehensive understanding of the synthesis, solubility, stability and photolysis of two highly water soluble c4m and pHP-based PAGs. The results are published in the article "Coumarin-4-ylmethyl and p-hydroxyphenacyl-based photoacid generators with high solubility in aqueous media: synthesis, stability and photolysis" in the journal *ChemPhotoChem* (Wiley-VCH).

In the future, these properties should enable the usage of c4m-ac and pHP-t for hydrogel modification reactions. One example could be a light-triggered pH shift of the hydrogel swelling agent for applications in solvent responsive hydrogels. Another more advanced application could be in the field of 3D printed hydrogel foams. This idea is based on the photo release of acid in a carbonate containing solution, which leads to CO_2 as foaming agent (Schlögl *et al.* 2012). A simultaneous foaming and curing reaction of the hydrogel, after the 3D printing of the hydrogel precursor solution, could pave the way to innovative 3D printable hydrogel foams.

By merging the two concepts of hydrogel foaming with c4m-ac or pHP-t PAGs and functionalizing the air-hydrogel interface with PFGE$_p$-b-PEG$_q$ macromonomers, a 3D printed hydrogel foam for post-synthetic modification reactions could be accessible (Figure 78).
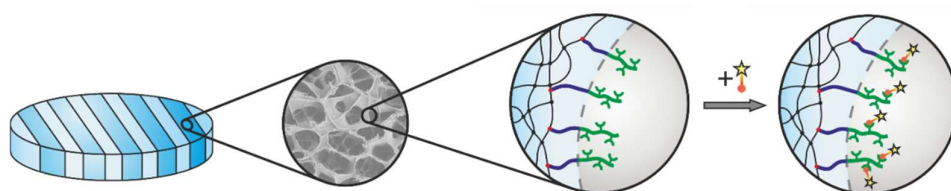

Figure 78: Schematic depiction of a 3D printed hydrogel foam for post-synthetic modification reactions.

Such 3D printed hydrogel foams for post-synthetic modification reactions could be highly valuable as polymer scaffold in tissue engineering.

11. Bibliography

Abd El-Mohdy, H. L.; Safrany, A., Preparation of fast response superabsorbent hydrogels by radiation polymerization and crosslinking of N-isopropylacrylamide in solution. *Radiat. Phys. Chem.* **2008,** *77* (3), 273-279.

Adams, M. L.; Kwon, G. S., The effects of acyl chain length on the micelle properties of poly(ethylene oxide)-block-poly(N-hexylL-aspartamide)-acyl conjugates. *J. Biomater. Sci. Polym. Ed.* **2002,** *13* (9), 991-1006.

Adams, M. L.; Kwon, G. S., Relative aggregation state and hemolytic activity of amphotericin B encapsulated by poly(ethylene oxide)-block–poly(N-hexyl-l-aspartamide)-acyl conjugate micelles: effects of acyl chain length. *J. Control. Release* **2003a,** *87* (1), 23-32.

Adams, M. L.; Lavasanifar, A.; Kwon, G. S., Amphiphilic block copolymers for drug delivery. *J. Pharm. Sci.* **2003b,** *92* (7), 1343-1355.

Adatia, K. K.; Keller, S.; Götz, T.; Tovar, G. E. M.; Southan, A., Hydrogels with multiple clickable anchor points: synthesis and characterization of poly(furfuryl glycidyl ether)-*block*-poly(ethylene glycol) macromonomers. *Polym. Chem.* **2019,** *10*, 4485 - 4494.

Adzima, B. J.; Tao, Y.; Kloxin, C. J.; DeForest, C. A.; Anseth, K. S.; Bowman, C. N., Spatial and temporal control of the alkyne–azide cycloaddition by photoinitiated Cu(II) reduction. *Nat. Chem.* **2011,** *3* (3), 256-259.

Ahmed, E. M., Hydrogel: Preparation, characterization, and applications: A review. *J. Adv. Res.* **2015,** *6* (2), 105-121.

Akhtar, M. F.; Hanif, M.; Ranjha, N. M., Methods of synthesis of hydrogels … A review. *Saudi Pharm. J.* **2016,** *24* (5), 554-559.

Al-Wahaibi, L. H.; Abu-Melha, H. M.; Ibrahim, D. A., Synthesis of Novel 1, 2, 4-Triazolyl Coumarin Derivatives as Potential Anticancer Agents. *J. Chem.* **2018,** *2018*, 8.

Alder, K., Nobel Lectures - Diene synthesis and related reaction types. **1950**, Stockholm, Sweden.

Allen, C.; Han, J.; Yu, Y.; Maysinger, D.; Eisenberg, A., Polycaprolactone–*b*-poly(ethylene oxide) copolymer micelles as a delivery vehicle for dihydrotestosterone. *J. Control. Release* **2000,** *63* (3), 275-286.

Altin, H.; Kosif, I.; Sanyal, R., Fabrication of "Clickable" Hydrogels via Dendron−Polymer Conjugates. *Macromolecules* **2010,** *43* (8), 3801-3808.

Anderson, J.; Reese, C., A photo-induced rearrangement involving aryl participation. *Tetrahedron Lett.* **1962,** *3* (1), 1-4.

Angelova, A.; Vollhardt, D.; Ionov, R., 2D−3D Transformations of Amphiphilic Monolayers Influenced by Intermolecular Interactions: A Brewster Angle Microscopy Study. *J. Phys. Chem. B.* **1996,** *100* (25), 10710-10720.

Atta, A. M.; Ismail, H. S.; Elsaaed, A. M., Application of anionic acrylamide-based hydrogels in the removal of heavy metals from waste water. *J. Appl. Polym. Sci.* **2012a,** *123* (4), 2500-2510.

Atta, S.; Ikbal, M.; Kumar, A.; Pradeep Singh, N. D., Application of photoremovable protecting group for controlled release of plant growth regulators by sunlight. *J. Photochem. Photobiol.* **2012b,** *111*, 39-49.

Atta, S.; Jana, A.; Ananthakirshnan, R.; Narayana Dhuleep, P. S., Fluorescent Caged Compounds of 2,4-Dichlorophenoxyacetic Acid (2,4-D): Photorelease Technology for Controlled Release of 2,4-D. *J. Agric. Food Chem.* **2010,** *58* (22), 11844-11851.

Ayub, N. F.; Hashim, S.; Jamaluddin, J.; Rasit Ali, R.; Adrus, N., UV LED Curing Formulation for Polyacrylamide Hydrogels. *Adv. Mat. Res.* **2015,** *1125*, 84-88.

Baekmark, T. R.; Elender, G.; Lasic, D. D.; Sackmann, E., Conformational Transitions of Mixed Monolayers of Phospholipids and Polyethylene Oxide Lipopolymers and Interaction Forces with Solid Surfaces. *Langmuir* **1995,** *11* (10), 3975-3987.

Bailey Jr., F. E.; Callard, R. W., Some properties of poly(ethylene oxide)1 in aqueous solution. *J. Appl. Polym. Sci.* **1959,** *1* (1), 56-62.

Baker, A. E. G.; Tam, R. Y.; Shoichet, M. S., Independently Tuning the Biochemical and Mechanical Properties of 3D Hyaluronan-Based Hydrogels with Oxime and Diels–Alder Chemistry to Culture Breast Cancer Spheroids. *Biomacromolecules* **2017,** *18* (12), 4373-4384.

Baoukina, S.; Monticelli, L.; Risselada, H. J.; Marrink, S. J.; Tieleman, D. P., The molecular mechanism of lipid monolayer collapse. *Proc. Natl. Acad. Sci.* **2008,** *105* (31), 10803-10808.

Barentin, C.; Muller, P.; Joanny, J. F., Polymer Brushes Formed by End-Capped Poly(ethylene oxide) (PEO) at the Air−Water Interface. *Macromolecules* **1998,** *31* (7), 2198-2211.

Barman, B. N.; Champion, D. H.; Sjoberg, S. L., Identification and quantification of polyethylene glycol types in polyethylene glycol methyl ether and polyethylene glycol vinyl ether. *J. Chrom. A.* **2009,** *1216* (40), 6816-6823.

Barman, S.; Mukhopadhyay, S. K.; Biswas, S.; Nandi, S.; Gangopadhyay, M.; Dey, S.; Anoop, A.; Pradeep Singh, N. D., A p-Hydroxyphenacyl–Benzothiazole–Chlorambucil Conjugate as a Real-Time-Monitoring Drug-Delivery System Assisted by Excited-State Intramolecular Proton Transfer. *Angew. Chem. Int. Ed.* **2016,** *55* (13), 4194-4198.

Barth, A.; Corrie, J. E.; Gradwell, M. J.; Maeda, Y.; Mäntele, W.; Meier, T.; Trentham, D. R., Time-resolved infrared spectroscopy of intermediates and products from photolysis of 1-(2-nitrophenyl) ethyl phosphates: reaction of the 2-nitrosoacetophenone byproduct with thiols. *J. Am. Chem. Soc.* **1997,** *119* (18), 4149-4159.

Barthel, M. J.; Mansfeld, U.; Hoeppener, S.; Czaplewska, J. A.; Schacher, F. H.; Schubert, U. S., Understanding and tuning the self-assembly of polyether-based triblock terpolymers in aqueous solution. *Soft Matter* **2013a,** *9* (13), 3509-3520.

Barthel, M. J.; Rudolph, T.; Crotty, S.; Schacher, F. H.; Schubert, U. S., Homo- and diblock copolymers of poly(furfuryl glycidyl ether) by living anionic polymerization: Toward reversibly core-crosslinked micelles. *J. Polym. Sci., Part A: Polym. Chem.* **2012,** *50* (23), 4958-4965.

Barthel, M. J.; Rudolph, T.; Teichler, A.; Paulus, R. M.; Vitz, J.; Hoeppener, S.; Hager, M. D.; Schacher, F. H.; Schubert, U. S., Self-Healing Materials via Reversible Crosslinking of Poly(ethylene oxide)-Block-Poly(furfuryl glycidyl ether) (PEO-b-PFGE) Block Copolymer Films. *Adv. Funct. Mater.* **2013b,** *23* (39), 4921-4932.

Beer, A., Determination of the absorption of red light in colored liquids. *Ann. Physik* **1852,** *162*, 78-88.

Bernardini, C.; Stoyanov, S. D.; Arnaudov, L. N.; Cohen Stuart, M. A., Colloids in Flatland: a perspective on 2D phase-separated systems, characterisation methods, and lineactant design. *Chem. Soc. Rev.* **2013,** *42* (5), 2100-2129.

Bialk, M.; Prucker, O.; Rühe, J., Grafting of polymers to solid surfaces by using immobilized methacrylates. *Colloids Surf. A* **2002,** *198-200*, 543-549.

Bijsterbosch, H. d.; De Haan, V.; De Graaf, A.; Mellema, M.; Leermakers, F.; Stuart, M. C.; Well, A. v., Tethered adsorbing chains: neutron reflectivity and surface pressure of spread diblock copolymer monolayers. *Langmuir* **1995,** *11* (11), 4467-4473.

Binder, W. H.; Sachsenhofer, R., 'Click' Chemistry in Polymer and Materials Science. *Macromol. Rapid Commun.* **2007,** *28* (1), 15-54.

Blodgett, K. B., Films built by depositing successive monomolecular layers on a solid surface. *J. Am. Chem. Soc.* **1935,** *57* (6), 1007-1022.

Bodour, A. A.; Miller-Maier, R. M., Application of a modified drop-collapse technique for surfactant quantitation and screening of biosurfactant-producing microorganisms. *J. Microbiol. Methods* **1998,** *32* (3), 273-280.

Bolourchian, N.; Mahboobian, M. M.; Dadashzadeh, S., The effect of PEG molecular weights on dissolution behavior of Simvastatin in solid dispersions. *J. Pharm. Pharm. Sci.* **2013,** *12* (Suppl), 11.

Bomze, D.; Knaack, P.; Liska, R., Successful radical induced cationic frontal polymerization of epoxy-based monomers by C–C labile compounds. *Polym. Chem.* **2015,** *6* (47), 8161-8167.

Bossard, F.; Aubry, T.; Gotzamanis, G.; Tsitsilianis, C., pH-Tunable rheological properties of a telechelic cationic polyelectrolyte reversible hydrogel. *Soft Matter* **2006,** *2* (6), 510-516.

Brocas, A.-L.; Mantzaridis, C.; Tunc, D.; Carlotti, S., Polyether synthesis: From activated or metal-free anionic ring-opening polymerization of epoxides to functionalization. *Prog. Polym. Sci.* **2013,** *38* (6), 845-873.

Brugger, B.; Vermant, J.; Richtering, W., Interfacial layers of stimuli-responsive poly-(N-isopropylacrylamide-co-methacrylicacid)(PNIPAM-co-MAA) microgels characterized by interfacial rheology and compression isotherms. *Phys. Chem. Chem. Phys.* **2010,** *12* (43), 14573-14578.

Brunchi, C.-E.; Ghimici, L., PEG in aqueous salt solutions. Viscosity and separation ability in a TiO2 suspension. *Rev. Roum. Chim.* **2013,** *58* (2-3), 183-188.

Brynda, E.; Houska, M.; Kysilka, J.; Přádný, M.; Lesný, P.; Jendelová, P.; Michálek, J.; Syková, E., Surface modification of hydrogels based on poly (2-hydroxyethyl methacrylate) with extracellular matrix proteins. *J. Mater. Sci. Mater. Med.* **2009,** *20* (4), 909-915.

Buckup, T.; Southan, A.; Kim, H.-C.; Hampp, N.; Motzkus, M., Optimisation of two-photon induced cleavage of molecular linker systems for drug delivery. *J. Photochem. Photobiol.* **2010,** *210* (2-3), 188-192.

Buenger, D.; Topuz, F.; Groll, J., Hydrogels in sensing applications. *Prog. Polym. Sci.* **2012,** *37* (12), 1678-1719.

Buono, P.; Duval, A.; Averous, L.; Habibi, Y., Thermally healable and remendable lignin-based materials through Diels–Alder click polymerization. *Polymer* **2017,** *133*, 78-88.

Buwalda, S. J.; Vermonden, T.; Hennink, W. E., Hydrogels for therapeutic delivery: Current developments and future directions. *Biomacromolecules* **2017,** *18* (2), 316-330.

Caló, E.; Khutoryanskiy, V. V., Biomedical applications of hydrogels: A review of patents and commercial products. *Eur. Polym. J.* **2015,** *65*, 252-267.

Cardenas-Valera, A.; Bailey, A., The interfacial rheological behaviour of monolayers of PEO/PMMA graft copolymers spread at the air/water and oil/water interfaces. *Colloids Surf. A* **1993,** *79* (1), 115-127.

Chausson, M.; Fluchère, A.-S.; Landreau, E.; Aguni, Y.; Chevalier, Y.; Hamaide, T.; Abdul-Malak, N.; Bonnet, I., Block copolymers of the type poly(caprolactone)-*b*-poly(ethylene oxide) for the preparation and stabilization of nanoemulsions. *Int. J. Pharm.* **2008,** *362* (1-2), 153-162.

Chen, E. M.; Quijano, A. R.; Seo, Y.-E.; Jackson, C.; Josowitz, A. D.; Noorbakhsh, S.; Merlettini, A.; Sundaram, R. K.; Focarete, M. L.; Jiang, Z., Biodegradable PEG-poly(ω-pentadecalactone-co-p-dioxanone) nanoparticles for enhanced and sustained drug delivery to treat brain tumors. *Biomaterials* **2018**.

Chen, R. T.; Marchesan, S.; Evans, R. A.; Styan, K. E.; Such, G. K.; Postma, A.; McLean, K. M.; Muir, B. W.; Caruso, F., Photoinitiated Alkyne–Azide Click and Radical Cross-Linking Reactions for the Patterning of PEG Hydrogels. *Biomacromolecules* **2012,** *13* (3), 889-895.

Chen, X.; Ma, C.; Kwok, W. M.; Guan, X.; Du, Y.; Phillips, D. L., A Theoretical Investigation of p-Hydroxyphenacyl Caged Phototrigger Compounds: An Examination

of the Excited State Photochemistry of p-Hydroxyphenacyl Acetate. *J. Phys. Chem.* **2006,** *110* (45), 12406-12413.

Chiappe, C.; Malvaldi, M.; Pomelli, C. S., The solvent effect on the Diels-Alder reaction in ionic liquids: multiparameter linear solvation energy relationships and theoretical analysis. *Green Chem.* **2010,** *12* (8), 1330-1339.

Ciamician, G.; Silber, P., Chemische Lichtwirkungen. *P. Chem. Ber* **1901,** *34* (2), 1530-1543.

Claaßen, C.; Claaßen, M. H.; Gohl, F.; Tovar, G. E.; Borchers, K.; Southan, A., Photoinduced Cleavage and Hydrolysis of o-Nitrobenzyl Linker and Covalent Linker Immobilization in Gelatin Methacryloyl Hydrogels. *Macromol. Biosci.* **2018,** *18* (9), 1800104.

Clop, E. M.; Corvalán, N. A.; Perillo, M. A., Langmuir films of dipalmitoyl phosphatidylethanolamine grafted poly (ethylene glycol). In-situ evidence of surface aggregation at the air-water interface. *Colloids Surf. B.* **2016,** *148*, 640-649.

Conrad, P. G.; Givens, R. S.; Weber, J. F.; Kandler, K., New Phototriggers: 1 Extending the p-Hydroxyphenacyl π− π* Absorption Range. *Org. Lett.* **2000,** *2* (11), 1545-1547.

Constantino, C.; Dhanabalan, A.; Oliveira Jr, O., Experimental artifacts in the surface pressure measurement for lignin monolayers in Langmuir troughs. *Rev. Sci. Instrum.* **1999,** *70* (9), 3674-3680.

Cornwell, D. J.; Daubney, O. J.; Smith, D. K., Photopatterned multidomain gels: multi-component self-assembled hydrogels based on partially self-sorting 1, 3: 2, 4-dibenzylidene-D-sorbitol derivatives. *J. Am. Chem. Soc.* **2015,** *137* (49), 15486-15492.

Crivello, J. V.; Lam, J. H. W., Diaryliodonium Salts. A New Class of Photoinitiators for Cationic Polymerization. *Macromolecules* **1977,** *10* (6), 1307-1315.

Crivello, J. V.; Lam, J. H. W., Dye-sensitized photoinitiated cationic polymerization. *J. Polym. Sci. A Polym. Chem.* **1978,** *16* (10), 2441-2451.

Crivello, J. V.; Lam, J. H. W., Photoinitiated cationic polymerization by triarylselenonium salts. *J. Polym. Sci. A Polym. Chem.* **1979,** *17* (4), 1047-1057.

Crivello, J. V.; Lee, J. L., Photosensitized cationic polymerizations using dialkylphenacylsulfonium and dialkyl(4-hydroxyphenyl)sulfonium salt photoinitiators. *Macromolecules* **1981,** *14* (5), 1141-1147.

Culp, J. T.; Park, J.-H.; Stratakis, D.; Meisel, M. W.; Talham, D. R., Supramolecular Assembly at Interfaces: Formation of an Extended Two-Dimensional Coordinate Covalent Square Grid Network at the Air−Water Interface. *J. Am. Chem. Soc.* **2002,** *124* (34), 10083-10090.

D'souza, A. A.; Shegokar, R., Polyethylene glycol (PEG): a versatile polymer for pharmaceutical applications. *Expert Opin. Drug Deliv.* **2016,** *13* (9), 1257-1275.

Da Silva, A. G.; Filipe, E.; d'Oliveira, J.; Martinho, J., Interfacial behavior of poly(styrene)-poly(ethylene oxide) diblock copolymer monolayers at the air-water interface. Hydrophilic block chain length and temperature influence. *Langmuir* **1996,** *12* (26), 6547-6553.

Das, K.; Kundu, S., Subphase pH induced monolayer to multilayer collapse of fatty acid Salt Langmuir monolayer at lower surface pressure. *Colloids Surf. A.* **2016,** *492,* 54-61.

De Witte, T.-M.; Fratila-Apachitei, L. E.; Zadpoor, A. A.; Peppas, N. A., Bone tissue engineering via growth factor delivery: from scaffolds to complex matrices. *Regen. Biomater.* **2018,** *5* (4), 197-211.

Decker, C.; Jenkins, A. D., Kinetic approach of oxygen inhibition in ultraviolet-and laser-induced polymerizations. *Macromolecules* **1985,** *18* (6), 1241-1244.

DeForest, C. A.; Anseth, K. S., Photoreversible Patterning of Biomolecules within Click-Based Hydrogels. *Angew. Chem. Int. Ed.* **2012,** *51* (8), 1816-1819.

DeLong, S. A.; Moon, J. J.; West, J. L., Covalently immobilized gradients of bFGF on hydrogel scaffolds for directed cell migration. *Biomaterials* **2005,** *26* (16), 3227-3234.

Deschênes, L.; Saint-Germain, F.; Lyklema, J., Langmuir monolayers of non-ionic polymers: Equilibrium or metastability? Case study of PEO and its PPO–PEO diblock copolymers. *J. Colloid Interface Sci.* **2015,** *449,* 494-505.

Dhanabalan, A.; Gaffo, L.; Barros, A. M.; Moreira, W. C.; Oliveira, O. N., Surface Pressure and Surface Potential Isotherms of Ytterbium Bisphthalocyanine Langmuir Monolayers. *Langmuir* **1999,** *15* (11), 3944-3949.

Diamant, H.; Witten, T. A.; Ege, C.; Gopal, A.; Lee, K. Y. C., Topography and instability of monolayers near domain boundaries. *Phys. Rev. E.* **2001,** *63* (6), 061602.

Diels, O.; Alder, K., Über die Ursachen der „Azoesterreaktion" . *Liebigs Ann. Chem.* **1926,** *450* (1), 237-254.

Ding, J.; Takamoto, D. Y.; von Nahmen, A.; Lipp, M. M.; Lee, K. Y. C.; Waring, A. J.; Zasadzinski, J. A., Effects of Lung Surfactant Proteins, SP-B and SP-C, and Palmitic Acid on Monolayer Stability. *Biophys. J.* **2001,** *80* (5), 2262-2272.

Dolatabadi-Farahani, T.; Vasheghani-Farahani, E.; Mirzadeh, H., Swelling behaviour of alginate-N, O-carboxymethyl chitosan gel beads coated by chitosan. *Iran. Poly. J.* **2006,** *15* (5), 405.

Drumheller, P. D.; Hubbell, J. A., Polymer networks with grafted cell adhesion peptides for highly biospecific cell adhesive substrates. *Anal. Biochem.* **1994,** *222* (2), 380-388.

Drury, J. L.; Mooney, D. J., Hydrogels for tissue engineering: scaffold design variables and applications. *Biomaterials* **2003,** *24* (24), 4337-4351.

Du, X.; Frei, H.; Kim, S.-H., Comparison of nitrophenylethyl and hydroxyphenacyl caging groups. *Biopolymers* **2001,** *62* (3), 147-149.

Dunne, A.; Delaney, C.; Florea, L.; Diamond, D., Solvato-morphologically controlled, reversible NIPAAm hydrogel photoactuators. *RSC Adv.* **2016,** *6* (86), 83296-83302.

Dworak, A.; Baran, G.; Trzebicka, B.; Wałach, W., Polyglycidol-*block*-poly(ethylene oxide)-*block*-polyglycidol: synthesis and swelling properties. *React. Funct. Polym.* **1999,** *42* (1), 31-36.

Dynarowicz-Łątka, P.; Dhanabalan, A.; Oliveira Jr, O. N., Modern physicochemical research on Langmuir monolayers. *Adv. Colloid Interface Sci.* **2001,** *91* (2), 221-293.

Edward Semple, J.; Sullivan, B.; Vojkovsky, T.; Sill, K. N., Synthesis and facile end-group quantification of functionalized PEG azides. *J. Polym. Sci. A Polym. Chem.* **2016a,** *54* (18), 2888-2895.

Edward Semple, J.; Sullivan, B.; Vojkovsky, T.; Sill, K. N., Synthesis and facile end-group quantification of functionalized PEG azides. *J. Polym. Sci. A Polym. Chem.* **2016b,** *54* (18), 2888-2895.

Ehrenhofer, A.; Elstner, M.; Wallmersperger, T., Normalization of hydrogel swelling behavior for sensoric and actuatoric applications. *Sens. Actuator B Chem.* **2018,** *255*, 1343-1353.

El-Sherbiny, I. M.; Yacoub, M. H., Hydrogel scaffolds for tissue engineering: Progress and challenges. *Glob. Cardiol. Sci. Pract.* **2013,** *2013* (3), 316-342.

Elter, J. K.; Sentis, G.; Bellstedt, P.; Biehl, P.; Gottschaldt, M.; Schacher, F. H., Core-crosslinked diblock terpolymer micelles - taking a closer look on crosslinking efficiency. *Polym. Chem.* **2018,** *9* (17), 2247-2257.

Fadhel, A. A.; Yue, X.; Ghazvini Zadeh, E. H.; Bondar, M. V.; Belfield, K. D., Pegylated and nanoparticle-conjugated sulfonium salt photo triggers necrotic cell death. *Int. J. Nanomed.* **2016,** *11*, 6161-6168.

Fan, M.; Ma, Y.; Zhang, Z.; Mao, J.; Tan, H.; Hu, X., Biodegradable hyaluronic acid hydrogels to control release of dexamethasone through aqueous Diels–Alder chemistry for adipose tissue engineering. *Mater. Sci. Eng. C.* **2015,** *56*, 311-317.

Faucher, J. A.; Koleske, J. V.; Jr., E. R. S.; Stratta, J. J.; III, C. W. W., Glass Transitions of Ethylene Oxide Polymers. *J. Appl. Phys.* **1966,** *37* (11), 3962-3964.

Faure, M.; Bassereau, P.; Carignano, M.; Szleifer, I.; Gallot, Y.; Andelman, D., Monolayers of diblock copolymer at the air-water interface: the attractive monomer-surface case. *Eur. Phys. J. B.* **1998,** *3* (3), 365-375.

Fauré, M. C.; Bassereau, P.; Lee, L. T.; Menelle, A.; Lheveder, C., Phase Transitions in Monolayers of PS−PEO Copolymer at the Air−Water Interface. *Macromolecules* **1999,** *32* (25), 8538-8550.

Fazio, V.; Komitov, L.; Lagerwall, S., Alignment of nematic liquid crystals on mixed Langmuir–Blodgett monolayers. *Thin Solid Films* **1998,** *327*, 681-685.

Feng, W.; Zhou, W.; Zhang, S.; Fan, Y.; Yasin, A.; Yang, H., UV-controlled shape memory hydrogels triggered by photoacid generator. *RSC Adv.* **2015,** *5* (100), 81784-81789.

Fiume, M. M.; Heldreth, B.; Bergfeld, W. F.; Belsito, D. V.; Hill, R. A.; Klaassen, C. D.; Liebler, D.; Marks Jr, J. G.; Shank, R. C.; Slaga, T. J., Safety assessment of alkyl PEG ethers as used in cosmetics. *Int. J. Toxicol.* **2012,** *31* (5_suppl), 169S-244S.

Flory, P. J., Molecular Size Distribution in Ethylene Oxide Polymers. *J. Am. Chem. Soc.* **1940,** *62* (6), 1561-1565.

Francis, R.; Taton, D.; Logan, J. L.; Masse, P.; Gnanou, Y.; Duran, R. S., Synthesis and Surface Properties of Amphiphilic Star-Shaped and Dendrimer-like Copolymers Based on Polystyrene Core and Poly(ethylene oxide) Corona. *Macromolecules* **2003,** *36* (22), 8253-8259.

Francis, W.; Dunne, A.; Delaney, C.; Florea, L.; Diamond, D., Spiropyran based hydrogels actuators—Walking in the light. *Sens. Actuator B. Chem.* **2017,** *250*, 608-616.

Fruijtier-Pölloth, C., Safety assessment on polyethylene glycols (PEGs) and their derivatives as used in cosmetic products. *Toxicology* **2005,** *214* (1-2), 1-38.

Furuta, T.; Takeuchi, H.; Isozaki, M.; Takahashi, Y.; Kanehara, M.; Sugimoto, M.; Watanabe, T.; Noguchi, K.; Dore, T. M.; Kurahashi, T., Bhc-cNMPs as either water-soluble or membrane-permeant photoreleasable cyclic nucleotides for both one-and two-photon excitation. *ChemBioChem* **2004,** *5* (8), 1119-1128.

Gandini, A., The furan/maleimide Diels–Alder reaction: a versatile click–unclick tool in macromolecular synthesis. *Prog. Polym. Sci.* **2013,** *38* (1), 1-29.

Gao, Y.; Wei, Z.; Li, F.; Yang, Z. M.; Chen, Y. M.; Zrinyi, M.; Osada, Y., Synthesis of a morphology controllable Fe 3 O 4 nanoparticle/hydrogel magnetic nanocomposite inspired by magnetotactic bacteria and its application in H 2 O 2 detection. *Green Chem.* **2014,** *16* (3), 1255-1261.

Gaplovsky, M.; Il'ichev, Y. V.; Kamdzhilov, Y.; Kombarova, S. V.; Mac, M.; Schwörer, M. A.; Wirz, J., Photochemical reaction mechanisms of 2-nitrobenzyl compounds: 2-nitrobenzyl alcohols form 2-nitroso hydrates by dual proton transfer. *Photochem. Photobiol. Sci.* **2005,** *4* (1), 33-42.

García-Astrain, C.; Gandini, A.; Coelho, D.; Mondragon, I.; Retegi, A.; Eceiza, A.; Corcuera, M.; Gabilondo, N., Green chemistry for the synthesis of methacrylate-based hydrogels crosslinked through Diels–Alder reaction. *Eur. Polym. J.* **2013,** *49* (12), 3998-4007.

García-Astrain, C.; Gandini, A.; Peña, C.; Algar, I.; Eceiza, A.; Corcuera, M.; Gabilondo, N., Diels–Alder "click" chemistry for the cross-linking of furfuryl-gelatin-polyetheramine hydrogels. *RSC Adv.* **2014,** *4* (67), 35578-35587.

Garg, S.; Garg, A., Hydrogel: Classification, Prperties, Preparationa and Technical Features. *Asian J. Biomat. Res,* **2016,** *2* (6), 163 - 170.

Gargava, A.; Arya, C.; Raghavan, S. R., Smart Hydrogel-Based Valves Inspired by the Stomata in Plants. *ACS Appl. Mater. Interfaces* **2016,** *8* (28), 18430-18438.

Gatzke, A. L., Chain transfer in anionic polymerization. Determination of chain-transfer constants by using carbon-14-labeled chain transfer agents. *J. Polym. Sci. Pol. Chem.* **1969,** *7* (8), 2281-2292.

Gaucher, G.; Dufresne, M.-H.; Sant, V. P.; Kang, N.; Maysinger, D.; Leroux, J.-C., Block copolymer micelles: preparation, characterization and application in drug delivery. *J. Control. Release* **2005,** *109* (1), 169-188.

Gauthier, M.; Stangel, I.; Ellis, T.; Zhu, X., Oxygen inhibition in dental resins. *J. Dent. Res.* **2005,** *84* (8), 725-729.

Gee, G.; Higginson, W.; Levesley, P.; Taylor, K., Polymerisation of epoxides: Some kinetic aspects of the addition of alcohols to epoxides catalysed by sodium alkoxides. *J. Chem. Soc.* **1959**, 1338-1344.

Geibel, S.; Barth, A.; Amslinger, S.; Jung, A. H.; Burzik, C.; Clarke, R. J.; Givens, R. S.; Fendler, K., P3-[2-(4-hydroxyphenyl)-2-oxo] ethyl ATP for the rapid activation of the Na+, K+-ATPase. *Biophys. J.* **2000,** *79* (3), 1346-1357.

Geißler, D.; Antonenko, Y. N.; Schmidt, R.; Keller, S.; Krylova, O. O.; Wiesner, B.; Bendig, J.; Pohl, P.; Hagen, V., (Coumarin-4-yl)methyl Esters as Highly Efficient, Ultrafast Phototriggers for Protons and Their Application to Acidifying Membrane Surfaces. *Angew. Chem. Int. Ed.* **2005,** *44* (8), 1195-1198.

Givens, R. S.; Heger, D.; Hellrung, B.; Kamdzhilov, Y.; Mac, M.; Conrad, P. G.; Cope, E.; Lee, J. I.; Mata-Segreda, J. F.; Schowen, R. L.; Wirz, J., The Photo-Favorskii Reaction of p-Hydroxyphenacyl Compounds Is Initiated by Water-Assisted, Adiabatic Extrusion of a Triplet Biradical. *J. Am. Chem. Soc.* **2008,** *130* (11), 3307-3309.

Givens, R. S.; Lee, J.-I., The *p*-hydroxyphenacyl photoremovable protecting group. *J. Photosci.* **2003,** *10* (1), 37-48.

Givens, R. S.; Matuszewski, B., Photochemistry of phosphate esters: an efficient method for the generation of electrophiles. *J. Am. Chem. Soc.* **1984,** *106* (22), 6860-6861.

Givens, R. S.; Park, C.-H., p-Hydroxyphenacyl ATP1: A new phototrigger. *Tetrahedron Lett.* **1996,** *37* (35), 6259-6262.

Givens, R. S.; Rubina, M.; Wirz, J., Applications of p-hydroxyphenacyl (p HP) and coumarin-4-ylmethyl photoremovable protecting groups. *Photochem. Photobiol. Sci.* **2012,** *11* (3), 472-488.

Givens, R. S.; Stensrud, K.; Conrad, P. G.; Yousef, A. L.; Perera, C.; Senadheera, S. N.; Heger, D.; Wirz, J., p-Hydroxyphenacyl photoremovable protecting groups— Robust photochemistry despite substituent diversity. *Can. J. Chem.* **2011,** *89* (3), 364-384.

Givens, R. S.; Weber, J. F. W.; Conrad, P. G.; Orosz, G.; Donahue, S. L.; Thayer, S. A., New Phototriggers 9: p-Hydroxyphenacyl as a C-Terminal Photoremovable Protecting Group for Oligopeptides. *J. Am. Chem. Soc.* **2000,** *122* (12), 2687-2697.

Gleede, T.; Rieger, E.; Blankenburg, J.; Klein, K.; Wurm, F. R., Fast Access to Amphiphilic Multiblock Architectures by the Anionic Copolymerization of Aziridines and Ethylene Oxide. *J. Am. Chem. Soc.* **2018,** *140* (41), 13407-13412.

Gopal, A.; Lee, K. Y. C., Morphology and Collapse Transitions in Binary Phospholipid Monolayers. *J. Phys. Chem. B.* **2001,** *105* (42), 10348-10354.

Goto, T. E.; Caseli, L., Understanding the Collapse Mechanism in Langmuir Monolayers through Polarization Modulation-Infrared Reflection Absorption Spectroscopy. *Langmuir* **2013,** *29* (29), 9063-9071.

Götz, T.; Schädel, N.; Petri, N.; Kirchhof, M.; Bilitewski, U.; Tovar, G. E.; Laschat, S.; Southan, A., Triazole-based cross-linkers in radical polymerization processes: tuning mechanical properties of poly (acrylamide) and poly (N, N-dimethylacrylamide) hydrogels. *RSC Adv.* **2018,** *8* (60), 34743-34753.

Gould, S. T.; Darling, N. J.; Anseth, K. S., Small peptide functionalized thiol–ene hydrogels as culture substrates for understanding valvular interstitial cell activation and de novo tissue deposition. *Acta Biomater.* **2012,** *8* (9), 3201-3209.

Grevesse, T.; Versaevel, M.; Circelli, G.; Desprez, S.; Gabriele, S., A simple route to functionalize polyacrylamide hydrogels for the independent tuning of mechanotransduction cues. *Lab Chip* **2013,** *13* (5), 777-780.

Grevesse, T.; Versaevel, M.; Gabriele, S., Preparation of hydroxy-PAAm hydrogels for decoupling the effects of mechanotransduction cues. *J. Vis. Exp.* **2014,** (90), 51010.

Griffin, W. C., Calculation of HLB Values of Non-Ionic Surfactants. *J. Cosmet. Sci.* **1954,** *5* (4), 249–256.

Griffin, W. C., Classification of surface-active agents by "HLB". *J. Cosmet. Sci.* **1949,** *1*, 311-326.

Guilherme, M. R.; Aouada, F. A.; Fajardo, A. R.; Martins, A. F.; Paulino, A. T.; Davi, M. F.; Rubira, A. F.; Muniz, E. C., Superabsorbent hydrogels based on polysaccharides for application in agriculture as soil conditioner and nutrient carrier: A review. *Eur. Polym. J.* **2015,** *72*, 365-385.

Gupta, P.; Vermani, K.; Garg, S., Hydrogels: from controlled release to pH-responsive drug delivery. *Drug Discov. Today* **2002,** *7* (10), 569-579.

Hagen, V.; Dekowski, B.; Kotzur, N.; Lechler, R.; Wiesner, B.; Briand, B.; Beyermann, M., {7-[Bis (carboxymethyl) amino] coumarin-4-yl} methoxycarbonyl Derivatives for Photorelease of Carboxylic Acids, Alcohols/Phenols, Thioalcohols/Thiophenols, and Amines. *Chem. Eur. J.* **2008,** *14* (5), 1621-1627.

Hagen, V.; Dekowski, B.; Nache, V.; Schmidt, R.; Geißler, D.; Lorenz, D.; Eichhorst, J.; Keller, S.; Kaneko, H.; Benndorf, K., Coumarinylmethyl esters for ultrafast release of high concentrations of cyclic nucleotides upon one-and two-photon photolysis. *Angew. Chem. Int. Ed.* **2005,** *44* (48), 7887-7891.

Hagen, V.; Kilic, F.; Schaal, J.; Dekowski, B.; Schmidt, R.; Kotzur, N., [8-[Bis(carboxymethyl)aminomethyl]-6-bromo-7-hydroxycoumarin-4-yl]methyl Moieties as Photoremovable Protecting Groups for Compounds with COOH, NH2, OH, and C=O Functions. *J. Org. Chem.* **2010,** *75* (9), 2790-2797.

Hamedi, H.; Moradi, S.; Hudson, S. M.; Tonelli, A. E., Chitosan based hydrogels and their applications for drug delivery in wound dressings: A review. *Carbohydr. Polym.* **2018,** *199*, 445-460.

Harris, J. M.; Hundley, N. H.; Shannon, T. G.; Struck, E. C., Polyethylene glycols as soluble, recoverable, phase-transfer catalysts. *J. Org. Chem.* **1982,** *47* (24), 4789-4791.

Hatchard, C.; Parker, C. A., A new sensitive chemical actinometer-II. Potassium ferrioxalate as a standard chemical actinometer. *Proc. Royal Soc. Lond.* **1956,** *235* (1203), 518-536.

Heinz, T.; Tom, H.; Shen, Y. R., Determination of molecular orientation of monolayer adsorbates by optical second-harmonic generation. *Phys. Rev. A* **1983,** *28* (3), 1883.

Hennink, W. E.; van Nostrum, C. F., Novel crosslinking methods to design hydrogels. *Adv. Drug Deliv. Rev.* **2002,** *54* (1), 13-36.

Hermanson, G., Immobilization of Ligands on Chromatography Supports. *Pierce Biotechnology,* **2013**, Rockford.

Herzberger, J.; Niederer, K.; Pohlit, H.; Seiwert, J.; Worm, M.; Wurm, F. R.; Frey, H., Polymerization of ethylene oxide, propylene oxide, and other alkylene oxides: synthesis, novel polymer architectures, and bioconjugation. *Chem. Rev.* **2015,** *116* (4), 2170-2243.

Hiller, A.; Borchers, K.; Tovar, G. E.; Southan, A., Impact of intermediate UV curing and yield stress of 3D printed poly(ethylene glycol) diacrylate hydrogels on interlayer connectivity and maximum build height. *Addit. Manuf.* **2017,** *18*, 136-144.

Hiyoshizo, K.; Kazuhiko, A.; Hiroyuki, O., Preparatively Useful Method for the Synthesis of Diels-Alder Adducts between Furan and Methyl Acrylate. *Bull. Chem. Soc. Jpn.* **1984,** *57* (11), 3339-3340.

Hoffman, A. S., Hydrogels for biomedical applications. *Adv. Drug Delivery Rev.* **2012,** *64* (0), 18-23.

Holm, A.; Kunz, L.; Riscoe, A. R.; Kao, K.-C.; Cargnello, M.; Frank, C. W., General Self-Assembly Method for Deposition of Graphene Oxide into Uniform Close-Packed Monolayer Films. *Langmuir* **2019,** *35* (13), 4460-4470.

Hörenz, C.; Rudolph, T.; Barthel, M. J.; Günther, U.; Schacher, F. H., Amphiphilic polyether-based block copolymers as crosslinkable ligands for Au-nanoparticles. *Polym. Chem.* **2015**.

Höring, H. R. S.; Ulbricht, J., On the anionic polymerization of ethylene oxide with monofunctional initiators. *Europ. Polym. J.* **1989,** *25* (11), 1113-1117.

Hotta, Y.; Kaneko, T.; Hayashi, R.; Yamamoto, A.; Morimoto, S.; Chiba, J.; Tomohiro, T., Photoinduced Electron Transfer-Regulated Protein Labeling With a Coumarin-Based Multifunctional Photocrosslinker. *Chem. Asian J.* **2019,** *14* (3), 398-402.

Hoyle, C. E.; Bowman, C. N., Thiol–Ene Click Chemistry. *Angew. Chem. Int. Ed.* **2010a,** *49* (9), 1540-1573.

Hoyle, C. E.; Lowe, A. B.; Bowman, C. N., Thiol-click chemistry: a multifaceted toolbox for small molecule and polymer synthesis. *Chem. Soc. Rev.* **2010b,** *39* (4), 1355-1387.

Hrubý, M.; Koňák, Č.; Ulbrich, K., Poly(allyl glycidyl ether)-block-poly(ethylene oxide): A novel promising polymeric intermediate for the preparation of micellar drug delivery systems. *J. Appl. Polym. Sci.* **2005,** *95* (2), 201-211.

Hu, X.; Tan, H.; Wang, X.; Chen, P., Surface functionalization of hydrogel by thiol-yne click chemistry for drug delivery. *Colloids Surf. A.* **2016,** *489*, 297-304.

Huang, J.; Wang, H.; Tian, X., Preparation of PEO with amine and sulfadiazine end groups by anion ring-opening polymerization of ethylene oxide. *J. Polym. Sci. A. Polym. Chem.* **1996,** *34* (10), 1933-1940.

Huisgen, R., 1,3-Dipolar Cycloadditions. Past and Future. *Angew. Chem. Int. Ed.* **1963,** *2* (10), 565-598.

Hussain, S.-A.; Bhattacharjee, D., Langmuir–Blodgett films and molecular electronics. *Mod. Phys. Lett. B* **2009,** *23* (29), 3437-3451.

Hynd, M. R.; Frampton, J. P.; Burnham, M.-R.; Martin, D. L.; Dowell-Mesfin, N. M.; Turner, J. N.; Shain, W., Functionalized hydrogel surfaces for the patterning of multiple biomolecules. *J. Biomed. Mater. Res. A.* **2007,** *81A* (2), 347-354.

Iijima, M.; Nagasaki, Y.; Okada, T.; Kato, M.; Kataoka, K., Core-polymerized reactive micelles from heterotelechelic amphiphilic block copolymers. *Macromolecules* **1999,** *32* (4), 1140-1146.

Il'ichev, Y. V.; Schwörer, M. A.; Wirz, J., Photochemical reaction mechanisms of 2-nitrobenzyl compounds: methyl ethers and caged ATP. *J. Am. Chem. Soc.* **2004,** *126* (14), 4581-4595.

Ivanova, T.; Panaiotov, I.; Georgiev, G.; Launois-Surpas, M. A.; Proust, J. E.; Puisieux, F., Surface pressure—area hysteresis of surface films formed by spreading of phospholipid liposomes. *Colloids Surf. A.* **1991,** *60*, 263-273.

Jang, H.-J.; Shin, C. Y.; Kim, K.-B., Safety evaluation of polyethylene glycol (PEG) compounds for cosmetic use. *Tox. res.* **2015,** *31* (2), 105.

Jaroque, G. N.; Sartorelli, P.; Caseli, L., Interfacial vibrational spectroscopy and Brewster angle microscopy distinguishing the interaction of terpineol in cell membrane models at the air-water interface. *Biophys. Chem.* **2019,** *246*, 1-7.

Ji, X.; Wang, C.; Xu, J.; Zheng, J.; Gattás-Asfura, K. M.; Leblanc, R. M., Surface Chemistry Studies of (CdSe) ZnS Quantum Dots at the Air− Water Interface. *Langmuir* **2005,** *21* (12), 5377-5382.

Jianqi, F.; Lixia, G., PVA/PAA thermo-crosslinking hydrogel fiber: preparation and pH-sensitive properties in electrolyte solution. *Eur. Polym. J.* **2002,** *38* (8), 1653-1658.

Joas, S.; Tovar, G. E. M.; Celik, O.; Bonten, C.; Southan, A., Extrusion-Based 3D Printing of Poly(ethylene glycol) Diacrylate Hydrogels Containing Positively and Negatively Charged Groups. *Gels* **2018,** *4* (3), 69.

Joncheray, T. J.; Denoncourt, K. M.; Mathieu, C.; Meier, M. A.; Schubert, U. S.; Duran, R. S., Langmuir and Langmuir− Blodgett films of poly(ethylene oxide)-*b*-poly(ε-caprolactone) star-shaped block copolymers. *Langmuir* **2006,** *22* (22), 9264-9271.

Kabanov, A. V.; Batrakova, E. V.; Alakhov, V. Y., Pluronic® block copolymers as novel polymer therapeutics for drug and gene delivery. *J. Control. Release* **2002,** *82* (2), 189-212.

Kaganer, V.; Brezesinski, G.; Möhwald, H.; Howes, P.; Kjaer, K., Positional order in Langmuir monolayers: An x-ray diffraction study. *Phys. Rev. E* **1999,** *59* (2), 2141.

Kaila, N.; Janz, K.; DeBernardo, S.; Bedard, P. W.; Camphausen, R. T.; Tam, S.; Tsao, D. H. H.; Keith, J. C.; Nickerson-Nutter, C.; Shilling, A.; Young-Sciame, R.; Wang, Q., Synthesis and Biological Evaluation of Quinoline Salicylic Acids As P-Selectin Antagonists. *J. Med. Chem.* **2007,** *50* (1), 21-39.

Kaleta, J.; Wen, J.; Magnera, T. F.; Dron, P. I.; Zhu, C.; Michl, J., Structure of a monolayer of molecular rotors on aqueous subphase from grazing-incidence X-ray diffraction. *Proc. Natl. Acad. Sci.* **2018,** *115* (38), 9373-9378.

Kamoun, E. A.; Kenawy, E.-R. S.; Chen, X., A review on polymeric hydrogel membranes for wound dressing applications: PVA-based hydrogel dressings. *J. Adv. Res.* **2017,** *8* (3), 217-233.

Kampf, J. P.; Frank, C. W.; Malmström, E. E.; Hawker, C. J., Stability and Molecular Conformation of Poly(benzyl ether) Monodendrons with Oligo(ethylene glycol) Tails at the Air−Water Interface. *Langmuir* **1999,** *15* (1), 227-233.

Kandler, K.; Katz, L. C.; Kauer, J. A., Focal photolysis of caged glutamate produces long-term depression of hippocampal glutamate receptors. *Nat. neurosci.* **1998,** *1* (2), 119.

Kankala, R.; Lu, F.-J.; Liu, C.-G.; Zhang, S.-S.; Chen, A.-Z.; Wang, S.-B., Effect of icariin on engineered 3d-printed porous scaffolds for cartilage repair. *Materials* **2018,** *11* (8), 1390.

Karateev, A.; Karyagin, A.; Litvinov, D.; Sumtsova, L.; Taranukha, Y., New network polymers based on furfurylglycidyl ether. *Chem. Chem.Technol.* **2008,** *2* (1), 19-26.

Kascholke, C.; Loth, T.; Kohn-Polster, C.; Möller, S.; Bellstedt, P.; Schulz-Siegmund, M.; Schnabelrauch, M.; Hacker, M. C., Dual-Functional Hydrazide-Reactive and Anhydride-Containing Oligomeric Hydrogel Building Blocks. *Biomacromolecules* **2017,** *18* (3), 683-694.

Kataoka, K.; Matsumoto, T.; Yokoyama, M.; Okano, T.; Sakurai, Y.; Fukushima, S.; Okamoto, K.; Kwon, G. S., Doxorubicin-loaded poly(ethylene glycol)–poly(β-benzyl-l-aspartate) copolymer micelles: their pharmaceutical characteristics and biological significance. *J. Control. Release* **2000,** *64* (1-3), 143-153.

Kawaguchi, H.; Fujimoto, K.; Nakazawa, Y.; Sakagawa, M.; Ariyoshi, Y.; Shidara, M.; Okazaki, H.; Ebisawa, Y., Modification and functionalization of hydrogel microspheres. *Colloids Surf. A.* **1996,** *109*, 147-154.

Klán, P.; Šolomek, T.; Bochet, C. G.; Blanc, A.; Givens, R.; Rubina, M.; Popik, V.; Kostikov, A.; Wirz, J., Photoremovable Protecting Groups in Chemistry and Biology: Reaction Mechanisms and Efficacy. *Chen. Rev.* **2013a,** *113* (1), 119-191.

Klán, P.; Šolomek, T.; Bochet, C. G.; Blanc, A.; Givens, R.; Rubina, M.; Popik, V.; Kostikov, A.; Wirz, J., Photoremovable Protecting Groups in Chemistry and Biology: Reaction Mechanisms and Efficacy. *Chem. Rev.* **2013b,** *113* (1), 119-191.

Klara, K.; Fabiola, P.; Buket, T.; Pascal, D.; Jörg, H., Self-assembling chitosan hydrogel: A drug-delivery device enabling the sustained release of proteins. *J. Appl. Polym. Sci.* **2018,** *135* (1), 45638.

Klein, R.; Wurm, F. R., Aliphatic Polyethers: Classical Polymers for the 21st Century. *Macromol. Rapid Commun.* **2015**.

Klíčová, Ĺ.; Šebej, P.; Šolomek, T.; Hellrung, B.; Slavíček, P.; Klán, P.; Heger, D.; Wirz, J., Adiabatic Triplet State Tautomerization of p-Hydroxyacetophenone in Aqueous Solution. *J. Phys. Chem. A* **2012,** *116* (11), 2935-2944.

Klikovits, N.; Knaack, P.; Bomze, D.; Krossing, I.; Liska, R., Novel photoacid generators for cationic photopolymerization. *Polym. Chem.* **2017,** *8* (30), 4414-4421.

Kobayashi, M.; Koide, T.; Hyon, S.-H., Tribological characteristics of polyethylene glycol (PEG) as a lubricant for wear resistance of ultra-high-molecular-weight polyethylene (UHMWPE) in artificial knee join. *J. Mech. Behav. Biomed. Mater.* **2014,** *38*, 33-38.

Koehler, K. C.; Alge, D. L.; Anseth, K. S.; Bowman, C. N., A Diels–Alder modulated approach to control and sustain the release of dexamethasone and induce osteogenic differentiation of human mesenchymal stem cells. *Biomaterials* **2013,** *34* (16), 4150-4158.

Kolb, H. C.; Finn, M. G.; Sharpless, K. B., Click Chemistry: Diverse Chemical Function from a Few Good Reactions. *Angew. Chem. Int. Ed.* **2001,** *40* (11), 2004-2021.

Komitov, L.; Stebler, B.; Gabrielli, G.; Puggelli, M.; Sparavigna, A.; Strigazzi, A., Amphiphilic Langmuir-Blodgett Films as a New Tool for Inducing Alignment Transition in Nematics. *Mol. Cryst. Liq. Cryst. Sci. Technol.* **1994,** *243* (1), 107-124.

Komoto, K.; Ishidoya, M.; Ogawa, H.; Sawada, H.; Okuma, K.; Ohata, H., Photopolymerization of vinyl ether by hydroxy- and methylthio-alkylphosphonium salts as novel photocationic initiators. *Polymers* **1994,** *35* (1), 217-218.

Konishcheva, E.; Daubian, D.; Gaitzsch, J.; Meier, W., Synthesis of Linear ABC Triblock Copolymers and Their Self-Assembly in Solution. *Helv. Chim. Acta* **2018,** *101* (2), e1700287.

Kovalenko, A.; Zimny, K.; Mascaro, B.; Brunet, T.; Mondain-Monval, O., Tailoring of the porous structure of soft emulsion-templated polymer materials. *Soft Matter* **2016,** *12* (23), 5154-5163.

Kowalczyk, A.; Fau, M.; Karbarz, M.; Donten, M.; Stojek, Z.; Nowicka, A. M., Hydrogel with chains functionalized with carboxyl groups as universal 3D platform in DNA biosensors. *Biosens. Bioelectron.* **2014,** *54*, 222-228.

Koyama, Y.; Umehara, M.; Mizuno, A.; Itaba, M.; Yasukouchi, T.; Natsume, K.; Suginaka, A.; Watanabe, K., Synthesis of Novel Poly(ethylene glycol) Derivatives Having Pendant Amino Groups and Aggregating Behavior of Its Mixture with Fatty Acid in Water. *Bioconjugate Chem.* **1996,** *7* (3), 298-301.

Kraut, G.; Yenchesky, L.; Prieto, F.; Tovar, G. E. M.; Southan, A., Influence of shear thinning and material flow on robotic dispensing of poly(ethylene glycol) diacrylate/poloxamer 407 hydrogels. *J. Appl. Polym. Sci.* **2017,** *134* (29), 45083.

Kumari, S.; Gusain, R.; Kumar, N.; Khatri, O. P., PEG-mediated hydrothermal synthesis of hierarchical microspheres of MoS2 nanosheets and their potential for lubrication application. *J. Ind. Eng. Chem.* **2016,** *42*, 87-94.

Kyeremateng, S. O.; Amado, E.; Blume, A.; Kressler, J., Synthesis of ABC and CABAC triphilic block copolymers by ATRP combined with 'click'chemistry. *Macromol. Rapid Commun.* **2008,** *29* (12-13), 1140-1146.

Laita, H.; Boufi, S.; Gandini, A., The Application of the Diels-Alder Reaction to Polymers Bearing Furan Moieties. *Eur. Polym. J.* **1997,** *33* (8), 1203-1211.

Langmuir, I., The constitution and fundamental properties of solids and liquids. *J. Am. Chem. Soc.* **1917,** *39* (9), 1848 - 1906.

Langmuir, I., Nobel Lectures - Surface chemistry. **1932**, Stockholm, Sweden.

Le, H. T.; Hong, B. N.; Lee, Y. R.; Cheon, J. H.; Kang, T. H.; Kim, T. W., Regulatory effect of hydroquinone–tetraethylene glycol conjugates on zebrafish pigmentation. *Bioorg. Med. Chem. Lett.* **2016,** *26* (2), 699-705.

Lee, K. Y.; Mooney, D. J., Hydrogels for Tissue Engineering. *Chem. Rev.* **2001,** *101* (7), 1869-1880.

Lee, K. Y. C., Collapse Mechanisms of Langmuir Monolayers. *Annu. Rev. Phys. Chem.* **2008,** *59* (1), 771-791.

Letchford, K.; Burt, H., A review of the formation and classification of amphiphilic block copolymer nanoparticulate structures: micelles, nanospheres, nanocapsules and polymersomes. *Eur. J. Pharm. Biopharm.* **2007,** *65* (3), 259-269.

Li, C.; Chen, P.; Shao, Y.; Zhou, X.; Wu, Y.; Yang, Z.; Li, Z.; Weil, T.; Liu, D., A Writable Polypeptide–DNA Hydrogel with Rationally Designed Multi-modification Sites. *Small* **2015,** *11* (9-10), 1138-1143.

Li, J.; Mooney, D. J., Designing hydrogels for controlled drug delivery. *Nat. Rev. Mater.* **2016,** *1* (12), 16071.

Liang, L.; Astruc, D., The copper(I)-catalyzed alkyne-azide cycloaddition (CuAAC) "click" reaction and its applications. An overview. *Coord. Chem. Rev.* **2011,** *255* (23), 2933-2945.

Lipp, M. M.; Lee, K. Y. C.; Takamoto, D. Y.; Zasadzinski, J. A.; Waring, A. J., Coexistence of Buckled and Flat Monolayers. *Phys. Rev. Lett.* **1998,** *81* (8), 1650-1653.

Liu, M.; Kira, A.; Nakahara, H., Complex Formation between Monolayers of a Novel Amphiphilic Thiazolylazo Dye and Transition Metal Ions at the Air/Water Interface. *Langmuir* **1997,** *13* (4), 779-783.

Liu, X.; Cole, J. M.; Low, K. S., Solvent effects on the UV–Vis absorption and emission of optoelectronic Coumarins: a comparison of three empirical solvatochromic models. *J. Phys. Chem. C.* **2013,** *117* (28), 14731-14741.

Lloyd, G. R.; Craig, D. Q. M.; Smith, A., An investigation into the melting behavior of binary mixes and solid dispersions of paracetamol and PEG 4000. *J. Pharm. Sci.* **1997,** *86* (9), 991-996.

Lowe, A. B., Thiol-ene "click" reactions and recent applications in polymer and materials synthesis. *Polym. Chem.* **2010,** *1* (1), 17-36.

Ma, C.; Kwok, W. M.; Chan, W. S.; Zuo, P.; Wai Kan, J. T.; Toy, P. H.; Phillips, D. L., Ultrafast Time-Resolved Study of Photophysical Processes Involved in the Photodeprotection of p-Hydroxyphenacyl Caged Phototrigger Compounds. *J. Am. Chem. Soc.* **2005,** *127* (5), 1463-1472.

Maget-Dana, R., The monolayer technique: a potent tool for studying the interfacial properties of antimicrobial and membrane-lytic peptides and their interactions with lipid membranes. *Biochim. Biophys. Acta* **1999,** *1462* (1), 109-140.

Mahou, R.; Wandrey, C., Versatile route to synthesize heterobifunctional poly(ethylene glycol) of variable functionality for subsequent pegylation. *Polymers* **2012,** *4* (1), 561-589.

Malkoch, M.; Vestberg, R.; Gupta, N.; Mespouille, L.; Dubois, P.; Mason, A. F.; Hedrick, J. L.; Liao, Q.; Frank, C. W.; Kingsbury, K.; Hawker, C. J., Synthesis of well-defined hydrogel networks using Click chemistry. *Chem. Commun.* **2006,** (26), 2774-2776.

Malzert, A.; Boury, F.; Saulnier, P.; Benoit, J.; Proust, J., Interfacial Properties of a PEG2000− PLA50 Diblock Copolymer at the Air/Water Interface. *Langmuir* **2001,** *17* (25), 7837-7841.

Mangold, C.; Obermeier, B.; Wurm, F.; Frey, H., From an Epoxide Monomer Toolkit to Functional PEG Copolymers With Adjustable LCST Behavior. *Macromol. Rapid Commun.* **2011,** *32* (23), 1930-1934.

Mangold, C.; Wurm, F.; Frey, H., Functional PEG-based polymers with reactive groups via anionic ROP of tailor-made epoxides. *Polym. Chem.* **2012,** *3* (7), 1714-1721.

Mangold, C.; Wurm, F.; Obermeier, B.; Frey, H., "Functional Poly(ethylene glycol)": PEG-Based Random Copolymers with 1,2-Diol Side Chains and Terminal Amino Functionality. *Macromolecules* **2010a,** *43* (20), 8511-8518.

Mangold, C.; Wurm, F.; Obermeier, B.; Frey, H., Hetero-Multifunctional Poly(ethylene glycol) Copolymers with Multiple Hydroxyl Groups and a Single Terminal Functionality. *Macromol. Rapid Commun.* **2010b,** *31* (3), 258-264.

Mann, B. K.; Gobin, A. S.; Tsai, A. T.; Schmedlen, R. H.; West, J. L., Smooth muscle cell growth in photopolymerized hydrogels with cell adhesive and proteolytically degradable domains: synthetic ECM analogs for tissue engineering. *Biomaterials* **2001,** *22* (22), 3045-3051.

Martin, C. J.; Rapenne, G.; Nakashima, T.; Kawai, T., Recent progress in development of photoacid generators. *J. Photochem. Photobiol.* **2018,** *34*, 41-51.

Masson, P.; Beinert, G.; Franta, E.; Rempp, P., Synthesis of polyethylene oxide macromers. *Polym. Bull.* **1982,** *7* (1), 17-22.

McCullough, E. J.; Yadavalli, V. K., Surface modification of fused deposition modeling ABS to enable rapid prototyping of biomedical microdevices. *J. Mater. Process Technol.* **2013,** *213* (6), 947-954.

McNaught, A. D.; Wilkinson, A., IUPAC- Compendium of Chemical Terminology, 2nd ed. **1997,** *Blackwell Scientific Publications,* , Oxford.

Miñones, J.; Conde, M. M.; Yebra-Pimentel, E.; Trillo, J. M., Behavior of Syndiotactic Poly(methyl methacrylate) Monolayers at the Air/Water Interface: Influence of Temperature and Molecular Weight on the Surface Pressure−Area Isotherms and Brewster Angle Microscopy Images. *J. Phys. Chem. C.* **2009,** *113* (40), 17455-17463.

Mizoguchi, K.; Hasegawa, E., Photoactive polymers applied to advanced microelectronic devices. *Polym. Adv. Technol.* **1996,** *7* (5-6), 471-477.

Modlińska, A.; Bauman, D., The Langmuir-Blodgett Technique as a Tool for Homeotropic Alignment of Fluorinated Liquid Crystals Mixed with Arachidic Acid. *Int. J. Mol. Sci.* **2011,** *12* (8), 4923-4945.

Mohammadzadeh Pakdel, P.; Peighambardoust, S. J., A review on acrylic based hydrogels and their applications in wastewater treatment. *J. Environ. Manage.* **2018,** *217*, 123-143.

Mori, S.; Barth, H. G., *Size exclusion chromatography*. Springer Science & Business Media: 2013.

Murugan, R.; Mohan, S.; Bigotto, A., FTIR and polarised Raman spectra of acrylamide and polyacrylamide. *J. Kor. Phys. Soc.* **1998,** *32* (4), 505-512.

Nad, S.; Pal, H., Unusual photophysical properties of coumarin-151. *J. Phys. Chem. A.* **2001,** *105* (7), 1097-1106.

Nagasaki, Y.; Kutsuna, T.; Iijima, M.; Kato, M.; Kataoka, K.; Kitano, S.; Kadoma, Y., Formyl-ended heterobifunctional poly (ethylene oxide): synthesis of poly (ethylene oxide) with a formyl group at one end and a hydroxyl group at the other end. *Bioconjugate Chem.* **1995,** *6* (2), 231-233.

Napoli, A.; Tirelli, N.; Wehrli, E.; Hubbell, J. A., Lyotropic behavior in water of amphiphilic ABA triblock copolymers based on poly(propylene sulfide) and poly(ethylene glycol). *Langmuir* **2002,** *18* (22), 8324-8329.

Nebhani, L.; Choudhary, V.; Adler, H.-J.; Kuckling, D., pH-and metal ion-sensitive hydrogels based on N-[2-(dimethylaminoethyl) acrylamide]. *Polymers* **2016,** *8* (6), 233.

Neckers, D. C.; Abu-Abdoun, I. I., *p,p'*-Bis((triphenylphosphonio)methyl)-benzophenone salts as photoinitiators of free radical and cationic polymerization. *Macromolecules* **1984,** *17* (12), 2468-2473.

Ni, Y.; Puthenkovilakom, R. R.; Huo, Q., Synthesis and Supramolecular Self-Assembly Study of a Novel Porphyrin Molecule in Langmuir and Langmuir−Blodgett Films. *Langmuir* **2004,** *20* (7), 2765-2771.

Nielen, M. W. F., Maldi time-of-flight mass spectrometry of synthetic polymers. *Mass Spectrom. Rev.* **1999,** *18* (5), 309-344.

Nimmo, C. M.; Owen, S. C.; Shoichet, M. S., Diels−Alder click cross-linked hyaluronic acid hydrogels for tissue engineering. *Biomacromolecules* **2011,** *12* (3), 824-830.

Nutting, G. C.; Harkins, W. D., Pressure-Area Relations of Fatty Acid and Alcohol Monolayers. *J. Am. Chem. Soc.* **1939,** *61* (5), 1180-1187.

Obermeier, B.; Frey, H., Poly(ethylene glycol-co-allyl glycidyl ether)s: A PEG-Based Modular Synthetic Platform for Multiple Bioconjugation. *Bioconjugate Chem.* **2011a,** *22* (3), 436-444.

Obermeier, B.; Wurm, F.; Frey, H., Amino Functional Poly(ethylene glycol) Copolymers via Protected Amino Glycidol. *Macromolecules* **2010,** *43* (5), 2244-2251.

Obermeier, B.; Wurm, F.; Mangold, C.; Frey, H., Multifunctional Poly(ethylene glycol)s. *Angew. Chem. Int. Ed.* **2011b,** *50* (35), 7988-7997.

Ohtsuki, T.; Kanzaki, S.; Nishimura, S.; Kunihiro, Y.; Sisido, M.; Watanabe, K., Phototriggered protein syntheses by using (7-diethylaminocoumarin-4-yl) methoxycarbonyl-caged aminoacyl tRNAs. *Nat. Commun.* **2016,** *7*, 12501.

Otsuka, H.; Nagasaki, Y.; Kataoka, K., Self-assembly of poly(ethylene glycol)-based block copolymers for biomedical applications. *Curr. Opin. Colloid Interface Sci.* **2001,** *6* (1), 3-10.

Owen, S. C.; Chan, D. P.; Shoichet, M. S., Polymeric micelle stability. *Nano Today* **2012,** *7* (1), 53-65.

Ozbas, B.; Kretsinger, J.; Rajagopal, K.; Schneider, J. P.; Pochan, D. J., Salt-triggered peptide folding and consequent self-assembly into hydrogels with tunable modulus. *Macromolecules* **2004,** *37* (19), 7331-7337.

Özçoban, C.; Halbritter, T.; Steinwand, S.; Herzig, L.-M.; Kohl-Landgraf, J.; Askari, N.; Groher, F.; Fürtig, B.; Richter, C.; Schwalbe, H.; Suess, B.; Wachtveitl, J.; Heckel, A., Water-Soluble Py-BIPS Spiropyrans as Photoswitches for Biological Applications. *Org. Lett.* **2015,** *17* (6), 1517-1520.

Pappas, S. P.; Pappas, B. C.; Gatechair, L. R.; Schnabel, W., Photoinitation of cationic polymerization. II. Laser flash photolysis of diphenyliodonium salts. *J. Polym. Sci. A Polym. Chem.* **1984,** *22* (1), 69-76.

Parente, M.; Ochoa Andrade, A.; Ares, G.; Russo, F.; Jiménez-Kairuz, Á., Bioadhesive hydrogels for cosmetic applications. *Int. J. Cosmet. Sci.* **2015,** *37* (5), 511-518.

Park, C.-H.; Givens, R. S., New Photoactivated Protecting Groups. 6. p-Hydroxyphenacyl: A Phototrigger for Chemical and Biochemical Probes1,2. *J. Am. Chem. Soc* **1997,** *119* (10), 2453-2463.

Park, S.-E.; Nho, Y.-C.; Lim, Y.-M.; Kim, H.-I., Preparation of pH-sensitive poly(vinyl alcohol-g-methacrylic acid) and poly(vinyl alcohol-g-acrylic acid) hydrogels by gamma ray irradiation and their insulin release behavior. *J. Appl. Polym. Sci.* **2004,** *91* (1), 636-643.

Patist, A.; Bhagwat, S. S.; Penfield, K. W.; Aikens, P.; Shah, D. O., On the measurement of critical micelle concentrations of pure and technical-grade nonionic surfactants. *J. Surfactants Deterg.* **2000,** *3* (1), 53-58.

Pella, D. A., Synthesis and applications of caged thiols for studying protein prenylation. **2012,** *Dissertation*, University of Minnesota, United States of America.

Pellá, M. G.; Lima-Tenório, M. K.; Tenório-Neto, E. T.; Guilherme, M. R.; Muniz, E. C.; Rubira, A. F., Chitosan-based hydrogels: From preparation to biomedical applications. *Carbohydr. Polym.* **2018**.

Pelliccioli, A. P.; Wirz, J., Photoremovable protecting groups: reaction mechanisms and applications. *Photochem. Photobiol. Sci.* **2002,** *1* (7), 441-458.

Pich, A.; Berger, S.; Ornatsky, O.; Baranov, V.; Winnik, M. A., The influence of PEG macromonomers on the size and properties of thermosensitive aqueous microgels. *Colloid Polym. Sci.* **2009,** *287* (3), 269-275.

Pockels, A., Surface tension. *Nature* **1891,** *43* (1115), 437-439.

Polizzotti, B. D.; Fairbanks, B. D.; Anseth, K. S., Three-Dimensional Biochemical Patterning of Click-Based Composite Hydrogels via Thiolene Photopolymerization. *Biomacromolecules* **2008,** *9* (4), 1084-1087.

Pramanik, N. B.; Mondal, P.; Mukherjee, R.; Singha, N. K., A new class of self-healable hydrophobic materials based on ABA triblock copolymer via RAFT polymerization and Diels-Alder "click chemistry". *Polymer* **2017,** *119*, 195-205.

Price, C. C.; Carmelite, D. D., Reactions of epoxides in dimethyl sulfoxide catalyzed by potassium t-butoxide. *J. Am. Chem. Soc.* **1966,** *88* (17), 4039-4044.

Qian, Y.; Lesage, K.; El Cheikh, K.; De Schutter, G., Effect of polycarboxylate ether superplasticizer (PCE) on dynamic yield stress, thixotropy and flocculation state of fresh cement pastes in consideration of the Critical Micelle Concentration (CMC). *Cem. Concr. Res.* **2018,** *107*, 75-84.

Qin, S.; Hui, L.-w.; Yang, L.-h.; Ma, M.-m., Solvent-triggered self-folding of hydrogel sheets. *Chin. J. Chem. Phys.* **2018,** *31* (5), 667-672.

Qiu, Y.; Park, K., Environment-sensitive hydrogels for drug delivery. *Adv. Drug Deliv. Rev.* **2001,** *53* (3), 321-339.

Ramírez, P.; Pérez, L. M.; Trujillo, L. A.; Ruiz, M.; Muñoz, J.; Miller, R., Equilibrium and surface rheology of two polyoxyethylene surfactants (CiEOj) differing in the number of oxyethylene groups. *Colloids Surf. A.* **2011,** *375* (1), 130-135.

Reichmanis, E.; Smith, B. C.; Gooden, R., O-nitrobenzyl photochemistry: Solution vs. solid-state behavior. *J. Polym. Sci. A Polym. Chem.* **1985,** *23* (1), 1-8.

Reinfelds, M.; von Cosel, J.; Falahati, K.; Hamerla, C.; Slanina, T.; Burghardt, I.; Heckel, A., A New Photocage Derived from Fluorene. *Chem. Eur. J.* **2018,** *24* (49), 13026-13035.

Reuss, V. S.; Obermeier, B.; Dingels, C.; Frey, H., *N, N*-diallylglycidylamine: a Key monomer for amino-functional poly(ethylene glycol) architectures. *Macromolecules* **2012,** *45* (11), 4581-4589.

Richards, D.; Szwarc, M., Block polymers of ethylene oxide and its analogues with styrene. *J. Chem. Soc. Faraday Trans.* **1959,** *55*, 1644-1650.

Richter, A.; Paschew, G.; Klatt, S.; Lienig, J.; Arndt, K.-F.; Adler, H.-J., Review on hydrogel-based pH sensors and microsensors. *Sensors* **2008,** *8* (1), 561-581.

Richter, A.; Wenzel, J.; Kretschmer, K., Mechanically adjustable chemostats based on stimuli-responsive polymers. *Sens. Actuator B Chem.* **2007,** *125* (2), 569-573.

Rideout, D. C.; Breslow, R., Hydrophobic acceleration of Diels-Alder reactions. *J. Am. Chem. Soc.* **1980,** *102* (26), 7816-7817.

Rieger, J.; Bernaerts, K. V.; Du Prez, F. E.; Jérôme, R.; Jérôme, C., Lactone End-Capped Poly(ethylene oxide) as a New Building Block for Biomaterials. *Macromolecules* **2004,** *37* (26), 9738-9745.

Ries Jr, H. E.; Swift, H., Twisted double-layer ribbons and the mechanism for monolayer collapse. *Langmuir* **1987,** *3* (5), 853-855.

Riess, G.; Labbe, C., Block copolymers in emulsion and dispersion polymerization. *Macromol. Rapid Commun.* **2004,** *25* (2), 401-435.

Rimmer, S.; Johnson, C.; Zhao, B.; Collier, J.; Gilmore, L.; Sabnis, S.; Wyman, P.; Sammon, C.; Fullwood, N. J.; MacNeil, S., Epithelialization of hydrogels achieved by amine functionalization and co-culture with stromal cells. *Biomaterials* **2007,** *28* (35), 5319-5331.

Rivera, E.; del Pilar Carreón-Castro, M.; Rodríguez, L.; Cedillo, G.; Fomine, S.; Morales-Saavedra, O. G., Amphiphilic azo-dyes (RED-PEGM). Part 2: Charge transfer complexes, preparation of Langmuir–Blodgett films and optical properties. *Dyes Pigm.* **2007,** *74* (2), 396-403.

Roberts, G. G., An applied science perspective of Langmuir-Blodgett films. *Adv. Phys.* **1985,** *34* (4), 475-512.

Rodríguez Patino, J. M.; Sánchez, C. C.; Rodríguez Niño, M. R., Morphological and structural characteristics of monoglyceride monolayers at the air− water interface observed by Brewster angle microscopy. *Langmuir* **1999,** *15* (7), 2484-2492.

Roos, K.; Dolci, E.; Carlotti, S.; Caillol, S., Activated anionic ring-opening polymerization for the synthesis of reversibly cross-linkable poly (propylene oxide) based on furan/maleimide chemistry. *Polym. Chem.* **2016,** *7* (8), 1612-1622.

Rosiak, J. M.; Yoshii, F., Hydrogels and their medical applications. *Nucl. Instrum. Methods Phys. Res. B.* **1999,** *151* (1), 56-64.

Rösler, A.; Vandermeulen, G. W.; Klok, H.-A., Advanced drug delivery devices via self-assembly of amphiphilic block copolymers. *Adv. Drug Deliv. Rev.* **2012,** *64*, 270-279.

Rostovtsev, V. V.; Green, L. G.; Fokin, V. V.; Sharpless, K. B., A Stepwise Huisgen Cycloaddition Process: Copper(I)-Catalyzed Regioselective "Ligation" of Azides and Terminal Alkynes. *Angew. Chem.* **2002,** *114* (14), 2708-2711.

Roy, S.; Biswas, B.; Mondal, J. A.; Singh, P. C., Heterodyne-Detected Vibrational Sum Frequency Generation Study of Air–Water–Fluoroalcohol Interface: Fluorocarbon Group-Induced Structural and Orientational Change of Interfacial Water. *J. Phys. Chem. C* **2018,** *122* (47), 26928-26933.

Sadeghi, M.; Hosseinzadeh, H., Synthesis of Starch—Poly(Sodium Acrylate-co-Acrylamide) Superabsorbent Hydrogel with Salt and pH-Responsiveness Properties as a Drug Delivery System. *J. Bioact. Compat. Polym.* **2008,** *23* (4), 381-404.

Saeva, F. D.; Morgan, B. P.; Luss, H. R., Photochemical conversion of sulfonium salts to sulfides via a 1,3-sigmatropic rearrangement. Photogeneration of Broensted acids. *J. Org. Chem.* **1985,** *50* (22), 4360-4362.

Safran, S. A.; Schick, M., Statistical Thermodynamics of Surfaces, Interfaces, and Membranes. *Phys. Today* **1996,** *49*, 68.

Saha, A.; SenGupta, S.; Kumar, A.; Naik, P. D., Interaction of l-Phenylalanine with Lipid Monolayers at Air–Water Interface at Different pHs: Sum-Frequency Generation Spectroscopy and Surface Pressure Studies. *J. Phys. Chem. C* **2018,** *122* (7), 3875-3884.

Sahebnazar, Z.; Mowla, D.; Karimi, G.; Yazdian, F., Zero-valent iron nanoparticles assisted purification of rhamnolipid for oil recovery improvement from oily sludge. *J. Environ. Chem. Eng.* **2018,** *6* (1), 917-922.

Sajeesh, S.; Bouchemal, K.; Sharma, C.; Vauthier, C., Surface-functionalized polymethacrylic acid based hydrogel microparticles for oral drug delivery. *Eur. J. Pharm. Biopharm.* **2010,** *74* (2), 209-218.

Sakurai, I.; Kawamura, Y., Lateral electrical conduction along a phosphatidylcholine monolayer. *Biochim. Biophys. Acta.* **1987,** *904* (2), 405-409.

Satoh, T.; Sumaru, K.; Takagi, T.; Kanamori, T., Light Dose-Dependent Thickness Control of Photoacid Generator-Bearing Hydrogel. *Macromol. Symp.* **2015,** *358* (1), 52-58.

Schade, B.; Hagen, V.; Schmidt, R.; Herbrich, R.; Krause, E.; Eckardt, T.; Bendig, J., Deactivation Behavior and Excited-State Properties of (Coumarin-4-yl)methyl Derivatives. 1. Photocleavage of (7-Methoxycoumarin-4-yl)methyl-Caged Acids with Fluorescence Enhancement. *J. Org. Chem.* **1999,** *64* (25), 9109-9117.

Schauenburg, D.; Gálvez, A. O.; Bode, J. W., Covalently functionalized amide cross-linked hydrogels from primary amines and polyethylene glycol acyltrifluoroborates (PEG-KATs). *J. Mat. Chem. B.* **2018,** *6* (29), 4775-4782.

Schlaad, H.; Kukula, H.; Rudloff, J.; Below, I., Synthesis of α, ω-heterobifunctional poly (ethylene glycol) s by metal-free anionic ring-opening polymerization. *Macromolecules* **2001,** *34* (13), 4302-4304.

Schlögl, S.; Reischl, M.; Ribitsch, V.; Kern, W., UV induced microcellular foaming—A new approach towards the production of 3D structures in offset printing techniques. *Prog. Org. Coat.* **2012,** *73* (1), 54-61.

Schmidt, R.; Geissler, D.; Hagen, V.; Bendig, J., Kinetics Study of the Photocleavage of (Coumarin-4-yl)methyl Esters. *J. Phys. Chem.* **2005,** *109* (23), 5000-5004.

Schmierer, T.; Laimgruber, S.; Haiser, K.; Kiewisch, K.; Neugebauer, J.; Gilch, P., Femtosecond spectroscopy on the photochemistry of ortho-nitrotoluene. *Phys. Chem. Chem. Phys.* **2010,** *12* (48), 15653-15664.

Scholz, N.; Behnke, T.; Resch-Genger, U., Determination of the Critical Micelle Concentration of Neutral and Ionic Surfactants with Fluorometry, Conductometry, and Surface Tension—A Method Comparison. *J. Fluoresc.* **2018,** *28* (1), 465-476.

Schramm, L.; Green, W., An absolute differential maximum bubble pressure surface tensiometer employing displaced capillaries. *Colloid Polym. Sci.* **1992,** *270* (7), 694-706.

Schuster, F.; Hirth, T.; Weber, A., Reactive inkjet printing of polyethylene glycol and isocyanate based inks to create porous polyurethane structures. *J. Appl. Polym. Sci.* **2019,** *136* (3), 46977.

Schuster, F.; Ngamgoue, F. N.; Goetz, T.; Hirth, T.; Weber, A.; Bach, M., Investigations of a catalyst system regarding the foamability of polyurethanes for reactive inkjet printing. *J. Mater. Chem. C* **2017,** *5* (27), 6738-6744.

Schwörer, M.; Wirz, J., Photochemical reaction mechanisms of 2-nitrobenzyl compounds in solution, I. 2-Nitrotoluene: thermodynamic and kinetic parameters of the aci-nitro tautomer. *Helv. Chim. Acta* **2001,** *84* (6), 1441-1458.

Serowy, S.; Saparov, S. M.; Antonenko, Y. N.; Kozlovsky, W.; Hagen, V.; Pohl, P., Structural Proton Diffusion along Lipid Bilayers. *Biophys. J.* **2003,** *84* (2), 1031-1037.

Shahi, S.; Zohuriaan-Mehr, M. J.; Omidian, H., Antibacterial superabsorbing hydrogels with high saline-swelling properties without gel blockage: Toward ideal superabsorbents for hygienic applications. *J. Bioact. Compat. Polym.* **2017,** *32* (2), 128-145.

Sheehan, J. C.; Umezawa, K., Phenacyl photosensitive blocking groups. *J. Org. Chem.* **1973,** *38* (21), 3771-3774.

Shembekar, V. R.; Chen, Y.; Carpenter, B. K.; Hess, G. P., Coumarin-caged glycine that can be photolyzed within 3 μs by visible light. *Biochemistry* **2007,** *46* (18), 5479-5484.

Shembekar, V. R.; Chen, Y.; Carpenter, B. K.; Hess, G. P., A Protecting Group for Carboxylic Acids That Can Be Photolyzed by Visible Light. *Biochemistry* **2005,** *44* (19), 7107-7114.

Shimizu, K.; Canongia Lopes, J. N.; Gonçalves da Silva, A. I. M., Ionic Liquid Films at the Water–Air Interface: Langmuir Isotherms of Tetra-alkylphosphonium-Based Ionic Liquids. *Langmuir* **2015,** *31* (30), 8371-8378.

Shinzawa, H.; Uchimaru, T.; Mizukado, J.; Kazarian, S. G., Non-equilibrium behavior of polyethylene glycol (PEG)/polypropylene glycol (PPG) mixture studied by Fourier transform infrared (FTIR) spectroscopy. *Vib. Spectrosc.* **2017,** *88*, 49-55.

Shirai, M.; Tsunooka, M., Photoacid and photobase generators: chemistry and applications to polymeric materials. *Prog. Polym. Sci.* **1996,** *21* (1), 1-45.

Sill, K. N.; Sullivan, B.; Carie, A.; Semple, J. E., Synthesis and Characterization of Micelle-Forming PEG-Poly (Amino Acid) Copolymers with Iron-Hydroxamate Cross-Linkable Blocks for Encapsulation and Release of Hydrophobic Drugs. *Biomacromolecules* **2017,** *18* (6), 1874-1884.

Singh, A.; Sharma, P. K.; Garg, V. K.; Garg, G., Hydrogels: A review. *Int. J. Pharm. Sci. Res.* **2010,** *4* (2), 97-105.

Singhal, R.; Gupta, K., A Review: Tailor-made Hydrogel Structures (Classifications and Synthesis Parameters). *Polym. Plast. Technol. Eng.* **2016,** *55* (1), 54-70.

Smets, G.; Aerts, A.; Erum, J. V., Photochemical Initiation of Cationic Polymerization and Its Kinetics. *Polym. J.* **1980,** *12*, 539.

Smith, L. J.; Taimoory, S. M.; Tam, R. Y.; Baker, A. E. G.; Binth Mohammad, N.; Trant, J. F.; Shoichet, M. S., Diels–Alder Click-Cross-Linked Hydrogels with Increased Reactivity Enable 3D Cell Encapsulation. *Biomacromolecules* **2018,** *19* (3), 926-935.

Soontornworajit, B.; Zhou, J.; Shaw, M. T.; Fan, T.-H.; Wang, Y., Hydrogel functionalization with DNA aptamers for sustained PDGF-BB release. *Chem. Commun.* **2010,** *46* (11), 1857-1859.

Southan, A., *Functional Poly(ethylene glycol)-based Polymers for Polymer Network Formation bey Side-product free Reactions* **2013,** *Dissertation*, University of Stuttgart.

Southan, A.; Lang, T.; Schweikert, M.; Tovar, G. E. M.; Wege, C.; Eiben, S., Covalent incorporation of tobacco mosaic virus increases the stiffness of poly(ethylene glycol) diacrylate hydrogels. *RSC Adv.* **2018,** *8* (9), 4686-4694.

Spencer, D. S.; Luu, B. C.; Beckman, D. W.; Peppas, N. A., Control of cationic nanogel PEGylation in heterogeneous ARGET ATRP emulsion polymerization with PEG macromonomers. *J. Polym. Sci. A Polym. Chem.* **2018,** *56* (14), 1536-1544.

Steven, V.; Graham, D., Oligonucleotide conjugation to a cell-penetrating (TAT) peptide by Diels–Alder cycloaddition. *Org. Biomol. Chem.* **2008,** *6* (20), 3781-3787.

Studer, K.; Decker, C.; Beck, E.; Schwalm, R., Overcoming oxygen inhibition in UV-curing of acrylate coatings by carbon dioxide inerting, Part I. *Prog. Org. Coat.* **2003,** *48* (1), 92-100.

Sugita, H.; Matsumura, N., I-line photoresist composed of multifunctional acrylate, photo initiator, and photo acid generator, which can be patterned after g-line photo-crosslinking. *Microelec. Eng.* **2018,** *195*, 86-94.

Swain, S.; Bal, T., Carrageenan-guar gum microwave irradiated micro-porous interpenetrating polymer network: A system for drug delivery. *Int. J. Polym. Mater.* **2018**, 1-10.

Taher, A. M.; Cates, D. M., A spectrophotometric investigation of the yellow color that accompanies the formation of furan derivatives in degraded-sugar solutions. *Carbohydr. Res.* **1974,** *34* (2), 249-261.

Takamoto, D. Y.; Lipp, M. M.; von Nahmen, A.; Lee, K. Y. C.; Waring, A. J.; Zasadzinski, J. A., Interaction of Lung Surfactant Proteins with Anionic Phospholipids. *Biophys. J.* **2001,** *81* (1), 153-169.

Tallawi, M.; Rosellini, E.; Barbani, N.; Cascone, M. G.; Rai, R.; Saint-Pierre, G.; Boccaccini, A. R., Strategies for the chemical and biological functionalization of scaffolds for cardiac tissue engineering: a review. *J. Royal Soc. Interface* **2015,** *12* (108), 20150254.

Tan, J.; Butterfield, D.; Voycheck, C.; Caldwell, K.; Li, J., Surface modification of nanoparticles by PEO/PPO block copolymers to minimize interactions with blood components and prolong blood circulation in rats. *Biomaterials* **1993,** *14* (11), 823-833.

Tang, J. D.; Mura, C.; Lampe, K. J., Stimuli-Responsive, Pentapeptide, Nanofiber Hydrogel for Tissue Engineering. *J. Am. Chem. Soc.* **2019,** *141* (12), 4886-4899.

Tasdelen, M. A., Diels–Alder "click" reactions: recent applications in polymer and material science. *Polym. Chem.* **2011,** *2* (10), 2133-2145.

Taton, D.; Le Borgne, A.; Sepulchre, M.; Spassky, N., Synthesis of chiral and racemic functional polymers from glycidol and thioglycidol. *Macromol. Chem. Phys.* **1994,** *195* (1), 139-148.

Tavakoli, J.; Tang, Y., Hydrogel based sensors for biomedical applications: An updated review. *Polymers* **2017,** *9* (8), 364.

Taylor, M.; Scurr, D.; Lutolf, M.; Buttery, L.; Zelzer, M.; Alexander, M., 3D chemical characterization of frozen hydrated hydrogels using ToF-SIMS with argon cluster sputter depth profiling. *Biointerphases* **2016,** *11* (2), 301.

Teissié, J.; Prats, M.; Soucaille, P.; Tocanne, J., Evidence for conduction of protons along the interface between water and a polar lipid monolayer. *Proc. Natl. Acad. Sci.* **1985,** *82* (10), 3217-3221.

Truong, T. T.; Thai, S. H.; Nguyen, H. T.; Vuong, V.-D.; Nguyen, L.-T. T., Synthesis of allyl end-block functionalized poly(ε-caprolactone)s and their facile post-functionalization via thiol–ene reaction. *J. Polym. Sci. Pol. Chem.* **2017,** *55* (5), 928-939.

Tsutsumi, H.; Kawamura, M.; Mihara, H., Osteoblastic differentiation on hydrogels fabricated from Ca2+-responsive self-assembling peptides functionalized with bioactive peptides. *Bioorg. Med. Chem.* **2018,** *26* (12), 3126-3132.

Ullah, F.; Othman, M. B. H.; Javed, F.; Ahmad, Z.; Akil, H. M., Classification, processing and application of hydrogels: A review. *Mater. Sci. Eng. C.* **2015,** *57*, 414-433.

Vojkovsky, T.; Sullivan, B.; Sill, K. N., Synthesis of heterobifunctional polyethylene glycols: Polymerization from functional initiators. *Polymers* **2016,** *105*, 72-78.

Wagner, M.; Barthel, M. J.; Freund, R. R.; Hoeppener, S.; Traeger, A.; Schacher, F. H.; Schubert, U. S., Solution self-assembly of poly (ethylene oxide)-block-poly (furfuryl glycidyl ether)-block-poly (allyl glycidyl ether) based triblock terpolymers: a field-flow fractionation study. *Polym. Chem.* **2014**.

Wang, G.; Jiang, M.; Zhang, Q.; Wang, R.; Zhou, G., Biobased multiblock copolymers: Synthesis, properties and shape memory performance of poly(ethylene 2,5-furandicarboxylate)-b-poly(ethylene glycol). *Polym. Degrad. and Stab.* **2017,** *144*, 121-127.

Wang, W. B.;   Xu, J. X.; Wang, A. Q., A pH-, salt- and solvent-responsive carboxymethylcellulose-g-poly(sodium acrylate)/medical stone superabsorbent composite with enhanced swelling and responsive properties. *Express Polymer Letters* **2011,** *5*, 385-400.

Webster, R.; Elliott, V.; Park, B. K.; Walker, D.; Hankin, M.; Taupin, P., PEGylated Protein Drugs: Basic Science and Clinical Applications. **2009,** *Birkhäuser*, Basel, Switzerland.

Wenande, E.; Garvey, L. H., Immediate-type hypersensitivity to polyethylene glycols: a review. *Clin. Exp. Allergy* **2016,** *46* (7), 907-922.

Wichterle, O.; Lim, D., Hydrophilic Gels for Biological Use. *Nature* **1960,** *185* (4706), 117-118.

Wiesenthal, T.; Baekmark, T. R.; Merkel, R., Direct Evidence for a Lipid Alkyl Chain Ordering Transition in Poly(ethylene oxide) Lipopolymer Monolayers at the Air−Water Interface Obtained from Infrared Reflection Absorption Spectroscopy. *Langmuir* **1999,** *15* (20), 6837-6844.

Williamson, A., Theory of etherification. *Philos. Mag.* **1850,** *37* (251), 350-356.

Wu, J.; Li, P.; Dong, C.; Jiang, H.; Bin, X.; Gao, X.; Qin, M.; Wang, W.; Bin, C.; Cao, Y., Rationally designed synthetic protein hydrogels with predictable mechanical properties. *Nat. Commun.* **2018,** *9* (1), 620.

Wu, K. J.; Odom, R. W., Characterizing Synthetic Polymers by MALDI MS. *Anal. Chem.* **1998,** *70* (13), 456A-461A.

Wurm, F.; Nieberle, J.; Frey, H., Synthesis and Characterization of Poly(glyceryl glycerol) Block Copolymers. *Macromolecules* **2008,** *41* (6), 1909-1911.

Xue, B.; Kozlovskaya, V.; Liu, F.; Chen, J.; Williams, J. F.; Campos-Gomez, J.; Saeed, M.; Kharlampieva, E., Intracellular Degradable Hydrogel Cubes and Spheres for Anti-Cancer Drug Delivery. *ACS Appl. Mater. Interfaces* **2015,** *7* (24), 13633-13644.

Yamamoto, Y.; Nagasaki, Y.; Kato, M.; Kataoka, K., Surface charge modulation of poly(ethylene glycol)–poly(D,L-lactide) block copolymer micelles: conjugation of charged peptides. *Colloids Surf. B* **1999,** *16* (1), 135-146.

Yang, H.; Shin, K.; Tae, G.; Satija, S. K., Structure of a monolayer of poly (ethylene glycol) end-capped with a fluoroalkyl group and its relationship with protein adsorption at the aqueous interface. *Soft Matter* **2009,** *5* (14), 2731-2737.

Yang, H.; Zhao, X.; Zhang, X.; Ma, L.; Wang, B.; Wei, H., Optimization of bioreducible micelles self-assembled from amphiphilic hyperbranched block copolymers for drug delivery. *J. Polym. Sci. A Polym. Chem.* **2018,** *56* (13), 1383-1394.

Yang, W.; Auciello, O.; Butler, J. E.; Cai, W.; Carlisle, J. A.; Gerbi, J. E.; Gruen, D. M.; Knickerbocker, T.; Lasseter, T. L.; Russell Jr, J. N., DNA-modified nanocrystalline diamond thin-films as stable, biologically active substrates. *Nat. Mater.* **2002,** *1* (4), 253.

Ybert, C.; Lu, W.; Möller, G.; Knobler, C. M., Collapse of a Monolayer by Three Mechanisms. *J. Phys. Chem. B.* **2002,** *106* (8), 2004-2008.

Yew, Y.; Ng, T.; Li, H.; Lam, K., Analysis of pH and electrically controlled swelling of hydrogel-based micro-sensors/actuators. *Biomed. Microdevices* **2007,** *9* (4), 487-499.

Yigit, S.; Sanyal, R.; Sanyal, A., Fabrication and Functionalization of Hydrogels through "Click" Chemistry. *Chem. Asian J.* **2011,** *6* (10), 2648-2659.

Yilmaz, G.; Kahveci, M. U.; Yagci, Y., A One Pot, One Step Method for the Preparation of Clickable Hydrogels by Photoinitiated Polymerization. *Macromol. Rapid Commun.* **2011,** *32* (23), 1906-1909.

Yoo, S.-Y.; Shin, H.-K.; Jeong, H.; Park, J.-C.; Kwon, Y.-S., Structure Analysis of Langmuir and Langmuir-Blodgett Films with Metal Complexes. *Mol. Cryst. Liq. Cryst. Sci. Technol.* **1999,** *337* (1), 357-360.

Yu, F.; Cao, X.; Zeng, L.; Zhang, Q.; Chen, X., An interpenetrating HA/G/CS biomimic hydrogel via Diels–Alder click chemistry for cartilage tissue engineering. *Carbohydr. Polym.* **2013,** *97* (1), 188-195.

Yu, H.; Li, J.; Wu, D.; Qiu, Z.; Zhang, Y., Chemistry and biological applications of photo-labile organic molecules. *Chem. Soc. Rev.* **2010,** *39* (2), 464-473.

Yue, X.; Yanez, C. O.; Yao, S.; Belfield, K. D., Selective Cell Death by Photochemically Induced pH Imbalance in Cancer Cells. *J. Am. Chem. Soc.* **2013,** *135* (6), 2112-2115.

Zhang, C.; Hekmatfer, S.; Karuri, N. W., A comparative study of polyethylene glycol hydrogels derivatized with the RGD peptide and the cell-binding domain of fibronectin. *J. Biomed. Mater. Res. B.* **2014,** *102* (1), 170-179.

Zhang, K.; Corrie, J. E.; Munasinghe, V. R. N.; Wan, P., Mechanism of photosolvolytic rearrangement of p-hydroxyphenacyl esters: evidence for excited-state intramolecular proton transfer as the primary photochemical step. *J. Am. Chem. Soc.* **1999,** *121* (24), 5625-5632.

Zhang, Y.; Li, Y.; Liu, W., Dipole–Dipole and H-Bonding Interactions Significantly Enhance the Multifaceted Mechanical Properties of Thermoresponsive Shape Memory Hydrogels. *Adv. Func. Mat.* **2015,** *25* (3), 471-480.

Zhu, J., Bioactive modification of poly(ethylene glycol) hydrogels for tissue engineering. *Biomaterials* **2010,** *31* (17), 4639-4656.

Zhu, J.; Beamish, J. A.; Tang, C.; Kottke-Marchant, K.; Marchant, R. E., Extracellular matrix-like cell-adhesive hydrogels from RGD-containing poly (ethylene glycol) diacrylate. *Macromolecules* **2006,** *39* (4), 1305-1307.

Zou, K.; Cheley, S.; Givens, R. S.; Bayley, H., Catalytic Subunit of Protein Kinase A Caged at the Activating Phosphothreonine. *J. Am. Chem. Soc.* **2002,** *124* (28), 8220-8229.

Zou, K.; Miller, W. T.; Givens, R. S.; Bayley, H., Caged thiophosphotyrosine peptides. *Angew. Chem. Int. Ed.* **2001,** *40* (16), 3049-3051.

IV. Appendix

Curriculum vitae

Karishma Katharina Reinold, geb. Adatia

_____

Education

03/2015 – 07/2020   PhD student at the Institute of Interfacial Process Engineering and Plasma Technology at the University of Stuttgart in cooperation with Fraunhofer IGB, Germany.

PhD thesis title: Synthesis and Characterization of Multifunctional Macromonomers and Photoacid Generators for the Modification of Hydrogels

10/2017 – 03/2018   Visiting researcher at the department of Chemical Engineering at Stanford University, USA.

Research topic: Structure-property Relations of Amphiphilic Poly(furfuryl glycidyl ether)-*block*-poly(ethylene glycol) Macromonomers at the Air-water Interface

04/2012 – 06/2014   Master of Science, chemistry, Technical University of Munich, Germany.

Master thesis title: Synthesis and Establishment of Base-cleavable Linkers for Activity-based Proteomics

10/2008 – 11/2011   Bachelor of Science, chemistry, University of Ulm, Germany.

Bachelor thesis title: Synthesis and Characterization of Biotinylated Multifunctional Dendrimer Branches

09/1999 – 06/2008   High school, Vöhlin Gymnasium Memmingen, Germany.

_____

Scholarships and Awards

10/2019   Leadership scholarship of the Karl-Schlecht foundation

06/2015 – 05/2018 PhD scholarship of the Evonik foundation

06/2017   Poster prize at the International NanoBioMater conference 2017

09/2016   Scholarship of the Young Titans summer academy: leadership and personality

01/2009 – 05/2014 Scholarship of the Friedrich Ebert foundation

06/2006 – 12/2008 Music scholarship of the Lions Club

Scientific contributions

Journal articles *(peer reviewed)*

Adatia, K. K.; Keller, S.; Götz, T.; Tovar, G. E. M.; Southan, A.: „Hydrogels with multiple clickable anchor points: synthesis and characterization of poly(furfuryl glycidyl ether)-*block*-poly(ethylene glycol) macromonomers", *Polym. Chem*. **2019**, *10*, 4485 - 4494.

Adatia, K. K.; Halbritter, T.; Reinfelds, M.; Michele, A.; Tran, M.; Laschat, S.; Heckel, A.; Tovar, G. E. M.; Southan, A.: "Coumarin-4-ylmethyl and *p*-hydroxyphenacyl-based photoacid generators with high solubility in aqueous media: synthesis, stability and photolysis", *ChemPhotoChem* **2020**, *4,* 207 - 217.

Adatia, K. K.; Holm, A.; Southan, A.; Frank, C. W.; Tovar, G. E. M.: „Structure-property relations of amphiphilic poly(furfuryl glycidyl ether)-*block*-poly(ethylene glycol) macromonomers at the air-water interface", *Polym. Chem*. **2020**, *11*, 5659 - 5668.

Conference contributions

Adatia, K. K.; Southan, A.; Tovar, G. E. M.: „Surface Characteristics and Structure Property Relations of Functional PEG-based Block Copolymers at the Water-Air Interface" (Presentation), *13th NanoBioMater workshop*, July 18th, Stuttgart, **2018**.

Adatia, K. K.; Southan, A.; Tovar, G. E. M.: „Synthesis and characterization of blockcopolymers for surface functionalization of hydrogels" (Presentation), *International NanoBioMater conference*, June 28th - June 30th, Bad Herrenalb, **2017**.

Adatia, K. K.; Southan, A.; Tovar, G. E. M.: „Synthesis and characterization of blockcopolymers for surface functionalization of hydrogels" (Poster presentation), *NanoBioMater summer school*, June 27th, Bad Herrenalb, **2017**.

Adatia, K. K.; Southan, A.: „Hydrogel Ink Design Principles for Robotic 3D Dispensing" (Poster presentation), *Macromolecular Colloquium*, February 15th - February 17th, Freiburg, **2017**.

Adatia, K. K.; Southan, A.; Tovar, G. E. M.: „Surface functionalization of Hydrogel Foams for Additive Manufacturing" (Poster presentation), *10th NanoBioMater workshop*, December 7th, Stuttgart, **2016**.

Adatia, K. K.; Southan, A.; Tovar, G. E. M.: „Surface functionalization of superporous hydrogels *via* self assembly of functionalized blockcopolymers for additive manufacturing" (Presentation), *Scholars Meeting Evonik Foundation*, April 15th, Darmstadt, **2016**.

Adatia, K. K.; Southan, A.; Tovar, G. E. M.: „Surface functionalization of Hydrogel Foams for Additive Manufacturing" (Poster presentation), *7th NanoBioMater workshop*, February 16th, Stuttgart, **2016**.

Adatia, K. K.; Southan, A.; Tovar, G. E. M.: „Surface functionalization of Hydrogel Foams for Additive Manufacturing" (Poster presentation), *NanoBioMater summer school*, June 22th - June 24th, Bad Herrenalb, **2015**.